Metabolic plasticity of vascular smooth muscle cells in vascular disease

Inaugural-Dissertation

to obtain the academic degree

Doctor rerum naturalium (Dr. rer. nat.)

submitted to the Department of Biology, Chemistry, Pharmacy

of Freie Universität Berlin

by

Kerstin Wöltje

2022

The work presented herein was performed under the supervision of PD Dr. med. Till Althoff at the Center for Cardiovascular Research at Charité-Universitätsmedizin Berlin between February 2015 and January 2020 in the research group ‘Atherogenesis’, headed by Prof. Dr. Karl Stangl and Prof. Dr. Verena Stangl.

1. Reviewer: PD Dr. med. Till Althoff
2. Reviewer: Prof. Dr. rer. nat. Sigmar Stricker

Date of defense: 25.11.2022

Acknowledgement

I would like to take this opportunity and thank everyone who contributed to the completion of this thesis.
First, I would like to thank my supervisor, Dr. Till Althoff, who initiated this project and entrusted me with it. Thank you for guiding and supporting me throughout this thesis and for your encouragement when I was struggling with unexpected results and seemingly insurmountable problems.
Thank you also to Prof. Karl Stangl and Prof. Verena Stangl for giving me the opportunity to perform this thesis in their lab.
Many thanks go to Prof. Sigmar Stricker who kindly agreed to review this thesis. Thank you for your time.

Heartfelt gratitude goes to all the members of the research group 'AG Stangl' at the CCR. Thank you, Mario Lorenz and Antje Ludwig, for your help and scientific advice and for always lending an ear to my problems. Huge thanks go to Andrea Weller without whom this project would not have been possible. Thank you for always taking care of the mice and of me and for finding solutions for most problems. Big thanks also go to Angelika Vietzke, Conny Bartsch, Anke Stach and Nicole Rösener for their help and advice in the lab.
I would also like to thank Dr. Carsten Grötzinger who kindly offered his support and whose advice I gladly took.

My warmest thank you to my fellow doctoral candidates. Thank you, Carmen Hannemann, Johannes Schecker, Shailey Twamley, Cathleen Drescher and Veronika Bobb, for your support, your companionship and for the often fun and sometimes sad times we shared in and outside of the lab.

I would like to express great thanks to my wonderful friends. Thank you for your continuous support, for always understanding when my time was scarce, for laughing and crying with me, for all your help, ranging from proof-reading this thesis over helping with the LaTeX formatting to distracting me when I needed it.

My biggest thank you goes to my beloved family. Thank you for your unwavering belief in me, for always encouraging me in whatever I wanted to do and giving me the support I needed to achieve it. Thank you for always being there for me.

Declaration of Independence

Herewith I certify that I have prepared and written my thesis independently and that I have not used any sources and aids other than those indicated by me. I also declare that I have not submitted the dissertation in this or any other form to any other institution as a dissertation.

Place, Date Kerstin Wöltje

Selbstständigkeitserklärung

Hierdurch versichere ich, dass ich meine Dissertation selbstständig verfasst und keine anderen als die von mir angegebenen Quellen und Hilfsmittel verwendet habe. Die Dissertation ist in keinem früheren Promotionsverfahren angenommen oder abgelehnt worden.

Ort, Datum Kerstin Wöltje

Contents

Abbreviations

AAA	abdominal aortic aneurysm
acetyl-CoA	acetyl coenzyme A
ACS	acute coronary syndrome
AUC	area under the curve
AVM	arteriovenous malformation
ADP	adenosine diphosphate
AMP	adenosine monophosphate
AMPK	AMP-dependent kinase
ApoE	apolipoprotein E
ATP	adenosine triphosphate
BCA	brachiocephalic artery
BSA	bovine serum albumin
CAD	coronary heart disease
Cat. No.	catalogue number
CLTI	critical limb-threatening ischemia
$CreER^{T2}$	cre recombinase with a modified estrogen receptor binding domain
CVD	cardiovascular disease
CVI	chronic venous insufficiency
DAPI	4,6-diamidino-2-phenylindole
DMEM	Dulbecco's Modified Eagle's Medium
DMSO	dimethyl sulfoxide
DNA	deoxyribonucleic acid
DPBS	Dulbecco's phosphate buffered saline
DSB	double-strand break
DVT	deep vein thrombosis
ECAR	extracellular acidification rate
ECM	extracellular matrix
EGFP	enhanced green fluorescent protein
$FADH_2$	dihydroflavine-adenine dinucleotide
FCCP	carbonyl cyanide-p-trifluoromethoxyphenylhydrazone
FCS	fetal calf serum
flox	floxed

GABP	GA-binding protein
H3K4dime	histone 3 lysine 4 dimethylations
HAVSMC	human vascular smooth muscle cells
HEPES	4-(2-hydroxyethyl)-1-piperazineethanesulfonic acid
HDL	high density lipoprotein
KLF4	Kruppel-like factor 4
KO	knock-out
LDL	low density lipoprotein
LDLR	low density lipoprotein receptor
mG	membrane-targeted enhanced green fluorescent protein
miRNA	microRNA
MOMP	mitochondrial outer membrane permeabilization
mRNA	messenger RNA
mT	membrane-targeted tandem dimer Tomato
mtDNA	mitochondrial DNA
mVSMC	mouse vascular smooth muscle cells
NADH/NAD^+	nicotinamide adenine dinucleotide
NADPH/$NADP^+$	nicotinamide adenine dinucleotide phosphate
NM	non-muscle
OCR	oxygen consumption rate
OXPHOS	oxidative phosphorylation
PAD	peripheral artery disease
PASMC	pulmonary arterial smooth muscle cell
pCA	β-actin core promoter with a CMV enhancer
PCR	polymerase chain reaction
PDGF	platelet-derived growth factor
PDGF-BB	platelet-derived growth factor BB
qPCR	quantitative PCR
rDNA	ribosomal DNA
RNA	ribonucleic acid
ROS	reactive oxygen species
rRNA	ribosomal RNA
RT-qPCR	reverse transcription qPCR
scRNA-seq	single-cell RNA sequencing

SEM	standard error of mean
SEM cells	cells that express markers for stem cells, endothelial cells and monocyte/macrophages
shRNA	small hairpin RNA
siRNA	small interfering RNA
SIRT6	sirtuin 6
SIRT7	sirtuin 7
SM	smooth muscle
SMA	smooth muscle actin
SM-MHC/SMMHC	smooth muscle myosin heavy chain
SMC	smooth muscle cell
SRF	serum response factor
STAC	sirtuin-activating compounds
TAA	thoracic aortic aneurysm
TC	total cholesterol
TCA	tricarboxylic acid
TG	triglyceride(s)
TIM	translocases of the inner mitochondrial membrane
TOM	translocases of the outer mitochondrial membrane
tRNA	transfer-RNA
VDAC	voltage-dependent anion channels
VLDL	very low density lipoprotein
VSMC	vascular smooth muscle cell
WT	wildtype

A complete list of mentioned genes, receptors and transcription factors can be found in 6.1.

List of Figures

List of Tables

Summary

Unlike cardiac or skeletal muscle cells, vascular smooth muscle cells (VSMCs) retain a remarkable degree of plasticity. On environmental cues they can dedifferentiate from a quiescent contractile state towards phenotypes of increased proliferation and migration as well as secretory capacity and inflammation. This ability to transition between different phenotypes is a prerequisite for physiological vascular remodeling processes, but also plays a key role in the pathogenesis of virtually all vascular diseases. These vascular diseases, above all atherosclerosis resulting in myocardial infarction or stroke, are still the leading cause of death worldwide.

Based on the respective metabolic requirements of proliferating versus quiescent cells it was hypothesised that VSMCs undergo metabolic changes during dedifferentiation. Therefore, the aim of this study was to investigate the metabolic adaptions VSMCs exhibit during phenotypic transition and identify possible regulators thereof.

Utilising two *in vitro* models and one *in vivo* model for VSMC dedifferentiation, this study showed that dedifferentiated VSMCs shift their energy generation from mitochondrial respiration towards elevated glycolysis and lactate production, reminiscent of the Warburg effect observed in cancer cells. Dedifferentiated VSMCs also displayed reduced expression of genes involved in mitochondrial respiration, lower mitochondrial abundance and altered mitochondrial shape, indicating a strong association between mitochondrial homeostasis and VSMC plasticity.

The second objective of this study was to investigate whether intervention in VSMC metabolism would affect VSMC plasticity and vascular remodeling. Two known regulators of metabolism, Sirt6 and Sirt7, were chosen for their regulatory function in glucose and mitochondrial metabolism, respectively. The effects of VSMC specific knock-outs of Sirt6 and Sirt7 on VSMC dedifferentiation and proliferation were assessed *in vitro* and *in vivo*. Both sirtuins were expected to display atheroprotective functions. This could be confirmed for Sirt7 as the VSMC-specific knock-out of Sirt7 resulted in elevated neointima formation in a carotid artery ligation mouse model and increased plaque sizes in an $ApoE^{-/-}$ atherosclerosis mouse model. VSMC-specific knock-out of Sirt6 did not impact both these parameters. Contrary to expectations, the effects of the Sirt7 knock-out did not seem to be mediated by regulation of mitochondrial homeostasis. The atheroprotective role shown in this study, nevertheless renders Sirt7 an interesting target for the treatment of vascular diseases.

Zusammenfassung

Im Gegensatz zu Skelettmuskelzellen weisen vaskuläre glatte Muskelzellen (VSMCs) eine hohe Plastizität auf. Verschiedene Stimuli können eine Dedifferenzierung des ruhenden, kontraktilen Phänotyps hin zu Phänotypen induzieren, die sich durch erhöhte Proliferation, Migration, gesteigerte Sekretion oder stärkere inflammatorische Eigenschaften auszeichnen. Diese phänotypische Fluidität bildet die Grundlage für physiologischen Gefäßumbau, aber auch für pathophysiologische Gefäßumbauprozesse in vaskulären Erkrankungen. Vaskuläre Erkrankungen, insbesondere Atherosklerose und deren klinische Manifestationen wie Myokardinfarkte und Schlaganfälle, sind gegenwärtig die häufigste Todesursache weltweit.

Basierend auf den unterschiedlichen metabolischen Anforderungen von proliferierenden gegenüber ruhenden Zellen, wurde die Hypothese aufgestellt, dass sich der Metabolismus von VSMCs der phänotypischen Umstellung anpasst. Das Ziel dieser Arbeit war deshalb die metabolischen Veränderungen in VSMCs während des phänotypischen Wandels zu untersuchen und mögliche Regulatoren zu identifizieren.
Mit Hilfe zweier *in vitro* und eines *in vivo* Modells für VSMC-Dedifferenzierung, konnte in dieser Arbeit gezeigt werden, dass VSMCs ihre Energiequelle von verstärkter mitochondrialer Atmung hin zu verstärkter Glykolyse and Laktatproduktion verschieben, ein Prozess, der an den aus Krebszellen bekannten Warburg Effekt erinnert. Dedifferenzierte VSMCs zeigten außerdem eine reduzierte Expression von Genen der mitochondrialen Atmung, eine geringere Anzahl an Mitochondrien und eine veränderte mitochondriale Form, was auf eine starke Assoziation zwischen Mitochondrien und der Plastizität glatter Muskelzellen schließen lässt.

Das zweite Ziel dieser Arbeit war es zu untersuchen, ob eine Intervention in den Metabolismus die Plastizität glatter Muskelzellen und den pathologischen Gefäßumbau beeinflussen würde. Zwei bekannte Stoffwechselregulatoren, Sirt6 und Sirt7, wurden auf Grund ihrer Funktionen im Glukosestoffwechsel zum einen und im mitochondrialen Metabolismus zum anderen, ausgewählt. Der Effekt glattmuskelspezifischer Sirt6 und Sirt7 Knock-Outs wurde in *in vitro* und in *in vivo* Modellen untersucht, wobei für beide Sirtuine eine atheroprotektive Wirkung erwartet wurde.
Diese Annahme konnte für Sirt7 bestätigt werden, da der glattmuskelspezifische Knock-Out von Sirt7 zu einer gesteigerten Bildung von Neointima in einem Carotis-Ligatur Mausmodell und zu größeren Plaques in einem $ApoE^{-/-}$ Atherosklerose Mausmodell führte. Der glattmuskelspezifische Sirt6 Knock-Out zeigte in dieser Studie

keine Effekte in den genannten Modellen. Entgegen den Erwartungen schienen die Effekte des Sirt7 Knock-Outs nicht durch eine Regulation der Mitochondrien vermittelt zu werden. Die hier gezeigte atheroprotektive Funktion, bestätigt Sirt7 als vielversprechendes Zielmolekül in der Erforschung und Behandlung von vaskulären Erkrankungen.

1 Introduction

1.1 The vascular system

All tissues in the mammalian body are dependent on an effective transport of gases, liquids, nutrients and signaling molecules. Their transport throughout the body is accomplished by an extensive, highly branched and connected tubular network, the vascular system [1]. The vascular system is comprised of two branching networks, the blood vasculature and the lymphatic vasculature, which are responsible for maintaining homeostasis in the organism, stabilising body temperature and for innate and adaptive immunity [2, 3]. The lymphatic vasculature consists of blind-ending lymphatic vessels that transport the lymph, a protein-rich fluid, and immune cells from distal tissues into the venous branch of the blood circulation via the thoracic duct [1, 3].

In contrast to the lymphatic system, the blood vasculature is a closed network which is built up from arteries, capillaries and veins. Arteries carry blood away from the heart towards smaller arteries, called arterioles, and further into the capillaries. Pulmonary arteries transport blood with low oxygen content from the right ventricle to the lungs while systemic arteries transport oxygenated blood from the left ventricle to the body tissues. Capillaries surround body cells and tissues to deliver and absorb oxygen, carbon dioxide, nutrients and other substances while veins return blood back towards the heart. The inner linings of all these blood vessels are formed by vascular endothelial cells. Pericytes and vascular smooth muscle cells (VSMCs), summarised as mural or perivascular cells, wrap around the vessel walls to provide mechanical strength and vasomotor control of the circulation. Pericytes are contractile cells that cover the endothelium of capillaries and are important for maintaining endothelial homeostasis [4–6]. Vascular smooth muscle cells, together with connective elastic tissue, wrap around the larger vessels, namely arteries and veins, and give them the necessary flexibility for constriction and relaxation [7].

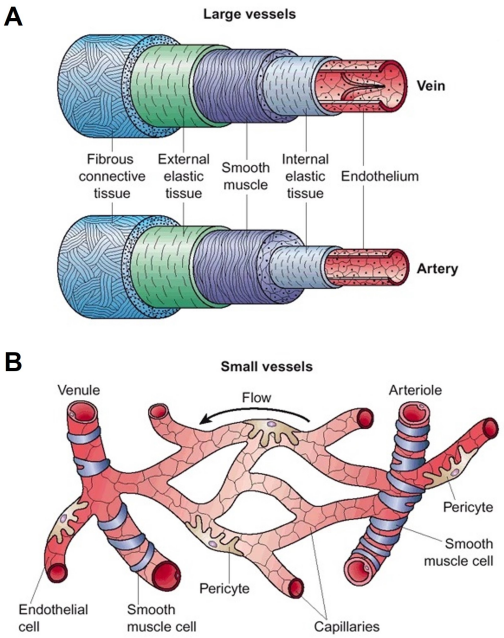

Figure 1 Types of blood vessels
Blood vessels show distinct wall compositions depending on their size. **A** Larger vessels are comprised of multiple layers, including cellular layers and layers consisting of extracellular materials. Arterial vessel walls are strong and elastic for withstanding and upkeeping blood pressure whereas veins have interior valves for preventing backflow of blood. **B** Capillaries, small vessels, are just comprised of the endothelium which is loosely covered by pericytes. Figure modified from [8].

The walls of larger vessels are comprised of three layers. The innermost layer, the tunica intima (also called tunica interna), consists of a monolayer of endothelial cells surrounded by a fine network of connective tissue and elastic fibers. The middle layer, the tunica media, is comprised of vascular smooth muscle cells which are oriented circular around the vascular lumen and form numerous layers. The tunica media provides support for the vessel and is able to adapt the vessel diameter to regulate blood flow and blood pressure. It is located between the tunica intima and tunica adventitia and is separated from these layers by the lamina elastica interna and the lamina elastica externa, respectively. The outermost layer, which attaches the vessel to the surrounding tissue, is the tunica externa or tunica adventitia. This layer is comprised of connective tissue which contains varying amounts of elastic and collagenous fibers, fibroblasts, nerves and, in bigger vessels, also small blood vessels supplying the vascular wall, called vasa vasorum. In addition, the tunica adventitia anchors blood vessels to the adjacent tissues.

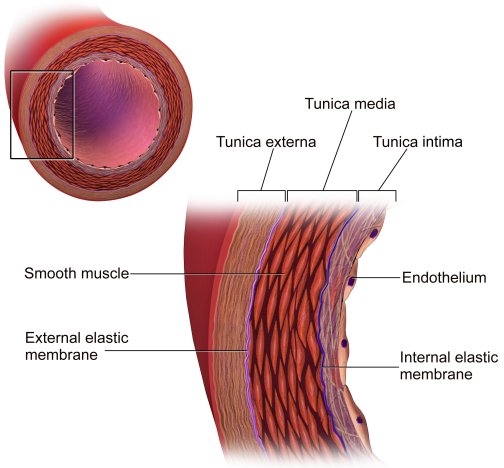

Figure 2 The structure of the arterial wall
Large arterial walls are divided into three layers, the tunica intima, tunica media and tunica externa (also tunica adventitia). The tunica intima consists of a monolayer of endothelial cells surrounded by a fine network of connective tissue and an internal elastic layer. Smooth muscle cells which are oriented circular around the vascular lumen in numerous layers form the tunica media while the tunica adventitia is comprised of connective tissue which contains varying amounts of elastic and collagenous fibers. Figure taken from [9].

The two most important cell types found in the vessel wall are endothelial cells and vascular smooth muscle cells (VSMCs). In the tunica intima, endothelial cells form a permeable barrier between vessels and tissue and control the exchange of cells, molecules and fluids between the bloodstream and the surrounding tissues. Among other processes, the endothelium is essential for the formation of new blood vessels, inflammatory processes and wound healing, forms the blood brain barrier and is involved in cardiovascular and other diseases. VSMCs form the tunica media and are critical to maintain structural integrity of the vessel. They regulate the vessel diameter by contracting and relaxing dynamically in response to vasoactive stimuli and participate in arterial wall remodeling. In contrast to skeletal muscle cells, they are not terminally differentiated but highly plastic (see 1.3.1).
Both endothelial cells and VSMCs, interact and communicate with each other as well as with the surrounding tissues through an extensive network of signaling pathways, small molecules, physical forces and other stimuli. Through this crosstalk as well as other factors, the vascular network is highly adaptive. Blood vessels can grow towards tissues in the body that are underoxygenated and can remodel according to changes in their surroundings. New blood vessel formation occurs through two distinct mechanisms, vasculogenesis and angiogenesis. Vasculogenesis describes

the formation and self-assembly of endothelial cells during embryonic development, whereas the growth and reorganisation of existing vessels during tissue repair, development and cancer is called angiogenesis [10, 11]. The initial formation of blood vessels is not terminal however, as developmental as well as other signaling pathways can initiate remodeling of artery walls during physiological and pathological adaptation to vessel wall injury, inflammation or chronic hypoxia. Moreover, vascular remodeling plays an important part in the pathophysiology of cardiovascular diseases, such as hypertension, restenosis, the development of aneurysms and, most prominently, atherosclerosis.

1.2 Vascular diseases

1.2.1 Overview

Cardiovascular diseases (CVDs) are pathological conditions affecting the heart and the blood vessels. Diseases specifically affecting the blood vessels are often summarised as vascular diseases. Among the most common vascular diseases are stroke, coronary artery disease (CAD), abdominal aortic aneurysm (AAA), restenosis and peripheral artery disease (PAD). Vascular diseases can affect all types of blood vessels manifesting in diseases like arteriovenous malformation (AVM), critical limb-threatening ischemia (CLTI), pulmonary embolism (blood clots), deep vein thrombosis (DVT) and chronic venous insufficiency (CVI). Cardiovascular diseases are the leading cause of death worldwide [12].

The underlying disease of major cardiovascular events, such as myocardial infarction, acute coronary syndrome (ACS) and stroke, is a chronic progressive inflammatory disease, atherosclerosis (see 1.2.2). Atherosclerosis can lead to the narrowing or blockage of vessels by plaques. Rupture of these plaques can then cause the mentioned cardiovascular events. For treatment, the artery can be cleared by angioplasty. For this, a catheter is guided through the aorta and into the coronary arteries of the heart where blocked arteries can be opened with a balloon positioned at the tip of the catheter. Angioplasty is often combined with the placement of a stent, a small wire mesh tube that serves as a scaffold that keeps the artery open [13]. The recurrence of a vessel blockage is called restenosis. One of the main underlying mechanisms of restenosis is increased and pathological proliferation of VSMCs. Therefore, most stents are now coated with drugs aiming for the inhibition of VSMC proliferation to keep the artery open after intervention [14].

Aortic aneurysms can occur in the ascending aorta (TAA) or abdominal aorta (AAA) and are defined as a progressive loss of the arterial wall's ability to withstand the wall tension generated by high intraluminal pressure. This results in a local dilation of the arterial wall which can lead to intramural or complete rupture. A common mechanism in the pathogenesis of aortic aneurysms is the degradation of extracellular matrix (ECM) by proteolytic enzymes. Usually, the insoluble fibrillary ECM which is synthesised by VSMCs should withstand the wall tension and ensure the integrity of the vessel [15].

1.2.2 Atherosclerosis

Atherosclerosis is a progressive, inflammatory disease of the large arteries and the primary cause of heart disease, like myocardial infarction and acute coronary syndrome (ACS), and stroke. It is characterised by the accumulation of lipids and fibrous material initiating a chronic inflammation of the vessel wall and the build-up of so-called plaques which may become unstable, rupture and thus cause thrombotic events which trigger cardiovascular events.

There are numerous risk factors for developing atherosclerosis which can be roughly divided into factors with a strong genetic component and environmental risk factors. Elevated levels of low density lipoprotein (LDL) or very low density lipoprotein (VLDL) are often due to genetic disposition and are among the highest risk factors for atherosclerosis. Similarly, reduced levels of high density lipoprotein (HDL) have been associated with the atherosclerosis development. High blood pressure and systemic inflammatory diseases as well as diabetes are also among risk factors. Not only genetic risk factors but also environmental factors can contribute to the development of atherosclerosis. Especially the lifestyle in highly developed westernised countries that often includes high-fat diets, smoking and little exercise gives rise to the development and progression of atherosclerosis [16].

Atherosclerotic lesions usually form at locations with a weakened endothelial barrier. One of the major physical forces acting on the endothelium is fluid shear stress. The endothelial cells in the vessel wall will alter their morphology according to the blood flow. Where the flow is laminar and uniform they will align in the direction of the flow whereas in areas with disturbed blood flow like in curvatures or areas of arterial branching, they will have no discrete orientation. Sites with disturbed blood flow are

preferential sites for atherosclerotic lesion formation, so-called predilection sites [17]. At predilection sites, low density lipoprotein (LDL) can diffuse passively through endothelial tight junctions and accumulate in the subendothelial matrix. Atherosclerosis may then develop from there. The LDL in the vessel wall will then get modified through oxidation, lipolysis, proteolysis and aggregation. The most significant LDL modification for the formation of early atherosclerotic lesions is lipid oxidation. Macrophages take up the oxidised LDL and turn into foam cells which will drive inflammation in the vessel wall. In contrast to LDL, of which high levels in the circulation will increase the risk for lipid accumulation in the subendothelium, HDL is strongly protective against atherosclerosis. HDL promotes the removal of excess cholesterol from peripheral tissues and inhibits lipoprotein oxidation, thereby reducing the inflammatory process [16]. When LDL is highly oxidised it can be taken up by macrophages to form foam cells. The oxidation is believed to stem from reactive oxygen species released by endothelial cells as well as the modification through several enzymes. The uptake of the highly oxidised LDL is mediated by a group of scavenger receptors.
In addition to the formation of foam cells, accumulation of oxidised LDL stimulates the endothelial cells to produce pro-inflammatory molecules such as adhesion molecules and growth factors like macrophage colony-stimulating factor (M-CSF). Through the adhesion molecules, monocytes can bind to the endothelium, first rolling along the surface and then adhering to selectins or intercellular adhesion molecule (ICAM). Further adhesion molecules, like integrins and vascular cell adhesion molecule 1 (VCAM-1), bind lymphocytes, enabling them to enter the subendothelial space (Figure 3). Other molecules such as monocyte chemotactic protein (MCP-1) and its receptor CCR2 also play a role in this process. M-CSF, released from endothelial cells, is a cytokine that stimulates the differentiation and proliferation of macrophages as well as the expression of some scavenger receptors. The formation of foam cells as well as the recruitment of monocytes and lymphocytes drive the inflammation in the vessel wall which is characteristic for the early stages of the atherosclerotic lesion.

During the development towards more advanced lesions, smooth muscle cells also start to play a role in the pathogenesis. Different stimuli initiate proliferation and migration of VSMCs from the tunica media into the atherosclerotic lesion, now forming an atherosclerotic plaque. There VSMCs produce large amounts of extracellular matrix. The accumulation of VSMCs and the VSMC-derived extracellular matrix come together to form a fibrous cap covering the inflamed lesion (Figure 3C). Historically, VSMCs in atherosclerotic lesions were perceived as plaque-stabilising and athero-

protective whereas macrophages are viewed as being destabilising. This perception, however, has had to be reassessed during the last years (see 1.3.2). It could be shown that VSMCs as well as macrophages can undergo an extensive phenotypic modification over the course of the disease which renders the definitive identification of these cells and their classification as one or the other extremely difficult. The role of phenotypic plasticity of VSMCs in this setting is further described in 1.3.3.

The major clinical consequences of atherosclerosis, such as myocardial infarction or stroke are not caused by the narrowing of the vessel but by thrombotic events. The occurrence of thrombi is initiated by the acute rupture or erosion of unstable plaques. Vulnerable or instable plaques usually have a thin or fragmented fibrous cap comprised of cells presumed to be derived from VSMCs, large numbers of inflammatory cells and cells presumed to be macrophages as well as a large necrotic core containing foam cells and lipids (Figure 3D) [18]. Factors fostering inflammation may influence thrombosis, as plaque rupture often occurs at the lesion edges where foam cells tend to accumulate. Tissue factor, a protein from the initiation of the coagulation cascade, is produced by endothelial cells and macrophages and is a major factor in the thrombogenicity of the lesion core.

Processes like calcification and neovascularisation which take place during formation of advanced lesions also influence plaque stability. Calcification of the intima is driven by pericyte-like cells that secrete a matrix scaffold that subsequently becomes calcified, similar to bone formation. Neovascularisation describes the growth of small vessels from the media which might provide a further entry point for inflammatory cells.

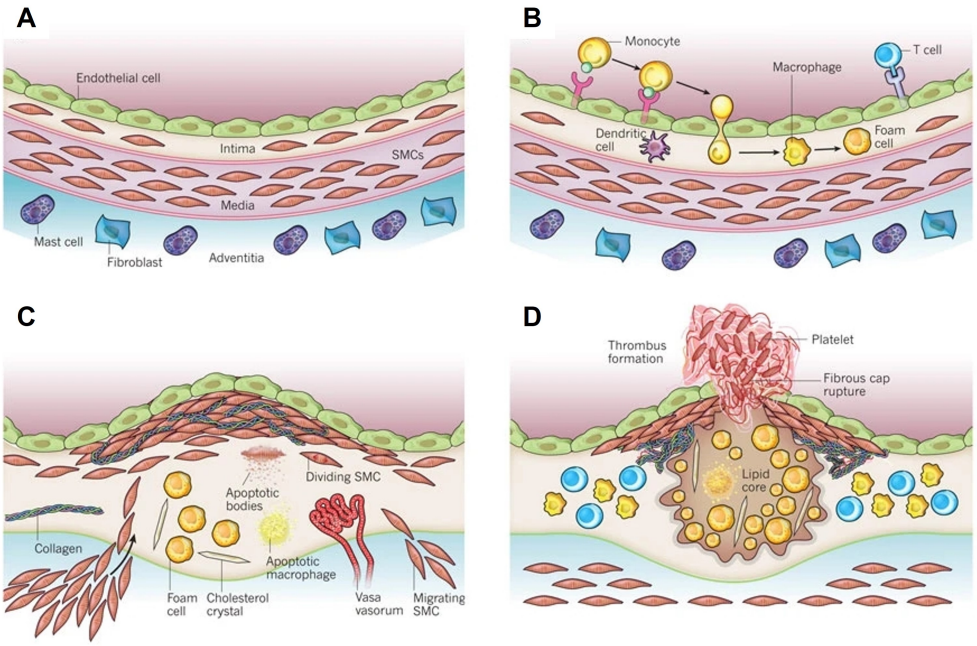

Figure 3 Development and progression of atherosclerosis
Shown are processes and cell changes during atherosclerosis progression in human arteries.
A The healthy artery is comprised of three layers, the tunica intima, tunica media and tunica adventitia. The tunica intima contains the endothelium surrounded by connective tissue and an internal elastic layer. The human intima also contains resident smooth muscle cells. The tunica media contains SMCs embedded in extracellular matrix. The outer layer of human arteries, the tunica adventitia, is comprised of connective tissue which contains elastic and collagenous fibers, nerve endings and micro vessels. **B** Atherosclerotic lesions usually form at locations with a weakened endothelial barrier. Blood leukocytes adhere to the activated endothelial monolayer and can migrate into the intima. Low density lipoprotein (LDL) diffuses passively through endothelial tight junctions and accumulates in the subendothelial matrix where it is oxidised. The recruited monocytes mature into macrophages which take up the oxidised LDL and turn into foam cells which will drive inflammation in the vessel wall. **C** During lesion progression SMCs in the media as well as resident intimal SMCs start proliferating and medial SMCs migrate from the media into the intima. SMCs undergo phenotypic modulation and synthesise and excrete large amounts of extracellular matrix components. SMCs as well as plaque macrophages can die in advancing lesions, some by apoptosis. If extracellular lipid accumulates in the central region of a plaque, the so-called lipid or necrotic core is formed. Advancing plaques also contain cholesterol crystals and micro vessels. **D** If the fibrous cap, formed by SMCs, fractures, blood coagulation and tissue factors from the plaque's interior form a thrombus which can extend into the vessel lumen where it can impede blood flow. If the thrombus breaks free from the plaque and enters the blood circulation, this can lead to heart attacks and strokes, the ultimate complications of atherosclerosis. Figure modified from [19].

1.2.3 Treatment of Atherosclerosis

One of the first aims during atherosclerosis therapy is the reduction of atherogenic risk factors through adaption of lifestyle. Dietary changes, physical activity and abstaining from smoking can largely benefit patients as well as improve their overall health [20, 21].

When the modification of environmental factors is not sufficient to prevent the disease, control of lipoprotein levels is essential. Hypercholesterolemia is one of the main triggers of atherosclerosis and lowering of LDL cholesterol levels remains, to date, the standard medical prevention and treatment of atherosclerotic disease [21]. Pharmacological reduction of LDL cholesterol levels is achieved by statins. Statins inhibit the endogenous cholesterol synthesis in the liver which leads to a reduction in intracellular cholesterol concentration. This triggers an increased surface expression of low density lipoprotein receptor (LDLR) on the cells, which results in increased uptake of LDL cholesterol from the blood stream. This lowers the plasma concentration of LDL cholesterol and other apoB-containing lipoproteins, including triglyceride (TG)-rich particles in the circulation [22]. The lowering of atherogenic lipoproteins by statins and the reduction of blood pressure through anti-hypertensive agents, dramatically decreased clinical events and mortality from atherosclerosis.

However, while conventional atherosclerosis treatment with statins and the control of blood pressure reduces the risk of cardiovascular events, heart disease and stroke are still the most common cause of death in westernised societies [21]. Therefore, new therapies are still needed and have been investigated over the course of the past decade. Among them are anti-inflammatory or inflammation-resolving therapies, agents that block the disease at the level of the vessel wall or raising of the anti-atherogenic HDL.

1.2.4 Mouse models of Atherosclerosis

The most widely used mouse models for atherosclerosis are apolipoprotein E knockout ($ApoE^{-/-}$) mice and low density lipoprotein receptor deficient mice ($Ldlr^{-/-}$), both of which develop hypercholesterolemia. Apolipoprotein E is synthesised by the liver and several peripheral tissues and cell types, including macrophages. It has various functions, like efficient hepatic uptake of lipoproteins, stimulation of cholesterol efflux from macrophage foam cells in the atherosclerotic lesion, and the regulation of immune and inflammatory responses [23]. ApoE deficient mice display poor lipoprotein clearance which leads to accumulation of cholesterol particles in the blood,

promoting the development of atherosclerotic plaques. Both ApoE deficient and LDLR deficient mice are frequently used to study the initiation, pathophysiology and progression of atherosclerosis [24].

1.3 Vascular smooth muscle cells

Vascular smooth muscle cells are highly specialised cells in the vasculature of adult humans and animals. Their main function is contraction which enables the regulation of blood vessel tone and diameter, both determining blood pressure and blood flow distribution. In the adult vessel VSMCs characteristically display very low proliferation and a very low synthetic activity. They also express a set of contractile proteins and signaling molecules distinguishable from other cell types. Another major difference to skeletal and cardiac muscle lies in the VSMCs' ability to undergo profound but reversible phenotypic changes in response to environmental cues, a characteristic that is called VSMC plasticity [25–27].

The quiescent, non-proliferative, contractile phenotype is characterised by an abundance of contractile fibres containing VSMC specific contractile proteins such as α-actin and the SM-1 and SM-2 myosin heavy chain isoforms as well as other proteins of the contractile apparatus. Although they share these characteristics, quiescent VSMCs are still highly heterogenous. The vessel wall contains contractile cells, synthetic cells specialised on extracellular matrix production and progenitor cells which are the source of VSMCs accumulating in the intima during vascular remodeling, such as neointimal hyperplasia and arteriosclerosis [28–30]. Upon different stimuli during vascular remodeling as well as during the onset and development of vascular diseases, VSMCs undergo phenotypic modulation, often referred to as phenotypic switching, towards synthetic and proliferative phenotypes which are often summarised as dedifferentiated phenotype.

During different stages of differentiation, VSMCs express a variety of differentiation markers. These markers can be divided into early, mid-term and late according to their appearance during embryonic development [27]. Most prominent early markers are smooth muscle (SM) α-actin, myocardin and SM22-α [31–33]. SM α-actin is the earliest known VSMC differentiation marker and is frequently used as a VSMC identifying marker. However, the expression of SM α-actin can be misleading as it is not exclusive to VSMCs but can also be expressed by other cell types [34]. Together with other proteins like calponin, SM α-actin is located in thin filaments

in VSMCs and contributes to the cell's cytoskeleton and contractility. Another early smooth muscle differentiation marker is SM22-α which is an actin-binding protein that is also contributing to the organisation of the actin cytoskeleton and enhances the contractility and mobility of VSMCs [35].
Arguably the most important of the early differentiation markers is myocardin. Myocardin is a transcriptional coactivator of serum response factor (SRF) and a master regulator of smooth muscle marker gene expression. Most smooth muscle marker genes contain essential binding sites for SRF. However, binding of SRF alone is not sufficient for expression of VSMC specific genes. Here, myocardin is needed as a transcriptional coactivator of SRF. Together the myocardin-SRF complex induces, among others, expression of SM α-actin, SM22-α, calponin and smooth muscle myosin heavy chain (SM-MHC). As myocardin is essential for VSMC differentiation, mice lacking it will die during embryogenesis from a lack of differentiated VSMCs. A reduction of myocardin, for example through proteasomal degradation, will promote phenotypic transition of VSMCs toward the synthetic and proliferative phenotype [36–38].

Early to mid-term differentiation markers include caldesmon and SM-calponin, both cytoskeletal proteins. Caldesmon occurs in two isoforms, high molecular weight caldesmon (h-caldesmon) and low molecular weight caldesmon (l-caldesmon). While h-caldesmon is found in adult and fully differentiated smooth muscle cells, l-caldesmon is present in non-muscle cells and in dedifferentiated VSMCs. Smooth muscle caldesmon interacts with actin, tropomyosin, myosin and calmodulin and plays a role in Ca^{2+}-dependent inhibition of smooth muscle contraction [39, 40].
Calponin is a regulatory protein associated with actin filaments. It occurs in three isoforms, all of which are expressed in smooth muscle cells but also in other cell types. Calponin 1-3 inhibit actin-activated myosin ATPase and stabilise the actin cytoskeleton. They are also involved in smooth muscle contractility and in processes in the cytoskeleton during embryogenesis, myogenesis and neuronal plasticity. In addition, they have tumor suppressing effects (calponin 1 and 2) and can serve as tumor markers in the serum of patients (calponin 2) [41–43].

Finally, late markers of VSMC differentiation include desmin, meta-vinculin, SM-1 and SM-2 isoforms of myosin heavy chain and smoothelin [31, 34, 44]. Desmin is a muscle specific protein and, together with vimentin, forms intermediate filaments in VSMCs. It is considered to be more prominent towards a more advanced differentiation status.

Meta-vinculin is a high-molecular form of vinculin, both of which are membrane-cytoskeletal proteins co-localised in focal adhesion plaques. There they are involved in the linkage of integrin adhesion receptors to the actin cytoskeleton. Meta-vinculin is considered to be a marker for well differentiated VSMCs and expression levels drop upon phenotypic modulation towards the dedifferentiated, synthetic, proliferative phenotype. This has been shown in human coronary arteries affected by arteriosclerosis or during cultivation of VSMCs [45, 46].
The most widely recognised marker for VSMC differentiation is smooth muscle myosin heavy chain (SM-MHC). It is located in thick filaments and occurs in two isoforms, SM-1 and SM-2 MHC whose expression is highly variable in VSMCs [31]. In addition to SM-1 and SM-2 myosin heavy chain, VSMCs express the non-muscle (NM) isoform of MHC which can also be found in other cell types like fibroblasts and macrophages [47]. During phenotypic modulation towards the dedifferentiated phenotype, e.g. during vascular disease, vascular surgery and cultivation of VSMCs, the expression of both SM isoforms decreases profoundly [31, 47, 48].
The last differentiation marker discussed here is smoothelin. Smoothelin (SMTN) is a cytoskeletal protein and occurs as SMTN-A, SMTN-B and SMTN-like protein (SMTNL1). All isoforms can be found in VSMCs where they are associated with the contractile apparatus, help maintain the contractile phenotype and contribute to vascular adaptions in physiological and pathophysiological processes [49, 50].

1.3.1 VSMC phenotypic plasticity in vascular remodeling and disease

Cells expressing high levels of the differentiation markers listed above are generally described as displaying a differentiated and mature phenotype. However, in contrast to other cell types, VSMCs are not terminally differentiated but retain profound plasticity. Upon environmental cues and extracellular signals VSMCs undergo phenotypic modulation, transitioning from the contractile, differentiated to a synthetic phenotype. This process is also often called phenotypic switching. Phenotypic modulation is characterised by a loss of contractile filaments, decreased expression of VSMC differentiation marker genes and is generally associated with increased smooth muscle cell proliferation and migration. It is referred to as the synthetic phenotype as these cells then typically express large amounts of extracellular matrix [18, 25, 27, 51].

Phenotypically modified VSMCs play a major role in vascular remodeling and in various vascular diseases. Pathological processes involving VSMCs in vascular diseases are intimal thickening, formation of atherosclerotic plaques, thickening

of the blood vessel wall during hypertension, stenosis or full obliteration of the vascular lumen and restenosis after intervention [18, 52, 53]. Phenotypic modulation also occurs when VSMCs are cultivated *in vitro*, particularly under conventional static conditions and in standard serum-supplemented media [27, 31, 54]. During phenotypic switching, the markers of VSMC differentiation are gradually lost [55, 56]. The first markers to disappear are the late markers of differentiation that were defined earlier. Upon an injury of the vessel wall for example, as occurring in atherosclerosis or restenosis, smoothelin-B is the first marker to disappear [7].

1.3.2 The role of VSMCs in atherosclerosis

The loss of VSMC marker genes during phenotypic modulation has made the investigation of VSMCs in vascular diseases difficult as they are increasingly harder to identify once the dedifferentiation process has started. This is also true for the investigation of the pathology of atherosclerosis and the role of VSMCs therein. VSMC phenotypic plasticity in atherosclerosis has been studied extensively but is still not completely understood [57]. One of the major obstacles in the investigation of the role of VSMC in atherosclerosis is the loss of VSMC marker genes on the one hand and the ability of phenotypically modulated VSMCs to express marker genes of other cell types like macrophages, on the other. In the past decade, this phenotypic transitioning during atherogenesis has been shifted into the focus of atherosclerosis research again through smooth muscle cell specific lineage tracing studies. In these studies, VSMCs are permanently labelled and stay identifiable by expression of a reporter gene like fluorescent proteins or β-galactosidase. All progeny of thus labelled VSMCs will continue to express the reporter gene and can therefore be traced, even if the cells loose expression of typical VSMC marker genes. Taking the results of these studies into account, former assumptions about the composition of atherosclerotic lesions must be re-evaluated. It seems that a major fraction of cells in atherosclerotic plaques have previously not been recognized as VSMC-derived cells or have been identified as another cell type.

Fate of VSMCs in the atherosclerotic lesion Utilizing lineage tracing models, it was shown, for instance, that over 80% of VSMC-derived cells within advanced plaques of ApoE$^{-/-}$ mice expressed genes like CD68, Lgals3/Mac2 and CD11b, which are commonly thought of as macrophage markers [58–60]. Similarly, in humans it could be shown that almost 20% of CD68 positive cells in advanced coronary plaques were actually of smooth muscle cell and not of myeloid origin. These results further

supported the widespread theory of VSMC-to-macrophage transdifferentiation during atherogenesis. However, the precise fate of VSMCs in the atherosclerotic lesion and the nature of their phenotypic states, are still controversial.

With a combined lineage tracing and scRNA-seq experiment, Alencar et al. recently identified several clusters of VSMCs in late-stage atherosclerotic lesions [61]. These included clusters characterised by inflammatory markers, stem-like markers, production of ECM and osteogenic markers, demonstrating the immense phenotypic diversity and complexity of VSMC dedifferentiation and transition during atherosclerosis. Furthermore, they identified a transitional VSMC population exhibiting Galectin 3 (Lgals3) expression. They called these cells pioneer cells. Despite their expression of Lgals3 which is typically thought of as a macrophage marker however, Alencar et al. postulated that these cells did not acquire a macrophage cellular state. They rather generated inflammatory, extracellular matrix and osteogenic cell states. Alencar et al. therefore proposed, that contractile VSMCs dedifferentiate towards transitional pioneer cells which go on towards non-macrophage cellular states which could also give rise to osteogenic cell states, usually seen as being plaque destabilising [61].
In line with these results Pan et al. identified a similar transitional cell state in atherosclerotic lesions which displayed expression of markers for stem cells, endothelial cells and monocyte/macrophages. Derived from these characteristics the cells were called SEM cells. Like pioneer cells they showed Lgals3 expression and were multipotent [62].

While the results from Pan et al.'s study as well as earlier findings suggest the transition of VSMC to macrophage like cell states, studies from Alencar et al. and Wirka et al. showed little evidence for the presence of VSMC-derived macrophage like cells in atherosclerotic lesions [61, 63]. Therefore, the theory of VSMC transdifferentiation to macrophages in the atherosclerotic lesion is still controversial and requires further research.

Fate of macrophages in the atherosclerotic lesion This is further complicated by the fact that until the usage of lineage tracing, cells that were not VSMC-derived were still identified as such due to their expression of SMC marker genes. It was shown that myeloid derived cells in lesions of ApoE knock-out mice were able to express early markers of SMCs, like SM-actin (Acta2) and SM22-α but not late stage markers such as MHC (Myh11) [64]. This is supported by studies of human coronary artery

lesions where myeloid cells did not acquire the SMC-specific MYH11 H3K4dime epigenetic signature [58]. There are also cells in atherosclerotic lesions that express both, markers perceived as VSMC-specific and markers perceived as specific for macrophages. For example, in a study by Allahverdian et al., 40% of foam cells within advanced human coronary artery lesions expressed both Acta2 and CD68 [65].
Taken together, these relatively new findings indicate that previous conceptions about the function of VSMCs and macrophages in atherosclerotic lesions may have been incorrect and need re-evaluation.

Origin of VSMCs in the vessel wall Lineage tracing has also enabled more precise investigation of where VSMC-like cells in the atherosclerotic lesion originate. It has been shown that even mature MYH11 expressing VSMCs from the vessel media are not terminally differentiated but can perform phenotypic transitioning in culture, after vascular injury and in atherosclerosis [58–60, 66]. The question remains, however, whether there is a number of VSMCs in the media predetermined to progress to the transitional cell state in the growing intima or if the selection is random. Although all contractile VSMCs seem to have the ability of phenotypic transition, studies indicate that not all cells from the media switch but that VSMCs in the plaque originate from specific progenitor cells in the vessel wall [67]. This concept is not new as healthy vessel walls show areas with monoclonal VSMCs formed by the expansion of progenitor cells during vascular development. Recent studies also support the theory of some VSMCs being predetermined for fate switching towards VSMC derived transitional cells in vascular disease [57, 68, 69]. Findings of monoclonality of VSMCs within clusters in atherosclerotic plaques further supports the theory of a subpopulation of MYH11 positive progenitor cells in the vessel media [18]. Whether transitional pioneer cells in the atherosclerotic lesion then continue to expand clonally, however, has not been fully elucidated yet.

VSMC proliferation, migration, apoptosis and senescence in atherosclerosis The role of VSMCs and the processes that they undergo in the atherosclerotic plaque are highly diverse and have recently been revisited due to the availability of new tools like lineage tracing. Generally, VSMCs are often associated with the stability of atherosclerotic plaques which depends on the thickness and integrity of the fibrous cap and the degree of cap inflammation. The population of VSMCs within the plaque is formed through a balance of cell proliferation and migration versus cell death and cell senescence. Cell death which is accompanied by the breakdown of collagen and

other ECM components promotes thinning of the fibrous cap and the vulnerability of the plaque. A major change that switching VSMCs undergo is their proliferative activity. In the healthy vessel VSMCs are barely proliferating and have a very slow turnover. Upon vascular injury and during early atherosclerosis however, VSMC proliferation increases drastically [70]. This effect ablates in advanced human atherosclerotic plaques and also in aged vessels where VSMC proliferation drops again. Fittingly, the expression pattern of cell cycle regulators in human plaque VSMCs and in normal human VSMCs undergoing replicative senescence are similar [18]. A decrease in proliferation upon aging was not found in rodents however, as aged VSMCs showed increased proliferation compared to younger animals [71–73]. As plaque stability is dependent on VSMCs thickening the fibrous cap, it might be beneficial to enhance VSMC proliferation in advanced lesions. Migration of VSMCs to the mature human plaque on the other hand is not very well understood as it is difficult to investigate due to the loss of marker genes and because human arteries also contain intimal VSMCs. In rodents however, VSMCs in lesions must arise from the media as healthy vessels do not contain intimal VSMCs.
Increased proliferation and migration of VSMCs into the plaque are opposed by cell death, mainly apoptosis. Apoptotic rate is low during the early stages but increases as the lesions develop [18, 74, 75]. Apoptosis occurs in the necrotic core and the fibrous cap and affects primarily VSMCs and macrophages. Apoptosis of VSMCs in atherosclerosis promotes plaque vulnerability as it can lead to a thinner fibrous cap, an enlarged necrotic core and macrophage infiltration into the cap [76]. Usually VSMC apoptosis, which also occurs in vascular aging and remodeling, is not associated with high inflammation. In atherosclerosis however, apoptosis of VSMCs is accompanied by and promotes inflammatory processes. This is in part due to inefficient clearance of apoptotic VSMCs and the release of cytokines by VSMCs surrounding apoptotic cells [18]. Phagocytosis is also delayed in hyperlipidemia and VSMCs that have undergone phenotypic switching towards macrophage like cells display defective phagocytosis [77].

As was touched on earlier, cell senescence also plays a role in the atherosclerotic lesion. Senescent cells have irreversibly lost their ability to divide. In replicative senescence, cells have exhausted their proliferative potential over time which is a characteristic of aging. It is accompanied by an induction of DNA damage due to a critical shortening of the telomers at chromosomal ends. Senescence can also be triggered prematurely through external stimuli which is then called stress-induced

senescence. It can be induced by oxidising agents and radiation and in contrast to replicative senescence is not associated with telomere shortening. Shortened telomers have been found in plaque VSMCs and endothelial cells compared to the normal vessel wall [78, 79]. An increase in the senescence associated marker, β-galactosidase, was observed in aged vessels and atherosclerotic lesions [78]. Moreover, aged VSMCs show upregulation of chemokines, adhesion molecules and innate immune receptors, promoting the inflammatory environment in the plaque [80]. Like other cell types, VSMCs will transition into a senescence-associated secretory phenotype upon aging [18].

Taken together, VSMC proliferation, migration, apoptosis and senescence form a complex cellular and extracellular environment which is embedded in the complex structure of the atherosclerotic plaque. While VSMC proliferation is no primary driver of plaque formation and is possibly even beneficial for plaque stability, VSMC apoptosis and senescence both promote atherogenesis and plaque vulnerability. Therefore, it would be desirable for new therapies to directly target and manipulate the different phenotypic transitions of VSMCs in atherosclerotic lesions to promote beneficial changes of phenotypes and inhibit detrimental ones to overall reduce plaque burden and increase plaque stability. For this however, the mechanisms of VSMC phenotypic switching as well as environmental cues need to be found and better understood.

1.3.3 Regulation of VSMC phenotypic transition in atherosclerosis

The mechanisms of VSMC phenotypic transition in atherosclerosis and other vascular diseases have been and still are extensively investigated and various influencing factors have been identified. One major regulator of VSMC marker gene expression and consequently VSMC phenotype is the myocardin-serum response factor regulatory module. As described in 1.3, myocardin via SRF is a major regulator of activating and repressing expression of most VSMC contractile genes. ApoE$^{-/-}$ mice with a heterozygous knock-out of myocardin developed increased atherosclerosis with heightened accumulation of macrophages or macrophage-like cells compared to the homozygous control. Consequently, gain of myocardin function inhibited inflammatory pathways and limited macrophage accumulation [37].

Tying into the myocardin-SRF axis, the transcription and stem cell factor Kruppel-like factor 4 (KLF4) is an important regulator of phenotypic plasticity. It has been found to be required in phenotypic transition of cultured VSMCs induced by different stimuli, such as platelet-derived growth factor BB (PDGF-BB), oxidised phospholipids and

interleukin-1β [81–85]. Transcriptional repression of VSMC markers in cells treated with these stimuli was dependent on the binding of KLF4 to a highly conserved G/C repressor element found in the promotors of many SMC maker genes. KLF4 also inhibits myocardin expression and therefore myocardin dependent gene activation of VSMC markers. Its expression is increased within atherosclerotic lesions of ApoE$^{-/-}$ mice as well as after vascular injury [18, 58, 86, 87]. VSMC specific knock-out of KLF4 reduced the number of VSMC derived macrophage-like cells, reduced plaque size but increased fibrous cap area in atherosclerosis. This indicates that KLF4 regulates the phenotypic transition towards macrophage-like cells [86, 88]. Additionally, in a recent study, Alencar et al. found Klf4 to impact the transitioning of VSMCs to the pioneer cell state they postulated in the respective study [61]. Moreover, in a ligation injury model, loss of KLF4 delayed phenotypic switching, supporting the assumption that KLF4 is required for the process [87].
Given the importance of the myocardin-SRF dependent activation or repression of VSMC markers, the accessibility of chromatin for the myocardin-SRF complex is also of importance for VSMC phenotypic modulation. Chromatin accessibility is regulated by epigenetic modifications. Epigenetic modifications are heritable through mitosis and often play a crucial role in cell differentiation and cell lineage determination. During VSMC differentiation, promoter regions of SMC marker genes acquire epigenetic modifications including histone acetylations and histone 3 lysine 4 dimethylations (H3K4dime). These modifications are believed to facilitate SRF/myocardin binding to CArG-containing regions by inducing chromatin relaxation. The H3K4dime is specific to smooth muscle cells and has been shown to persist even when VSMCs undergo phenotypic switching *in vitro* and *in vivo*, making it one of the most reliable markers of SMC origin detected so far [51, 59, 89].

Besides myocardin and KLF4, there are several other transcription factors that can regulate VSMC phenotypic switching. The transcription factor Oct4, for example, has been shown to regulate VSMC phenotypic transition and plays an important role in the pathogenesis of atherosclerosis [61, 90].
In their study giving rise to the VSMC to SEM cell transition theory mentioned earlier (see 1.3.2), Pan et al. identified cellular retinoic acid-binding protein 2 as a potential master regulator of the VSMC to SEM cell transition. Retinoids had been shown before to impact VSMC phenotype by inhibiting VSMC growth and migration [91]. In the study by Pan et al. all-trans retinoic acid inhibited the VSMC to SEM transition *in vitro* and *in vivo*. They also showed that all-trans retinoic acid reduced the intimal

area in atherosclerotic lesions [62].
Another possible regulator of VSMC phenotypes was proposed by Wirka et al. They showed that transcription factor 21 (Tcf21) reduced VSMC phenotypic modulation and resulted in less fibromyocytes at the fibrous cap [57, 63].

Evidence has accumulated that VSMC phenotypic plasticity is also regulated by non-coding RNAs, including microRNAs (miRNA). MiRNAs are small single-stranded non-coding RNAs that bind to specific messenger RNAs (mRNAs), either repressing their translation or promoting mRNA degradation, thereby repressing protein expression. MiRNAs that promote the contractile VSMC phenotype are miR-1 and miR-143/145. miR-1 expression is induced by myocardin and targets KLF4 which in turn inhibits myocardin and induced VSMC transition towards the macrophage-like phenotype [92]. miR-143/145 is driven by the myocardin coactivator SRF and, similarly to miR-1, sustains VSMC differentiation. Without miR-143/145, VSMCs are locked in the synthetic phenotype and decreased miR-143/145 expression was found in atherosclerotic plaques. miR-143/145 can target KLF4, ETS Like-1 protein (Elk1) and angiotensin-converting enzyme (Ace). *In vitro* cholesterol treatment induces VSMC transition towards the macrophage-like phenotype which was mediated by miR-143/145 [93–95]. In contrast, there are miRNAs that promote the synthetic phenotype. miR-221 and miR-222 both induce VSMC proliferation and can trigger a transition towards an osteogenic phenotype which is characterised by high calcification activity [96, 97]. MiR-24 and miR-26a play a role in PDGF-BB driven dedifferentiation of VSMCs. PDGF-BB has been shown to induce phenotypic switching in VSMCs *in vitro* by suppressing SMC marker gene expression and promoting proliferation and migration [98, 99]. It is not yet fully understood whether PDGF-BB is as potent a regulator of VSMC differentiation *in vivo* as was shown *in vitro* [99].

During atherosclerosis, there are some more factors that can influence VSMC phenotypic plasticity. One factor thought to be driving VSMC transition to macrophage-like cells might be the accumulation of lipids in the plaque. It was shown that cultured VSMCs that were exposed to cholesterol suppressed expression of VSMC marker genes and elevated expression of macrophage markers. Cholesterol treatment also increased expression of proinflammatory genes and induced phagocytic activity. All of these phenotypic adjustments were KLF4 dependent [58, 88, 100]. However, these macrophage-like VSMCs still differ from classical macrophages in their gene expression and display reduced ability of phagocytosis. Reduced phagocytosis is a

characteristic of advanced atherosclerotic lesions and promotes the formation of a necrotic core. Therefore, the reduced ability to clear lipids, dying cells and necrotic debris of VSMCs transitioned to macrophage-like cells may worsen the clearance and promote inflammation in the plaque [77].
In addition to the accumulation of lipids, the environment surrounding VSMCs can also impact phenotypic plasticity. The interplay between VSMCs and the extracellular matrix is complex. Usually, VSMCs synthesise and are embedded in an ECM which is assumed to suppress phenotypic switching. However, breakdown of ECM, for example by matrix metalloproteinases released by both, macrophages and VSMCs themselves, promotes phenotypic modulation as well as proliferation and migration of cells [18, 101, 102]. As with phenotypic modulation, ECM synthesis can be both beneficial and detrimental. Fibronectin deposition at sites of early lesions, for instance, promotes atherosclerosis but also enables the formation of the protective fibrous cap [103].

Although the regulation of VSMC phenotypic modulation has been studied intensively, many aspects remain that are still not understood. Several factors influencing the dedifferentiated transitional VSMC have been identified but the regulation of these factors themselves is largely unknown. It is also still unclear how the fate of VSMCs in the atherosclerotic lesion is decided and which factors will lead to the transition towards the respective phenotypes, like inflammatory, macrophage-like or osteogenic phenotype. Therefore, the molecular signatures of VSMC derived cell types in atherosclerotic lesions need to be further investigated. Finally, although evidence suggests that VSMCs can transition towards a macrophage-like phenotype, the question whether they can also acquire macrophage-like functions, still remains unanswered.

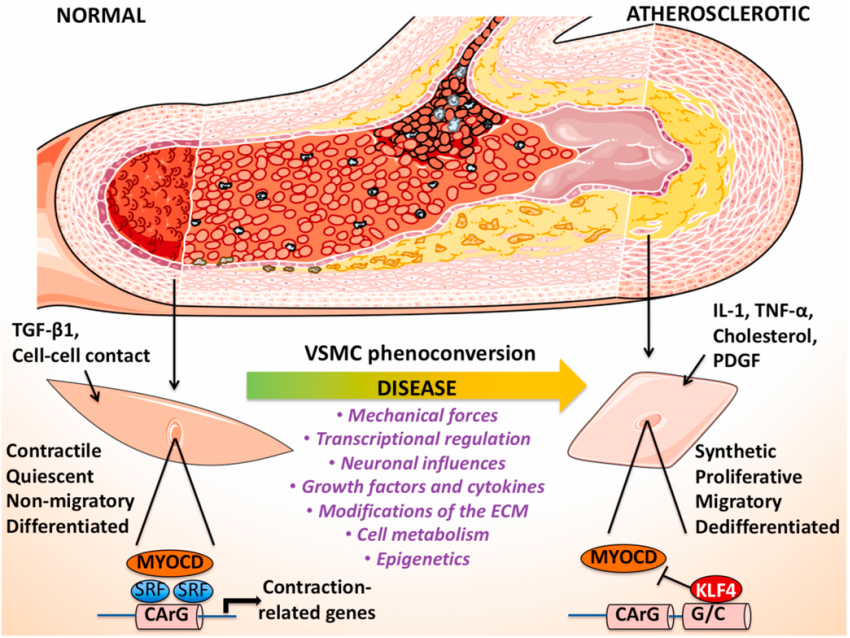

Figure 4 Phenotypic plasticity of vascular smooth muscle cells
Phenotypic plasticity of VSMCs is characterised by a transition from the so-called differentiated, contractile, quiescent, non-migratory phenotype towards synthetic, inflammatory, proliferative or migratory phenotypes, often summarised as dedifferentiated phenotype. Phenotypic transition is induced and regulated by a variety of factors, including mechanical forces, transcription factors, neuronal influences, growth factors and cytokines, modifications in the ECM, cell metabolism and epigenetics. The myocardin-SRF complex is the main driver of VSMC marker gene expression. These marker genes are mainly contraction-related genes. Tying into the myocardin-SRF axis, the transcription and stem cell factor Kruppel-like factor 4 (KLF4) is an important regulator of phenotypic plasticity. It inhibits myocardin expression and therefore myocardin-dependent gene activation of VSMC markers. Figure taken from [104].

1.4 Cell metabolism

Cell metabolism has increasingly moved into focus as a key regulator of cell function and fate. It has been shown, for instance, that a cell's metabolism can determine its differentiation status and vice versa.

1.4.1 Overview

Cell metabolism is defined as the entirety of biochemical reactions involved in biomolecular synthesis (anabolism), maintenance, and breakdown (catabolism). The sum of these processes defines the energetic status of the cell. Involved are basic cellular building blocks such as lipids, amino acids, carbohydrates and nucleotides, and numerous enzymes and cofactors that participate in metabolic reactions. The uptake of nutrients provides these cellular building blocks and thus influences metabolic reactions in the cell.

Lipids, or fats, are a heterogenous group of molecules that provide energy for cell functions and serve as building blocks for cellular structures such as membranes and cell organelles. Lipids can be stored long-term and can be mobilised again during times of nutritional or energetic deficiency. Important lipids taken up from food are triglycerides and cholesterol, both of which are essential for organismal function but can also play a major role in the onset of vascular diseases like atherosclerosis.
A common component of complex lipids are fatty acids which are both a source and storage unit of energy in the cell. They play a major role in cellular signaling and can thus influence cellular function. Fatty acids differ in chain length and the number and position of double bonds. These structural variations result in functional differences and different impacts upon cell and tissue responses and consequently metabolism. Fatty acids are synthesised from acetyl coenzyme A (acetyl-CoA) and nicotinamide adenine dinucleotide phosphate (NADPH), a process catalysed by fatty acid synthase. Acetyl-CoA is generated during glycolysis, the breakdown of glucose which also provides glycerol. Together, fatty acids and glycerol form triglycerides as well as phospholipids. Phospholipids serve many functions within the cell and are the major building block of cell membranes. Fatty acid β-oxidation, the process of fatty acid breakdown into their acetyl-CoA subunits, takes place in the mitochondria where the acetyl-CoA is shuttled into the citric acid cycle.

Most of the energy needed by the body is provided by glucose. It can be taken up by all tissues in the body and can be stored as glycogen primarily in liver and muscle cells. When blood glucose levels drop, glycogen can be rapidly hydrolysed back into glucose and provide energy when needed. During glycolysis, glucose is converted into pyruvic acid (pyruvate) in a series of enzyme catalysed steps. The energy released in this process is used to generate adenosine triphosphate (ATP) and reduced nicotinamide adenine dinucleotide (NADH). In contrast to other metabolic pathways, glycolysis does not require oxygen and is therefore the predominant energy providing pathway in anaerobic organisms. When oxygen is limited, other organisms also rely more on glycolysis for generation of energy.

A key step in cell metabolism is the conversion of pyruvate, the end product of glycolysis, into acetyl-CoA by the enzyme pyruvate dehydrogenase. This step connects glycolysis and the citric acid cycle and takes place in the mitochondrial matrix. Acetyl-CoA is shuttled into the citric acid cycle where a series of redox reactions generate the high-energy molecules NADH, dihydroflavine-adenine dinucleotide ($FADH_2$) and ATP as well as carbon dioxide and water as byproducts. Each glucose molecule renders two pyruvates which fuel two run-throughs of the citric acid cycle and the generation of two carbon dioxide molecules, three NADH, one $FADH_2$ and one ATP for each turn. The citric acid cycle itself does not produce much ATP but generates NADH and $FADH_2$ which are needed as electron carriers in the electron transport chain during oxidative phosphorylation. Oxidative phosphorylation (OXPHOS) is the final stage of cellular respiration and takes place across the inner mitochondrial membrane. A linked set of protein complexes in the inner mitochondrial membrane forms an electron transport chain. Electron transport along this chain creates potential energy which is ultimately used to generate ATP.

As illustrated, the products of glycolysis are necessary for cellular respiration and are shunted into the citric acid cycle and oxidative phosphorylation. However, glucose-6-phosphate which is generated in the first step of glycolysis is also shuttled into the pentose phosphate pathway. This cytosolic pathway generates NADPH, pentose sugars and ribose 5-phosphate, which serve as precursor molecules for nucleotide synthesis, necessary for DNA and RNA production.
This shows the intricate network of biochemical reactions that are summarised as cell metabolism [105–108].

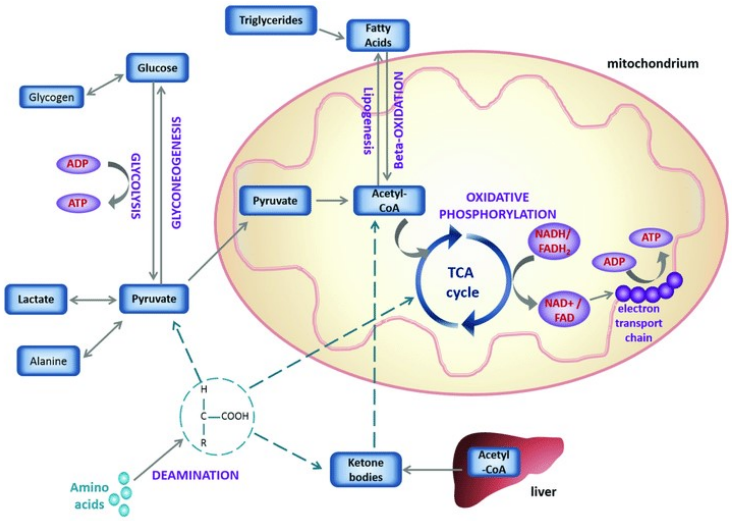

Figure 5 Metabolic pathways in the cell
Cells metabolise nutrients to generate energy and cellular building blocks. Figure modified from [109].

1.4.2 Mitochondria

The mitochondrial network Mitochondria are cell organelles that fulfil several essential functions in the cell. They are comprised of two compartments, the matrix and the intermembrane space. These compartments are divided by two structurally and functionally distinct membranes, the outer and the inner membrane. The inner membrane is almost completely non-permeable as it effectively blocks even small molecules and ions. It is highly folded and forms cristae which increases the membrane's surface area. The outer membrane is more permeable and most molecules with a molecular weight less than 5 kDa can pass through it [110, 111].

Mitochondria form a dynamic interconnected network within the cell which is constantly changing by fusion and fission processes. However, when looked at through microscopes they often appear as single round or oblong shapes. This is due to the thin sectioning needed for imaging techniques like electron microscopy, and the limited two-dimensional view that most microscopes provide [110]. The dynamics of fusion and fission processes are tightly regulated by GTPases. Dynamin-related protein 1 (DRP1) is responsible for mitochondrial fission while mitofusin 1 and 2 (MFN1, MFN2) and optic atrophy 1 (OPA1) regulate fusion. The balance of fission and fusion determines the shape of the mitochondrial network and can influence mitochondrial function [112, 113]. It can mediate energy output, production of reactive oxygen species (ROS) and mitochondrial quality control. During the cell cycle, mitochondrial

shape is synchronised to accommodate the energy demands of a proliferating cell [114, 115].
In addition to fusion and fission events, the mitochondrial network is shaped by the turnover of mitochondria through mitochondrial biogenesis and mitophagy.

Mitochondrial biogenesis Mitochondria are comprised of a large number and variety of proteins, most of which are encoded in the nucleus. Nuclear coded proteins are synthesised on cytoplasmic ribosomes and imported post-translationally into the mitochondrion. However, mitochondria contain multiple copies of their own circular DNA, which encodes for two ribosomal RNAs (rRNAs), 22 transfer-RNAs (tRNAs) and 13 protein subunits and is transcribed and translated within the mitochondrion. Mitochondrial DNA (mtDNA) does not encode any transcription factors but is dependent on nuclear transcription factors. Nuclear respiratory factor (NRF) 1 and 2 are nuclear transcription factors that control both mtDNA genes and nuclear genes while mitochondrial transcription factors A and B (TFAM, TFBM) exclusively regulate mtDNA genes. In addition to the transcription factors, transcription requires an RNA polymerase (POLRMT) and a termination factor. Mitochondrial ribosomes are formed by ribosomal RNA that is encoded by and transcribed from mitochondrial DNA and ribosomal proteins that are encoded by the nucleus and imported from the cytoplasm [110, 116, 117]. The expression of mtDNA is vital for the assembly and functioning of the oxidative phosphorylation complexes as thirteen of their subunits are encoded by the mitochondrial genome. Defects in mtDNA gene expression can lead to disturbed assembly of these complexes and consequently to mitochondrial disease [118].

Mitochondrial biogenesis is regulated by multiple factors, including the transcription factors NRF1 and NRF2. These were the first nuclear transcription factors found to be involved in multiple mitochondrial functions. NRF1 regulates multiple target genes encoding proteins of the respiratory complex, the mitochondrial import machinery and the transcription of mtDNA (transcription factor A mitochondrial, TFAM, transcription factor B1 mitochondrial, TFB1M, and transcription factor B2 mitochondrial TFB2M) [116, 119]. NRF2 was identified as a transcriptional activator of the cytochrome c oxidase subunit IV (COXIV) promotor and regulates the expression of mitochondrial transcription factors (TFAM, TFB1M, TFB2M). Its mouse-ortholog is the GA-binding protein (GABP), an ETS-domain (E26 transformation-specific) transcription factor [120]. GABP is comprised of a tetrameric complex which includes two distinct proteins, GABPα and GABPβ. GABPα binds to DNA through its ETS domain and

recruits GABPβ to the DNA. GABPβ1 is deacetylated by SIRT7 which triggers its binding to GABPα and enhances GABP transcriptional activity [121]. GABPα was shown to regulate transcription of TFB1M, an RNA dimethyltransferase that regulates mitochondrial protein translation [122]. Together the GABP complex regulates the expression of a plethora of mitochondrial proteins and transcription factors and is thus an essential regulator of mitochondrial biogenesis.
Other transcription factors involved in mitochondrial biogenesis include nuclear receptors like peroxisome proliferator-activated receptor alpha (PPARα) and estrogen-related receptors (ERRs) as well as nuclear transcriptions factors like YY1, MEF2 and c-myc [117, 123, 124].

Since an important function of mitochondria is to provide the cell with energy by generating ATP from nutrients, they are vulnerable to metabolic stress. The homeostasis of mitochondria is thus tightly controlled through mechanisms like mitochondrial biogenesis and mitophagy, the degradation of mitochondria by autophagy. Adaptions to cellular energetic and metabolic stress are controlled by transcription factors and transcriptional coregulators, such as PPARγ coactivator 1α (PGC-1α), other PGC-1 coactivators and sirtuins. PGC-1α, for example, coactivates NFR1, which in turns activates transcription of the transcription factor TFAM, a regulator of mtDNA synthesis [117, 125].
The sirtuin family also links cellular energetic and metabolic stress to transcriptional coregulation (see 1.6). Several other mechanisms play important roles in mitochondrial biogenesis. Mitochondrial protein import, mtDNA replication, transcription and translation have all been shown to be essential for biogenesis [116, 117].

Mitochondrial functions The main function of mitochondria is cellular respiration. In an initial step, pyruvate and fatty acids are shuttled into mitochondria from the cytoplasm via membrane bound permeases and are then converted to acetyl-CoA. Pyruvate decarboxylation, the conversion of pyruvate to acetyl-CoA, is catalysed by a complex of three enzymes, the pyruvate dehydrogenase complex. Fatty acids are first converted to their CoA ester derivative in the cytosol. However, the mitochondrial membranes are not permeable to medium- and long-chain acyl-CoAs with hydrocarbon chains longer than 12 carbons. They are therefore translocated through a carnitine-dependent process involving isoforms of the enzyme carnitine palmitoyltransferase (CPT) on the mitochondrial outer and inner membranes. Once inside the mitochondrion, fatty acids are broken down in a series of enzyme catalysed

steps that are repeated until only acetyl-CoA remains. Acetyl-CoA is then oxidised in the citric acid or tricarboxylic acid (TCA) cycle to yield carbon dioxide and reduced electron carriers NADH and FADH2. During oxidative phosphorylation, electrons from these carriers are then passed along a series of electron donors and acceptors organised into four complexes (I-IV) [105, 108].

The initial step in the respiratory chain is the transfer of two electrons by oxidation of NADH to NAD^+ and reduction of ubiquinone, a lipid-soluble quinone that is found in the mitochondrion membrane [126]. Succinate dehydrogenase (complex II) oxidizes succinate to fumarate and reduces ubiquinone and is therefore part of the electron transport chain as well as the citric acid cycle. This reaction does not contribute to the proton gradient across the mitochondrial membrane [127]. Outside the complexes, electron transfer flavoprotein-ubiquinone oxidoreductase (ETF-Q oxidoreductase) is an important enzyme in the respiratory chain. It accepts electrons from electron-transferring flavoprotein in the mitochondrial matrix and uses these electrons to reduce ubiquinone. This metabolic pathway is important in β-oxidation of fatty acids as it accepts electrons from acetyl-CoA dehydrogenases [128]. Cytochrome c reductase (complex III) catalyses the oxidation of ubiquinol and the reduction of cytochrome c, a heme protein that is localized in the compartment between the inner and outer mitochondrial membranes [129]. The final protein complex in the electron transport chain is cytochrome c oxidase (complex IV). It oxidises cytochrome c and transfers electrons to oxygen and hydrogen while pumping protons across the membrane. Oxygen, the terminal electron acceptor in the chain, is reduced to water which releases energy [130].
The electron transport through these four complexes is directly linked to the establishment of a proton gradient by pumping of protons across the mitochondrial membrane from matrix to intermembrane space. Subsequent dissipation of this gradient is coupled to the formation of ATP. In the final step of oxidative phosphorylation, the ATP-synthase (also called complex V) utilises the movement of protons back across the inner membrane to synthesise ATP from ADP and phosphate [131]. The shuttling of adenosine diphosphate (ADP) and phosphate into the mitochondria in exchange for ATP is also powered by the proton-motive force. Three ATPs are produced and released into the cytosol for each NADH that is oxidised through the electron transfer chain [105, 110].

In addition to ATP production, mitochondria also play essential roles in other metabolic pathways. They have key functions in heme, steroid and iron-sulfur cluster biosynthesis and are important for cellular calcium homeostasis. They are also an essential part of apoptosis. Mitochondria protect cells from oxidative stress induced by reactive oxygen species (ROS). ROS are normal by-products of mitochondrial metabolism and energy generation. In the vascular system their production is increased by stimuli like endothelin I, angiotensin II, TNFa and mechanical stretch. To prevent cell damage by ROS they are regulated by antioxidant mechanisms, which includes the manganese superoxide dismutase (Mn-SOD) in the mitochondria as well as cytosolic and extracellular SODs [132, 133]. Mitochondria have further been shown to influence signaling pathways, affect gene expression and thus play roles in cell proliferation, cell aging and determine cell differentiation [134].

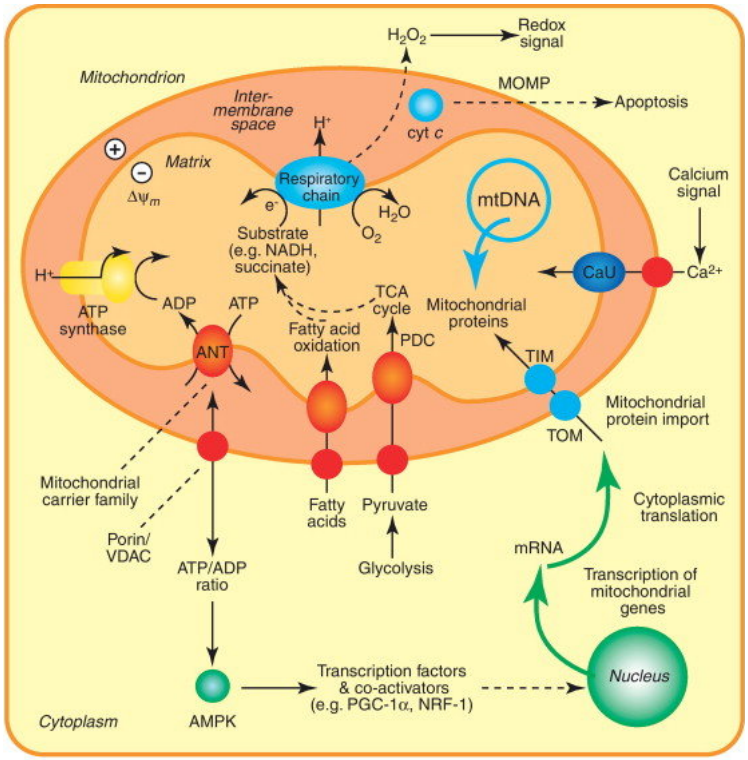

Figure 6 Mitochondrial functions

Shown are different mitochondrial functions and aspects of mitochondrial biogenesis. One of the main functions of mitochondria is the production of ATP. Initially, glucose is broken down to pyruvate through glycolysis in the cytosol. Pyruvate as well as other small molecules can pass through the outer mitochondrial membrane through voltage-dependent anion channels (VDACs). AMP-dependent kinase (AMPK) is activated by low ATP/ADP ratios and can regulate mitochondrial functions and output by targeting transcription factors and coactivators. ADP can be imported and ATP exported by the adenine nucleotide translocase (ANT). Mitochondrial proteins are encoded by mitochondrial DNA (mtDNA) and nuclear DNA. Translocases of the inner and outer mitochondrial membrane (TIM and TOM) transport nuclear-encoded proteins into mitochondria. Mitochondria can take up calcium into the mitochondrial matrix through the calcium uniporter (CaU) and thus play a role in calcium signaling. Mitochondria also play a major role in apoptosis. Upon apoptotic signals the mitochondrial outer membrane becomes compromised, a process called mitochondrial outer membrane permeabilization (MOMP). The permeabilization of the membrane leads to the release of cytochrome c (cyt c) and other pro-apoptotic proteins from the intermembrane space into the cytosol. There they induce apoptotic cell death. Figure modified from [135].

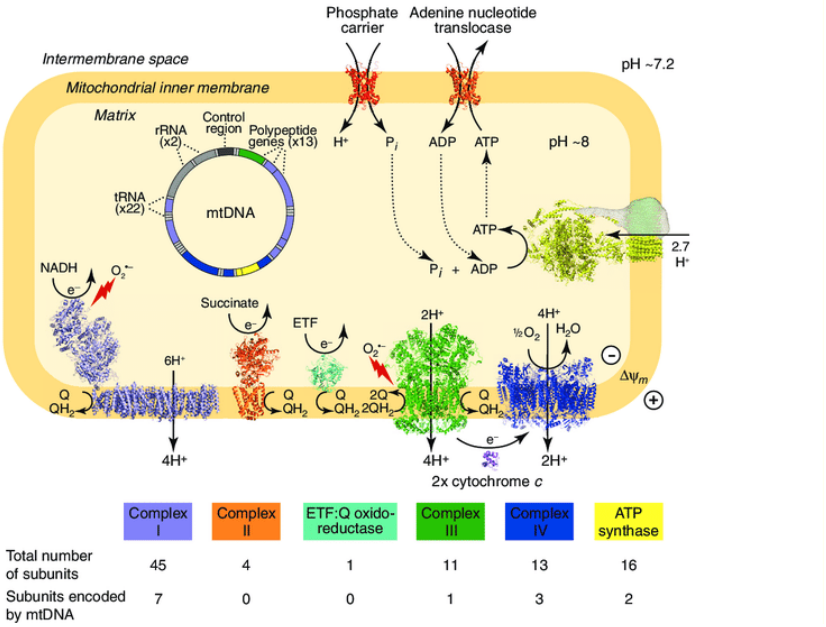

Figure 7 Oxidative phosphorylation
Shown are the components necessary for oxidative phosphorylation and details on the respiratory chain complexes. Figure modified from [135].

1.5 Metabolic regulation of cell functions

There is evidence for numerous cases in which metabolism can influence cellular function and vice versa. The cellular metabolism is highly adaptable and reacts to changes in the cell environment as well as to the availability of nutrients and metabolites. Generally, cells rely on the metabolism of glucose, amino acids and fatty acids to maintain overall energy homeostasis. However, increasing evidence suggests that the favouring of specific metabolic pathways, the levels of available substrates and their intermediates can modulate specific molecular activities. Metabolites such as acetyl-CoA, for instance, directly connect metabolism to the regulation of protein function and chromatin modification. Evidence for a role of metabolism in modulating cellular function can be found in various contexts. These areas include the tumour microenvironment and the immune system but also the vascular system.

The metabolic changes in tumour cells are probably the best studied example of metabolic adaption to a cell's requirements. Usually, cells need to be stimulated by growth factors to take up nutrients from their environment from which they can then gain the energy needed for proliferation. Cancer cells, however, often acquire mutations that constitutively activate these pathways so that they are no longer

dependent on growth factors. This can lead to an increased uptake of nutrients, especially glucose which then delivers the required energy for cancer cell proliferation [136–138]. While differentiated cells primarily rely on oxidative phosphorylation to generate energy from glucose, most cancer cells rely on aerobic glycolysis instead. When oxygen is limited, the pyruvate generated through glycolysis is not shuttled into the mitochondria for oxidative phosphorylation but is directly converted into lactate by lactate dehydrogenase (LDH), a process called anaerobic glycolysis. The observation that cancer cells tend to generate lactate from glucose even in the presence of sufficient oxygen, a process termed aerobic glycolysis, is called the Warburg effect [136, 139, 140]. Studies have shown that mitochondrial function is not impaired in most cancer cells suggesting another reason for aerobic glycolysis in these cells [141, 142]. This is puzzling, as generating ATP from aerobic glycolysis is less efficient than the complete metabolization of glucose through oxidative phosphorylation.

Therefore, it is probably not the generation of energy in form of ATP but other metabolic requirements, that drive this effect in proliferating cells. As proliferating cells need to replicate their cellular content in order to create new cells, they have a large need for cellular building blocks like nucleotides, amino acids and lipids. To meet this need not all glucose can be catabolised completely as part of its carbon chain are needed as basis for other molecules. Acetyl-CoA, for example, is needed as a building block for acyl chains to synthesise lipids. Another important pathway that generates NADPH, pentose sugars and ribose 5-phosphate, which serve as precursor molecules for nucleotide synthesis is the pentose phosphate pathway. Glucose-6-phosphate which is generated in the first step of glycolysis is shunted into this pathway [136].

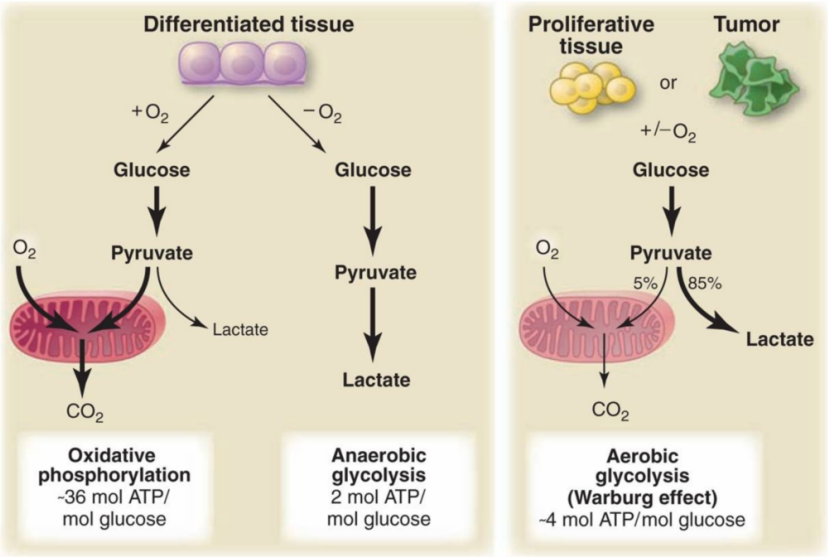

Figure 8 The Warburg effect
Illustration of oxidative phosphorylation, anaerobic glycolysis, and aerobic glycolysis (Warburg effect) in differentiated and proliferative and cancer tissue, respectively. In cells in nonproliferating (differentiated) tissues most of the pyruvate generated by glycolysis is shunted into the mitochondria where it is oxidised during oxidative phosphorylation. This process is oxygen dependent. When oxygen is limiting, cells can redirect the pyruvate and generate lactate (anaerobic glycolysis). Warburg found that cancer cells tend to convert most glucose to lactate regardless of whether oxygen is present (aerobic glycolysis). This has also been found in normal proliferating cells. Figure taken from [136].

In the vascular system, glycolysis has been shown to be an important regulator of endothelial cells in vessel sprouting. De Bock et al. found that endothelial cells relied on glycolysis rather than on oxidative phosphorylation for ATP production. The glycolytic activator phosphofructokinase-2/fructose-2,6-bisphosphatase 3 (PFKFB3) was shown to regulate endothelial cell proliferation as well as directional migration. Consequently, silencing of PFKFB3 impaired vessel sprouting, suggesting that glycolysis even overrules the Notch signaling pathway as the master regulator of endothelial proliferation and migration [143].

Metabolism can also determine the phenotype of plastic cells as was shown for the polarisation of macrophages. Macrophages are highly plastic and adaptable but can be roughly simplified into two extremes, a pro-inflammatory phenotype (M1) and an anti-inflammatory phenotype (M2). The phenotypic and functional changes of macrophages are accompanied by drastic changes in metabolism. M1 macrophages rely mainly on glycolysis and have an impaired TCA cycle. The break in the TCA cycle leads to an accumulation of succinate which stabilises hypoxia

inducible factor 1α (HIF1α). HIF1α activates the transcription of glycolytic genes, keeping glycolytic metabolism in M1 macrophages on a high level. M2 macrophages on the other hand are more dependent on oxidative phosphorylation and have an intact TCA cycle. Pathways that regulate lipid and amino acid metabolism are also differentially activated in M1 and M2 macrophages. These metabolic adaptations support macrophage activities of the two phenotypes and help sustain their polarisation [144].

These findings provide evidence that metabolism is an important regulator of cell function and cell fate and can determine the phenotype of plastic cells. Vascular smooth muscle cells are highly plastic and frequently undergo phenotypic transitions in physiology and pathology. It would stand to reason that metabolism could also play a role in these processes.

1.5.1 Metabolism and VSMCs

In the healthy vessel, VSMCs rely on both, glycolysis and oxidative phosphorylation, for the generation of energy. Glycolysis however, seems to play an important role in proliferation as well as for the phenotypic transition towards the synthetic phenotype. Even under fully oxygenated conditions, VSMCs metabolise a notable part of their glucose to lactate [145, 146]. In a cell culture model, incubation of VSMCs with lactate lead to a more synthetic phenotype. This suggests that a lactate rich environment might promote the dedifferentiated phenotype [147]. PDGF treatment of cultured cells induced glycolytic flux, further suggesting a link between increased glycolysis and the dedifferentiated, synthetic phenotype. PDGF has also been shown to promote the Warburg effect in pulmonary arterial smooth muscle cells supporting the theory that an adaptive metabolism plays an important role in smooth muscle cell proliferation [148]. In the disease setting, human atherosclerotic plaques were reported to exhibit enhanced glycolysis and pentose phosphate pathways as well as increased hexokinase 2 expression [145].

In addition to glycolysis, mitochondria have also been associated with VSMC phenotypic plasticity. PDGF treatment of cultured VSMCs lead to enhanced mitochondrial respiration in some studies while it was reduced in others. Several studies have found connections between mitochondrial fission and neointima formation [53, 114, 149, 150].

Mitochondrial DNA damage has been repeatedly linked to atherosclerosis. It was shown that mtDNA damage was present in the vessel wall as well as in circulating cells already in early stages of atherosclerosis and that mtDNA damage was found in atherosclerotic plaques in humans [151]. MtDNA defects also promoted atherosclerosis and plaque vulnerability in an ApoE knock-out mouse model of atherosclerosis [152]. MtDNA damage can lead to mitochondrial dysfunction. As mitochondria are regulators of various cell functions, mitochondrial dysfunction can lead to cell death, inflammation, oxidative stress and alterations of metabolism. Docherty et al. identified a subset of human plaque VSMCs that showed increased mitochondrial dysfunction and decreased oxidative phosphorylation linking possibly dedifferentiated VSMCs with an altered metabolic state [153].

These studies suggest that phenotypic plasticity of VSMCs is tightly linked to adaptions in metabolism and mitochondrial integrity. However, most studies of VSMC metabolism have been conducted in cultured cells, a setting lacking the microenvironment of cell-cell interactions, extracellular elastic fibers, hemodynamic factors and cytokines that all influence and regulate VSMC phenotype. Furthermore, studies investigating mitochondrial respiration in PDGF treated cultured VSMC have rendered contradictory results. Therefore, it was one of the aims of this study to further elucidate the role of metabolism in VSMC phenotypic plasticity *in vitro* and especially *in vivo*.

1.6 Sirtuins

A group of enzymes that link the nutritional state of the cell and regulation of metabolism and cell functions are the sirtuins. Sirtuins are the mammalian homologue of silent regulator 2 (Sir2) that was originally discovered in yeast as a regulator of aging [154].
There are seven Sir2 homologues in mammals, SIRT1-SIRT7, which belong to the class III histone acetylases. Sirtuins are NAD dependent histone deacetylases and share a conserved catalytic domain that contain a large, structurally homologous Rossmann-fold domain for NAD^+- binding and a smaller, more structurally diverse zinc-binding domain [155].
Deacetylation of histones leads to a more compact DNA conformation, which prevents or hinders the binding of transcription factors to the DNA. Thus, through deacetylation, sirtuins can regulate gene transcription. The different sirtuins have variable N- and C-terminal extensions and their cellular localisation, activities and functions differ

widely. SIRT1 is found in the nucleus and the cytoplasm, SIRT2 is localised in the cytoplasm while SIRT3,4 and 5 are located in the mitochondria. SIRT6 and SIRT7 are nuclear sirtuins. Similar to the originally found Sir2 in yeast, mammalian sirtuins have been shown to play beneficial roles in aging, longevity and stress responses [156, 157]. They also have various functions in transcription regulation, modulation of energy metabolism, cell survival, DNA repair and apoptosis [158, 159].

SIRT1 is the most extensively studied sirtuin. In addition to its function as a histone deacetylase it regulates transcription factors, such as p53, forkhead box (FOXOs), nuclear factor kappa-light-chain-enhancer of activated B cells (NFκB) and DNA repair proteins like poly-ADP-ribose-polymerase 1 (PARP1) [160–163]. SIRT1 has also been shown to regulate PGC-1α, an important coactivator in mitochondrial biogenesis [164, 165]. In cardiovascular diseases like atherosclerosis protective effects of SIRT1 have been shown [165, 166]. SIRT1 expression was reduced in atherosclerotic plaques of ApoE knock-out mice and a smooth muscle specific knock-out of SIRT1 in ApoE$^{-/-}$ mice lead to increased atherosclerosis [167]. It also plays a role in maintaining endothelial functions as inhibition of SIRT1 was associated with endothelial dysfunction and increased artery stiffness [168]. SIRT1 has also been found to play a role in angiogenesis, ischemia-reperfusion injury and other cardiovascular contexts, like hypertrophy and heart failure, hypertension and arrythmias [165].

The role of other sirtuins in cardiovascular diseases are not as well understood. SIRT3 has been associated with angiogenesis, hypertension as well as hypertrophy and fibrosis while SIRT5 was shown to have a protective role in ischemia reperfusion injury and prevents age-related hypertrophy and fibrosis in mice. Most sirtuins have also been shown to play roles in metabolic diseases, like dyslipidemia, obesity and type 2 diabetes [165].

Their broad spectrum of regulatory functions in all areas of cellular function make them interesting targets for further research and disease therapies. This study focuses on two sirtuins, SIRT6 and SIRT7.

1.6.1 Sirtuin 6

Sirtuin 6 is one of the nuclear located sirtuins and acts as a NAD^+-dependent deacetylase of acetyl groups and long-chain fatty-acyl groups [169–171]. It also functions as an ADP-ribosylase [172]. SIRT6 has been found to play important roles in the regulation of DNA repair, telomere maintenance and glucose and lipid metabolism and thus contributes to longevity and a healthy homeostasis [173]. SIRT6 also impacts genome integrity, genomic stability and DNA repair [173]. Loss of SIRT6 leads to dysfunctional telomers and genomic instability which can induce premature cell senescence [169]. Sirt6 also senses and regulates DNA double strand break (DSB) repair via multiple ways [173, 174]. Upon oxidative stress, for instance, SIRT6 was found to interact with PARP1 which was necessary for DSB repair [172].

An important area of SIRT6 function is in cellular metabolism. SIRT6 has been found to be a central regulator of glucose homeostasis, regulating both glycolysis and gluconeogenesis. SIRT6-deficient mice showed severe hypoglycaemia and an increased glucose uptake upon SIRT6 depletion was found in various cell types *in vivo* and *in vitro* [175, 176]. SIRT6 deficiency also led to an increase in GLUT1 expression, an enhanced glycolysis and a reduced mitochondrial respiration. SIRT6 was found to interact with hypoxia-HIF1α and to deacetylate histone 3 lysine 9 (H3K9) at the promoter of HIF1α target genes. Therefore, SIRT6 directly suppresses the expression of HIF1α target genes, such as PDK1, LDH, PFK1 and GLUT1 [176]. SIRT6 has also been found to control gluconeogenesis by modulating PGC-1α [173]. In lipid metabolism, evidence suggests that SIRT6 acts as a negative regulator of triglyceride synthesis [177]. It also promotes hepatic β-oxidation through the activation of PPARα [178].

SIRT6 has also been increasingly studied in the field of cancer. The enhanced glycolysis and inhibited mitochondrial respiration upon SIRT6 depletion is reminiscent of the Warburg effect observed in cancer cells [173, 176]. Fittingly, SIRT6 expression was found to be reduced in several cancer types, leading to enhanced expression of HIF1α target genes and enhanced glycolysis. It was therefore suggested that SIRT6 acts as a tumour suppressor by repressing HIF1α and thus inhibiting aerobic glycolysis [179].

1.6.2 Sirtuin 7

Like SIRT6, sirtuin 7, is located in the nucleus. SIRT7 however, has been shown to be predominantly located in the nucleolus [180]. SIRT7 is a highly selective histone 3 lysine 18 (H3K18) deacetylase but has also been shown to have a variety of non-histone substrates [181, 182]. Through regulating polymerase expression and activity, SIRT7 is involved in regulating ribosome biogenesis and protein translation [182]. Similar to other sirtuins, SIRT7 also promotes genomic stability and protects against cellular senescence. Different groups have shown that SIRT7 is recruited to DSB in a PARP1-dependent manner and that it can regulate p53 to promote genomic stability [183, 184]. SIRT7 is suggested to have a critical role in aging as SIRT7 knock-out mice had a shorter lifespan than control mice [121]. SIRT7 expression gradually declines with age and SIRT7 as well as SIRT6 expression levels are decreased in senescent cells [121, 182, 185]. Dysregulation of this mechanism is implicated in various diseases. High and low SIRT7 expression have both been associated with different cancers and are considered predictors of poor patient outcome [182]. The contradictory data found for SIRT7 in cancer, illustrate the complexity and variety of SIRT7 interactions and cellular functions [182].

Like SIRT6, SIRT7 plays an important role in metabolic regulation. It has been shown to be sensitive to low glucose levels and to protect the cell from nutritional stress. Upon glucose deprivation SIRT7 translocates from the nucleolus to the nucleoplasm where it inhibits ribosomal DNA (rDNA) transcription to preserve energy [186]. SIRT7 was found to impact glycolysis by regulating the activity of PGK1 in liver cancer cells and to be involved in gluconeogenesis [187, 188]. SIRT7 also negatively regulates the expression of HIF-1α and HIF-2α proteins. Over-expression of SIRT7 reduced the levels of HIF proteins and their transcriptional targets, consequently repressing glycolysis [189]. In addition to its role in glucose metabolism SIRT7 has been shown to be an important regulator of mitochondrial homeostasis. In a study by Ryu et al., SIRT7 knock-out mice showed multi-systemic mitochondrial dysfunction as well as lactate accumulation. SIRT7 regulates mitochondrial biogenesis by deacetylating GABPβ1 which forms a hetero-tetramer complex with GABPα [121]. Together the GABP complex regulates the transcription of a variety of nuclear-encoded mitochondrial target genes and is thus considered an essential regulator of mitochondrial biogenesis [122]. In another study, SIRT7 interacted with NRF1, a master regulator of mitochondrial biogenesis, to regulate mitochondria size and activity of the respiratory chain [190].

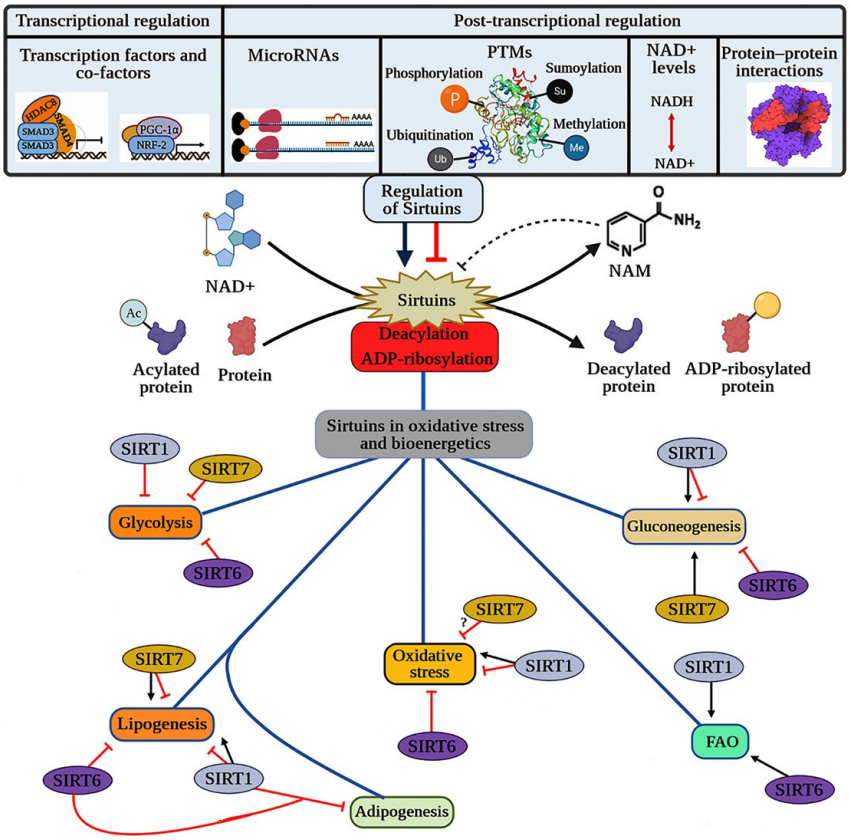

Figure 9 Overview sirtuins
Schematic overview of the regulation of sirtuins and the role of SIRT1, SIRT6 and SIRT7 in metabolic pathways. Figure modified from [191].

1.7 Aim of the study

The aim of this study was to investigate the association between VSMC plasticity and VSMC metabolism in vascular disease. As was shown for other cell types, cell metabolism can regulate cell functions and cell fate in physiological as well as pathophysiological conditions. In an experiment preceding this study the expression pattern in dedifferentiated versus differentiated VSMCs was acquired with a proteomics approach. Interestingly, there was a major shift in expression levels of proteins involved in cell metabolism. Most prominent was a drop in the abundance of mitochondrial proteins after induction of dedifferentiation with PDGF.

From this experiment and evidence in the literature (see 1.5.1), the hypothesis that VSMC phenotypic transition is accompanied by an adaption of the metabolism according to the requirements of the respective phenotype was generated. In this study, this hypothesis was to be tested in two *in vitro* and one *in vivo* mouse model of VSMC dedifferentiation.

The second part of this study aimed at manipulating VSMC metabolism through deletion of known metabolic regulators Sirt6 and Sirt7 and determining whether direct intervention in the cells' metabolism would impact VSMC plasticity in an *in vitro* and *in vivo* model of VSMC dedifferentiation and in an atherosclerosis mouse disease model. Based on the literature, the working hypothesis was that Sirt6 and Sirt7 might counteract the observed metabolic changes in VSMCs and thus would act atheroprotectively.

To summarise, the aim of this study was to investigate the metabolic adaptions VSMCs exhibit during phenotypic transition and identify possible regulators thereof.

2 Materials and Methods

2.1 Materials

2.1.1 Chemicals

All chemicals were obtained from Carl Roth or Sigma-Aldrich if not indicated otherwise.

Table 1 Chemicals

Name	Supplier	Cat.No.
BSA (bovine serum albumin), Fraction V	Merck	2930-100GM
Collagenase II	Worthington	LS004176
DAPI (4',6-Diamidino-2-phenylindole)	Sigma-Aldrich	D9564
Elastase	Worthington	LS002292
Epon resin	Serva	
Lead citrate	Sigma-Aldrich	15326
Mygliol 812	Caelo	3274
Neo-Clear	Merck	1.09843.5000
Neo-Mount	Merck	1.09016.0500
Osmium tetroxide	Science Services	E19140
Paraffin type 6 & 9	Fisher Scientific	8337
Roti-Histofix 4% (Phosphate buffered formaldehyde solution 4%)	Carl Roth	P087.3
Tamoxifen	Sigma-Aldrich	T5648
Vectashield with DAPI	BIOZOL	VEC-H-1200

2.1.2 Reagents, Inhibitors etc.

Table 2 Reagents, Inhibitors etc.

Name	Supplier	Cat. No.
Antimycin A	Sigma-Aldrich	A8674
Cholesterol-methyl-β-cyclodextrin	Sigma-Aldrich	C4951
FCCP	Sigma-Aldrich	C2920
Mitotracker™ Deep Red FM	Thermo Fisher Scientific	M22426
Oligofectamine™ Transfection Reagent	Thermo Fisher Scientific	12252011
Oligomycin A	Sigma-Aldrich	75351
ON-TARGETplus Non-targeting Control siRNA	Dharmacon	D-001810-01-05
ON-TARGETplus SMARTpool Sirt7 siRNA	Dharmacon	L-086898-02-0005
PDGF-BB from rat, recombinant	Sigma-Aldrich	P4056
Proteinase K	Qiagen	19131
Rotenone	Sigma-Aldrich	R8875

2.1.3 Cells

Table 3 Cells

Name	Description	Source
A7r5	thoracic aorta, smooth muscle cells from rat	ATCC®CRL-1444™
mVSMCs	vascular smooth muscle cells from mouse	isolated from carotid arteries and aorta from mice

2.1.4 Animals

Table 4 Mouse strains

Strain	Source	Reference
C57BL/6	Jackson Laboratory	-
SMMHC-CreER^{T2}	kindly provided by Angela Wirth, Institute of Pharmacology, University of Heidelberg, Heidelberg, Germany	[192]
mT/mG	kindly provided by Stefan Offermanns, Max Planck Institute for Heart and Lung Research, Bad Nauheim, Germany	[193]
ApoE$^{-/-}$	kindly provided by Stefan Offermanns, Max-Planck-Institute for Heart and Lung Research, Bad Nauheim, Germany	-
Sirt6 flox	kindly provided by Thomas Braun, Max-Planck-Institute for Heart and Lung Research, Bad Nauheim, Germany	[194]
Sirt7 flox	kindly provided by Eva Bober, Max-Planck-Institute for Heart and Lung Research, Bad Nauheim, Germany	[195]
SM-mT/mG	in-house breeding	
SM-Sirt6	in-house breeding	
SM-Sirt6-mT/mG	in-house breeding	
SM-Sirt6-ApoE$^{-/-}$	in-house breeding	
SM-Sirt7	in-house breeding	
SM-Sirt7-mT/mG	in-house breeding	
SM-Sirt7-ApoE$^{-/-}$	in-house breeding	
SM-Sirt7-ApoE$^{-/-}$-mT/mG	in-house breeding	

2.1.5 Cell culture

Cell culture consumables were purchased from Sarstedt, BD Falcon, Corning and B. Braun.

Table 5 Cell culture

Name	Supplier	Cat. No.
DMEM/F-12 1:1	Thermo Fisher Scientific (Gibco)	31330038
DMEM 4.5 g/l glucose	Thermo Fisher Scientific (Gibco)	41966-029
DMEM powder, basic (no glucose, no NaHCO3, no L-glutamine, no phenol red, no sodium pyruvate, no HEPES)	Sigma-Aldrich	D5030
DMSO (Dimethyl Sulfoxide)	Sigma-Aldrich	D2650
DPBS (Dulbecco's phosphate buffered saline)	Thermo Fisher Scientific (Gibco)	14190250
Fetal calf serum (FCS)	Biochrom AG	S0115
Opti-MEM	Thermo Fisher Scientific (Gibco)	31985062
Penicillin/Streptomycin (P/S)	Thermo Fisher Scientific (Gibco)	15140122
Trypsin-EDTA (0.05%)	Thermo Fisher Scientific (Gibco)	5300054

2.1.6 Consumables

All consumables not specifically listed here, were purchased from Sarstedt, BD Falcon, Corning and B. Braun.

Table 6 Consumables

Name	Supplier	Cat. No.
Histo Bond	Microscope Slides	Marienfeld 810000
Microscope Slides Superfrost PLUS	Thermo Fisher Scientific (Menzel)	J1800AMNZ
Microtome blade S35	Feather	S35
Sakura Finetek Tissue-Tek OCT Compound	Fisher Scientific	12351753
Sakura Finetek Tissue-Tek Cryomold Biopsy square (10 x 10 x 5 mm), 4565	Fisher Scientific	10690461
Sakura Finetek Tissue-Tek Cryomold Intermediate square (15 x 15 x 5 mm), 4566	Fisher Scientific	10844231
XFe96 FluxPak	Agilent	102416

2.1.7 Kits

Table 7 Commercial Kits

Name	Supplier	Cat. No.
DNeasy Blood and Tissue Kit	Qiagen	69504
Elastic Stain Kit	Sigma-Aldrich	HT25A
Fluitest CHOL (cholesterol)	Analyticon	4248
High-Capacity cDNA Reverse Transcription kit	Thermo Fisher Scientific	4374966
RNeasy Micro Kit	Qiagen	74004
Rneasy Mini Kit	Qiagen	74104
TaqMan Gene Expression Master Mix	Thermo Fisher Scientific	4369016
TG (Triglycerides)	Analyticon	5052
Quant-iT™ PicoGreen™ dsDNA Assay Kit	Thermo Fisher Scientific	P7589

2.1.8 Primer

Table 8 Taqman Assays used for quantitative PCR (qPCR)

Gene ID	Gene name	TaqmanAssay ID
Targeting Mouse		
Abca1	ATP-binding cassette, sub-family A (ABC1), member 1	Mm00442646_m1
Acadm	acyl-Coenzyme A dehydrogenase, medium chain	Mm01323360_g1
Aco2	aconitase 2, mitochondrial	Mm00475673_g1
Acta2	actin, alpha 2, smooth muscle	Mm00725412_s1
Aldoa	aldolase A	Mm00833172_g1
Atp5h	ATP synthase, H+ transporting, mitochondrial F0 complex, subunit D	Mm02392026_g1
Atp5o	ATP synthase, H+ transporting, mitochondrial F1 complex, O subunit	Mm01611862_g1
CD68	CD68 antigen	Mm03047343_m1
Clpp	caseinolytic mitochondrial matrix peptidase proteolytic subunit	Mm00489940_m1
Cpt1a	carnitine palmitoyltransferase 1a	Mm01231183_m1
Dnm1l	dynamin 1-like	Mm01342903_m1
Echs1	enoyl-CoA hydratase, short chain 1	Mm01276347_m1
Eef2	eukaryotic translation elongation factor 2	Mm05700170_g1
Eno1	enolase 1	Mm01619597_g1
Etfa	electron transfer flavoprotein subunit alpha	Mm00521254_m1
Fh1	fumarate hydratase 1	Mm01321349_m1
Got2	glutamatic-oxaloacetic transaminase 2	Mm00494703_m1
Idh2	isocitrate dehydrogenase 2 (NADP+)	Mm00612429_m1
Ldha	lactate dehydrogenase A	Mm01612132_g1
Lgals3	galectin 3 / lectin, galactose binding, soluble 3	Mm00802901_m1
Mfn1	mitofusin 1	Mm00612599_m1
Mfn2	mitofusin 2	Mm00500120_m1
Mrpl49	mitochondrial ribosomal protein L49	Mm00782916_s1
Mrps5	mitochondrial ribosomal protein S5	Mm01281573_m1
Mrps9	mitochondrial ribosomal protein S9	Mm00469845_m1

Gene ID	Gene name	TaqmanAssay ID
mt-Nd1	NADH dehydrogenase 1, mitochondrial	Mm04225274_s1
Myh11	myosin heavy chain 11, smooth muscle	Mm00443013_m1
Ndufa13	NADH:ubiquinone oxidoreductase subunit A13	Mm00445751_m1
Ndufs1	NADH:ubiquinone oxidoreductase core subunit S1	Mm00523640_m1
Pcx	pyruvate carboxylase	Mm00500992_m1
Pdha1	pyruvate dehydrogenase E1 subunit alpha 1	Mm00468675_m1
Pdhb	pyruvate dehydrogenase E1 subunit beta	Mm00499323_m1
Pdhx	pyruvate dehydrogenase complex, component X	Mm00558275_m1
Pdk2	pyruvate dehydrogenase kinase 2	Mm00446681_m1
Pdpr	pyruvate dehydrogenase phosphatase regulatory subunit	Mm01243524_m1
Pfkfb3	6-phosphofructo-2-kinase/fructose-2,6-biphosphatase 3	Mm00504650_m1
Pfkm	phosphofructokinase, muscle	Mm01309576_m1
Pgk1	phosphoglycerate kinase 1	Mm00435617_m1
Polrmt	RNA polymerase mitochondrial	Mm00553272_m1
Sirt6	sirtuin 6	Mm01149042_m1
Sirt7 E5-6	sirtuin 7 exon 5-6	Mm00461897_m1
Sirt7 E9-10	sirtuin 7 exon 9-10	Mm01248607_m1
Slc2a1	solute carrier family 2 member 1	Mm00441480_m1
Tfam	transcription factor A, mitochondrial	Mm00447485_m1
Tigar	Trp53 induced glycolysis regulatory phosphatase	Mm00621530_m1
Uqcrh	ubiquinol-cytochrome c reductase hinge protein	Mm00835199_g1
Housekeeper		
Rpl19	ribosomal protein L19	Mm02601633_g1
Targeting Rat		
Abca1	ATP-binding cassette, sub-family A (ABC1) member 1	Rn00710172_m1
Acadm	acyl-Coenzyme A dehydrogenase, medium chain	Rn00566390_m1

Gene ID	Gene name	TaqmanAssay ID
Aco2	aconitase 2, mitochondrial	Rn00577876_m1
Acta2	actin, alpha 2, smooth muscle	Rn01759928_g1
Atp5o	ATP synthase, H+ transporting, mitochondrial F1 complex, O subunit	Rn00756345_m1
Ccnd1	cyclin D1	Rn00432359_m1
CD68	CD68 antigen	Rn01495634_g1
Clpp	caseinolytic mitochondrial matrix peptidase proteolytic subunit	Rn01527475_m1
Cpt1a	carnitine palmitoyltransferase 1a	Rn00580702_m1
Ctnnb1	catenin beta 1	Rn00584431_g1
Echs1	enoyl-CoA hydratase, short chain 1	Rn01454617_m1
Etfa	electron transfer flavoprotein subunit alpha	Rn01766950_m1
Idh2	isocitrate dehydrogenase 2 (NADP+)	Rn01478119_m1
Ldha	lactate dehydrogenase A	Rn00820751_g1
Lgals3	galectin 3 / lectin, galactose binding, soluble 3	Rn04219572_m1
Mfn1	mitofusin 1	Rn00594496_m1
Mfn2	mitofusin 2	Rn00672763_m1
Mki67	marker of proliferation Ki-67	Rn01451446_m1
Mrpl49	mitochondrial ribosomal protein L49	Rn01501728_m1
Mrps5	mitochondrial ribosomal protein S5	Rn01513191_m1
Mrps9	mitochondrial ribosomal protein S9	Rn01437394_m1
Myh11	myosin heavy chain 11, smooth muscle	Rn01530321_m1
Ndufa13	NADH:ubiquinone oxidoreductase subunit A13	Rn01766950_m1
Pfkfb3	6-phosphofructo-2-kinase/fructose-2,6-biphosphatase 3	Rn00678825_m1
Polrmt	RNA polymerase mitochondrial	Rn01748691_m1
Sirt7 E5-6	sirtuin 7 exon 5-6	Rn01471420_m1
Sirt7 E9-10	sirtuin 7 exon 9-10	Rn01471424_m1
Slc2a1	solute carrier family 2 member 1	Rn01417099_m1
Tfam	transcription factor A, mitochondrial	Rn00580051_m1
Housekeeper		
Rps11	ribosomal protein S11	Rn00821284_g1

All Taqman Assays were purchased from Thermo Fisher Scientific.

Table 9 Primers for genotyping of mice

Gene	Primer sequence
SMMHC-CreER^{T2}	(1) TGA CCC CAT CTC TTC ACT CC (2) AAC TCC ACG ACC ACC TCA TC (3) AGT CCC TCA CAT CCT CAG GTT
mT/mG	(1) CTC TGC TGC CTC CTG GCT TCT (2) TCA ATG GGC GGG GGT CGT T (3) CGA GGC GGA TCA CAA GCA ATA
Sirt6	(1) AAC TGA CTG TTG CGG CAG AG (2) CCT GTC CCA TTC TGA GGA AC
Sirt7	(1) ACT CCT CAT GAA TGA ACT GGG (2) ACT GAT GGC GAG CTC AGA CC (3) GGC TGC ACA CCA TCT GTG G
ApoE$^{-/-}$	(1) GCC TAG CCG AGG GAG AGC CG (2) TGT GAC TTG GGA GCT CTG CAG C (3) GCC GCC CCG ACT GCA TCT

All primers were purchased from TIB MOLBIO.

2.1.9 Buffers and Solutions

Lysis buffer for DNA measurement

10 mM	Tris-HCl pH 7.4
1 mM	EDTA
0.1%	Triton X-100

Fixating solution for electron microscopy

2.5%	Glutaraldehyde
0.1 M	0.1 M sodium cacodylate buffer

2.1.10 Laboratory instruments

Table 10 Laboratory instruments

Name	Description	Supplier
BD FACSAria™ II	Cell sorter	BD Biosciences
BZ 9000 (Biorevo)	Fluorescence microscope	Keyence
CyAn ADP Analyzer 3 laser (405, 488 and 635 nm)	Flow cytometer	Beckman Coulter
Electron Microscope EM 906	Electron microscope	Carl Zeiss
Embedding center EC 350-2	Paraffin tissue block embedding station	Microm International GmbH
HM 325 Rotary Microtome	Microtome	Thermo Fisher Scientific
Jung Frigocut 2800 E	Cryostat	Leica
Leica DMIL	Light microscope	Leica
Leica MZ6	Stereomicroscope	Leica
MACSQuant Analyzer 10	Flow cytometer	Miltenyi Biotec
Seahorse XF96e Flux Analyzer	Metabolic flux analyser	Agilent
Shandon Citadel 1000	Automated tissue processor for paraffin embedding	Thermo Electron Corporation
Spectramax 340PC384	Plate reader	Molecular Devices
Spectramax GEMENI EM	Fluorescence plate reader	Molecular Devices
TissueLyser	Tissue Homogeniser	Retsch
QuantStudio 7 RT-PCR	Real-Time PCR System	Thermo Fisher Scientific

2.1.11 Software

Table 11 Software

Name	Supplier/Company
FCSalyzer	Open-source software
ImageJ	National Institutes of Health (NIH)
Prism Version 8	GraphPad
Summit V4.3.02	Beckman Coulter
QuantStudio Real-Time PCR Software	Thermo Fisher Scientific
Wave	Agilent

2.2 Methods

2.2.1 Cell culture

A7r5 A7r5 rat aortic smooth muscle cells were obtained from ATCC (ATCC CRL-1444) and cultured in DMEM (4.5 g/l glucose, L-glutamine, pyruvate) supplemented with 10% FCS and 1% penicillin/streptomycin. For passaging, cells were washed with PBS and incubated with 0.02% trypsin for 3-5 min. Growth medium was added to stop enzyme activity and cells were either transferred directly to a new cell culture vessel or were centrifuged at 1000 x g for 5 min before being resuspended in fresh growth medium.

Isolation of primary mouse VSMCs from aorta and carotids Mice were euthanized and thoracic and abdominal aorta, as well as both carotid arteries, were dissected. Connective tissue was removed and the exposed vessels were transferred to a petri dish with serum-free DMEM/F12 where they were cleaned of all remaining perivascular tissue. After dissection and tissue removal, vessels were placed in serum-free media and stored on ice until all vessels were collected and digestion could be started. For digestion, vessels were cut into small cross-sections and were placed in 700 µl of enzyme solution (serum-free DMEM/F12 with 1 mg/ml collagenase II and 0.5 mg/ml elastase) for 3 h 30 min at 37℃. 3 ml of growth medium (DMEM-F12 supplemented with 10% FCS and 1% penicillin/streptomycin) were added to the solution which was then centrifuged at 800 x g for 5 min. Cells were resuspended in

1 ml growth medium and seeded into a 24-well plate. Hereby, cells originating from one mouse were seeded into one well of a 24-well plate, respectively.

Cultivation of primary mouse VSMCs Isolated primary mouse vascular smooth muscle cells (mVSMCs) were cultivated in DMEM/F12 media supplemented with 10% FCS and 1% penicillin/streptomycin. For passaging, cells were washed with PBS twice and incubated with 0.02% trypsin for 5-7 min. Growth medium was added to stop enzyme activity and cells were either transferred directly to a new cell culture vessel or were centrifuged at 800 x g for 5 min before being resuspended in fresh growth medium. Cells up to passage 4 were used for experiments.

PDGF treatment For gene expression analysis, mVSMCs at passage 3 were seeded into a 12-well plate at 100 000 cells per well and left undisturbed for one day. Growth medium was then changed to serum free DMEM/F-12 medium and left over night. Cells were then treated with 50 ng/ml PDGF-BB (solved in 4 mM HCL containing 0.1% BSA) or vehicle in serum-free medium for 48 h.
For metabolic flux analysis, mVSMCs at passage 3 were seeded into a 12-well plate at 100 000 cells per well and left undisturbed for one day. Growth medium was then changed to serum free DMEM/F-12 medium and left over night. Cells were then treated with 50 ng/ml PDGF-BB or vehicle in serum-free medium for 6 days. They were seeded into 96-well cell culture microplates (Agilent) at a seeding density of 15 000 cells per well and further incubated with PDGF or vehicle. Flux analysis was performed the next day, after 7 days of PDGF treatment in total.

Cholesterol treatment mVSMCs at passage 3 were seeded into a 12-well plate at 100 000 cells per well and left undisturbed for one day. Growth medium was then changed to serum free DMEM/F-12 medium supplemented with 0.2% BSA and left over night. The next day, cells were either treated with 5 µg/ml water-soluble cholesterol (Cholesterol-methyl-β-cyclodextrin) or with vehicle, both in serum free DMEM/F-12 containing 0.2% BSA. For gene expression analysis, cholesterol and vehicle treated cells were lysed and collected after 24 h, 48 h and 72 h, respectively. For metabolic flux analyses cells were seeded into 96-well cell culture microplates (Agilent) at 15 000 cells per well. Cholesterol treatment was then carried out as described above and measurement took place 72 h after addition of cholesterol to the cells.
A7r5 cells were seeded into 6-well plates at 300 000 cells per well and left undisturbed

for one day. Growth medium was then changed to serum free DMEM medium supplemented with 0.2% BSA and left over night. The next day, cells were either treated with 5 µg/ml water-soluble cholesterol (Cholesterol–methyl-β-cyclodextrin) or with vehicle, both in serum free DMEM containing 0.2% BSA. For gene expression analysis, cholesterol and vehicle treated cells were lysed and collected after 24 h and 48 h, respectively. For metabolic flux analyses cells were seeded into 96-well cell culture microplates (Agilent) at 15 000 cells per well. Cholesterol treatment was then carried out as described above and measurement took place 48 h after addition of cholesterol to the cells.

siRNA transfection A7r5 cells were seeded in a 12-well cell culture plate at 100 000 cells per well. Two days after seeding, cells were transfected with 20 nM siRNA following the manufacturer's instructions. 1.5 µl Oligofectamine were added to 6 µl Opti-MEM and incubated for 10 min while siRNA was diluted in Opti-MEM. The Oligofectamine solution was added to the diluted siRNA before incubating for another 20 min at room temperature. Cells were washed once with Opti-MEM and then 400 µl Opti-MEM were dispersed per well. For transfection, 100 µl Oligofectamine and siRNA mix was added to each well. After 6 hours 1.5 ml of growth medium were added to each well. The procedure was repeated the next day for a total of two transfections. For gene expression analysis, cells were analysed 72 h after first transfection. For metabolic flux analyses with the Seahorse XFe96 Analyzer cells were transfected as described above, trypsinised 48 h after first transfection and seeded into Agilent cell culture microplates. Flux analysis was then performed 72 h after transfection.

Proliferation assay For assessing the proliferation of cells with repressed expression of Sirt7, A7r5 cells were seeded and transfected as described above. 48 h after first transfection, cells were trypsinised and seeded into 48-well plates at a density of 20 000 cells per well. The cells were then trypsinised and counted using a MACSQuant flow cytometer after 24 h, 48 h and 72 h. 4 wells were analysed per condition and time point. To account for differences in cell seeding, cell numbers after 24 h were set to 1 and growth rates were calculated based on this value.

2.2.2 Gene expression analysis

RNA isolation, reverse transcription, qPCR RNA isolation was performed with the RNeasy Mini Kit or RNeasy Micro Kit from Qiagen, depending on the starting material. RNA isolation from tissue was always performed with the RNeasy Micro

Kit. Here, the manufacturer's protocol for purification of total RNA from fibrous tissue was used. 3 to 4 mouse carotid arteries or one mouse aorta were placed in 150 µl of the supplied lysis buffer supplemented with 1% β-Mercaptoethanol. Tubes were placed in a TissueLyser which was operated for 4 min at 20 Hz. 295 µl RNase-free water was added to the homogenate as well as 5 µl Proteinase K (20 mg/ml) for a final concentration of 0.33 mg/ml and incubated at 55℃ for 10 min. The solution was centrifuged for 3 min at 10 000 x g at room temperature and the supernatant was transferred to a new tube. RNA isolation, including DNA digestion, was then carried out according to protocol. RNA isolation from mVSMCs was also performed with the RNeasy Micro Kit according to manufacturer's instructions. RNA isolation from A7r5 cells was carried out with the RNeasy Mini Kit. Reverse Transcription (RT) was performed with the High Capacity cDNA Reverse Transcription Kit with addition of RNAse inhibitor according to the manual. TaqMan assays were used to quantify the expression of selected genes (see Table 8 in 2.1.8) in 8-10 ng of cDNA (assayed in duplicate) using the Quantstudio 7 Real-Time-PCR System. Expression of target genes was calculated relative to the expression of a housekeeping gene (Rpl19 for mVSMCs and mouse tissue and Rps11 for rat A7r5 cells) using the comparative ΔCt method. Relative mRNA expression levels are presented as $2^{-\Delta\Delta Ct}$-values.

DNA isolation, qPCR DNA from mouse tissue was isolated using the DNeasy Blood and Tissue Kit. 1-2 carotid arteries were placed in 100 µl of the provided lysis buffer containing 0.6 mg/ml proteinase K and incubated at 56℃ for 2 h. DNA isolation was then performed according to the manufacturer's protocol. Relative copy numbers of nucleic and mitochondrial genes were determined with qPCR using TaqMan assays. Values are shown as Ct value of mitochondrial gene divided by Ct value of nuclear gene.

2.2.3 Metabolic flux analysis

Metabolic flux measurement Metabolic flux analyses were performed with a "Seahorse" XF96e Flux Analyzer. Cells were seeded into the appropriate 96-well cell culture microplates at a seeding density of 10 000 or 15 000 cells per well. The outer ring of wells was left without cells to serve as background measurement. Cells were seeded in their standard growth medium and left to attach overnight. The medium was exchanged to Seahorse Assay Medium one hour before beginning the measurement. Seahorse Assay Medium was prepared by adding glucose, glutamin and pyruvate to Seahorse Basal Medium which consists of unbuffered, phenolred-free

DMEM complemented with 1.85 g/l NaCl and adjusted to pH 7.4. For experiments on primary mVSMCs, 17.5 mM glucose and 2.5 mM glutamine were added to the medium. For experiments on A7r5, 25 mM glucose, 2 mM glutamine and 1 mM pyruvate were used. After exchanging the growth medium to Assay Medium the cell culture microplate was incubated at 37 °C in a non-CO_2 incubator. Sensor plates were hydrated according to the manufacturer's instructions the day before the experiment and left in a non-CO_2 incubator at 37 °C overnight. Ports were loaded with 25 µl of Oligomycin (Port A), FCCP (Port B) and Antimycin A and Rotenone (Port C) each. For experiments on primary mVSMCs, a final concentration of 3 µM Oligomycin, 0.5 µm FCCP, 1.5 µM Rotenone and 1 µM Antimycin A was used. For experiments on A7r5 2 µM Oligomycin, 0.75 µM FCCP, 0.5 µM Rotenone and 0.5 µM Antimycin A was applied to the cells during the measurement. Three data points were acquired for the baseline measurement as well as after addition of oligomycin, FCCP and Rotenone + Antimycin A, respectively. Parameters were calculated as shown in Figure 10 using the Wave software.

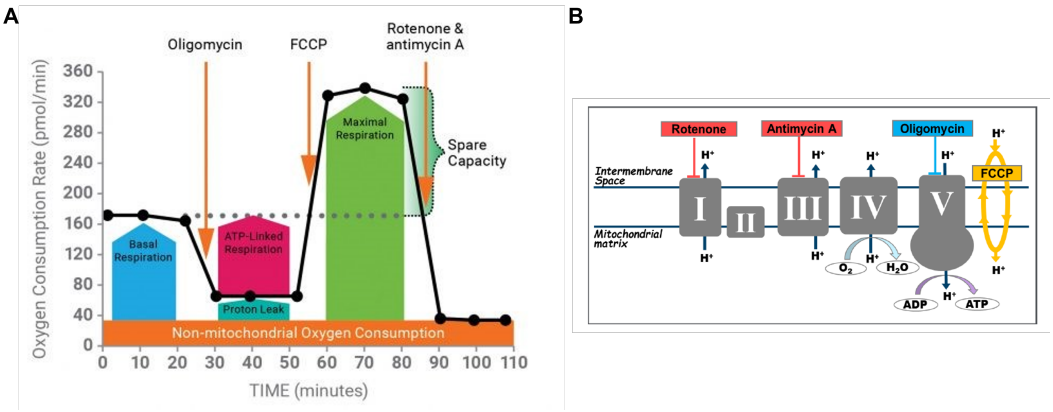

Figure 10 Metabolic flux measurement
A An exemplary metabolic flux measurement is shown. Oxygen consumption rate is measured in pmol/min. Three data points were acquired for the baseline measurement as well as after addition of oligomycin, FCCP and Rotenone + Antimycin A (black line). Basal respiration, ATP-linked respiration, proton leak, maximal respiration, spare respiratory capacity and non-mitochondrial oxygen consumption were calculated as shown. **B** Shown are the functions of the four compounds added during the measurement. Rotenone and Antimycin A are inhibitors of the respiratory complexes I and III, respectively. Oligomycin is an inhibitor of ATP-synthase (complex V) of the respiratory chain. FCCP uncouples oxidative phosphorylation by transporting protons across the mitochondrial membrane. Figure modified from [196].

Normalisation of metabolic flux data Data generated during the metabolic flux analyses were normalised to DNA content per well. For this purpose, the assay medium from the cell culture microplates was removed and the plates were frozen at -20 °C directly after the measurements. DNA content per well could then be determined at a suitable time point. For this, plates were set to thaw at room temperature before adding 50 µl of lysis buffer (10 mM Tris-HCL pH 7.4, 1 mM EDTA, 0.1% Triton X-100) to each well and placing the plate on a shaker for 30 min. The lysate was transferred to individual tubes which were placed on ice and in order to make sure to collect all the cells from the well, another 50 µl of lysis buffer was added to the wells. The plate was then placed at -20 °C for 30 min until the buffer was frozen, thawed again and placed on a shaker for another 30 min. The lysis buffer containing the remaining lysed cells was then combined with the previously obtained 50 µl of lysate to generate a total of 100 µl of lysate from each well. Next, 0.1 mg/ml proteinase K was added to each tube which were then incubated for 2 h at 50 °C. The DNA content was then measured with the Quant-iT™ PicoGreen™ dsDNA Assay Kit in 25 µl of the lysate in duplicate. Oxygen consumption rates and extracellular acidification rates obtained during the metabolic flux measurements were then normalised to the DNA content in each well.

2.2.4 Flow cytometry

Staining and analysis of mitochondria with flow cytometry For the analysis of mitochondria with Mitotracker™ Deep Red, cells were isolated from carotid arteries, stained and analysed with flow cytometry. Carotid arteries, taken from mice that underwent carotid artery ligation surgery, were sliced into small pieces and then digested with 1 mg/ml collagenase II and 0.5 mg/ml elastase in serum-free DMEM/F12 for 3 h 30 min at 37 °C. Released cells were then centrifuged, resuspended and tissue debris was filtered with a cell strainer. Cells were then stained with 5 nM Mitotracker™ Deep Red FM in serum-free DMEM/F12 for 15 min, spun down and resuspended in 500 µl serum-free DMEM/F12. The fluorescence intensity of the stained cells was then measured with a CyAn ADP Analyzer flow cytometer.

Sorting of VSMCs with FACS For cell sorting, carotid arteries and aorta were dissected from mice and connective tissue was removed. The vessels were cut into small cross-sections and were placed in enzyme solution (serum-free DMEM/F12 with 1 mg/ml collagenase II and 0.5 mg/ml elastase) for 3 h 30 min at 37 °C. Released cells were then centrifuged, resuspended and tissue debris was filtered with a cell

strainer. Cells were centrifuged again, resuspended in 500 µl of PBS and sorted with an Aria II cell sorter according to their displayed fluorescence from the mT/mG reporter construct.

2.2.5 Electron microscopy

Carotid arteries of 8-week old wildtype mice were ligated as described below. 4 weeks after ligation mice were euthanized and the vessels were perfused via the left ventricle with 10 ml PBS and 10 ml fixing solution containing 2.5% glutaraldehyde. Ligated and control carotid arteries were then dissected, connective tissue was removed and the vessels were cut in half longitudinally. The two halves were placed and stored in fixating solution for at least 24 h. Further processing of the tissue was then performed at the core facility for electron microscopy at Charité, Berlin. The samples were postfixed with 1% osmium tetroxide and 0.8% potassium ferrocyanide II in 0.1 M cacodylate buffer for 1.5 h at room temperature. The samples were then dehydrated in a graded ethanol series and embedded in Epon resin. Ultrathin sections of the samples (70 nm) were stained with 4% uranyl acetate and Reynolds lead citrate. Images were taken with a Zeiss EM 906 electron microscope at 80 kV acceleration voltage. Images were analysed with ImageJ software. Cell boundaries and mitochondrial shapes were tracked manually of which area and circularity were calculated by the software. Mitochondrial number was calculated per visible cell area.

2.2.6 Animal models

At all times, mice were housed in a 12 h dark/ 12 h light cycle at a constant room temperature (22℃) and had access to food and water ad libitum. All conducted animal experiments described in the following were approved (G0202/13, G0150/15 and G0139/19) by the local authority (Landesamt für Gesundheit und Soziales, Berlin, Germany) and performed according to the guidelines of Charité University Medicine Berlin.

Mouse strains All the mouse strains used in this study were created by in-house breeding of existing mouse strains which are briefly described in the following. The origins of these strains and where they were obtained is summarised in Table 4 in 2.1.4.

SMMHC-CreER^{T2} (SM) This transgenic mouse strain expresses a fusion protein of the cre recombinase with a modified estrogen receptor binding domain (CreER^{T2}) under the control of the smooth muscle myosin heavy chain (SMMHC) promoter. SMMHC is almost exclusively expressed in smooth muscle cells and is therefore considered a specific marker for VSMCs. This means that after treating these mice with tamoxifen and thus activating the cre recombinase, cre-mediated recombination occurs exclusively in smooth muscle cells. This construct is therefore used for smooth muscle cell specific genetic modifications like knock-outs of genes of interest [192].

mT/mG These mice have a cell membrane-targeted, two-colour fluorescent cre-reporter allele. Prior to cre-mediated recombination, cell membrane-localised td-Tomato (mT) fluorescence protein is expressed in all cells and tissues. Upon recombination the red fluorescence is replaced by cell membrane-localised EGFP (mG) fluorescence in cre recombinase expressing cells and all new cells derived from these cells [193].

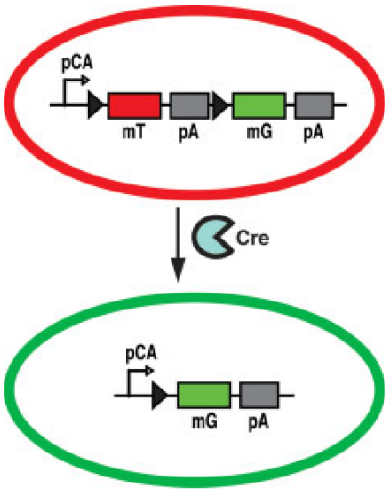

Figure 11 The mT/mG construct before and after cre-mediated recombination
Shown is a schematic overview of the mT/mG construct before and after cre-mediated recombination. The mT/mG construct contains a chicken β-actin core promoter with a CMV enhancer (pCA). The promoter drives a membrane-targeted tandem dimer Tomato (mT) sequence which results in the expression of membrane localised tdTomato. The sequence is flanked by loxP sites for cre-mediated recombination, represented by triangles. Upon cre-mediated recombination, the mT sequence is cut and the pCA promoter then drives the expression of membrane-targeted enhanced green fluorescent protein (mG) instead. pA stands for polyadenylation sequence. Figure taken from [193].

Sirt6 flox The exons 4-6 of the Sirt6 gene are flanked by loxP sites. Upon cre-mediated recombination they are eliminated from the gene [194].

Sirt7 flox The exons 6-9 of the Sirt7 gene are flanked by loxP sites. Upon cre-mediated recombination they are eliminated from the gene [195].

ApoE$^{-/-}$ These mice have a global knock-out of the ApoE$^{-/-}$ gene. For more information see section 2.2.6 Atherosclerosis mouse model.

SM-mT/mG This mouse strain was created by crossing the SMMHC-CreER^{T2} and the mT/mG line to serve as a genetic lineage tracing mouse model. Membranous tandem dimer Tomato fluorescent protein, tdTomato (mT), is globally expressed in all cells. Upon cre-mediated recombination, tdTomato is silenced in VSMCs expressing SMMHC and membranous enhanced green fluorescent protein (EGFP) is expressed instead. This results in permanent labelling of VSMCs with EGFP while all other cells continue expressing tdTomato. All progeny of the thus labelled VSMCs will also express EGFP.

All mouse strains used in this study were created by crossing the respective lines. Details on the different genotypes are shown in Table 12.

Table 12 Overview of mouse strains

Gene	SMMHC-CreER^{T2}	Sirt6	Sirt7	mT/mG	ApoE$^{-/-}$
C57BL/6	-	wt	wt	-	-
SM-mT/mG	+	wt	wt	+	-
SM-Sirt6-wildtype	+	wt	wt	-	-
SM-Sirt6-floxed	+	floxed	wt	-	-
SM-Sirt6-wildtype-mT/mG	+	wt	wt	+	-
SM-Sirt6-floxed-mT/mG	+	floxed	wt	+	-
SM-Sirt6-wildtype-ApoE$^{-/-}$	+	wt	wt	-	+
SM-Sirt6-floxed-ApoE$^{-/-}$	+	floxed	wt	-	+
SM-Sirt7-wildtype	+	wt	wt	-	-
SM-Sirt7-floxed	+	wt	floxed	-	-
SM-Sirt7-wt-mT/mG	+	wt	wt	+	-
SM-Sirt7-floxed-mT/mG	+	wt	floxed	+	-
SM-Sirt7-wildtype-ApoE$^{-/-}$	+	wt	wt	-	+
SM-Sirt7-floxed-ApoE$^{-/-}$	+	wt	floxed	-	+
SM-Sirt7-wildtype-ApoE$^{-/-}$-mT/mG	+	wt	wt	+	+
SM-Sirt7-floxed-ApoE$^{-/-}$-mT/mG	+	wt	floxed	+	+

Induction of cre recombinase with Tamoxifen Tamoxifen was diluted in Mygliol at 20 mg/ml and was dissolved by continuous rotation for at least three hours. Once prepared the solution was protected from light and could be stored up to one week at 4℃. Mice were given 1 mg Tamoxifen per mouse per day for five consecutive days. After disinfection of the injection site Tamoxifen injections were given intraperitoneal alternately into the left and right lower quadrant of the abdomen to minimise scarring. During long-term atherosclerosis experiments, Tamoxifen injection was repeated after 6 weeks.

Carotid artery ligation model The carotid artery ligation model is a highly feasible, reproducible model to investigate vascular smooth muscle cell behaviour in response to injury in mice as well as the controlling factors thereof. In this model, complete ligation of the common carotid artery induces smooth muscle cell dedifferentiation, proliferation and migration. Smooth muscle cells migrate across the internal elastic lamina, forming a neointima in the vessel. Gene expression changes and vascular remodelling start immediately after ligation and a stable lesion is formed within 3 to 4 weeks. Lineage-tracing studies have shown that the majority of neointimal cells are derived of medial vascular smooth muscle cell origin, demonstrating the highly plastic nature of smooth muscle cells and showing the lack of other cell types, like invading immune cells, in the neointima [197].

Important features of this model include lumen narrowing by neointimal lesion formation and by constrictive remodelling of the artery with maintenance of an intact endothelium, low levels of mechanical injury and no major inflammatory response. This allows for investigation of factors controlling vascular remodelling as well as smooth muscle cell phenotypic plasticity in a non-inflammatory environment. In addition, the carotid artery ligation model is technically simple and relatively easy to perform which leads to a high reproducibility of the vascular remodelling and neointima formation.
Although highly reproducible, the extent of the neointima formation can be dependent on the used mouse strain [198]. In general, however, the extent of generated neointima decreases with distance from the ligation. In wild-type mice, for example, the most severe neointima formation usually occurs within the first 500 µm of the ligation. Due to the constrictive nature of the remodelling process in this model, cross sections of the artery will display wavy elastic lamellae as in Figure 12 [199, 200].

For changes in gene expression and VSMC proliferation, arteries are examined at earlier time points. In this study, gene expression analysis and investigation of mitochondria was carried out at 3 and 7 days after ligation, respectively. As the composition of the neointima will continue to change a few weeks after ligation, neointimal size is usually examined at later times. In this study, intimal lesion size was assessed 4 weeks after ligation. There is a variety of factors and mediators that control the remodelling and neointimal response, including growth factors, adhesion molecules, transcriptional regulators, cytokine and hormone signaling and many more. An overview can be found in a review by Peterson et al. [197].

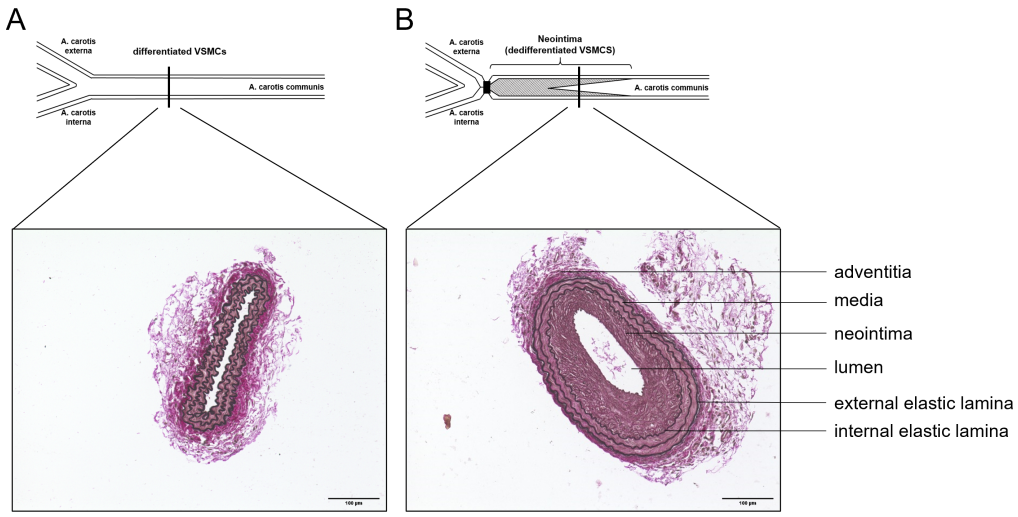

Figure 12 Carotid artery ligation
Shown are representative cross sections of **A** the right sham-ligated common carotid artery which serves as control and **B** the left common carotid artery 4 weeks after ligation

Carotid artery ligation - procedure In this model for smooth muscle cell dedifferentiation, the left carotid artery (carotis communis) was ligated directly below the bifurcation at the distal end of the vessel. Anesthesia was performed with an intraperitoneal injection of Ketamin 10% (0.1 µl/g body weight) and Xylazin 2% (0.05 µl/g body weight). Mice were placed onto a heating pad to preserve body temperature and salve was applied for eye protection. After hair removal a midline cervical incision was made and the left carotid artery was exposed. It was ligated directly below the bifurcation at the distal end of the vessel with a 7.0 silk thread. The wound was flushed with NaCl and the skin was sutured with a 6.0 silk thread. Animals were kept under a heating lamp until recovery and pain medication was applied when necessary.

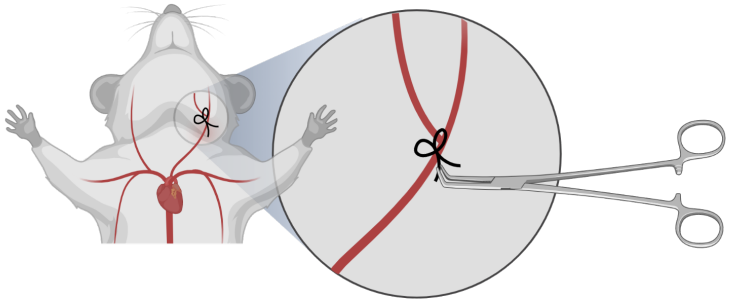

Figure 13 Carotid artery ligation - procedure
For the carotid artery ligation model, the left carotid artery (carotis communis) was ligated directly below the bifurcation at the distal end of the vessel as shown. Figure created with BioRender [201].

Atherosclerosis mouse model The mouse model for atherosclerosis used in this study is the apolipoprotein E knock-out ($ApoE^{-/-}$) model. In this model, $ApoE^{-/-}$ knock-out mice develop hypercholesterolemia and subsequently develop atherosclerotic lesions. Apolipoprotein E is synthesised by the liver and several peripheral tissues and cell types, including macrophages. It has various functions, like efficient hepatic uptake of lipoproteins, stimulation of cholesterol efflux from macrophage foam cells in the atherosclerotic lesion, and the regulation of immune and inflammatory responses [23]. ApoE deficient mice display poor lipoprotein clearance which leads to accumulation of cholesterol particles in the blood, promoting the development of atherosclerotic plaques. ApoE deficient mice are frequently used to study the initiation, pathophysiology and progression of atherosclerosis [24]. An example of an atherosclerotic plaque in a $ApoE^{-/-}$ knock-out mice in this study is presented in Figure 14. In this study, for atherosclerosis experiments, the plaque development was analysed in the brachiocephalic artery (BCA) which is sometimes considered a surrogate for human coronary plaques [202].

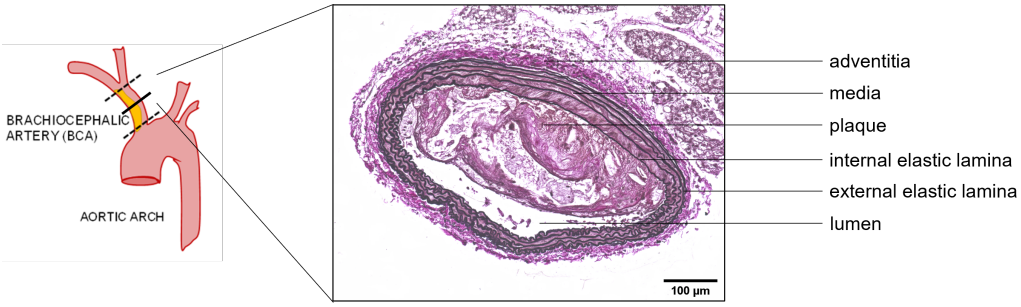

Figure 14 Atherosclerosis mouse model
Shown is an atherosclerotic plaque in a cross section from the brachiocephalic artery (BCA) of an ApoE$^{-/-}$ mouse fed a high fat diet for 12 weeks.

Sirt6 8-week-old SM-Sirt6-wildtype-ApoE$^{-/-}$ and SM-Sirt6-floxed-ApoE$^{-/-}$ mice were injected with tamoxifen for five consecutive days (see 2.2.6). From the following week onward, the mice were then fed a Western type diet containing 21.2% butter fat and 0.3% cholesterol (TD88137 mod., ssniff, Soest, Germany) for 12 weeks. Tamoxifen was injected again during week 6 of the experiment. General health and body weight of the mice were monitored weekly.
After 12 weeks tissues were harvested and processed as described below. Analysis of plaque sizes was carried out in paraffin sections.

Sirt7 8-week-old SM-Sirt7-wildtype-ApoE$^{-/-}$ and SM-Sirt7-floxed-ApoE$^{-/-}$ mice were subjected to the same regimen as Sirt6-ApoE$^{-/-}$ mice (see above). Tissues were also harvested after 12 weeks and processed as described below. Analysis of plaque sizes was also carried out in paraffin sections.

Sirt7-mT/mG 8-week-old SM-Sirt7-wildtype-ApoE$^{-/-}$-mT/mG and SM-Sirt7-floxed-ApoE$^{-/-}$-mT/mG mice were subjected to the same regimen as Sirt6-ApoE$^{-/-}$ and Sirt7-ApoE$^{-/-}$ mice (see above). After 12 weeks tissues were harvested and processed as described below. In contrast to the two experiments above, the analysis of plaque sizes was carried out in cryosections instead of paraffin sections in order to preserve fluorescence.

2.2.7 Processing of animal samples

Tissue harvesting - Carotid artery ligation model Mice were euthanized and vessels were perfused with 10 ml PBS and 10 ml fixating solution (4% paraformaldehyde, Roti-Histofix) via the left ventricle. Carotid arteries were dissected under a stereomicroscope and connective tissue was removed. Carotids were fixed in PFA for 24 h and then stored in 70% ethanol. Tissue harvesting for electron microscopy is described in 2.2.5.

Tissue harvesting - Atherosclerosis mouse model Mice were euthanized and blood was withdrawn from the heart. Serum was obtained by centrifugation at 8000 x g for 10 min. Vessels were flushed with 0.9% NaCl via left ventricular perfusion. Carotid arteries were dissected under a stereomicroscope and connective tissue was removed. For later generation of paraffin sections, carotids were fixed in PFA for 24 h and then stored in 70% ethanol before being embedded in paraffin. For cryosections, vessels were fixed in 4% PFA (Roti-Histofix) for 1 h on ice, then washed in cold PBS three times and embedded in Tissue-Tek O.C.T. Compound. For this, carotids were placed longitudinally into cryomolds, covered with O.C.T. compound, frozen on dry ice and stored at -80℃.

Determination of serum lipid levels Cholesterol and triglyceride concentrations in serum samples from Western type diet fed mice were measured using enzymatic colorimetric assays (Fluitest CHOL and TG) according to the manufacturer's instructions. For measuring of triglycerides (TG), serum samples were diluted 1 to 5 in 0.9% NaCl. For determination of total cholesterol serum levels, samples were diluted 1 to 10 before assaying. Preceding the concentration measurement of high-density lipoprotein cholesterol (HDL-C), apolipoprotein B (apoB)-containing lipoproteins were removed with phosphotungstate magnesium precipitation. Briefly, 40 µl of serum were mixed with 4 µl sodium phosphotungstate solution (40 g/l of phosphotungstic acid in 160 mM NaOH) and 1 µl 2 M $MgCl_2$ and centrifuged at 8000 x g for 10 min at 4℃ for separation. HDL-C was measured in the supernatant.

Histological analysis of tissues

Paraffin Left and right carotid arteries from ligation and atherosclerosis experiments were dehydrated and embedded in paraffin type 9 and cut into cross sections of 5 µm. Ligated left carotid arteries were cut starting from the point of ligation. The first

unobstructed view of the whole artery circumference below the ligating knot was set as 0 and the vessel was cut continuously from there. For atherosclerosis experiments the brachiocephalic artery (BCA) was analysed. Sections were cut beginning from the proximal side of the BCA and ended with the branching of the right subclavial artery. For morphological assessment, sections were stained with an Elastica Van Giesson staining kit. Elastic Van Giesson staining was performed according to manufacturer's instructions:

5 min	NeoClear
5 min	NeoClear
1 min	98% ethanol
1 min	80% ethanol
1 min	70% ethanol
1 min	60% ethanol
2 min	deionised water
10 min	elastic stain iodine solution
	3x rinsing in deionised water
2 min	ferric chloride solution
1 min	rinsing in tap water
1 min	95% ethanol
	rinse in deionised water
1 min	van Giesson solution
	dip in 95% ethanol
1 min	99% ethanol
5 min	NeoClear
5 min	NeoClear

Briefly, slides were hydrated, stained with elastic stain iodine solution and then differentiated in ferric chloride solution before being stained with van Giesson solution. Sections were then dehydrated again and slides were mounted with NeoMount mounting medium. Images were taken with the BZ 9000 microscope.

Cryosections Vessels were embedded and frozen as described above. Cryosections were made at -20℃ with 5 µm thickness. In preparation for imaging, sections were thawed, left to dry for a few minutes and then fixed in ice-cold acetone for 10 min at -20℃. Slides were washed in PBS once and then stained with 0.5 µg/ml DAPI in PBS for 10 min in the dark. After washing in PBS, slides were mounted with

Vectashield Antifade Mounting Medium and images were taken with the BZ 9000 microscope.

Analysis of histological sections of carotid arteries from carotid artery ligation model Cross sections from carotid arteries were analysed at predetermined intervals. The first unobstructed view of the whole artery circumference below the ligating knot was set as 0 and the vessel was cut and analysed continuously from there. Sections at 100 µm, 200 µm, 400 µm, 700 µm, 1000 µm, 1500 µm, 2000 µm and 3000 µm distance from starting point 0 were analysed. The neointimal area in ligated carotid arteries was measured by manually tracking the elastica interna and the vessel lumen using the ImageJ software (for illustration see Figure 12). Sections with signs of complete thrombotic occlusion of the artery were excluded from the analysis. Two sections were analysed per distance and the mean neointima size was plotted against the distance from the starting point. The area under the curve (AUC) was calculated to obtain the neointima volume.

Analysis of histological sections of the BCA from the atherosclerosis mouse model For atherosclerosis experiments the brachiocephalic artery (BCA) was analysed. Cross sections were cut beginning from the proximal side of the BCA and ended with the branching of the right subclavial artery. Sections at 0 µm, 100 µm, 200 µm, 300 µm, 400 µm, 500 µm, 600 µm, 700 µm, 800 µm and 900 µm were analysed from the BCA. Plaque sizes were also measured by manually tracking each plaque. Two sections were analysed per distance and the mean plaque size was plotted against the distance from the starting point. The area under the curve (AUC) was calculated to obtain the plaque volume.

2.2.8 Statistical Analysis

Data analysis was performed using Prism (GraphPad) software version 7. All data are represented as individual values, mean ± standard deviation or mean ± standard error of the mean (SEM). Outliers, identified using the ROUT method (Q=1%), were excluded. Comparison between two groups was made using unpaired or paired Student's t-test as indicated. Prerequisite for Student's t-tests was the confirmation of normal distribution of the data with D'Agostino and Pearson tests. Comparisons between more than two groups were made using two-way analysis of variance (ANOVA) followed by Tukey's or Dunnett's multiple comparison test.
A p-value < 0.05 was considered statistically significant.

3 Results

To investigate the mutual effects of VSMC dedifferentiation and metabolic adaptation of VSMCs, two approaches were taken. First, VSMCs were prompted to dedifferentiate in a number of different *in vitro* and *in vivo* models and the resulting changes in cell metabolism were observed. Second, the impact of known regulators of cell metabolism, namely Sirtuin 6 and Sirtuin 7, on VSMC dedifferentiation was investigated.

3.1 Effects of VSMC dedifferentiation on metabolism

3.1.1 Effects of PDGF treatment on VSMC dedifferentiation and metabolism

Different *in vitro* models and one *in vivo* model of VSMC dedifferentiation were used to assess the shifts in metabolic pathways occurring after prompting VSMCs to dedifferentiate. An *in vitro* model for VSMC dedifferentiation was set up according to previously published protocols that used platelet-derived growth factor (PDGF) to prompt smooth muscle cells to dedifferentiate (Figure 15A). It is known that the dedifferentiation process manifests among other changes in a reduced expression of VSMC marker genes α-smooth muscle actin (α-SMA) and myosin heavy chain 11 (Myh11). As a proof of concept after setting up the PDGF driven *in vitro* model for dedifferentiation, the expression of these genes was analysed after 48 h of PDGF treatment compared to vehicle control. As expected, the expression of both genes decreased significantly, to 0.37 ± 0.04 for α-SMA and 0.27 ± 0.05 for Myh11 (Figure 15B).

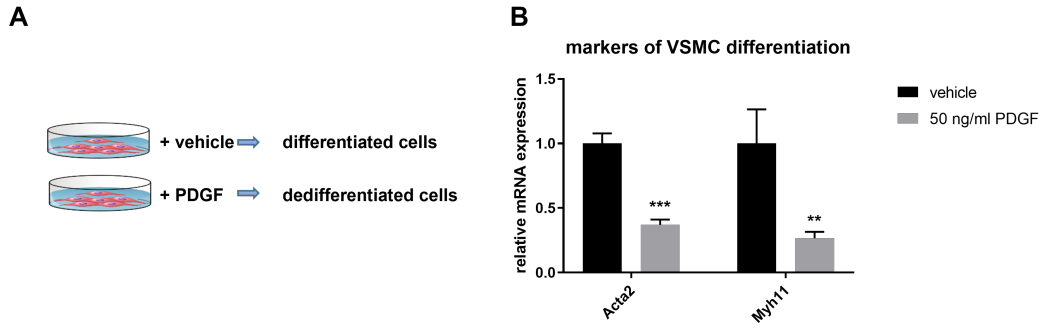

Figure 15 Relative mRNA expression of smooth muscle cell marker genes in mVSMCs after treatment with PDGF
A Primary mouse vascular smooth muscle cells (mVSMCs) were grown in serum-free media for 24 h before being treated with either vehicle or 50 ng/ml platelet-derived growth factor (PDGF) for 48 h **B** Relative mRNA expression of smooth muscle marker genes was analysed by RT-qPCR. Data are shown as mean ± standard deviation. Three independent experiments were carried out (n=3). mVSMCs were isolated from 3-4 mice and pooled for each experiment. ** $p < 0.01$, *** $p < 0.001$ indicate significance versus vehicle by Student's t-test.

In a previous experiment in the working group, the expression pattern in differentiated versus dedifferentiated VSMCs was acquired with a proteomics approach. For this, VSMCs directly isolated from mouse aortas and carotid arteries were compared to previously isolated VSMCs that were cultured and treated with PDGF for several days. As expected, protein levels of VSMC markers, including Myh11, Acta2, SM-22α and calponin were severely reduced or not detectable in PDGF treated cells versus freshly isolated cells. Interestingly, there was a major shift in expression levels of proteins involved in cell metabolism. Most prominent was a drop in the abundance of mitochondrial proteins after PDGF treatment. From this experiment, the hypothesis that VSMC phenotypic transition is accompanied by an adaption of the metabolism towards the requirements of the respective phenotype, was generated.
Aiming to confirm and further develop the results from this proteomics-based approach, the expression of genes involved in metabolic pathways that were regulated in those experiments were tested in the PDGF driven *in vitro* model using RT-qPCR (Figure 16).

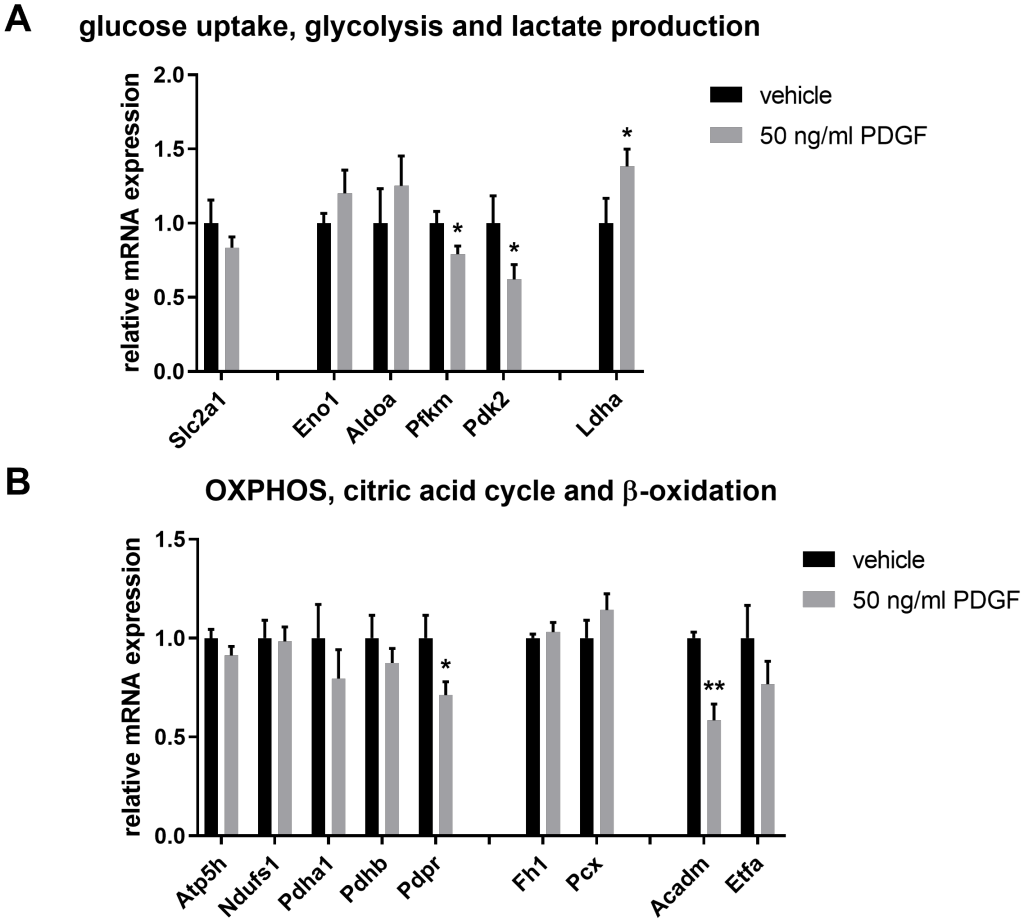

Figure 16 Relative mRNA expression of metabolic genes in mVSMCs after treatment with PDGF

Primary mVSMCs were grown in serum-free media for 24 h before being treated with either vehicle or 50 ng/ml PDGF for 48 h. Relative mRNA expression of genes involved in **A** glucose uptake, glycolysis and lactate production as well as **B** genes involved in oxidative phosphorylation (OXPHOS), the citric acid cycle and β-oxidation was analysed by qPCR. Data are shown as mean ± standard deviation. Three independent experiments were carried out (n=3). mVSMCs were isolated from 3-4 mice and pooled for each experiment. * $p < 0.05$, ** $p < 0.01$ indicate significance versus vehicle by Student's t-test.

After 48 h of PDGF treatment, expression of the glycolytic genes Aldolase A (Aldoa) and Enolase 1 (Eno1) was upregulated to 1.25 ± 0.2 and 1.2 ± 0.16, respectively. Lactate dehydrogenase (Ldha) expression was elevated significantly to 1.38 ± 0.12. (Figure 16A) Expression of Ndufs1, encoding the largest subunit of NADH dehydrogenase type I and Atp5h, part of the ATP synthase, was not altered in this model of PDGF driven dedifferentiation. The same was true for Fumarate hydratase 1 (Fh1) and Pyruvate carboxylase (Pcx), both enzymes of the citric acid cycle. Acyl-CoA dehydrogenase medium chain (Acadm) was significantly less expressed (0.59 ± 0.08 -fold)

after 48 h of PDGF treatment. Expression of the three subunits of Pyruvate dehydrogenase Pdpr, Pdhb and Pdha1 was also lowered (Figure 16B).
These results largely correlated with the results obtained in the proteomics-based approach. Expression of glycolytic enzymes and Ldha was upregulated while expression of genes involved in OXPHOS, the citric acid cycle and β-oxidation was lowered in PDGF treated cells compared to vehicle control.

To investigate whether this changed expression of genes related to glycolysis and mitochondrial oxidation also has an impact on the overall cell metabolism, cells were analysed for oxygen consumption and extracellular acidification, an indicator of lactate production, with an XFe Flux Analyzer. Following treatment with PDGF or vehicle for 7 days, the oxygen consumption rate (OCR) and extracellular acidification rate (ECAR) of these cells was measured. In addition to measuring the basal rate, different compounds were added to inhibit specific metabolic pathways. First added was oligomycin, an inhibitor of ATP synthase (complex V of the mitochondrial respiration chain), then FCCP, an uncoupler of mitochondrial oxidative phosphorylation and lastly rotenone and antimycin A, complex I and complex III inhibitors, respectively. Figure 17A shows the unprocessed data for the measured OCR after 7 days of treatment with either vehicle or PDGF. Important parameters calculated from the obtained curve are shown in Figure 17E. Cells grown with PDGF displayed a higher basal respiration as well as higher maximal respiration (185 ± 49 vs. 109 ± 36 pmol/min), spare respiratory capacity (117 ± 27 vs. 65 ± 35 pmol/min) and ATP production. ECAR was also elevated in PDGF treated cells throughout the whole measurement compared to control (Figure 17C).

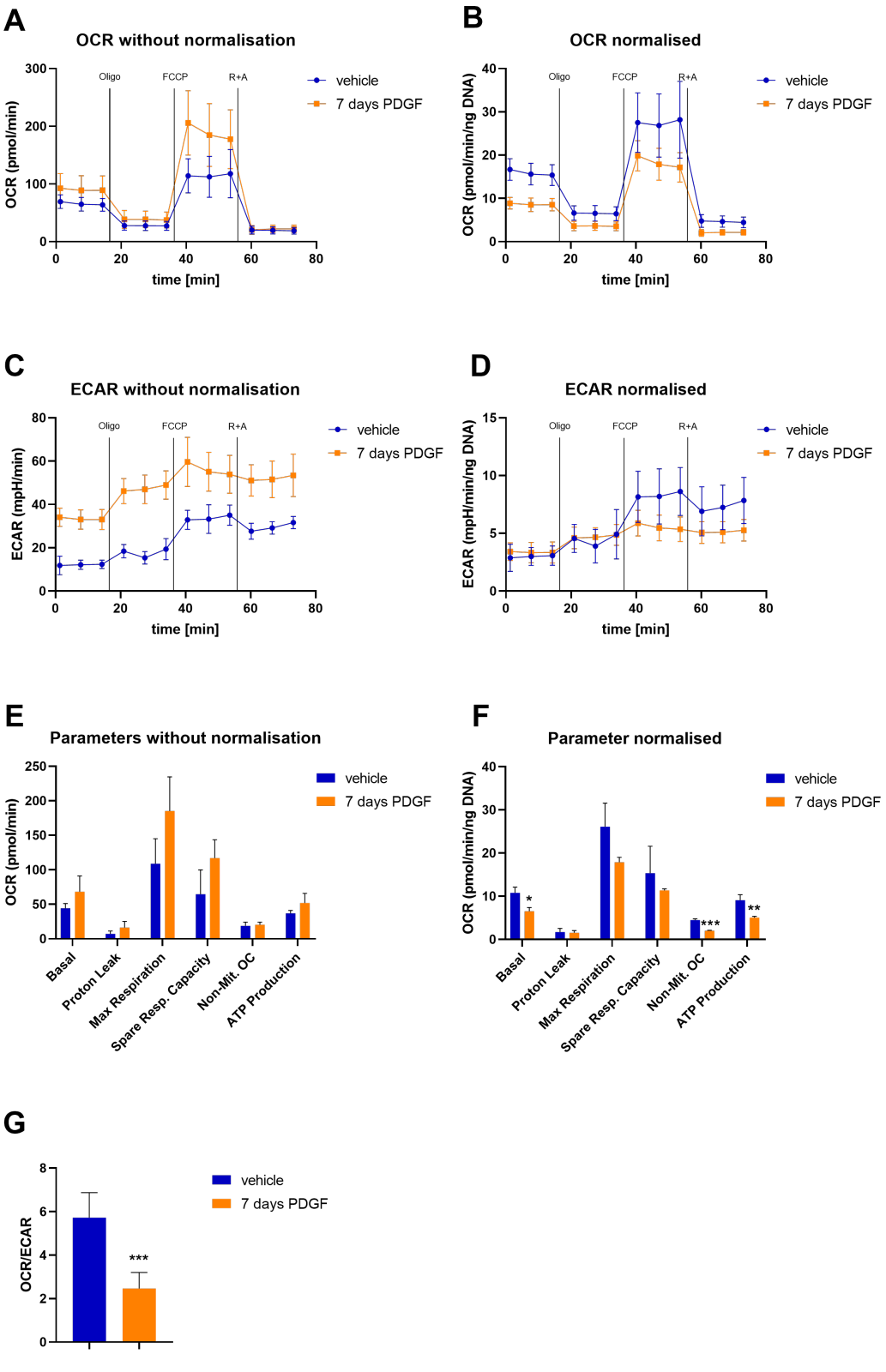
A
OCR without normalisation
OCR (pmol/min)
time [min]
Oligo
FCCP
R+A
vehicle
7 days PDGF
B
OCR normalised
OCR (pmol/min/ng DNA)
C
ECAR without normalisation
ECAR (mpH/min)
D
ECAR normalised
ECAR (mpH/min/ng DNA)
E
Parameters without normalisation
Basal
Proton Leak
Max Respiration
Spare Resp. Capacity
Non-Mit. OC
ATP Production
F
Parameter normalised
G
OCR/ECAR
***

Figure 17 XFe Flux Analysis of VSMCs after 7 days of PDGF treatment
Oxygen consumption rate (OCR) and extracellular acidification rate (ECAR) were measured with an XFe96 Flux Analyzer in primary VSMCs that received 50 ng/ml PDGF or vehicle for 7 days before as well as during the measurement. Oligomycin (Oligo), FCCP and rotenone and antimycin A (R+A) were added at indicated timepoints during the measurement. **A** OCR measured over time and **B** normalised to DNA content. **C** ECAR measured over time and **D** normalised to DNA content. **E** Parameters calculated from OCR values over time from non-normalised curve (A) as well as **F** parameters calculated from OCR values over time from normalised curve (B). **G** OCR over ECAR ratios calculated from basal values. Data are shown as mean ± standard deviation. At least three independent experiments were performed (n=3). * $p < 0.05$, ** $p < 0.01$, *** $p < 0.001$ indicate significance versus vehicle by Student's t-test.

However, it is a known feature of the method that the measurement largely correlates with the number of cells present in the observed wells. Therefore, different normalisation methods are employed. Here, the normalisation was based on the amount of DNA in each well, measured with a Quant-iT™ PicoGreen™ DNA Assay Kit. Upon normalisation the results looked reversed. Basal respiration was then significantly lower in PDGF treated cells compared to control. Non-mitochondrial oxygen consumption and ATP production were both significantly reduced by 54% and 44%, respectively. Other parameters such as maximal respiration and spare respiratory capacity were also reduced in PDGF treated cells (Figure 17F). Normalised ECAR values did not show any difference between treatment and control until FCCP injection during the measurement whereupon the acidification rate in control cells was higher than in PDGF treated cells (Figure 17D). Figure 17G shows the OCR/ECAR ratio calculated from the basal values for OCR and ECAR which was significantly different in PDGF treated cells compared to the control (2.5 vs. 5.7).

3.1.2 Effects of cholesterol treatment on VSMC dedifferentiation and metabolism

The second *in vitro* model of VSMC dedifferentiation was cholesterol-driven. Treatment of VSMCs with cholesterol has been previously reported to result in VSMC transdifferentiation towards a macrophage-like phenotype [100].

Here, isolated primary mouse VSMCs were treated with cholesterol or vehicle for 24 h, 48 h and 72 h, respectively (Figure 18A). As illustrated in Figure 18B, expression of the VSMC marker genes α-SMA and Myh11 was already reduced after 24 h treatment and declined further the longer the treatment lasted. In contrast, expression of macrophage marker genes CD68 (microsialin) and Lgals3 (galectin-3, also known as galactose binding lectin 3 or Mac-2), was elevated consistently after 24 h, 48 h and 72 h of cholesterol treatment compared to control. The expression of ABC transporter Abca1 was also strongly increased upon cholesterol treatment.

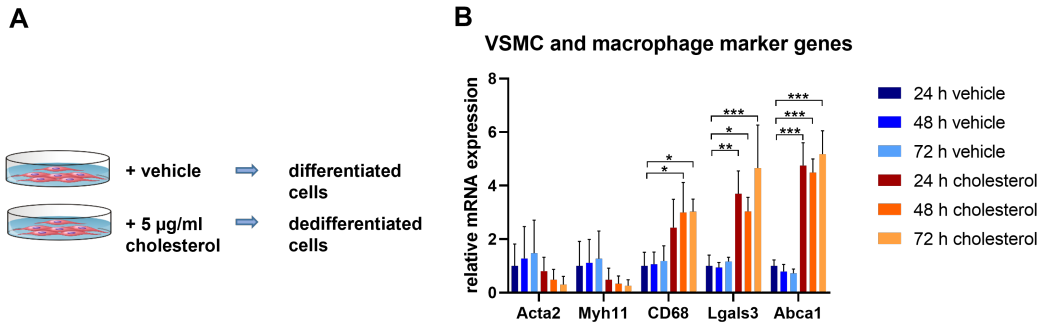

Figure 18 Relative mRNA expression of smooth muscle cell and macrophage marker genes in mVSMCs after treatment with cholesterol

A Primary mVSMCs were grown in serum-free media for 24 h before being treated with either vehicle or 5 µg/ml cholesterol for 24 h, 48 h and 72 h, respectively. **B** Relative mRNA expression of smooth muscle cell and macrophage marker genes was analysed by RT-qPCR. Data are shown as mean ± standard deviation. Three independent experiments were carried out (n=3). mVSMCs were isolated from 3-4 mice and pooled for each experiment.* $p < 0.05$, ** $p < 0.01$, *** $p < 0.001$ indicate significance versus 24 h vehicle by Two-way ANOVA followed by Dunnett's multiple comparisons test.

As with the PDGF driven model, the expression of genes involved in metabolic pathways upon cholesterol treatment was analysed.

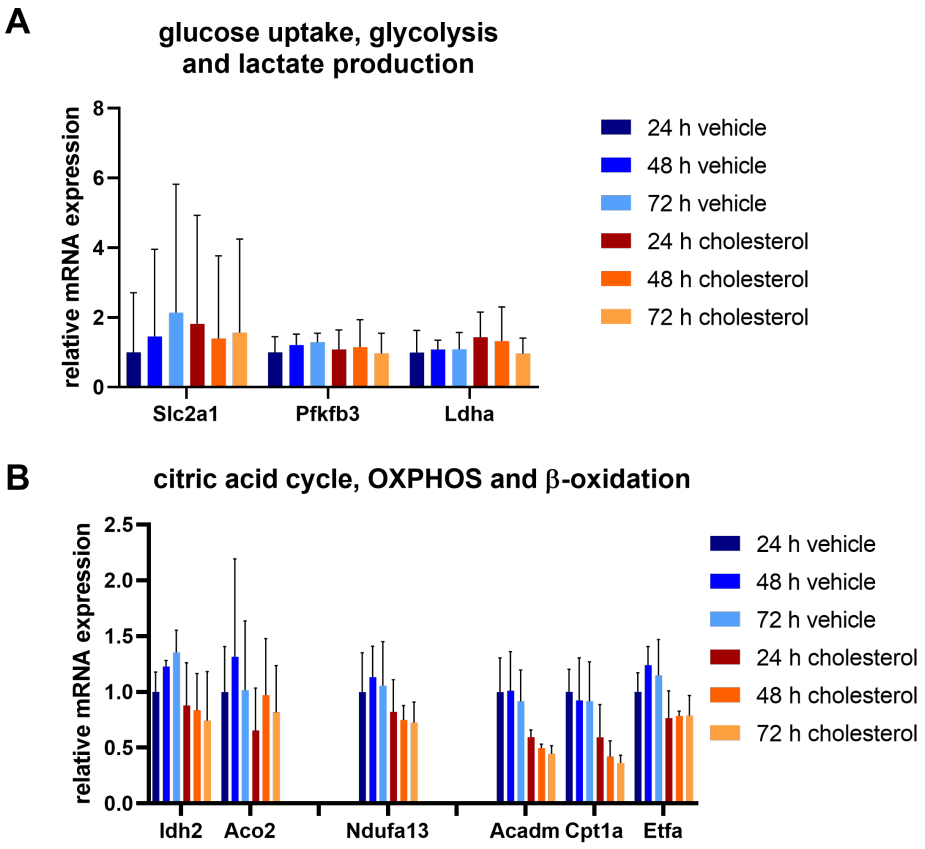

Figure 19 Relative mRNA expression of metabolic genes in mVSMCs after treatment with cholesterol
Primary mVSMCs were grown in serum-free media for 24 h before being treated with either vehicle or 5 µg/ml cholesterol for 24 h, 48 h and 72 h, respectively. Relative mRNA expression of genes involved in **A** glucose uptake, glycolysis and lactate production as well as **B** genes involved in oxidative phosphorylation (OXPHOS), the citric acid cycle and β-oxidation was analysed by RT-qPCR. Data are shown as mean ± standard deviation. Three independent experiments were carried out (n=3). mVSMCs were isolated from 3-4 mice and pooled for each experiment.

When looking at genes involved in glucose uptake, glycolysis and lactate production, expression of Slc2a1 (coding for glucose transporter 1 (Glut1)) and of Pfkfb3 (6-phosphofructo-2-kinase/fructose-2,6-biphosphatase 3) was not significantly changed while there was a slight trend of increased lactate dehydrogenase expression after 24 h and 48 h of treatment (Figure 19A). However, expression of isocitrate dehydrogenase 2 (Idh2) and aconitase 2 (Aco2), enzymes in the citric acid cycle, was reduced upon cholesterol treatment. The same was true for the expression

of NADH dehydrogenase subunit 13 (Ndufa13) in the respiration chain which was lowered to 0.72 ± 0.19 as well as acyl-Coenzyme A dehydrogenase medium chain (Acadm), carnitine palmitoyltransferase 1A (Cpt1a) and electron-transfer-flavoprotein alpha subunit (Etfa), all playing a role in fatty acid oxidation. Acadm expression was reduced to 0.44 ± 0.07, Cpt1a expression to 0.36 ± 0.07 and Etfa expression to 0.79 ± 0.18.

Along the lines of the analyses of the PDGF-driven VSMC dedifferentiation model, flux analyses were also performed for the cholesterol-driven transdifferentiation model. Figure 20 illustrates that there were no major differences in oxygen consumption rate between cholesterol treated and control cells. All calculated parameters such as maximal respiration, spare respiratory capacity and ATP production were not significantly different between groups. Normalisation to DNA content did not result in any larger shift in the data. Extracellular acidification rate before as well as after normalisation was consistently elevated in cholesterol-treated compared to control cells (Figure 20C and D). The OCR/ECAR ratios calculated from basal values were significantly different between both groups (6.9 control vs. 4.0 cholesterol) (Figure 20G).

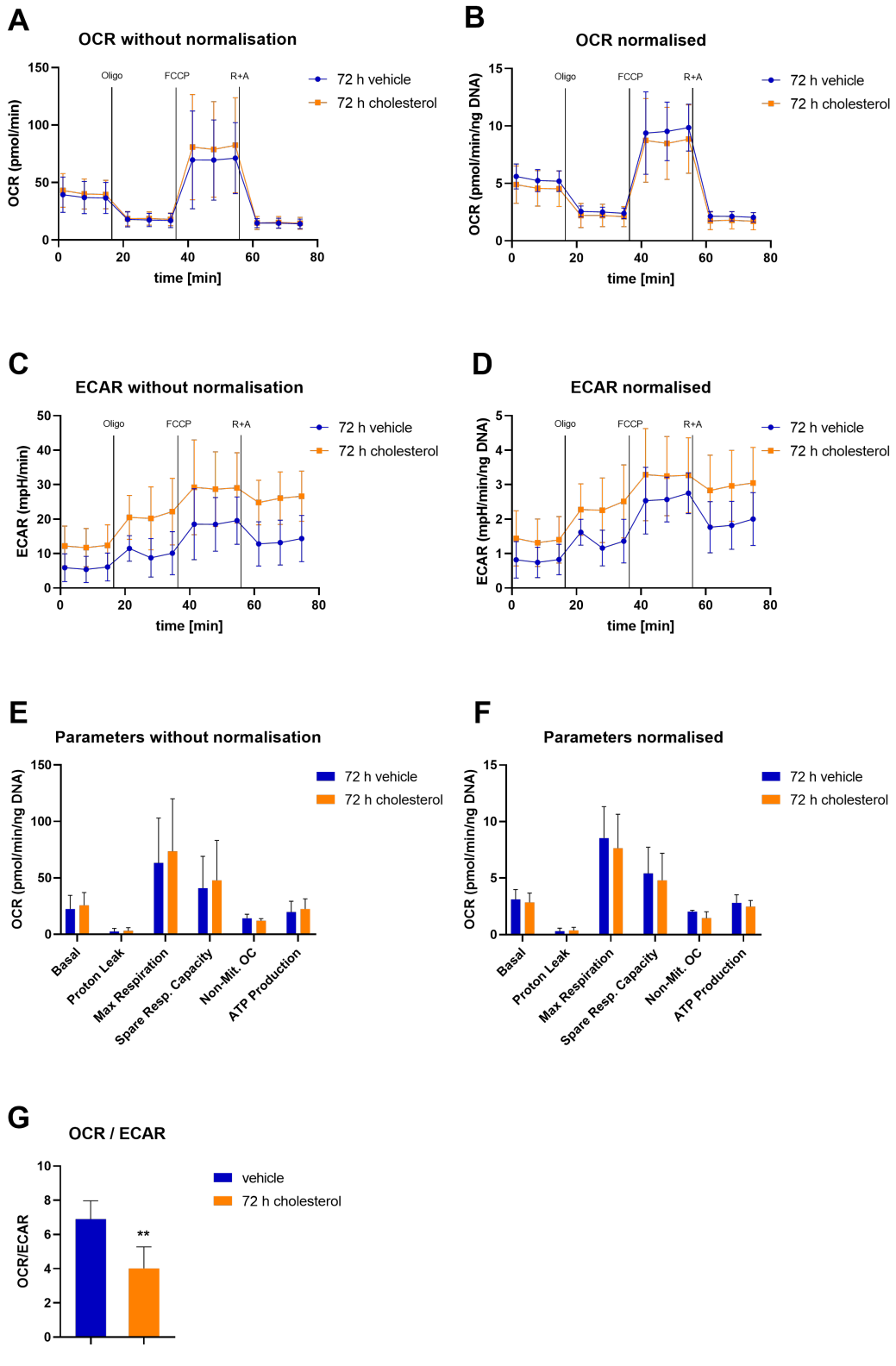
A
OCR without normalisation
OCR (pmol/min)
time [min]
Oligo
FCCP
R+A
72 h vehicle
72 h cholesterol
B
OCR normalised
OCR (pmol/min/ng DNA)
C
ECAR without normalisation
ECAR (mpH/min)
D
ECAR normalised
ECAR (mpH/min/ng DNA)
E
Parameters without normalisation
F
Parameters normalised
Basal
Proton Leak
Max Respiration
Spare Resp. Capacity
Non-Mit. OC
ATP Production
G
OCR / ECAR
OCR/ECAR
vehicle
72 h cholesterol
**

Figure 20 XFe Flux Analysis of VSMCs after 72 h of cholesterol treatment
Oxygen consumption rate (OCR) and extracellular acidification rate (ECAR) were measured with an XFe96 Flux Analyzer in primary VSMCs that were incubated with 5 µg/ml cholesterol or vehicle for 72 h before the measurement. Oligomycin (Oligo), FCCP and rotenone and antimycin A (R+A) were added at indicated timepoints during the measurement. **A** OCR measured over time and **B** normalised to DNA content. **C** ECAR measured over time and **D** normalised to DNA content. **E** Parameters calculated from OCR values over time from non-normalised curve (A) as well as **F** parameters calculated from OCR values over time from normalised curve (B). **G** OCR over ECAR ratios calculated from basal values. Data are shown as mean ± standard deviation. At least three independent experiments were performed (n=3). ** $p < 0.01$ indicate significance versus vehicle by Student's t-test.

3.1.3 *In vivo* effects of VSMC dedifferentiation on metabolism

Analyses of gene expression upon carotid artery ligation Following the *in vitro* experiments, the next aim was to confirm and expand those results in an *in vivo* model of VSMC dedifferentiation. For this, a carotid artery ligation mouse model was employed. In this experimental system, the left common carotid artery (arteria carotis communis) is ligated directly below the carotid bifurcation, where the common carotid artery divides into internal and external carotid arteries (see 2.2.6). This ligation disrupts the blood flow in that area which subsequently leads to a dedifferentiation and immigration of VSMCs into the intima of the vessel, forming the so-called neointima (see 2.2.6 and Figure 21A).

For the following analyses, tissue from the ligated left carotid artery was compared to the right carotid artery, which served as control.

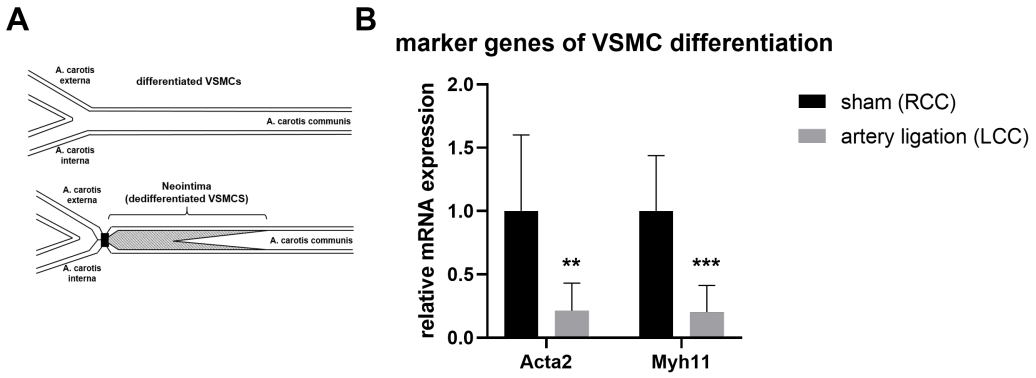

Figure 21 Relative mRNA expression of smooth muscle cell marker genes 3 days after carotid artery ligation
A The left common carotid artery (artery carotis communis) of 8 week-old mice was ligated directly below the carotid bifucation where the common carotid artery divides into internal and external carotid arteries. The right carotid artery was left in its orinigal state and served as internal control. **B** Relative mRNA expression of VSMC marker genes was analysed in ligated left carotid arteries (artery ligation (LCC)) vs. control right carotid arteries (sham (RCC)) by qPCR 3 days after surgery. Data are shown as mean ± standard deviation. Three indepent experiments were performed (n=3). For each experiment, RNA was isolated from LCCs and RCCs from 3-4 mice. ** $p < 0.01$, *** $p < 0.001$ indicate significance versus sham (RCC) by Student's t-test.

As a first experiment, the carotid arteries of wildtype mice were ligated and the tissue harvested 3 days post surgery for RT-qPCR analysis. Since one carotid artery does not render sufficient tissue material for RNA isolation and subsequent qPCR analysis carotid arteries from three individual mice were pooled and analysed. As a proof of concept, it was first checked whether the VSMC marker genes α-SMA and Myh11 were downregulated in the ligated vessel.
As presented in Figure 21B, expression of both VSMC marker genes was largely decreased three days after surgery compared to control. Both, expression of α-SMA and Myh11 was reduced to 0.2 ± 0.2. From this, it is evident that a major part of the VSMCs in the vessel undergo a dedifferentiation process.

After confirming that ligation of the artery sets dedifferentiation processes in motion, the expression of further genes was investigated.

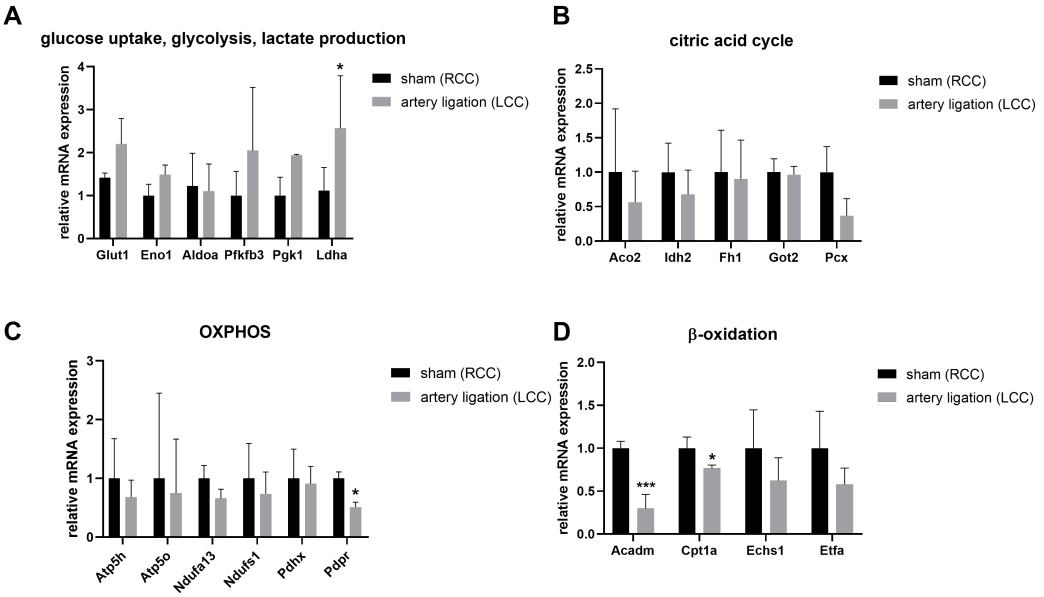

Figure 22 Relative mRNA expression of metabolic genes 3 days after carotid artery ligation

Relative mRNA expression of genes involved in **A** glucose uptake, glycolysis and lactate production, **B** genes involved in the citric acid cycle, **C** genes involved in oxidative phosphorylation (OXPHOS) and **D** genes involved in β-oxidation was analysed in ligated left carotid arteries (artery ligation (LCC)) vs. control right carotid arteries (sham (RCC)) by RT-qPCR 3 days after surgery. Data are shown as mean ± standard deviation. 3-6 experiments were performed (n=3-6). For each experiment, RNA was isolated from LCCs and RCCs from 3-4 mice. * $p < 0.05$, *** $p < 0.001$ indicate significance versus sham (RCC) by Student's t-test.

Figure 22A shows the mRNA levels of genes encoding for proteins and enzymes in glucose uptake and glycolytic activity. Expression of the genes Pfkfb3 and Pgk1, encoding 6-phosphofructo-2-kinase/fructose-2,6-biphosphatase 3 and phosphoglycerate kinase 1 was elevated to 2 and 1.9, respectively. Similarly, the expression of Slc2a1 encoding the glucose transporter 1 (Glut1) was increased to 1.4 while the largest shift in expression was found for lactate dehydrogenase A (Ldha) which was expressed 2.3-fold in tissue from the ligated arteries.

The expression of enzymes from the citric acid cycle was lowered to 0.56 and 0.7 for Idh2 and Aco2. Expression levels of glutamatic-oxaloacetic transaminase 2 (Got2) and fumarate hydratase 1 (Fh1) were not altered significantly (Figure 22B).

The expression of genes encoding subunits of different respiratory chain complexes NADH:ubiquinone oxidoreductase subunit A13 (Ndufa13) and NADH:ubiquinone oxidoreductase core subunit S1 (Ndufs1), ATP synthase, H+ transporting, mitochondrial F1 complex, O subunit (Atp5o) and pyruvate dehydrogenase complex,

component X (Pdhx) was decreased in the carotid artery tissue after ligation (Figure 22C).
Figure 22D shows the results for genes involved in the β-oxidation process. Expression of Cpt1a, enoyl Coenzyme A hydratase short chain 1 (Echs1) and Etfa was reduced to 0.77, 0.62 and 0.58. The strongest decrease in expression level was found for Acadm with a reduction to 0.3.
Overall, there was an increase in expression of genes involved in glucose uptake and glycolysis while genes encoding for enzymes in the citric acid cycle, fatty acid oxidation and for components of the respiratory chain complexes were down-regulated.

3.1.4 Analysis of mitochondrial abundance upon carotid artery ligation

The decreased expression of several genes encoding for enzymes in the citric acid cycle, fatty acid oxidation and for components of the respiratory chain complexes led to the assumption that the processes induced by the artery ligation have a direct or indirect impact on the cells' mitochondria. A series of experiments was performed to investigate whether the down regulation of mRNA expression led to fewer mitochondria or if mitochondrial integrity was affected. One means to investigate the abundance of mitochondria in cells is to determine the amount of mitochondrial DNA present in the cell and normalize this to the nuclear DNA. This relies on the fact that there are as many copies of mitochondrial DNA present in the cell as there are mitochondria while there is only one copy of nuclear DNA.

Employing the carotid artery ligation model again (Figure 23A), tissue was collected 4 weeks after surgery from which DNA was isolated and analysed with qPCR. For measuring mitochondrial DNA the amount of NADH dehydrogenase 1 (mt-Nd1) gene was determined while eukaryotic translation elongation factor 2 (Eef2) represented the nuclear DNA.

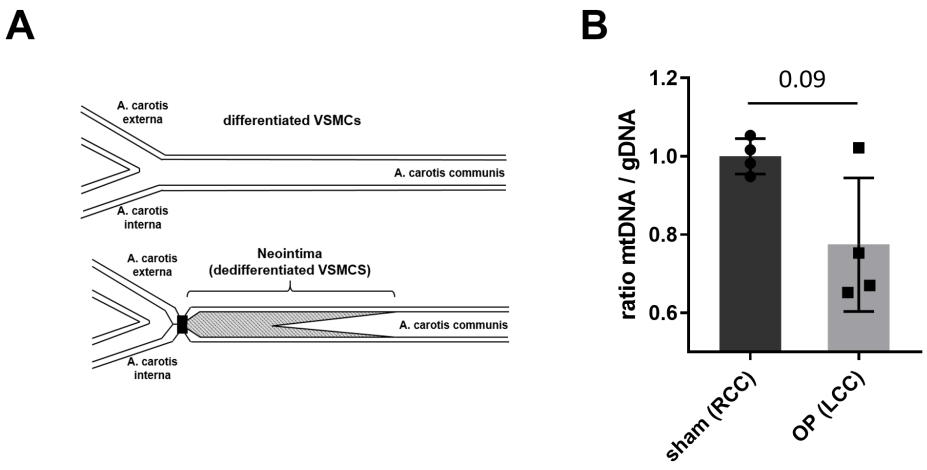

Figure 23 Amount of mitochondrial DNA 4 weeks after carotid artery ligation
A The left common carotid artery (arteria carotis communis) of 8-week-old mice was ligated directly below the carotid bifurcation where the common carotid artery divides into internal and external carotid arteries. The right carotid artery was left in its original state and served as internal control. **B** The amount of DNA for the mt-Nd1 gene, representing mitochondrial DNA (mtDNA), and the amount of DNA for the Eef2 gene, representing nuclear genomic DNA (gDNA), was determined in ligated left carotid arteries (artery ligation (LCC)) vs. control right carotid arteries (sham (RCC)) by qPCR 4 weeks after surgery. The ratio of mt-Nd1/Eef2 was calculated and shown here as ratio mtDNA/gDNA. Data are shown as mean ± standard deviation. 4 experiments were performed (n=4). For each experiment, DNA was isolated from LCCs and RCCs from 1-2 mice. p=0.09 versus sham (RCC) by Student's t-test.

Figure 23B shows that 4 weeks after ligation the mtDNA to nuclear DNA ratio decreased by 25% to 0.85. The calculated p-value is 0.09 suggesting there might be a significant difference in comparison to the control.

As a second approach to determine the abundance of mitochondria in dedifferentiated VSMCs, mitochondria were stained with MitoTracker™Deep Red FM and cells were analysed with flow cytometry. For this experiment, ligated and sham operated carotid arteries were harvested 7 days after surgery and digested to release individual cells which were then stained with MitoTracker™Deep Red FM to label mitochondria. In order to be able to differentiate between vascular smooth muscle cells and other cell types like endothelial cells that are also released from the tissue by the enzymatic digestion, a genetic lineage tracing mouse model (SM-mT/mG) was used here. Membranous red fluorescent protein (mTomato) is globally expressed in all cells. Upon Cre-mediated recombination, mTomato is silenced in VSMCs expressing SMMHC and membranous green fluorescent protein GFP is expressed instead. This results

in labelling of VSMCs with GFP while all other cells continue expressing mTomato. Thus, VSMCs from tissue taken from these mice can be identified with flow cytometry.

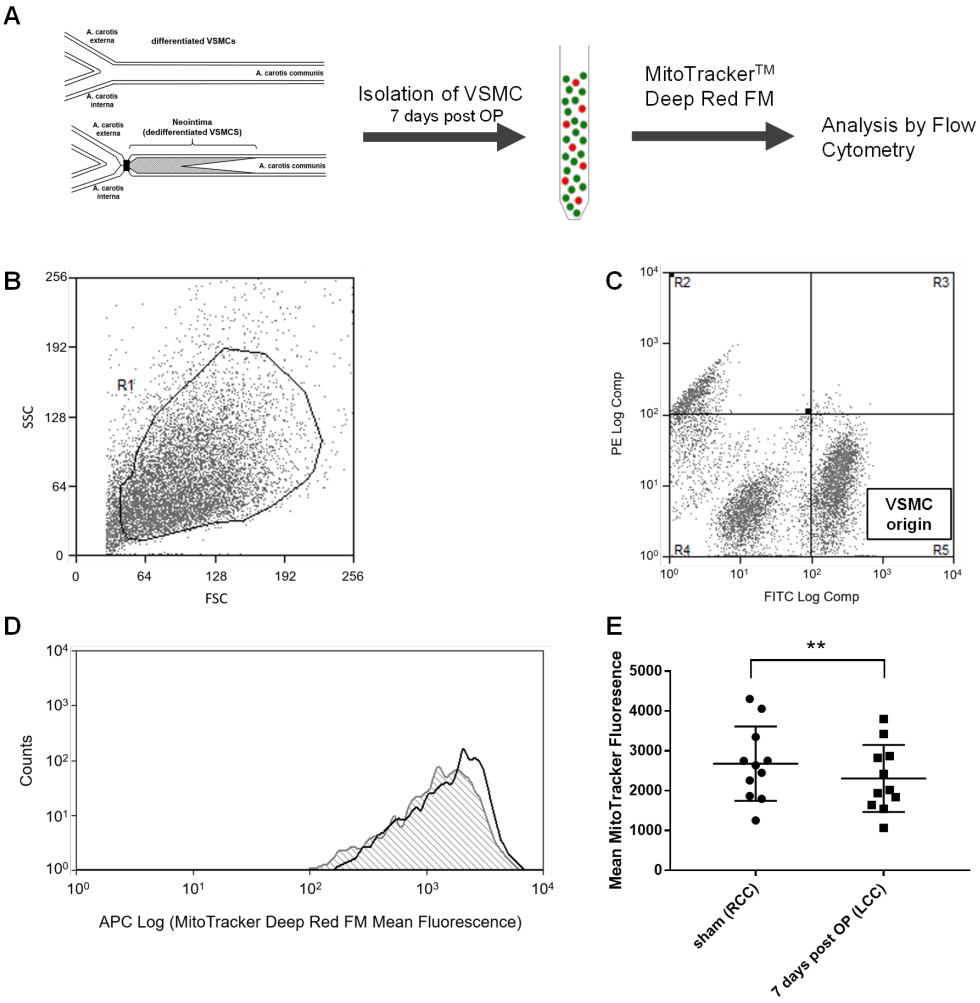

Figure 24 Mitochondrial abundance 7 days after carotid artery ligation
A The left common carotid artery (arteria carotis communis) of 8 week-old mice was ligated directly below the carotid bifurcation where the common carotid artery divides into internal and external carotid arteries. The right carotid artery was left in its original state and served as internal control. 7 days after surgery, vessels were digested to release cells from the tissue which were then stained with MitoTracker™ Deep Red FM and analysed by flow cytometry. **B** Forward vs. Side scatter: Only cells from Gate R1 were used for further analyses **C** Red fluorescence as PE compensated versus the GFP fluorescence as FITC compensated: Cells accumulating in the upper left quadrant (R2) display red fluorescence and accordingly are not from VSMC origin while cells in the lower right quadrant (R5) display green fluorescence and are thus from VSMC origin. **D** MitoTracker™ Deep Red staining of cells from R5 only **E** Mean MitoTracker Fluorescence from cells isolated from sham operated carotids (control) vs. ligated carotid arteries 7 days after surgery. Data are shown as individual values and mean ± standard deviation. n=11, ** $p < 0.01$ indicate significance versus sham (RCC) by paired Student's t-test.

Figure 24C shows the red fluorescence as PE compensated versus the GFP fluorescence as FITC compensated. Cells accumulating in the upper left quadrant display red fluorescence and accordingly are not from VSMC origin while cells in the lower right quadrant display green fluorescence and are thus from VSMC origin. Cells in the lower left quadrant which show little red and little green fluorescence, were shown to be dead cells by DAPI staining. Cells with VSMC origin (from the lower right quadrant) were analysed for MitoTracker™Deep Red staining (Figure 24D). Figure 24E shows the mean MitoTracker fluorescence for cells from ligated carotid arteries (LCC) compared to cells from control vessels (RCC). 7 days after ligation, cells from ligated arteries showed significantly less fluorescence compared to control.

To gain further insight into how the ligation-induced dedifferentiation of VSMCs influenced mitochondria, electron microscopy was employed. Electron microscopy allows a closer look at the size, shape and integrity of mitochondria. Figure 25 shows the different morphologies of ligated vessels and control vessels. Figure 25A i) and ii) illustrate how the control vessel is comprised of the adventitia or outer layer, the tunica media which contains the VSMCs and an endothelial layer on the lumen side of the vessel. Elastic fibers run through the vessel and stabilise it. Differentiated VSMCs are positioned longitudinally between the fibers and thus display an elongated, stretched out phenotype (Figure 25A ii)). In the ligated vessels, dedifferentiated VSMCs newly form the neointima which then extends between the media and the endothelium. As can be observed in Figure 25A i) and ii) VSMCs in the neointima did not display any uniform orientation but are scattered throughout the new layer. In the larger 12930x magnification (iii-v) it becomes evident that VSMCs from the media in the control vessels and VSMCs in the neointima in ligated vessels displayed a very different phenotype. While VSMCs in the media were elongated, spindly and quite large, VSMCs in the neointima appeared smaller, more circular and did not show consistent orientation. Mitochondria in the two different cell types displayed similar qualities. Mitochondria in differentiated VSMCs in the media were more elongated than in dedifferentiated VSMCS in the neointima. This is also reflected in the significantly higher circularity that was determined by analysing mitochondria in both cell types (Figure 25D). This different shape however, did not affect the overall size of the mitochondria (Figure 25C). Since electron microscopy is only two-dimensional, the size that is given here is equal to the area measured and does not provide any information on the actual volume of the mitochondria. In addition to mitochondrial area and circularity, mitochondria were also counted. Since cells often were not

completely depicted in one image, mitochondrial number was not calculated per cell but per visible cell area (Figure 25E). There was no difference in number of mitochondria per cell area detected.

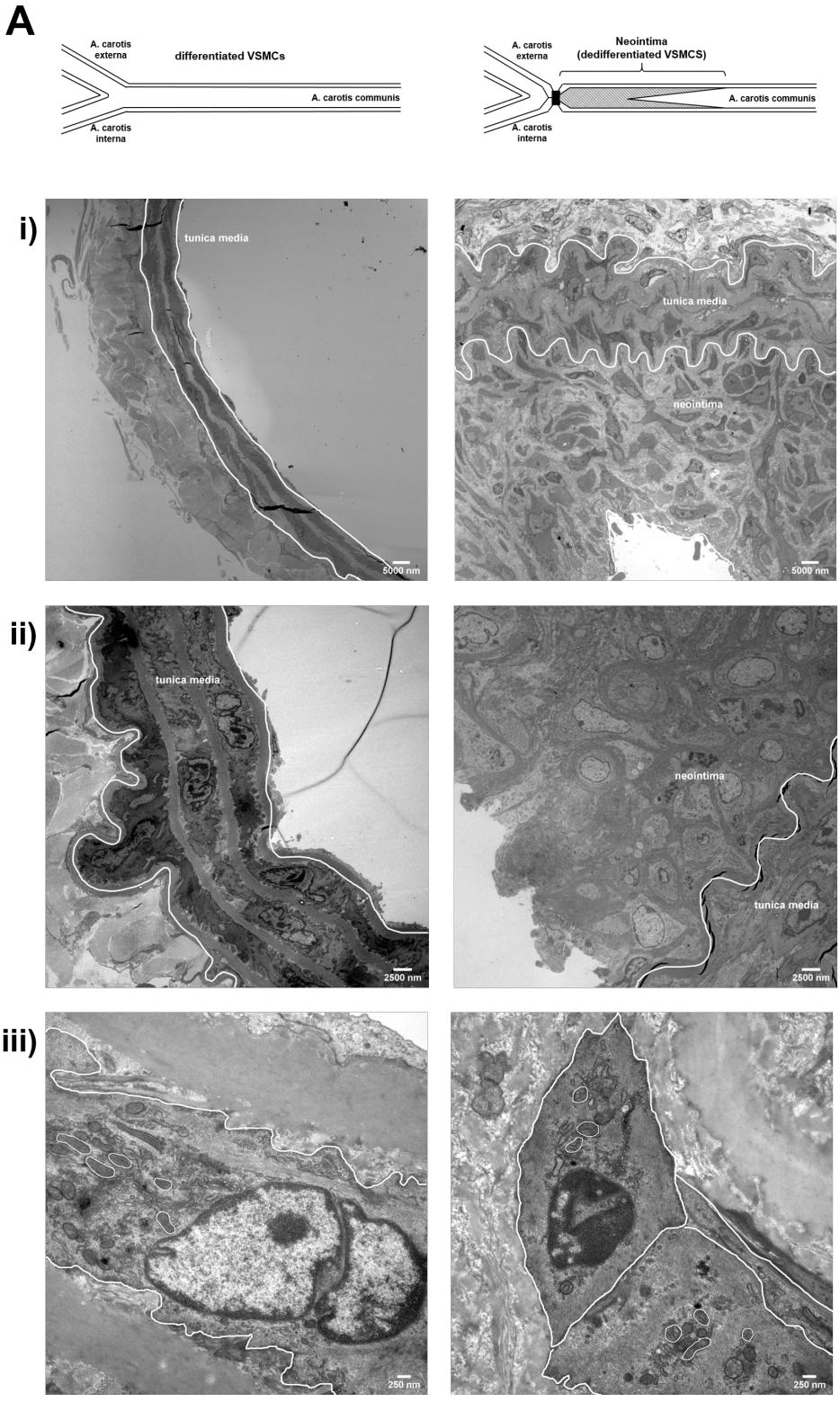
A
A. carotis externa
differentiated VSMCs
A. carotis communis
A. carotis interna
A. carotis externa
Neointima (dedifferentiated VSMCS)
A. carotis communis
A. carotis interna
i)
tunica media
5000 nm
tunica media
neointima
5000 nm
ii)
tunica media
2500 nm
neointima
tunica media
2500 nm
iii)
250 nm
250 nm

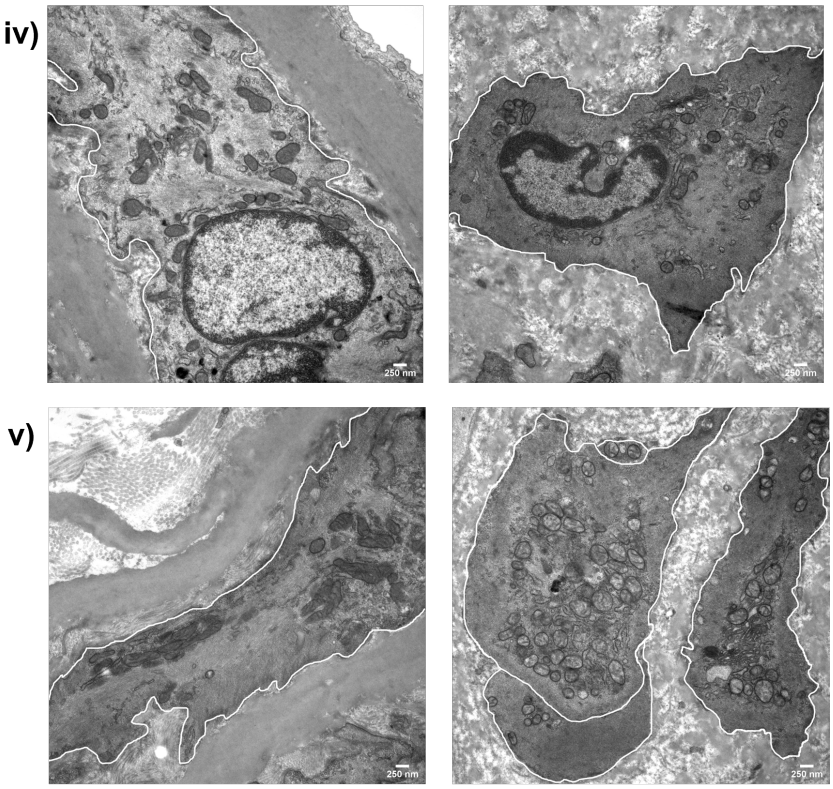

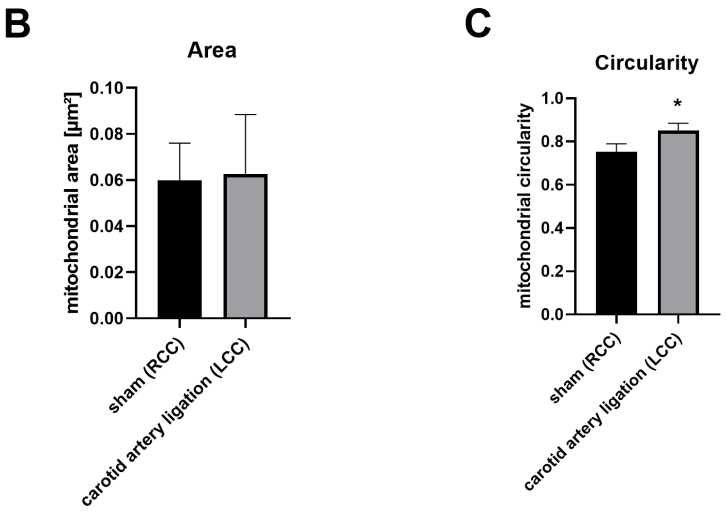

D

	sham (RCC)	carotid artery ligation (LCC)
number/cell area	1,2	1,1
	0,8	0,3
	0,7	0,8
mean	**0,9**	**0,7**
SD	0,26	0,40

Figure 25 Mitochondrial size, shape and number 4 weeks after carotid artery ligation **A** The left common carotid artery (arteria carotis communis) of 8 week-old mice was ligated directly below the carotid bifurcation. The right carotid artery was left in its original state and served as internal control. Sections of ligated and control vessels were imaged with electron microscopy 4 weeks after surgery. **i)** 775x magnification of control vessel (left) and ligated vessel (right), white lines indicate respective tissue layers **ii)** 1670x magnification of control vessel (left) and ligated vessel (right), white lines indicate respective tissue layers **iii-v)** 12930x magnification of control vessel (left) and ligated vessel (right), white lines indicate cell boundaries and mark mitochondria **B** mean mitochondrial size (area) in cells from control and ligated vessels **C** mean circularity of mitochondria in cells from control and ligated vessels **D** number of mitochondria per cell area in three control vessels and three ligated vessels. Data are shown as mean ± standard deviation. Carotids from three mice were analysed (n=3). 50 pictures were analysed per condition. * $p < 0.05$ indicate significance versus sham (RCC) by Student's t-test.

3.2 The role of Sirtuin 6 and Sirtuin 7 in VSMC dedifferentiation

Histone deacetylases sirtuin 6 (Sirt6) and sirtuin 7 (Sirt7) are known regulators of cell metabolism. Sirt6 has been shown to play a major role in the regulation of glycolytic genes. Sirt7 was identified as an important regulator of mitochondrial biogenesis mediated through its impact on GA-binding protein (GABP)β1, a master regulator of nuclear-encoded mitochondrial genes. Global Sirt7 deficiency in mice has been shown to induce multi-systemic mitochondrial dysfunction. As the activity of these sirtuins depends on the citric acid cycle intermediate NAD as a substrate, they are also considered as sensors of cellular nutritional demands that regulate metabolism accordingly (see 1.6). Due to this sensitivity towards the metabolic state of cells and their own functional role in regulation metabolism, Sirt6 and Sirt7 are interesting targets to investigate in the context of VSMC dedifferentiation and the concomitant shift in metabolism explored in 3.1.

3.2.1 Effect of VSMC dedifferentiation on Sirt6 and Sirt7 expression

As a first step, the cholesterol-driven *in vitro* model of VSMC dedifferentiation was utilized to investigate whether dedifferentiation affects the expression of Sirt6 and Sirt7 (Figure 26A). mRNA levels of Sirt6 and Sirt7 were slightly but not significantly lowered in cells that were treated with cholesterol.
In addition to the *in vitro* model, this question was also addressed in the *in vivo* artery ligation model (Figure 26B). Here, a moderate decrease of Sirt6 expression as well as a slight increase in Sirt7 expression was found three days after surgery.

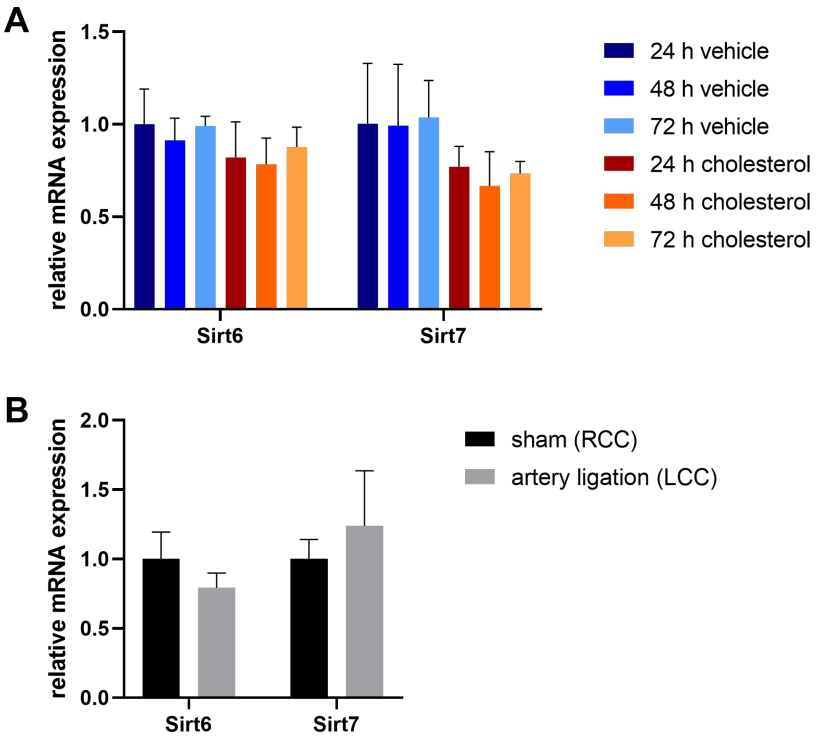

Figure 26 Relative mRNA expression of Sirt6 and Sirt7 *in vitro* and *in vivo*
A Primary mVSMCs were grown in serum-free media for 24 h before being treated with either vehicle or 5 µg/ml cholesterol for 24 h, 48 h and 72 h, respectively. Relative mRNA expression of Sirt6 and Sirt7 was analysed by RT-qPCR. Data are shown as mean ± standard deviation. Three independent experiments were carried out (n=3). mVSMCs were isolated from 3-4 mice and pooled for each experiment. **B** Relative mRNA expression of Sirt6 and Sirt7 was analysed in ligated left carotid arteries (artery ligation (LCC)) vs. control right carotid arteries (sham (RCC)) by RT-qPCR 3 days after surgery. Data are shown as mean ± standard deviation. 4 experiments were performed (n=4). For each experiment, RNA was isolated from LCCs and RCCs from 3-4 mice.

3.2.2 Establishment and validation of knock-out mouse models

To investigate the role of Sirt6 and Sirt7 in VSMCs specifically, conditional knock-out mouse models were created, containing a smooth-muscle cell specific cre recombinase and floxed Sirt6 and Sirt7 alleles, respectively. Upon cre recombinase activation by administration of tamoxifen the floxed areas of the Sirt6 or Sirt7 gene were eliminated from cells with VSMC origin. For each strain respective wildtype controls have been bred, resulting in genotypes SM-Sirt6-WT, SM-Sirt6-floxed, SM-Sirt7-WT and SM-Sirt7-floxed, in the following referred to as Sirt6 WT, Sirt6 KO, Sirt7 WT and Sirt7 KO. These floxed mice were then also crossed with the SM-mT/mG lineage tracing reporter mouse strain to create SM-Sirt6-WT/floxed-mT/mG and

SM-Sirt7-WT/floxed-mT/mG strains (for further details on the mouse strains see 2.1.4 and 2.2.6).

To validate whether recombination by the activated cre recombinase leads to the desired elimination of exons 4-6 of the Sirt6 and exons 6-9 of the Sirt7 gene respectively, carotids and aorta from SM-Sirt6-mT/mG and SM-Sirt7-mG/mT reporter mice were taken, digested and cells were sorted by FACS. The cells showing green fluorescence, indicating their VSMC origin, were collected and analysed with RT-qPCR. As Figure 27 shows, expression of Sirt6 and Sirt7 is almost completely abolished 10 days after completed tamoxifen administration.
Thus, the knock-down of Sirt6 and Sirt7 in their respective mouse strain was confirmed and the mouse lines were deemed suitable for further analysis of the role of Sirt6 and Sirt7 in VSMC dedifferentiation and metabolism.

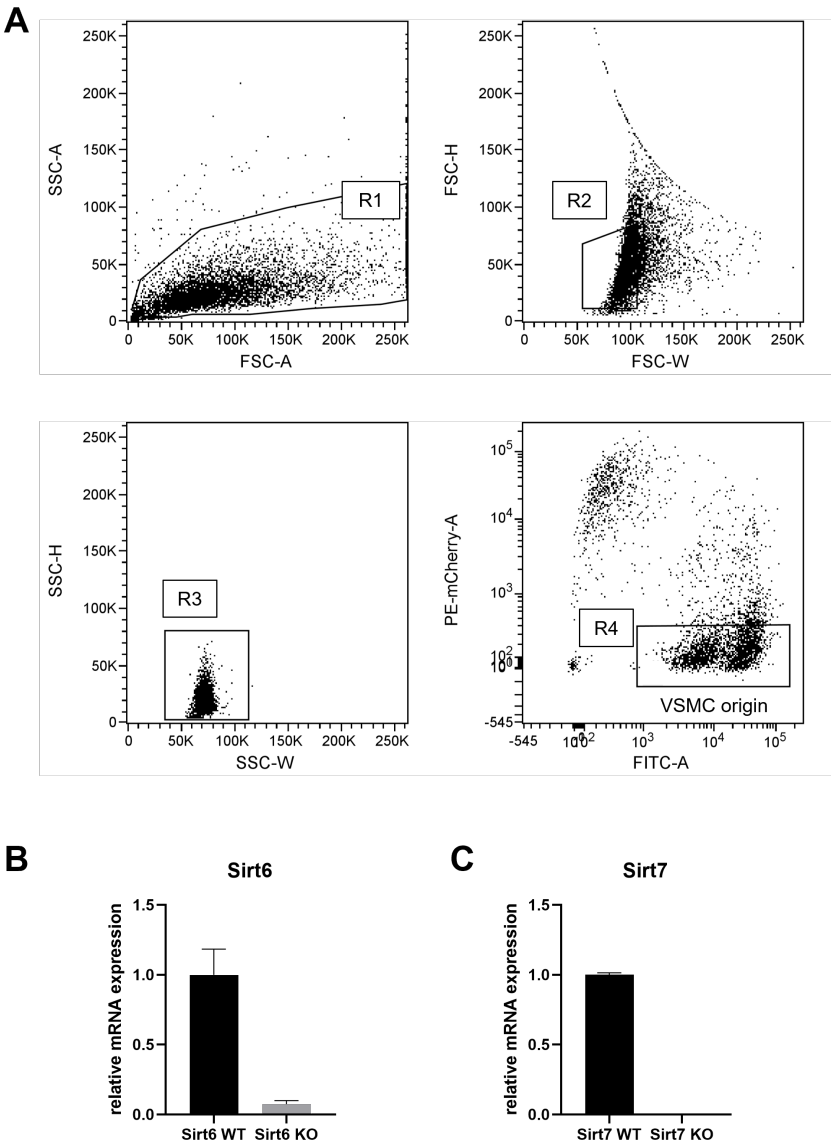

Figure 27 Validation of Sirt6 and Sirt7 knock-out in mouse models
8-week old SM-Sirt6-floxed-mT/mG and SM-Sirt6-WT-mT/mG as well as SM-Sirt7-floxed-mT/mG and SM-Sirt7-WT-mT/mG mice were injected with tamoxifen for five consecutive days. 10 days after the last injection the aorta and carotid arteries were harvested and digested to release individual cells. Cells were then sorted with FACS. **A** Cells were gated according to size and granularity (Forward vs. side scatter FCS-A vs. SSC-A) and double and multiple cells were excluded (FSC-H vs. FSC-W and SSC-H vs. SSC-W). Only cells exhibiting green fluorescence (R4) that were thus from VSMC origin were sorted and further analysed with RT-qPCR. **B** Relative mRNA expression of Sirt6 in sorted VSMCs from Sirt6 floxed and Sirt6 wildtype mice. **C** Relative mRNA expression of Sirt7 in sorted VSMCs from Sirt7 floxed and Sirt7 wildtype mice. Data are shown as mean ± standard deviation within one experiment (n=1). Sorted cells from 4 Sirt6 wildtype and 4 Sirt6 floxed mice were pooled and analysed (n per genotype = 4). Sorted cells from 3 Sirt7 wildtype and 5 Sirt7 floxed mice were pooled and analysed (n per genotype = 3-5).

3.2.3 The influence of Sirt6 on VSMC dedifferentiation and metabolism

The influence of Sirt6 on VSMC dedifferentiation in an *in vivo* carotid artery ligation model To investigate whether a Sirt6 knock-out in VSMCs affects their dedifferentiation process during remodeling, mice from the SM-Sirt6 line were subjected to carotid artery ligation inducing VSMC dedifferentiation. The resulting phenotype was analysed based on histological cross sections of the ligated vessels. The area and volume of the neointima formed upon vessel ligation in knock-out mice were compared to that forming in the carotids of wildtype mice.
4 weeks after carotid artery ligation, no difference was observed in neointima area or volume in the vessels of Sirt6 KO mice compared to wildtype (Figure 28).

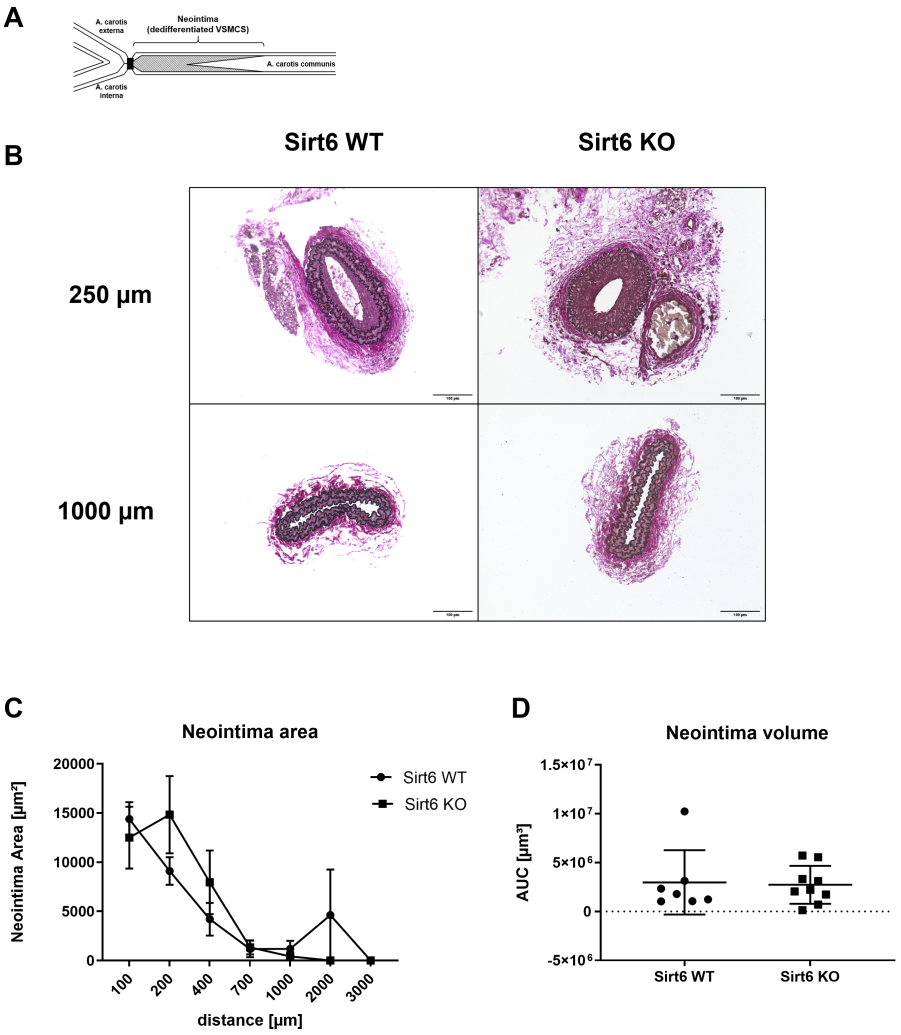

Figure 28 Histological analysis of ligated carotid arteries from Sirt6 conditional knock-out mice

8-week old SM-Sirt6 floxed and SM-Sirt6 wildtype mice were injected with tamoxifen for five consecutive days. **A** 10 days after the last injection, the left common carotid artery (arteria carotis communis) was ligated directly below the carotid bifurcation where the common carotid artery divides into internal and external carotid arteries. **B** 4 weeks after surgery the vessels were harvested and processed for histological analysis. The cross section directly below the ligation knot was defined as starting point and cross sections with defined distances from the ligation were analysed. Representative images of cross sections 250 µm and 1000 µm from the starting point are shown. **C** The area of the formed neointima at indicated distances was measured and **D** the volume of the neointima was defined as the calculated area under the curve. Data are shown as mean ± standard error of mean (SEM) for the measured area and individual values with mean ± standard deviation for the calculated volume. Analysed were 7 Sirt6 wildtype mice and 9 Sirt6 floxed mice (n per genotype= 7-9).

Expression profile of Sirt6 knock-out mice after carotid artery ligation Since Sirt6 is, among other functions, a known regulator of cell metabolism it was investigated whether the VSMCs from the respective knock-out mice showed altered expression patterns regarding key metabolic genes. Expression was compared between VSMCs from untreated control vessels (right carotid arteries) from knock-out versus wildtype mice. In addition, it was looked at whether the shift in expression of metabolic genes that occurs in VSMCs upon carotid artery ligation, as was found and shown in 3.1.3, were also observed in Sirt6 knock-out animals or whether there were differences to be found.

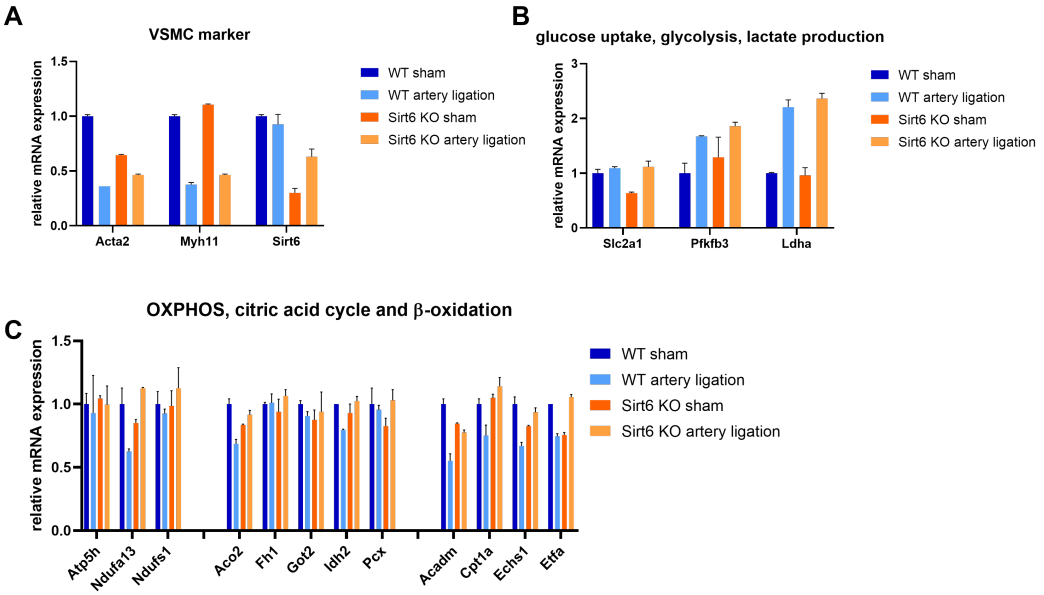

Figure 29 Relative mRNA expression of metabolic genes in Sirt6 knock-out versus wildtype 3 days after carotid artery ligation
8-week-old SM-Sirt6 floxed and SM-Sirt6 wildtype mice were injected with tamoxifen for five consecutive days. 10 days after the last injection, the left common carotid artery (arteria carotis communis) was ligated. Relative mRNA expression of **A** VSMC marker genes and Sirt6, **B** expression of genes involved in glucose uptake, glycolysis and lactate production and **C** genes involved in oxidative phosphorylation (OXPHOS), in the citric acid cycle and in β-oxidation was analysed in ligated left carotid arteries (artery ligation (LCC)) vs. control right carotid arteries (sham (RCC)) by RT-qPCR 3 days after surgery. Data are shown as mean ± standard deviation. 1-2 experiments were performed (n=1-2). For each experiment, RNA was isolated from LCCs and RCCs from 3-4 mice.

Expression of VSMC marker genes upon artery ligation was similarly down-regulated in Sirt6 WT and Sirt6 KO cells (Figure 29). There was also no difference in expression patterns for genes Slc2a1, Pfkfb3 and Ldha. As was found in the previous analysis of expression patterns after carotid artery ligation (3.1.3), expression of many genes

involved in oxidative phosphorylation, the citric acid cycle and β-oxidation was decreased after the surgery. This could also be observed in this experiment for the Sirt6 WT mice. Expression of these genes was also lowered in Sirt6 KO cells.

Influence of Sirt6 on the development of atherosclerosis in an ApoE$^{-/-}$ atherosclerosis mouse model While the carotid artery ligation model is useful to investigate the dedifferentiation of VSMCs *in vivo*, it cannot depict the complex pathology of real vascular diseases. Therefore, the effects of Sirt6 depletion in VSMCs were also investigated in a mouse model for atherosclerosis. For this purpose, in addition to the creation of the SM-Sirt6 and SM-Sirt6-mT/mG mouse strains, the SM-Sirt6 line was also crossed with ApoE knock-out mice (ApoE$^{-/-}$) to create the SM-Sirt6-ApoE$^{-/-}$ mouse strain. In these mice the apolipoprotein E (ApoE) is globally knocked-out and they possess floxed Sirt6 alleles as well as the smooth-muscle cell specific cre recombinase.

SM-Sirt6-floxed-ApoE$^{-/-}$ (referred to as Sirt6 KO ApoE$^{-/-}$) and SM-Sirt6-wildtype-ApoE$^{-/-}$ mice (referred to as Sirt6 WT ApoE$^{-/-}$) were fed a Western type diet for 12 weeks to induce the development of atherosclerosis. They were then analysed for cholesterol levels in the blood as well as the plaque burden in the diseased vessels. Body weight of Sirt6 WT ApoE$^{-/-}$ mice increased from 25.6 ± 1.8 g at the beginning of the experiment to 38.0 ± 3.1 g at the end of the experiment. Sirt6 KO ApoE$^{-/-}$ mice gained weight in a similar fashion, starting at 26.9 ± 3.0 g and ending at 37.4 ± 3.8 g (Figure 30A). Total cholesterol as well as high density lipoprotein (HDL) and triglyceride levels were similar in Sirt6 WT ApoE$^{-/-}$ and Sirt6 KO ApoE$^{-/-}$ mice after 12 weeks of Western type diet (Figure 30B,C and D). To determine the atherosclerotic plaque burden, the brachiocephalic artery (BCA) was analysed histologically. Cross sections were made beginning at the branch-off from the aortic arch and sections were analysed at fixed intervals. The plaque area in Sirt6 WT ApoE$^{-/-}$ and Sirt6 KO ApoE$^{-/-}$ mice was similar up to 500 µm from the branch-off. Towards the end of the BCA however, the plaque area in Sirt6 KO ApoE$^{-/-}$ mice was slightly larger than in Sirt6 WT ApoE$^{-/-}$ mice (Figure 30F). The calculated area under curve which depicts the plaque volume was not significantly different in Sirt6 WT ApoE$^{-/-}$ and Sirt6 KO ApoE$^{-/-}$ mice although there was a small trend towards higher plaque volume in Sirt6 KO ApoE$^{-/-}$ mice (Figure 30G).

In summary, neointima formation as well as atherosclerotic plaque size were not

significantly different in Sirt6 KO compared to Sirt6 WT mice. Screening of metabolic gene expression upon carotid artery ligation also did not show obvious differences between Sirt6 WT and Sirt6 KO mice.

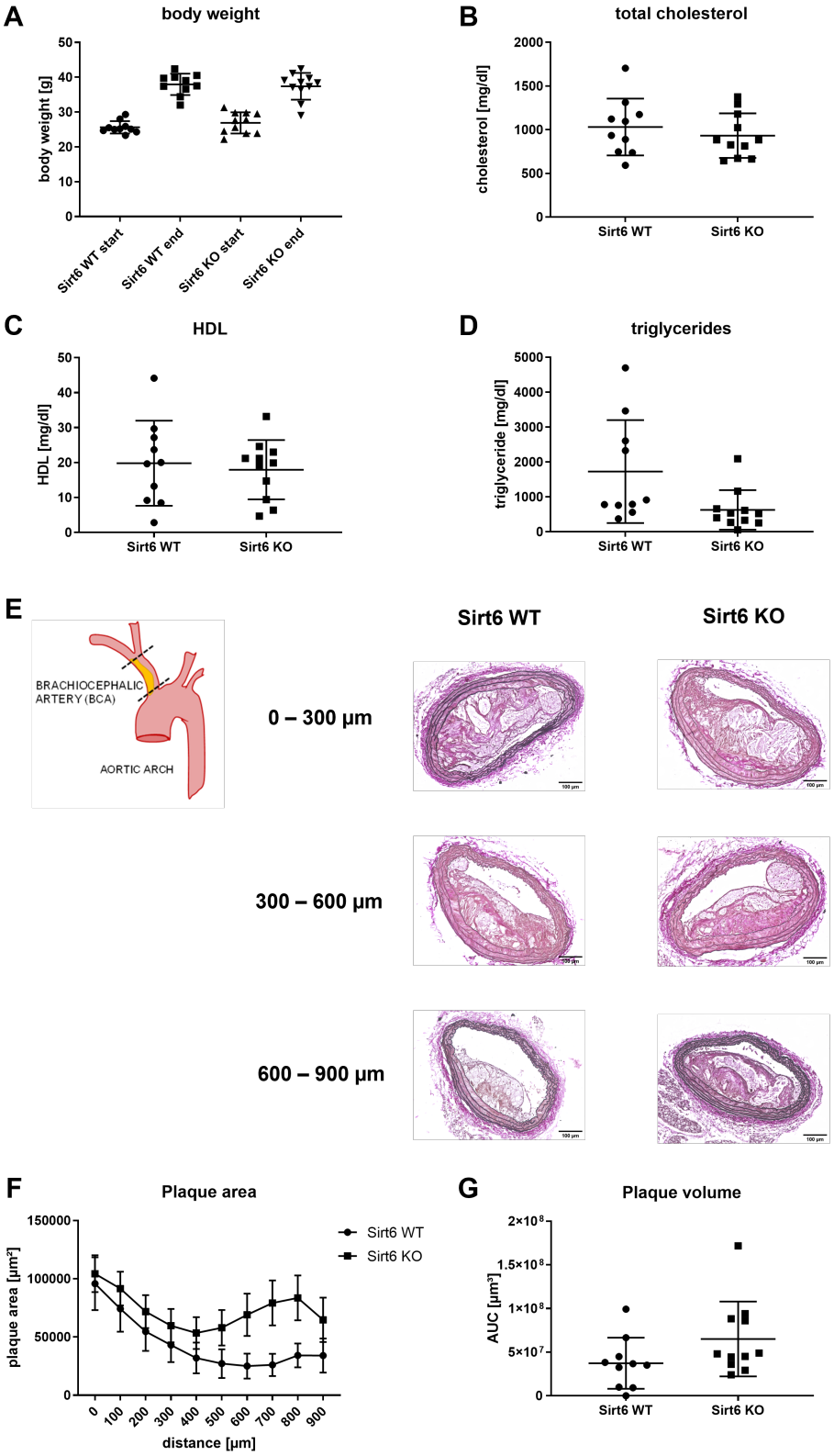
A
body weight
body weight [g]
Sirt6 WT start
Sirt6 WT end
Sirt6 KO start
Sirt6 KO end
B
total cholesterol
cholesterol [mg/dl]
Sirt6 WT
Sirt6 KO
C
HDL
HDL [mg/dl]
Sirt6 WT
Sirt6 KO
D
triglycerides
triglyceride [mg/dl]
Sirt6 WT
Sirt6 KO
E
BRACHIOCEPHALIC ARTERY (BCA)
AORTIC ARCH
Sirt6 WT
Sirt6 KO
0 – 300 µm
300 – 600 µm
600 – 900 µm
F
Plaque area
plaque area [µm²]
Sirt6 WT
Sirt6 KO
distance [µm]
G
Plaque volume
AUC [µm³]
Sirt6 WT
Sirt6 KO

Figure 30 Development of atherosclerosis in Sirt6 deficient ApoE$^{-/-}$ mice compared to Sirt6 wildtype ApoE$^{-/-}$
8-week-old SM-Sirt6-floxed-ApoE$^{-/-}$ and SM-Sirt6-WT-ApoE$^{-/-}$ mice were injected with tamoxifen for five consecutive days. The mice were then fed a Western type diet for 12 weeks. Shown is **A** body weight at beginning and end of the experiment, **B** levels of total cholesterol in the blood serum after 12 weeks of Western type diet, **C** levels of high density lipoprotein (HDL) in the blood serum after 12 weeks of Western type diet and **D** levels of triglycerides at the end of the experiment without prior fasting. **E** Representative images of cross sections of the brachiocephalic artery (BCA) 0-300 µm, 300-600 µm and 600-900 µm distal from the branch-off from the aortic arch. **F** Plaque area was measured in cross sections of the BCA at indicated distances from the branch-off from the aortic arch. **G** The area under the curve was calculated and defined as plaque volume. Data are shown as individual values (A, B, C, D and G) with mean ± standard deviation or as mean ± standard error of mean (SEM) (E). Analysed were 10 Sirt6-wildtype-ApoE$^{-/-}$ mice and 11 Sirt6-floxed-ApoE$^{-/-}$- mice (n per genotype = 10-11).

3.2.4 The influence of Sirt7 on VSMC dedifferentiation and metabolism

The influence of Sirt7 on VSMC dedifferentiation in an *in vivo* carotid artery ligation model To investigate whether a Sirt7 knock-out in VSMCs affects their dedifferentiation process during remodeling, mice from the SM-Sirt7 line were subjected to carotid artery ligation inducing VSMC dedifferentiation. The resulting phenotype was analysed based on histological cross sections of the ligated vessels. The area and volume of the neointima formed upon vessel ligation in knock-out mice were compared to that forming in the carotids of wildtype mice.
Figure 31 illustrates the results for the carotid artery ligation of Sirt7 knock-out mice. Here, a significant increase in neointima formation could be observed throughout the length of the vessel. Consequently, the calculated volume of the neointima was significantly larger in Sirt7 KO mice compared to control. The exemplary images show a pronounced hypertrophy in the Sirt7 KO vessel compared to control (Figure 31B).

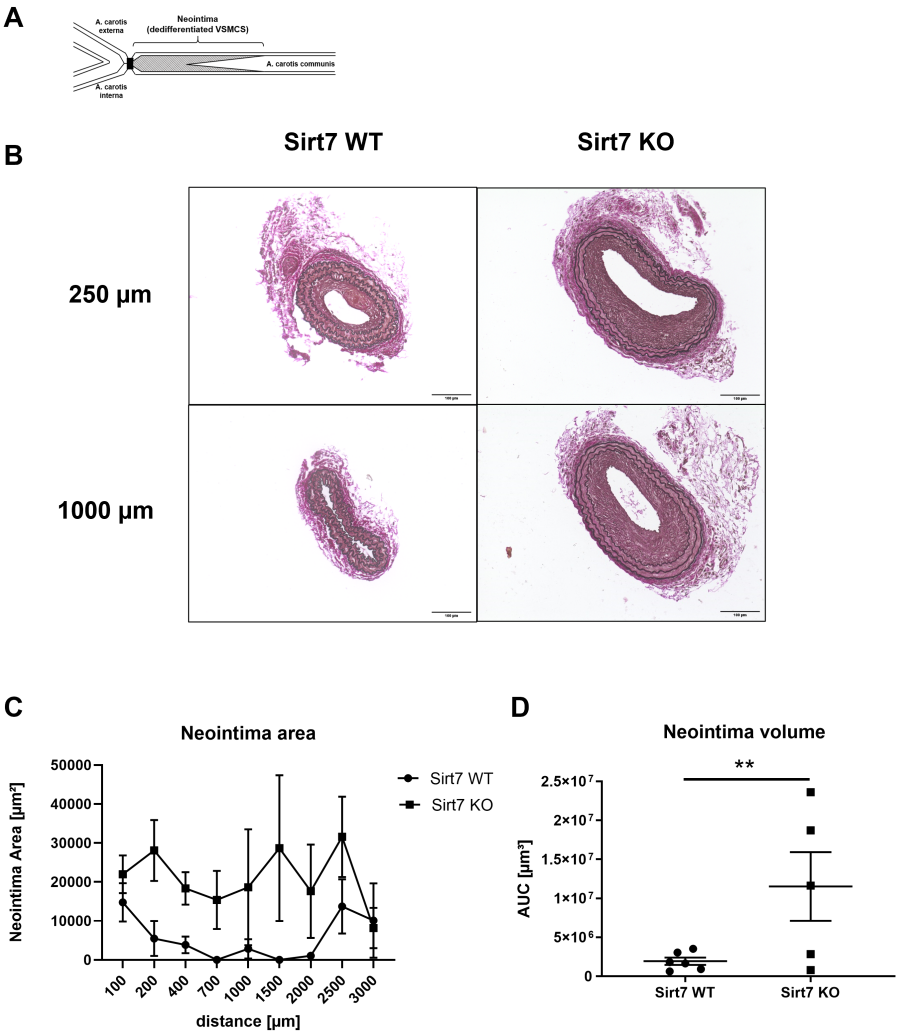

Figure 31 Histological analysis of ligated carotid arteries from Sirt7 conditional knock-out mice

8-week old SM-Sirt7 floxed and SM-Sirt7 wildtype mice were injected with tamoxifen for five consecutive days. **A** 10 days after the last injection, the left common carotid artery (arteria carotis communis) was ligated directly below the carotid bifurcation where the common carotid artery divides into internal and external carotid arteries. **B** 4 weeks after surgery the vessels were harvested and processed for histological analysis. The cross section directly below the ligation knot was defined as starting point and cross sections with defined distances from the ligation were analysed. Representative images of cross sections 250 µm and 1000 µm from the starting point are shown. **C** The area of the formed neointima at indicated distances was measured and **D** the volume of the neointima was defined as the calculated area under the curve. Data are shown as mean ± standard error of mean (SEM) for the measured area and individual values with mean ± standard deviation for the calculated volume. Analysed were 6 Sirt7 wildtype mice and 5 Sirt7 floxed mice (n per genotype= 5-6) ** $p < 0.01$ indicate significance versus wildtype by Student's t-test.

Expression profile of Sirt6 knock-out mice after carotid artery ligation Since Sirt7, like Sirt6, is a known regulator of cell metabolism it was investigated whether the VSMCs from Sirt7 knock-out mice showed altered expression patterns regarding key metabolic genes. Expression was compared between VSMCs from untreated control vessels (right carotid arteries) from knock-out versus wildtype mice. In addition, it was looked at whether the shift in expression of metabolic genes that occurs in VSMCs upon carotid artery ligation, as was found and shown in 3.1.3, was also observed in Sirt7 knock-out animals or whether there were differences to be found.

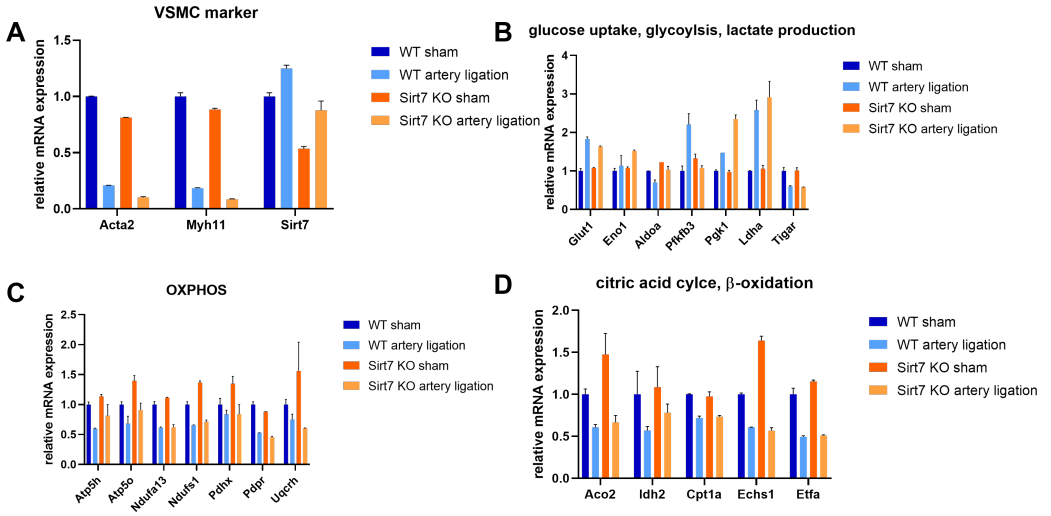

Figure 32 Relative mRNA expression of metabolic genes in Sirt7 knock-out versus wildtype 3 days after carotid artery ligation
8-week-old SM-Sirt7 floxed and SM-Sirt7 wildtype mice were injected with tamoxifen for five consecutive days. 10 days after the last injection, the left common carotid artery (arteria carotis communis) was ligated. Relative mRNA expression of **A** VSMC marker genes and Sirt7, **B** expression of genes involved in glucose uptake, glycolysis and lactate production, **C** genes involved in oxidative phosphorylation (OXPHOS) and **D** genes involved in the citric acid cycle and in β-oxidation was analysed in ligated left carotid arteries (artery ligation (LCC)) vs. control right carotid arteries (sham (RCC)) by RT-qPCR 3 days after surgery. Data are shown as mean ± standard deviation. 1-2 experiments were performed (n=1-2). For each experiment, RNA was isolated from LCCs and RCCs from 3-4 mice.

Expression of VSMC marker genes upon artery ligation was similarly reduced in Sirt7 WT and Sirt7 KO cells. As was found in the previous analysis of expression patterns after carotid artery ligation (3.1.3), expression of genes involved in glucose uptake, glycolysis and lactate production was increased after the surgery. In this experiment this was confirmed for Sirt7 WT vessels and was also largely true for the Sirt7 KO arteries. Down-regulation of the master regulator of glycolysis, Tigar, was also consistent in both genotypes. Expression of genes involved in oxidative

phosphorylation, the citric acid cycle and β-oxidation was also reduced in a similar fashion in Sirt7 WT ligated vessels as well as in Sirt7 KO ligated vessels compared to control.

Influence of Sirt7 on the development of atherosclerosis in an ApoE$^{-/-}$ atherosclerosis mouse model While the carotid artery ligation model is useful to investigate the dedifferentiation of VSMCs *in vivo*, it cannot depict the complex pathology of real vascular diseases. Therefore, the effects of Sirt7 depletion in VSMCs were also investigated in a mouse model for atherosclerosis. For this purpose, in addition to the creation of the SM-Sirt7 and SM-Sirt7-mT/mG mouse lines, the SM-Sirt7 strain was also crossed with ApoE knock-out mice (ApoE$^{-/-}$) to create the SM-Sirt7-ApoE$^{-/-}$ mouse strain. In these mice the apolipoprotein E (ApoE) is globally knocked out and they possess floxed Sirt7 alleles as well as the smooth-muscle cell specific cre recombinase.

As in the experiment with Sirt6 mice, SM-Sirt7-floxed-ApoE$^{-/-}$ (referred to as Sirt7-KO ApoE$^{-/-}$) and SM-Sirt7-wildtype-ApoE$^{-/-}$ mice (referred to as Sirt7 WT ApoE$^{-/-}$) were fed a Western type diet for 12 weeks to induce the development of atherosclerosis. They were then analysed for cholesterol levels in the blood as well as the plaque burden in the diseased vessels. Body weight of Sirt7 WT ApoE$^{-/-}$ mice increased from 26.7± 2.8 g at the beginning of the experiment to 34.8 ± 5.7 g at the end of the experiment. Sirt7 KO ApoE$^{-/-}$ mice gained weight in a similar fashion, starting at 23.9 ± 1.6 g and ending at 33.0 ± 3.8 g (Figure 33A). Total cholesterol as well as HDL and triglyceride levels were not different in Sirt7 WT ApoE$^{-/-}$ and Sirt7 KO ApoE$^{-/-}$ mice after 12 weeks of Western type diet (Figure 33B,C and D). The plaque area in Sirt7 KO ApoE$^{-/-}$ mice was significantly larger compared to Sirt7 WT ApoE$^{-/-}$ mice over the whole length of the BCA (Figure 33F). Consequently, the plaque volume was significantly higher in Sirt7 KO ApoE$^{-/-}$ mice than in Sirt7 WT ApoE$^{-/-}$ mice (Figure 33G).

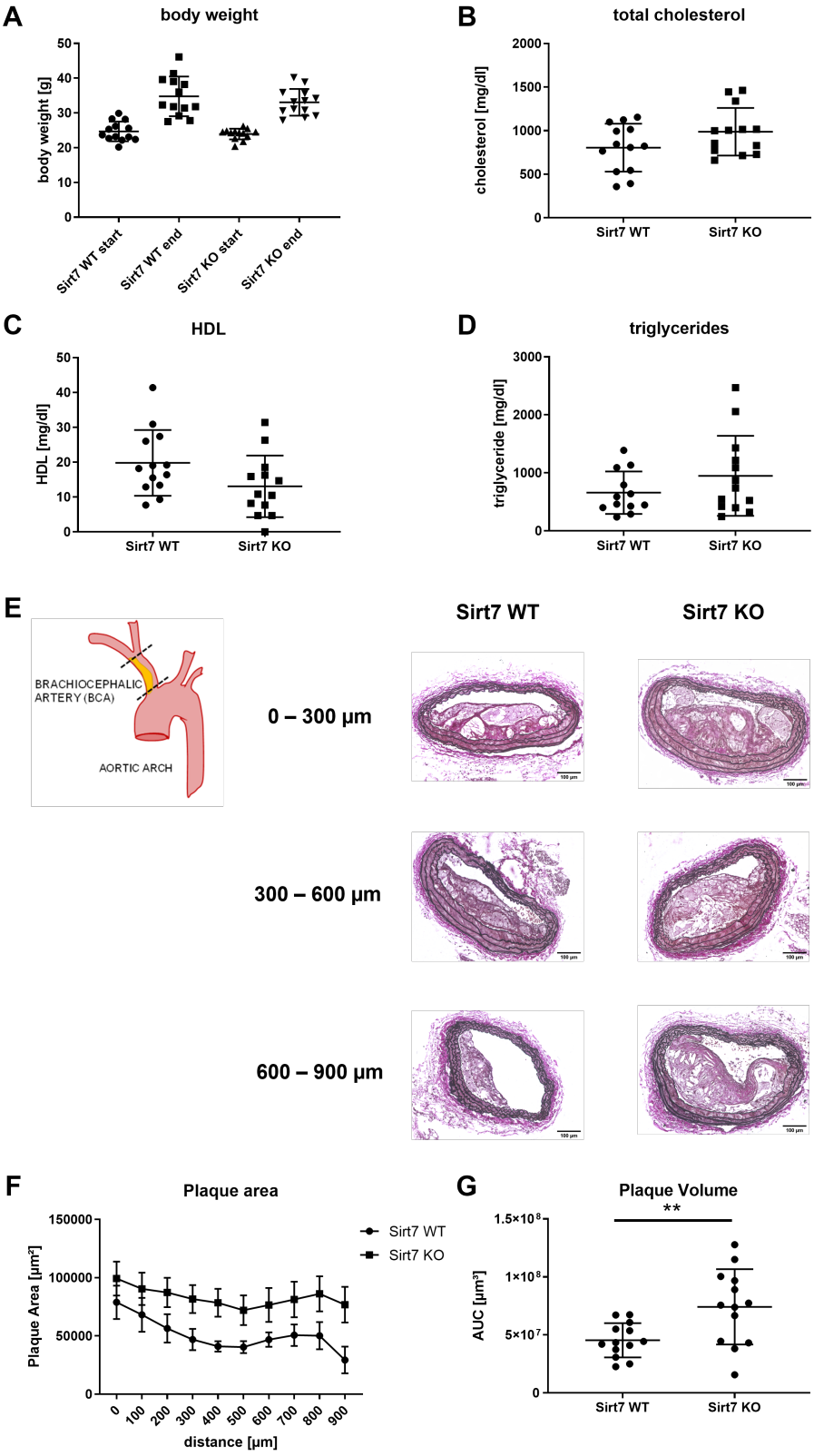
A
body weight
body weight [g]
50
40
30
20
10
0
Sirt7 WT start
Sirt7 WT end
Sirt7 KO start
Sirt7 KO end
B
total cholesterol
cholesterol [mg/dl]
2000
1500
1000
500
0
Sirt7 WT
Sirt7 KO
C
HDL
HDL [mg/dl]
50
40
30
20
10
0
Sirt7 WT
Sirt7 KO
D
triglycerides
triglyceride [mg/dl]
3000
2000
1000
0
Sirt7 WT
Sirt7 KO
E
BRACHIOCEPHALIC ARTERY (BCA)
AORTIC ARCH
Sirt7 WT
Sirt7 KO
0 – 300 µm
300 – 600 µm
600 – 900 µm
F
Plaque area
Plaque Area [µm²]
150000
100000
50000
0
0
100
200
300
400
500
600
700
800
900
distance [µm]
Sirt7 WT
Sirt7 KO
G
Plaque Volume
**
AUC [µm³]
1.5×10⁸
1×10⁸
5×10⁷
0
Sirt7 WT
Sirt7 KO

Figure 33 Development of atherosclerosis in Sirt7 deficient ApoE$^{-/-}$ mice compared to Sirt7 wildtype ApoE$^{-/-}$ mice
8-week-old SM-Sirt7-floxed-ApoE$^{-/-}$ and SM-Sirt7-WT-ApoE$^{-/-}$ mice were injected with tamoxifen for five consecutive days. The mice were then fed a Western type diet for 12 weeks. Shown is **A** body weight at beginning and end of the experiment, **B** levels of total cholesterol in the blood serum after 12 weeks of Western type diet, **C** levels of high density lipoprotein (HDL) in the blood serum after 12 weeks of Western type diet and **D** levels of triglycerides at the end of the experiment without prior fasting. **E** Representative images of cross sections of the brachiocephalic artery (BCA) 0-300 µm, 300-600 µm and 600-900 µm distal from the branch-off from the aortic arch. **F** Plaque area was measured in cross sections of the BCA at indicated distances from the branch-off from the aortic arch. **G** The area under the curve was calculated and defined as plaque volume. Data are shown as individual values (A, B, C, D and G) with mean ± standard deviation or as mean ± standard error of mean (SEM) (E). Analysed were 13 Sirt7 wildtype ApoE$^{-/-}$ mice and 13 Sirt7 floxed ApoE$^{-/-}$ mice (n per genotype = 13), ** $p < 0.01$ indicate significance versus wildtype by Student's t-test.

In summary, mice with a VSMC-specific Sirt7 knock-out showed increased neointima formation upon carotid artery ligation and developed larger atherosclerotic plaques compared to wildtype mice. These results indicate that Sirt7 regulates VSMC dedifferentiation in these models. Therefore, the next step was to identify how Sirt7 affects VSMC homeostasis and dedifferentiation.

3.2.5 Mechanistic effects of Sirt7 on VSMC homeostasis

Establishment of a Sirt7 knock-down cell culture model Before further investigations into the role of Sirt7 in VSMCs could be implemented, a cell culture model for a Sirt7 knock-down was needed. Due to animal welfare the experiments aimed at elucidating the basic function of Sirt7 and the effects of its knock-out could not and were not carried out exclusively with the help of animal experiments. Therefore, a cell culture model with a known and widely used VSMC cell line, A7r5, was established. Sirt7 knock-down was achieved by small interference RNA (siRNA) transfection.

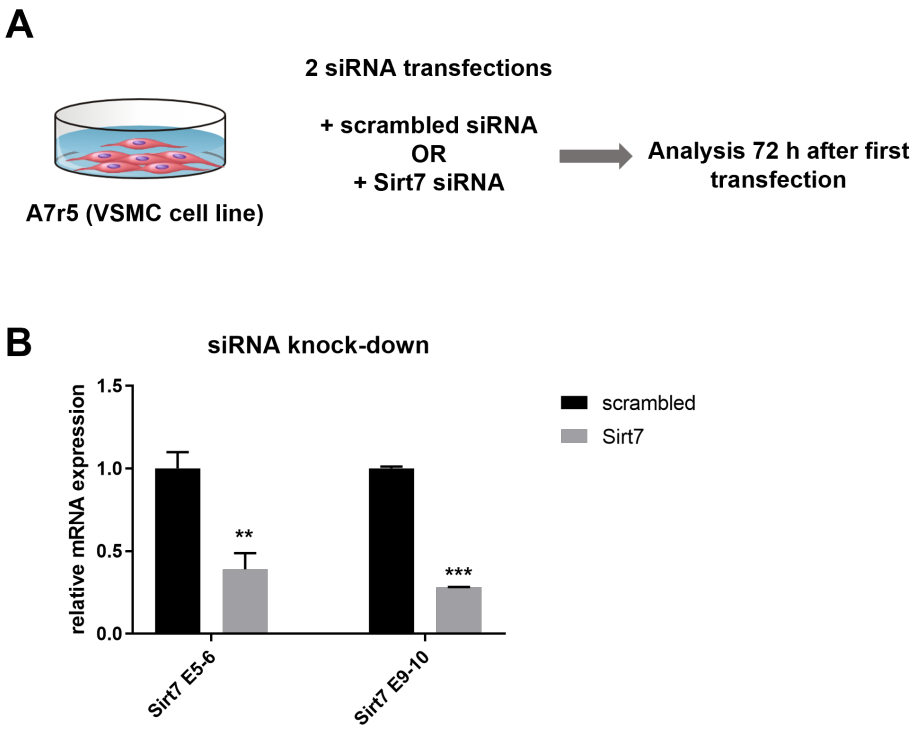

Figure 34 Establishing a Sirt7 knock-down cell culture model
A A7r5 cells were transfected with either scrambled or Sirt7 siRNA on two consecutive days. Cells were then harvested 72 h after the first transfection and **B** expression of Sirt7 was analysed with RT-qPCR. Two different primer sets were used, detecting exon 5-6 and exon 9-10 of Sirt7 cDNA. Data are shown as mean ± standard deviation. Three independent experiments were performed (n=3). ** $p < 0.01$, *** $p < 0.001$ indicate significance versus scrambled by Student's t-test.

As Figure 34 illustrates, a knock-down of 60-70% with a remaining Sirt7 expression of 30-40% could be achieved with two consecutive siRNA transfections. In spite of additional testing of different conditions and siRNA concentrations, a complete knock-down of Sirt7 could not be achieved. Therefore, this model was used in the following analyses despite the remaining Sirt7 mRNA and probably also protein.

Expression of Sirt7 target and key metabolic genes upon Sirt7 knock-down *in vitro* In their publication from 2014, Ryu et al. found that Sirt7 regulates the GA-binding protein which in turn is a master regulator of mitochondrial biogenesis. Consequently, a lot of genes involved in mitochondrial biogenesis were strongly down-regulated upon Sirt7 knock-down or knock-out [121]. The lowered expression of Sirt7 target genes was confirmed in hepatocytes as well as cardiomyocytes but up until now they were not investigated in VSMCs.
The mRNA levels of several of these target genes were analysed in the established

siRNA Sirt7 knock-down cell culture model. As Figure 35 shows, a significant decline in mRNA levels upon Sirt7 knock-down was only observed for mitofusin 1 (Mfn1), mitofusin 2 (Mfn2) (0.74 ± 0.08) and mitochondrial polymerase (Polrmt) with 0.83 ± 0.02. A downwards trend could also be observed for mitochondrial ribosomal protein 5 (Mrps5) with a p-value of 0.07. Although these down-regulations were significantly different from the control the observed decline in expression was not very large. In the publication of Ryu et al., the effects of Sirt7 depletion on these target genes was a lot more pronounced.

In addition to the target genes proposed from the mentioned publication, it was also checked whether Sirt7 knock-down had an impact on the expression of other genes important for cell metabolism (Figure 35B and C). However, there was no difference in expression of genes involved in glycolysis (Slc2a1, Pfkfb3, Ldha), in oxidative phosphorylation (Atp5o, Ndufa13), the citric acid cycle (Aco2, Idh2) or β-oxidation (Cpt1a, Echs1, Etfa).

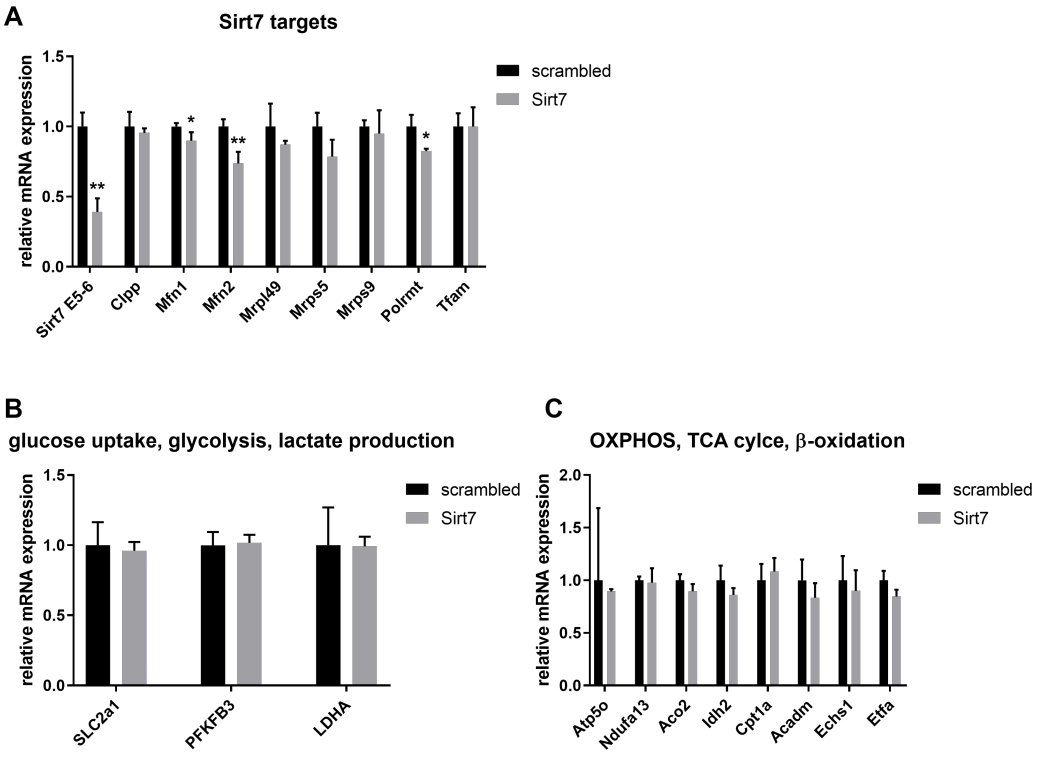

Figure 35 Relative mRNA expression of Sirt7 target genes and chosen metabolic genes upon Sirt7 siRNA knock-down
A7r5 cells were transfected with either scrambled or Sirt7 siRNA on two consecutive days. Cells were then harvested 72 h after the first transfection and **A** expression of Sirt7 and several of its target genes, **B** genes involved in glucose uptake, glycolysis and lactate production and **C** genes involved in oxidative phosphorylation (OXPHOS), in the citric acid cycle and in β-oxidation was analysed with RT-qPCR. Data are shown as mean ± standard deviation. Three independent experiments were performed (n=3) * $p < 0.05$, ** $p < 0.01$ indicate significance versus scrambled by Student's t-test.

Expression of Sirt7 target genes upon VSMC-specific Sirt7 knock-out *in vivo*

In addition to the exploration of Sirt7 depletion and its effects on the expression of published Sirt7 target genes *in vitro*, the expression was also investigated *in vivo*. SM-Sirt7 floxed and SM-Sirt7 wildtype mice were injected with tamoxifen for 5 consecutive days. Vessels were harvested and the expression of Sirt7 target genes analysed with RT-qPCR.

As Figure 36 illustrates, there was a strong knock-down of Sirt7 in Sirt7 floxed mice after tamoxifen injection as shown with primers for two different deleted exons. However, there was no effect on the expression of the Sirt7 target genes, published by Ryu et al., to be observed [121].

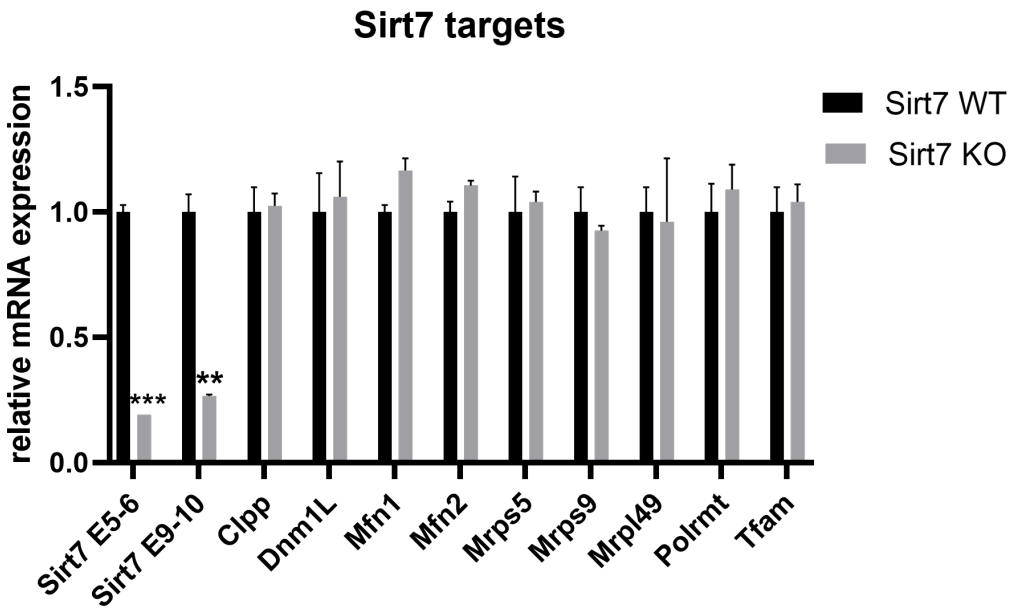

Figure 36 Relative mRNA expression of Sirt7 target genes in Sirt7 knock-out mice compared to wildtype
8-week-old SM-Sirt7 floxed and SM-Sirt7 wildtype mice were injected with tamoxifen for five consecutive days. 14 days after the last injection, carotid arteries and the aorta were harvested from these mice. Expression of Sirt7 and several of its target genes was analysed with RT-qPCR. Data are shown as mean ± standard deviation. Tissue was taken from two Sirt7 floxed and two wildtype mice (n per genotype = 2) ** $p < 0.01$, *** $p < 0.001$ indicate significance versus wildtype by Student's t-test.

The effect of Sirt7 knock-down on metabolic output To investigate whether the knock-down of Sirt7 and its postulated effects on the expression of mitochondrial genes affects the overall cell metabolism, cells were analysed for oxygen consumption and extracellular acidification, an indicator of lactate production, with an XFe Flux Analyzer. Oxygen consumption rate (OCR) and extracellular acidification rate (ECAR) were measured following two consecutive siRNA transfections. Figure 37 illustrates that there were no major differences in oxygen consumption rate in Sirt7 knock-down cells compared to control cells. All calculated parameters such as maximal respiration, spare respiratory capacity and ATP production were not significantly different between groups. Normalisation to DNA content did not result in any larger shift in the data. Extracellular acidification rate before as well as after normalisation was similar in Sirt7 knock-down and control cells (Figure 37C and D). The OCR/ECAR ratios calculated from basal values were not significantly different although the OCR/ECAR ratio in Sirt7 depleted cells was slightly lower than in the control (Figure 37G).

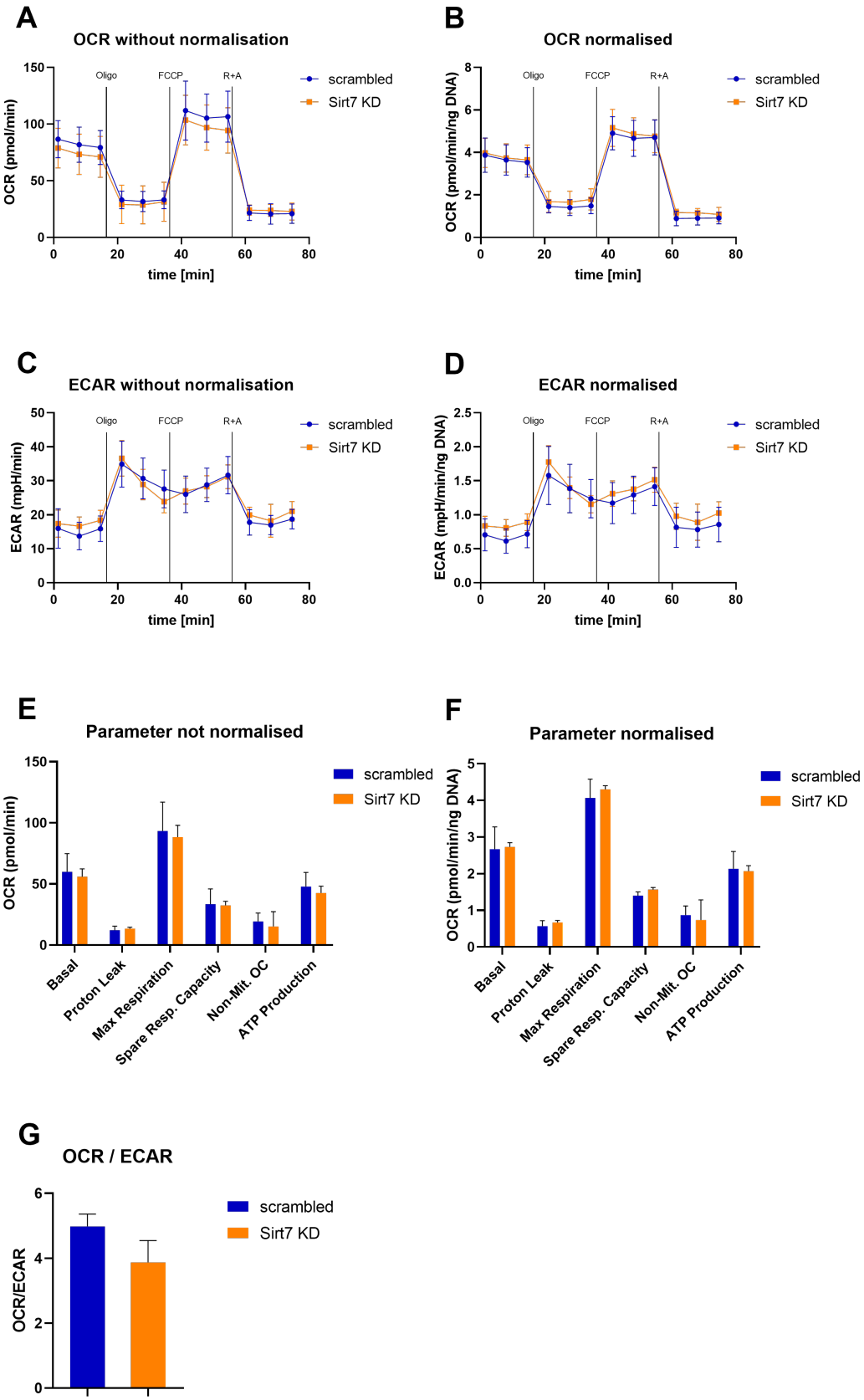
A
OCR without normalisation
OCR (pmol/min)
time [min]
Oligo
FCCP
R+A
scrambled
Sirt7 KD
B
OCR normalised
OCR (pmol/min/ng DNA)
C
ECAR without normalisation
ECAR (mpH/min)
D
ECAR normalised
ECAR (mpH/min/ng DNA)
E
Parameter not normalised
F
Parameter normalised
Basal
Proton Leak
Max Respiration
Spare Resp. Capacity
Non-Mit. OC
ATP Production
G
OCR / ECAR
OCR/ECAR

Figure 37 XFe Flux Analysis of VSMCs after Sirt7 siRNA knock-down
Oxygen consumption rate (OCR) and extracellular acidification rate (ECAR) were measured with an XFe96 Flux Analyzer in A7r5 cells which were transfected with either scrambled or Sirt7 siRNA on two consecutive days. Cells were transferred into the measurement plate 48 h after first transfection and measured 72 h after first transfection. During the measurement Oligomycin (Oligo), FCCP and rotenone and antimycin A (R+A) were added at indicated timepoints during the measurement. **A** OCR measured over time and **B** normalised to DNA amount. **C** ECAR measured over time and **D** normalised to DNA amount. **E** Parameters calculated from OCR values over time from non-normalised curve (A) as well as **F** parameters calculated from OCR values over time from normalised curve (B). **G** OCR over ECAR ratios calculated from basal values. Data are shown as mean ± standard deviation. At least three independent experiments were performed (n=3).

Influence of Sirt7 knock-down on metabolic output in VSMCs upon cholesterol-induced dedifferentiation Using the cholesterol-driven dedifferentiation cell culture model, it was tested whether Sirt7 knock-down had any influence on the changes in metabolism occurring in VSMCs upon dedifferentiation. A7r5 cells were transfected with Sirt7 or scrambled siRNA, treated with cholesterol for 48 h and cells were analysed for oxygen consumption and extracellular acidification with an XFe Flux Analyzer.

In both Sirt7 depleted and control cells, the oxygen consumption rate dropped noticeably upon cholesterol treatment which was probably due to a lower cell number in these wells as normalisation to DNA content abolished this effect. In fact, after normalisation there was no difference in oxygen consumption between the four different groups. The same was true for all calculated parameters such as maximal respiration, spare respiratory capacity and ATP production. Consistent with the results from 3.1.2 (Figure 20), extracellular acidification rate after normalisation was elevated in cholesterol-treated compared to control cells (Figure 38D). However, there was no difference between Sirt7-depleted and control cells. The OCR/ECAR ratios calculated from basal values, were significantly lowered in the cholesterol treated group but similar in Sirt7-depleted and control cells (Figure 38G).

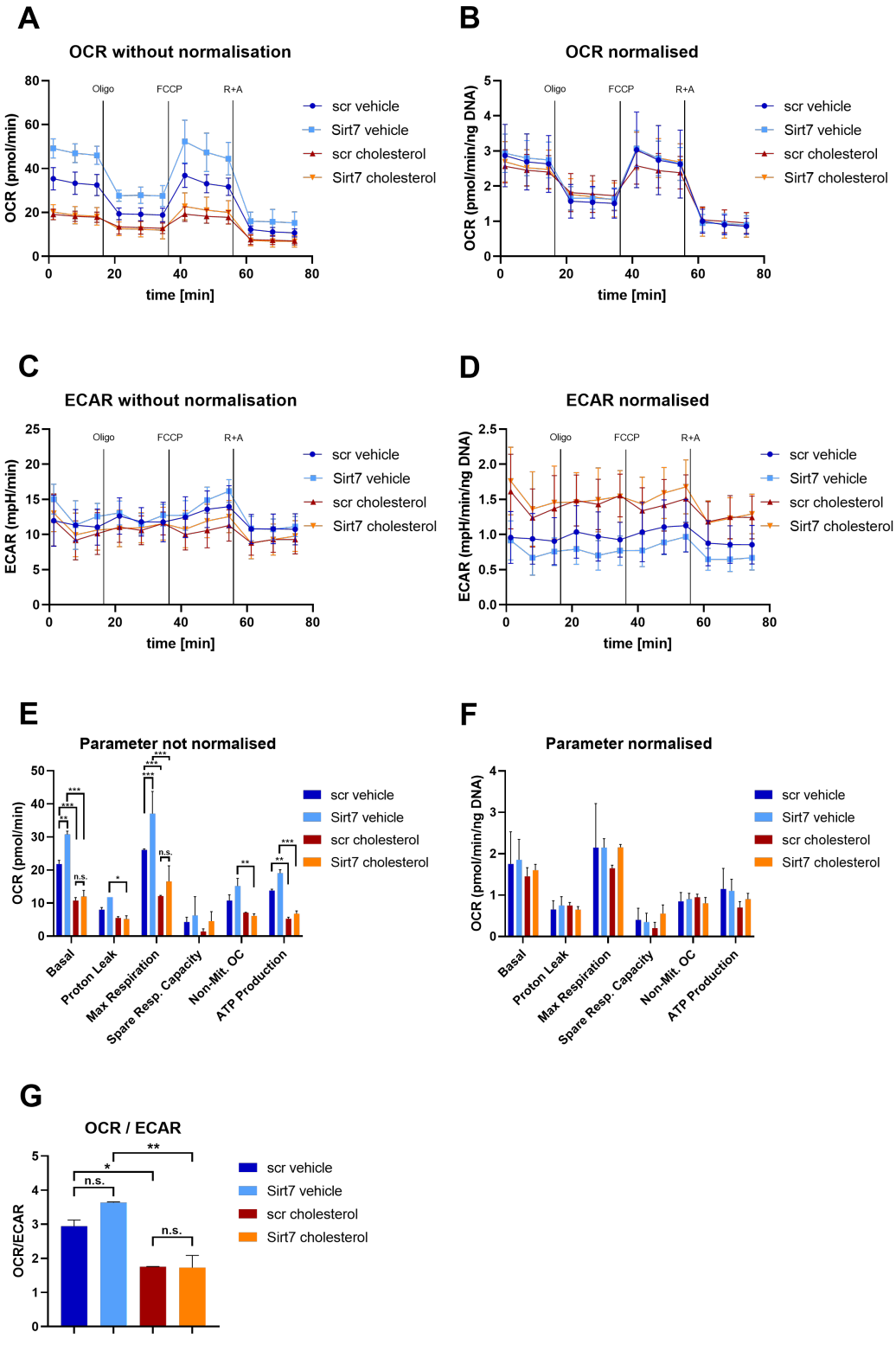
A
OCR without normalisation
OCR (pmol/min)
time [min]
Oligo
FCCP
R+A
scr vehicle
Sirt7 vehicle
scr cholesterol
Sirt7 cholesterol
B
OCR normalised
OCR (pmol/min/ng DNA)
C
ECAR without normalisation
ECAR (mpH/min)
D
ECAR normalised
ECAR (mpH/min/ng DNA)
E
Parameter not normalised
Basal
Proton Leak
Max Respiration
Spare Resp. Capacity
Non-Mit. OC
ATP Production
F
Parameter normalised
G
OCR / ECAR
OCR/ECAR
n.s.

Figure 38 Flux Analysis of VSMCs after Sirt7 siRNA knock-down and cholesterol treatment
Oxygen consumption rate (OCR) and extracellular acidification rate (ECAR) were measured with an XFe96 Flux Analyzer in A7r5 cells which were transfected with either scrambled or Sirt7 siRNA on two consecutive days. Cells were incubated with serum-free media before being treated with 5 µg/ml cholesterol or vehicle for 48 h. The measurement took place 5 days after the first siRNA transfection and after 48 h of cholesterol incubation. During the measurement Oligomycin (Oligo), FCCP and rotenone and antimycin A (R+A) were added at indicated timepoints during the measurement. **A** OCR measured over time and **B** normalised to DNA amount. **C** ECAR measured over time and **D** normalised to DNA amount. **E** Parameters calculated from OCR values over time from non-normalised curve (A) as well as **F** parameters calculated from OCR values over time from normalised curve (B). **G** OCR over ECAR ratios calculated from basal values. Data are shown as mean ± standard deviation. Two independent experiments were performed (n=2).* $p < 0.05$, ** $p < 0.01$, *** $p < 0.001$ indicate significance versus siRNA or treatment as indicated by Two-way ANOVA, followed by Tukey's multiple comparison test.

Analyses of the abundance of mitochondria in Sirt7 knock-out versus wildtype vessels upon carotid artery ligation In 3.1.4 the abundance of mitochondria in dedifferentiated VSMCs was analysed with flow cytometry by staining mitochondria with MitoTracker™ Deep Red FM. For this experiment, ligated and sham operated carotid arteries from SM-Sirt7-floxed-mT/mG and SM-Sirt7-WT-mT/mG mice were harvested 7 days after surgery and digested to release individual cells which were then stained with MitoTracker™ Deep Red FM to label mitochondria. As in the previous flow cytometry experiment (Figure 24) the genetic lineage tracing mouse strain was used in order to be able to differentiate between VSMCs and other cell types.

Figure 39B shows the absolute values of Mitotracker fluorescence in VSMCs from sham operated carotid arteries and ligated carotid arteries from wildtype as well as from Sirt7 knock-out mice. There was no observable difference between the absolute Mitotracker fluorescence between these groups. Since the experiments with wildtype and Sirt7 knock-out mice were not carried out on the same day and absolute values can vary due to differences in the staining process on separate days, data were normalised by calculating ratios of ligated and control arteries (Figure 39C). As seen previously, Mitotracker fluorescence in cells isolated from ligated wildtype arteries declines after surgery which results in a ratio lower than 1. Ratios from Sirt7 knock-out mice were not significantly different from those in wildtype mice indicating that depletion of Sirt7 did not influence the effect of artery ligation on Mitotracker fluorescence.

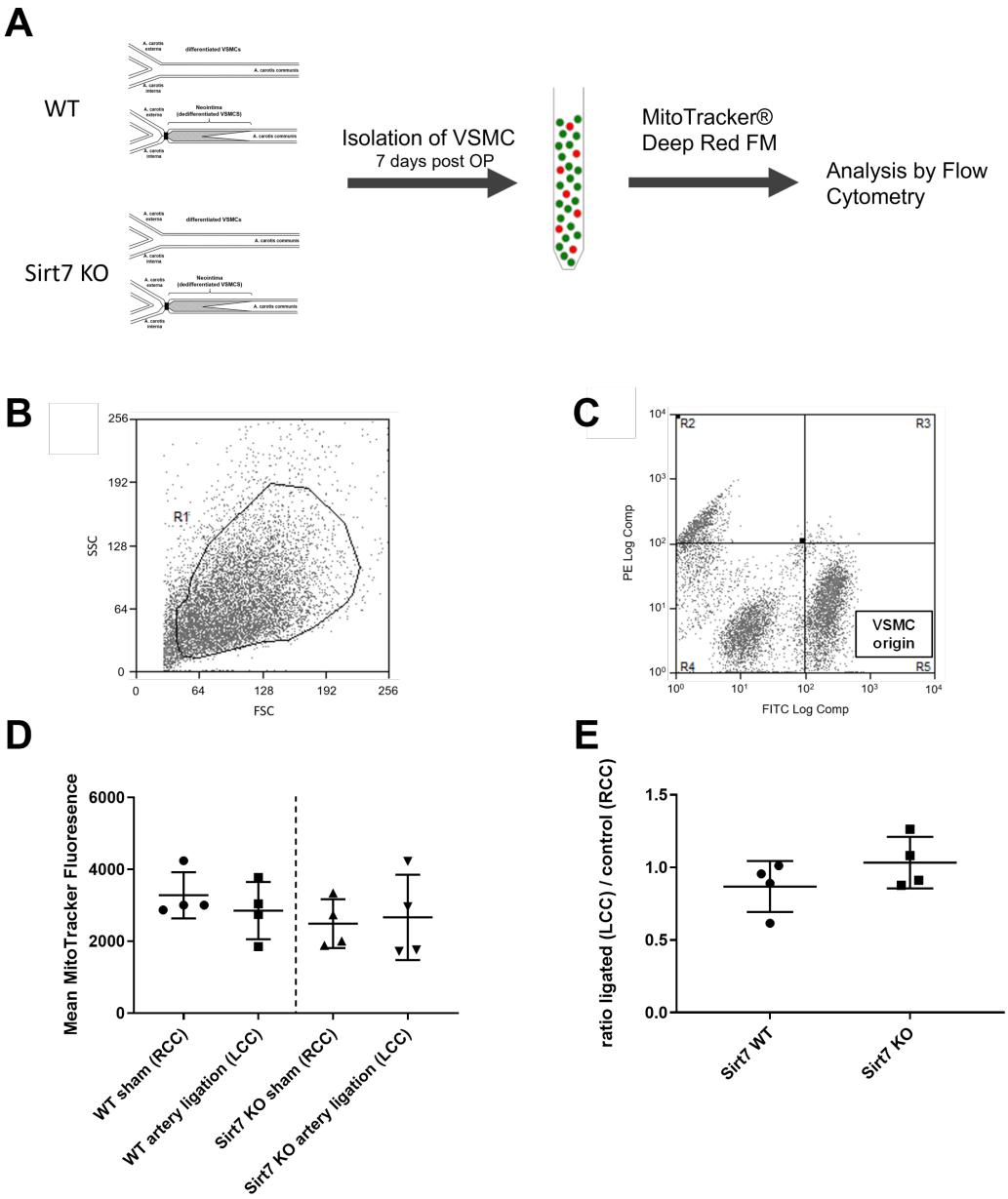
A
WT
Sirt7 KO
differentiated VSMCs
Neointima
(dedifferentiated VSMCS)
Isolation of VSMC
7 days post OP
MitoTracker®
Deep Red FM
Analysis by Flow
Cytometry
B
SSC
FSC
R1
C
PE Log Comp
FITC Log Comp
R2
R3
R4
R5
VSMC
origin
D
Mean MitoTracker Fluoresence
WT sham (RCC)
WT artery ligation (LCC)
Sirt7 KO sham (RCC)
Sirt7 KO artery ligation (LCC)
E
ratio ligated (LCC) / control (RCC)
Sirt7 WT
Sirt7 KO

Figure 39 Mitochondrial abundance in Sirt7 knock-out versus wildtype mice 7 days after carotid artery ligation
A 8-week-old SM-Sirt7-floxed-mT/mG and SM-Sirt7-WT-mT/mG mice were injected with tamoxifen for five consecutive days. The left common carotid artery (arteria carotis communis) was ligated directly below the carotid bifurcation where the common carotid artery divides into internal and external carotid arteries. The right carotid artery was left in its original state and served as internal control. 7 days after surgery, vessels were harvested and digested to release cells from the tissue which were then stained with MitoTracker™ Deep Red FM and analysed by flow cytometry. **B** Forward vs. Side scatter: Only cells from Gate R1 were used for further analyses **C** Red fluorescence as PE compensated versus the GFP fluorescence as FITC compensated: Cells accumulating in the upper left quadrant (R2) display red fluorescence and accordingly are not from VSMC origin while cells in the lower right quadrant (R5) display green fluorescence and are thus from VSMC origin. **D** Mean MitoTracker fluorescence of cells (from R5 only) isolated from sham operated carotids (control) vs. ligated carotid arteries 7 days after surgery of wildtype or Sirt7 knock-out mice. **E** Ratio of MitoTracker fluorescence of cells (from R5 only) from ligated carotid arteries (LCC) and control right carotid arteries (sham RCC) for each genotype. Data are shown as individual values with mean ± standard deviation. Analysed were 4 Sirt7 wildtype mice and 4 Sirt7 floxed mice (n per genotype= 4).

3.2.6 Proliferation of VSMCs after Sirt7 knock-down

In their publication from 2018, Zheng et al. postulated that Sirt7 regulates VSMC proliferation via the Wnt / β-catenin signaling pathway [203]. To check whether these results could be reproduced, a proliferation assay with A7r5 cells that were transfected with Sirt7 siRNA was performed. Additionally, cells with knocked-down Sirt7 were analysed for expression of genes from the canonical Wnt-signaling pathway.

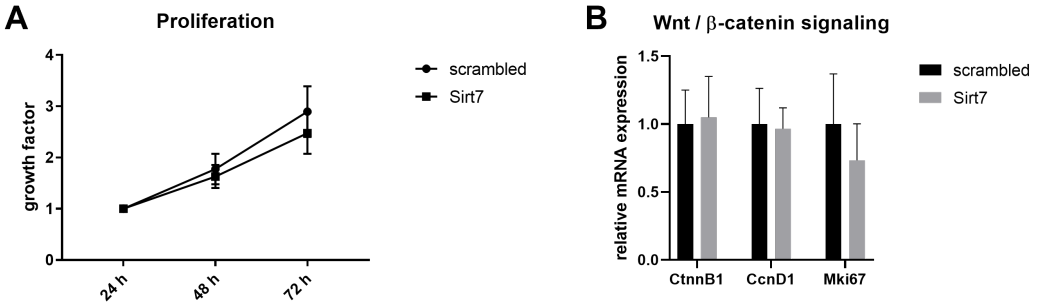

Figure 40 Proliferation of and Wnt-signaling in VSMCs after Sirt7 siRNA knock-down
A7r5 cells were transfected with either scrambled or Sirt7 siRNA on two consecutive days. **A** Cells were then seeded with the same density into wells of a 24 well plate. 24 h, 48 h and 72 h after seeding, the cells from 4 wells were trypsinised and counted. The cell number 24 h after seeding was set as the baseline and a growth factor was calculated.
B Expression of genes involved in the canonical Wnt-pathway and in proliferation was analysed with RT-qPCR 72 h after the first transfection. Data are shown as mean ± standard deviation. Six independent experiments were performed for **A** (n=6). Three independent experiments were performed for **B** (n=3).

There was no difference observed in proliferation of VSMCs after Sirt7 knock-down. Moreover, there was no difference in expression of β-catenin (CtnnB1) or cyclin D1 (CcnD1), both directly involved in the Wnt / β-catenin signalling pathway. Expression of the proliferation marker Ki67 (Mki67) was also not significantly changed after siRNA mediated knock-down of Sirt7.

3.2.7 Composition of atherosclerotic plaques in Sirt7 deficient ApoE$^{-/-}$ mice

As shown in Figure 33 Sirt7-KO-ApoE$^{-/-}$ mice developed larger atherosclerotic plaques after 12 weeks of a Western type diet than Sirt7-WT-ApoE$^{-/-}$ mice. Since the Sirt7 knock-out was only present in the VSMCs, it was then of interest to determine whether the number of VSMCs within the plaques was altered in the Sirt7 knock-out animals. However, as described before it can be difficult up to impossible to differentiate between cells that originate from VSMCs and other cells in the plaque that just assume a VSMC-like phenotype. To address this difficulty, genetic lineage tracing was employed again. SM-Sirt7-floxed-ApoE$^{-/-}$-mT/mG and SM-Sirt7-wildtype-ApoE$^{-/-}$-mT/mG mice were fed a Western type diet for 12 weeks to induce the development of atherosclerosis. They were then analysed for cholesterol levels in the blood as well as the VSMC content within the plaques.

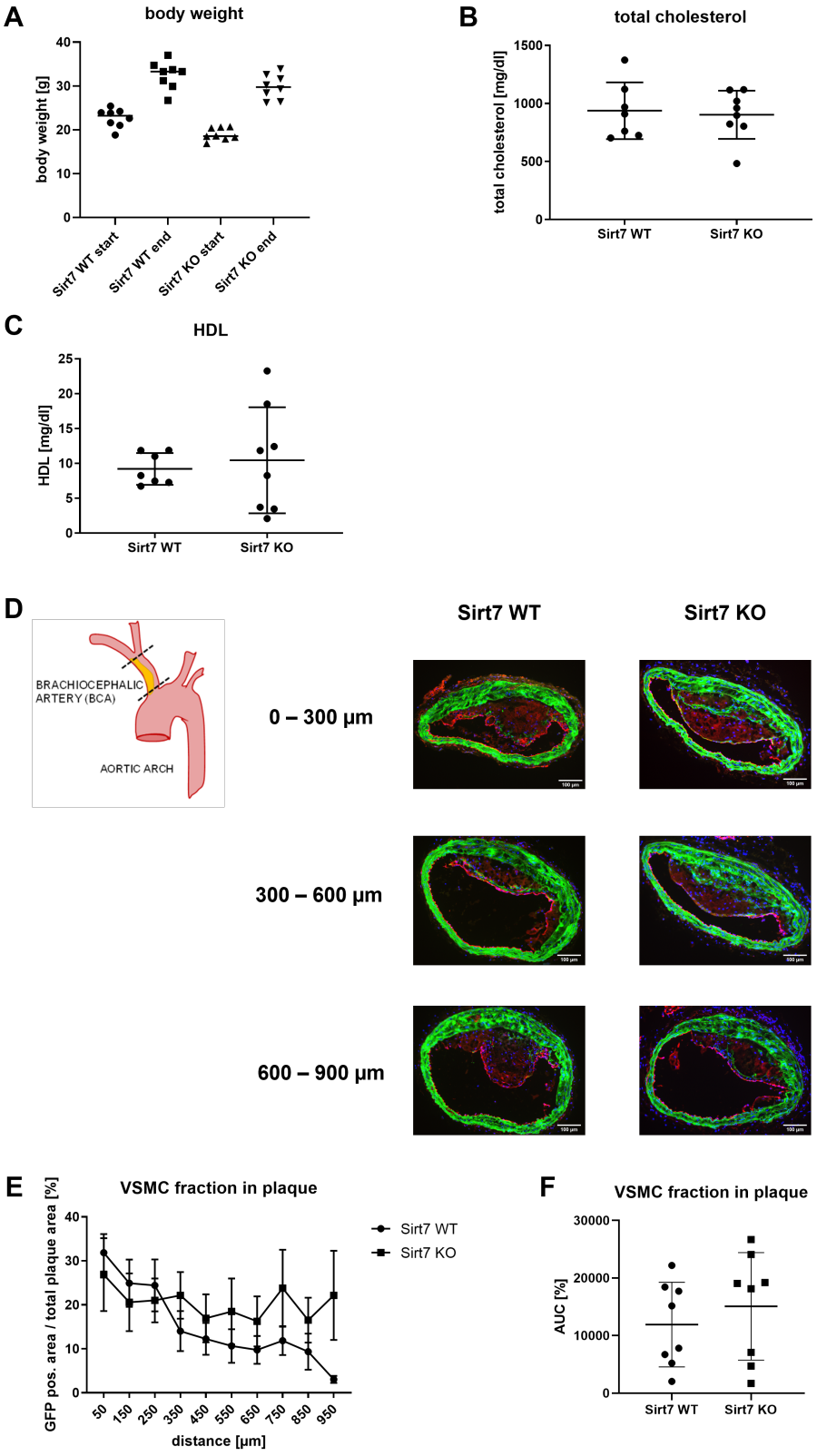
A
body weight
body weight [g]
40
30
20
10
0
Sirt7 WT start
Sirt7 WT end
Sirt7 KO start
Sirt7 KO end
B
total cholesterol
total cholesterol [mg/dl]
1500
1000
500
0
Sirt7 WT
Sirt7 KO
C
HDL
HDL [mg/dl]
25
20
15
10
5
0
Sirt7 WT
Sirt7 KO
D
Sirt7 WT
Sirt7 KO
BRACHIOCEPHALIC ARTERY (BCA)
AORTIC ARCH
0 – 300 µm
300 – 600 µm
600 – 900 µm
E
VSMC fraction in plaque
GFP pos. area / total plaque area [%]
40
30
20
10
0
50
150
250
350
450
550
650
750
850
950
distance [µm]
Sirt7 WT
Sirt7 KO
F
VSMC fraction in plaque
AUC [%]
30000
20000
10000
0
Sirt7 WT
Sirt7 KO

Figure 41 Plaque composition in Sirt7 deficient ApoE$^{-/-}$ mice compared to Sirt7 wild-type ApoE$^{-/-}$mice
8-week-old SM-Sirt7-floxed-ApoE$^{-/-}$-mT/mG and SM-Sirt7-WT-ApoE$^{-/-}$-mT/mG mice were injected with tamoxifen for five consecutive days. The mice were then fed a Western type diet for 12 weeks. Shown is **A** body weight at beginning and end of the experiment, **B** levels of total cholesterol in the blood serum after 12 weeks of Western type diet and **C** levels of HDL in the blood serum after 12 weeks of Western type diet. **D** Representative images of cross sections of the brachiocephalic artery (BCA) 0-300 µm, 300-600 µm and 600-900 µm distal from the branch-off from the aortic arch. **E** The GFP positive area was measured in cross sections of the BCA at indicated distances from the branch-off from the aortic arch and is shown as percentage of the total plaque area. **F** The area under the curve was calculated and shows the relative content of VSMCs in relation to the total plaque volume. Data are shown as individual values (A, B, C, D and G) with mean ± standard deviation or as mean ± standard error of mean (SEM) (E). Analysed were 8 SM-Sirt7-wildtype-ApoE$^{-/-}$ mice and 8 SM-Sirt7-floxed-ApoE$^{-/-}$ mice (n per genotype = 8).

There was no difference in body weight at the beginning and end of the experiment between the two groups (Figure 41A). There was also no difference in total cholesterol and HDL levels in Sirt7-floxed-ApoE$^{-/-}$-mT/mG and Sirt7-WT-ApoE$^{-/-}$-mT/mG mice (Figure 41B and C). The GFP positive area, indicating the cells of VSMC origin, was measured and shown as percentage of the total plaque area. There was no difference in the VSMC fraction of total plaque area over the length of the BCA between Sirt7 knock-out and wildtype mice (Figure 41E). Therefore the calculated volume of VSMC-derived cells within the plaques was also not different between Sirt7 knock-out and wildtype mice (Figure 41F).

4 Discussion

The aim of this study was to investigate the association between VSMC dedifferentiation and VSMC metabolism in vascular disease. It was tested whether metabolic processes adapt to the requirements of the new phenotype during VSMC dedifferentiation. This was investigated in two *in vitro* and one *in vivo* mouse model of VSMC dedifferentiation. The second part of this study aimed at manipulating VSMC metabolism through deletion of known metabolic regulators Sirt6 and Sirt7 and determining whether direct intervention in the cells' metabolism would impact VSMC dedifferentiation in an *in vitro* and *in vivo* model of VSMC dedifferentiation and in an atherosclerosis mouse disease model.

4.1 Effects of VSMC dedifferentiation on metabolism

4.1.1 PDGF regulates VSMC dedifferentiation and metabolism

As smooth muscle cell plasticity, also referred to as phenotypic switching, phenotypic modulation or phenotypic transition, is an intrinsic and complex process, it is an ongoing challenge to find suitable models that fully represent it. In this study, different cell culture models, an *in vivo* artery ligation model and an atherosclerosis disease model were used to study VSMC phenotypic switching *in vitro* and *in vivo*. A cell culture model that has been used widely and frequently is the induction of VSMC dedifferentiation by the growth factor PDGF-BB. Cultured VSMCs treated with PDGF-BB have been shown to exhibit increased proliferation and migration which is accompanied by a decrease in smooth muscle marker gene expression [98, 204]. In this study, the effect of PDGF treatment for 48 h on the mRNA levels of two smooth muscle markers, SMα-actin (Acta2) and myosin heavy chain (Myh11), was assessed in isolated mouse VSMCs. As expected, expression of both genes declined significantly upon PDGF treatment (Figure 15). Therefore, the PDGF-driven dedifferentiation model of mVSMCs was established and was then used for following experiments. In a previous experiment in the working group, the expression pattern in differentiated versus dedifferentiated VSMCs was acquired with a proteomics approach. For this, VSMCs directly isolated from mouse aortas and carotid arteries were compared to previously isolated VSMCs that were cultured and treated with PDGF for several days. As expected, protein levels of VSMC markers, including Myh11, Acta2, SM-22α and calponin were severely reduced or not detectable in PDGF treated cells versus freshly isolated cells. Interestingly,

there was a major shift in expression levels of proteins involved in cell metabolism. Most prominent was a drop in the abundance of mitochondrial proteins after PDGF treatment. From this experiment and evidence in the literature (see 1.5.1), the hypothesis that VSMC phenotypic transition is accompanied by an adaption of the metabolism towards the requirements of the respective phenotype, was generated.

To verify this hypothesis, the mRNA levels of selected genes involved in glucose uptake, glycolysis, lactate production, oxidative phosphorylation and fatty acid oxidation were measured after 48 h of PDGF treatment. Expression of two glycolytic enzymes, Aldoa and Eno1, was elevated while glucose transporter 1 (Glut1) was not changed significantly. This could indicate a higher glycolytic rate but no increased glucose uptake. Most prominent was the increase in Ldha expression which leads to speculation whether the acetyl-coA generated in an accelerated glycolysis is increasingly converted to lactate. An increase of Ldha expression as well as elevated lactate production after PDGF treatment was also demonstrated by Perez et al. [149]. While glycolysis seemingly increased, genes coding for different subunits of complexes in the respiratory chain were down-regulated (pyruvate dehydrogenase subunits Pdpr, Pdhb and Pdha1) or not altered (Atp5h, Ndufs1) in this PDGF-BB driven model.

Taken together, the gene expression analysis does indicate that PDGF-BB driven dedifferentiation is accompanied by changes in metabolic pathways. Gene expression alone, however, cannot depict the overall metabolic turnover and whether it is altered during VSMC phenotypic switching. Therefore, the oxygen consumption and lactate production of VSMCs treated with PDGF-BB were measured with a flux analyser. Cells grown with PDGF displayed a higher basal respiration as well as higher maximal respiration, spare respiratory capacity and ATP production. Extracellular acidification rate (ECAR), indicative of lactate production, was also elevated in PDGF treated cells throughout the whole measurement compared to control (Figure 17C). However, it is a known feature of the method that the measurement largely correlates with the number of cells present in the observed wells. Therefore, the measured values were normalised to DNA amount in each well. Upon this normalisation, the picture looked reversed. Basal respiration was then significantly lower in PDGF treated cells compared to control. ATP production, maximal respiration and spare respiratory capacity were also reduced in PDGF treated cells (Figure 17F). Normalised ECAR values did not show any difference between treatment and control until FCCP

injection during the measurement whereupon the acidification rate in control cells was higher than in PDGF treated cells. These drastic changes show that the cell number in the PDGF treated wells must have increased substantially. This could be expected as PDGF has been shown to increase VSMC proliferation before. Normalisation to different parameters such as protein levels or, like in this case, DNA content is important and necessary but might not be able to fully negate the effects of a large difference in cell number during the measurement. As VSMC dedifferentiation leads to a more synthetic phenotype which is characterised by the expression and secretion of a variety of proteins, it is also questionable whether the increase in protein content is correlative to the increase in cell number. These difficulties might be one reason for the contradictory results when looking at flux analysis of PDGF treated cells.
Perez et al., for instance, found that PDGF treatment increased both mitochondrial respiration, most prominently the spare respiratory capacity, and lactate production significantly [149]. In their study, they normalised the flux data to protein content in the wells to compensate for increased cell proliferation. These results match the results obtained in this study before the normalisation was applied. Once normalised however, the results contradict each other as Perez et al. have shown increased mitochondrial activity and lactate production whereas they are reduced or not significantly altered in the study presented here. These differences might be due to the different normalisation methods used as well as to the different durations of PDGF treatment. Perez et al. treated VSMCs with PDGF for 24 h before the measurement while cells in this study were treated for 7 days before being reseeded and measured. In addition, the amounts of substrates, like glucose and glutamine, added during the measurement were different. Perez et al. performed their experiments in rat aortic smooth muscle cells while cells from mouse aortas and carotid arteries were used here.

A better indicator of the metabolic shift during phenotypic switching is probably the OCR/ECAR ratio as it is based on the measured values from the same well and circumvents the problem of the difference in cell number. PDGF-treated cells displayed a significantly lower ratio compared to control cells, indicating a shift towards increased lactate production. This correlates with the elevated mRNA levels of Ldha after PDGF treatment as higher expression of Ldha could directly lead to an increased lactate production. Perez et al. have also shown an increase in Ldha protein expression and enzyme activity and have shown this upregulation to be dependent on the PI3K pathway.

Increased lactate production is often a direct effect of an increased glycolysis. There are reports that glycolysis can directly regulate VSMC proliferation by affecting cell cycle protein expression and phosphorylation. This was found using 2-desoxyglucose (2-DG) to inhibit glycolysis [149, 205]. This concept has also been shown for endothelial cells, where glycolysis is a key regulator of vessel sprouting, a process in which endothelial cells proliferate to form new vessels [206]. As endothelial proliferation during vessel sprouting and VMSC proliferation during phenotypic switching are similar processes, it stands to reason that the regulatory mechanisms might also be similar.
The effects of PDGF on metabolic pathways was also shown in pulmonary arterial smooth muscle cells (PASMCs). Xiao et al. demonstrated that PDGF promotes PASMC proliferation accompanied by an increase in lactate production as well as LDH and Glut1 expression while cellular ATP production and pyruvate dehydrogenase (PDH) expression was decreased [148]. This is indicative of the Warburg effect, a metabolic phenomenon by which cancer cells produce lactate from glucose even under non-hypoxic conditions. Xiao et al. showed an enhanced Warburg effect in PDGF treated PASMCs. They found the PI3K/AKT/mTOR/HIF-1α signaling pathway to be involved in promoting this process. HIF-1α has been shown to play an important role in regulating the Warburg effect in tumour cells by activating the gene expression of pyruvate dehydrogenase kinase 1 (PDK1). Increased PDK1 inhibits PDH, which in turn inhibits the TCA cycle and enhances the Warburg effect. Xiao et al. also found a feedback regulation between the Warburg effect and HIF-1α. Thus, they demonstrated that PDGF promotes the Warburg effect by activating the PI3K/AKT/mTOR/HIF-1a signaling pathway in PASMC proliferation [148].
The results from the present study confirm that PDGF has similar effects in mouse VSMCs. The significantly lower OCR/ECAR ratio compared to control and elevated Ldha mRNA levels after PDGF treatment indicate a shift towards increased lactate production which strongly suggests that PDGF enhances the Warburg effect in mVSMCs. Whether this is a consequence or the driving force of VSMC dedifferentiation, could not be resolved in this experiment.
Experiments in other models are thus needed to further understand the link between VSMC dedifferentiation and metabolism.

4.1.2 Cholesterol treatment affects VSMC phenotypic plasticity and metabolism

The second *in vitro* model of VSMC phenotypic switching used in this study was the treatment of mVSMCs with cholesterol. As the accumulation and uptake of

cholesterol plays a fundamental role in the development of atherosclerotic lesions it might be the model better suited to depict the processes in this disease. Incubation of isolated mVSMCs with free cholesterol, complexed to methyl-β-cyclodextrin which enhances the solubility of the cholesterol, leads to a phenotypic transition towards a macrophage-like phenotype as was demonstrated by Rong et al. [100]. Expression of VSMC marker genes like SMα-actin, MHC and calponin-h1 decreased drastically after 72 h of cholesterol treatment while macrophage markers CD68 and Mac2 expression was significantly elevated. Expression of Abca1, a key regulator of cholesterol efflux, was also increased upon cholesterol treatment. VSMCs incubated with cholesterol acquired phagocytic activity, further converging towards the macrophage phenotype. The authors refer to this phenotypic transition towards the macrophage-like cells as transdifferentiation.
These findings were confirmed in this study as cholesterol treatment for 24 h, 48 h and 72 h reduced the expression of smooth muscle marker genes and significantly elevated macrophage markers and Abca1 (Figure 18).
After establishing the model, it was used to analyse the expression of several genes involved in metabolic pathways. When looking at genes involved in glucose uptake, glycolysis and lactate production, mRNA expression levels were not significantly changed except for a slight trend of increased Ldha expression after 24 h and 48 h. However, mRNA levels of enzymes from the citric acid cycle, the respiration chain and fatty acid oxidation, all associated with mitochondria, were downregulated upon cholesterol treatment, suggesting that transdifferentiation is accompanied by a metabolic shift.
Flux analysis showed no difference in mitochondrial respiration but a significant increase in lactate production resulting in a shifted OCR to ECAR ratio towards increased ECAR. In contrast to the PDGF driven model, cholesterol did not have an impact on VSMC proliferation and the data did not change significantly upon normalisation to DNA content. As is the case with PDGF, cholesterol probably can also directly impact cell metabolism. Cholesterol accumulation in liver mitochondria was shown to disrupt mitochondrial functional performance and the organisation of respiratory supercomplexes in a recent study [207].

Taken together, both *in vitro* models suggest changes in VSMC metabolism upon induction of phenotypic switching. An elevated lactate production and data suggesting an increased glycolysis were observed with both methods upon phenotypic transition. This would indicate that VSMCs undergo similar processes as endothelial cells during

angiogenesis which also rely on glycolysis and lactate production to render energy faster and in a hypoxic environment. Cancer cells are also known to shift their energy generation from mitochondrial respiration towards glycolysis and lactate production, known as the Warburg effect. It stands to reason that VSMCs, in order to adapt to proliferative and synthetic phenotypes, underly the same mechanism. Whether a shift in metabolism is a driver of VSMC phenotypic switching or the shift happens in reaction to external dedifferentiation-inducing stimuli, is not fully understood.

4.1.3 Effects of VSMC dedifferentiation on VSMC metabolism *in vivo*

Cell culture models are useful to study specific processes in a contained reproducible environment. VSMC phenotypic plasticity, however, is an intrinsic and complex process that is influenced by the cells' microenvironment, cell-cell interactions, extracellular matrix, hemodynamic factors and cytokines. Crosstalk between endothelial cells and VSMCs, for example, has effects on both the contractile and the synthetic VSMC phenotype. The current cell culture models cannot depict this *in vivo* environment and are thus limited. To study VSMC phenotypic switching *in vivo*, a carotid artery ligation model was used in this study. The ligation of the artery induces VSMC dedifferentiation and proliferation and leads to neointima formation (similar to restenosis processes, see 1.2 and 2.2.6) VSMC dedifferentiation in this model was confirmed by determining the expression of VSMC differentiation markers α-SMA and Myh11 which were significantly down-regulated in ligated arteries (Figure 21).

In a next step, the expression of genes involved in glycolysis, the TCA cycle, oxidative phosphorylation and fatty acid oxidation three days after carotid artery ligation was measured. Expression of Slc2a1 encoding the glucose transporter 1 (Glut1) was increased in ligated arteries. As Glut1 is the domineering isoform of the GLUT family in VSMCs, an elevated expression could suggest an increased glucose uptake in VSMCs upon ligation induced dedifferentiation. Expression of Pfkfb3, an important activator of glycolysis, was also upregulated in dedifferentiated VSMCs. As Pfkfb3 was shown to play an important role in the regulation of endothelial proliferation through glycolysis, it is likely that it is also involved in an enhanced glycolytic activity and possibly VSMC proliferation [206]. Expression of Pgk1 which catalyses the first ATP-generating step of the glycolytic pathway, was also significantly elevated after carotid artery ligation. Together with the upregulation of other glycolytic enzymes like Eno1 this indicates an enhanced glycolytic activity in dedifferentiating VSMCs. It was demonstrated by Li et al. that conditions like hypoxia and oncogenic mutations

that lead to the activation of ERK signaling, can induce translocation of Pgk1 to the mitochondria. Mitochondrial PGK1 phosphorylates pyruvate dehydrogenase kinase 1 (PDK1) which in turn inhibits the pyruvate dehydrogenase complex (PDH). This suppresses mitochondrial pyruvate metabolism and increases lactate production, effectively promoting the Warburg effect [208]. The upregulation of Pgk1 and the fact that the VSMC dedifferentiation in this model is at least partly hypoxia driven, invite to speculate that the same mechanism is at work during phenotypic switching of VSMCS.
An essential enzyme in cell metabolism is lactate dehydrogenase. In this setting, expression of Ldha was upregulated significantly upon dedifferentiation of VSMC. Higher expression of Ldha suggests an increased lactate production, possibly also under oxygen rich conditions. In other studies lactate was shown to mediate the regulation of proliferation, migration, gene transcription and synthetic phenotype modulation in VSMCs [147]. Depletion of LDHA suppressed the viability, proliferation, migration and invasive abilities of human and rat aortic smooth muscle cells [209, 210].

Supporting the theory of a Warburg like effect in switching VSMCs, expression of enzymes from the TCA cycle and subunits from the respiration complexes was down-regulated upon artery ligation. Idh2 expression, for example, was reduced three days after ligation. Impaired function of Idh2 through mutations is known from many cancers and other diseases [211]. This parallel between reduced Idh2 activity in cancer cells and in proliferating VSMCs could further indicate a Warburg-like effect in proliferating VSMCs.
Expression of critical enzymes involved in the oxidation of fatty acids was also significantly reduced in dedifferentiated VSMCs in this model. This suggests a decrease in fatty acid oxidation in the VSMC synthetic phenotype. Two other groups however have found an increased fatty acid oxidation in dedifferentiated VSMCs and postulated a shift in metabolism from glucose-based substrates to free fatty acids [150, 212]. These studies, however, were carried out in cell culture models of VSMC dedifferentiation, whereas the data presented here stem from an *in vivo* model. Due to the different conditions and setups, discrepancies between the behaviour of switching VSMCs *in vitro* and *in vivo* could have surfaced. Additionally, in the present study only gene expression analysis was carried out. It is possible that lower gene expression of fatty acid oxidation enzymes does not reflect in the actual metabolic output of the cell. Since no metabolic flux analyses were done on the tissue, changes in the metabolic output of VSMCs *in vivo* can only be speculated upon based on the

gene expression pattern.

Taken together, the gene expression analysis in dedifferentiated cells from ligated carotid arteries strongly suggests a metabolic shift in switching VSMCs. Upon dedifferentiation, glycolysis seems to be enhanced in VSMCs while mitochondrial respiration is reduced. Significantly increased expression of Ldha indicates that dedifferentiated VSMCs turn towards aerobic glycolysis and metabolise pyruvate to lactate instead of shunting it into the TCA cycle and respiration chain. These processes are reminiscent of the Warburg effect in cancer cells. It is assumed that it is not the generation of energy in form of ATP but other metabolic requirements that drive the Warburg effect in proliferating cells. As proliferating cells need to replicate their cellular content in order to create new cells, they have a large need for cellular building blocks like nucleotides, amino acids and lipids. To meet this need, not all glucose can be catabolised completely as parts of its carbon chain are needed as basis for other molecules. Acetyl-CoA, for example, is needed as a building block for acyl chains to synthesise lipids.
Another important pathway, the pentose phosphate pathway, generates NADPH, pentose sugars and ribose 5-phosphate, which serve as precursor molecules for nucleotide synthesis. Glucose-6-phosphate which is generated in the first step of glycolysis is shunted into this pathway [136].

Based on the results from this study it seems likely that VSMCs also rely on the Warburg effect with increased glycolysis and lactate production in order to meet their metabolic requirements upon the increased proliferation and synthetic activity of the dedifferentiated phenotype. Elevated lactate levels and production in synthetic VSMCs has been shown before [147]. Lactate production, however, could also not only be due to aerobic glycolysis but also to anaerobic glycolysis as the occlusion of the blood vessel by the ligation could lead to a lack of oxygen, inducing HIF1α and energy generation through anaerobic means. It has also been shown that low mechanical shear stress induces HIF1α in endothelial cells. As ligation of the vessel reduces the blood flow in the carotid artery and consequently alters the shear stress, the same mechanisms could be in place in this model and not only apply to endothelial cells but also to the underlying VSMCs [213]. This also presents a drawback of this model which is the possible contamination with endothelial cells. As there is only one layer of endothelium and a whole media of VSMCs, the overwhelming number of VSMCs in relation to endothelial cells should make

endothelial cells negligible. Nevertheless, influences by endothelial mRNA can still not be excluded.

Taken together, the data from the *in vivo* ligation model match the data obtained from the cell culture models that also indicated a metabolic shift in VSMCs during phenotypic switching. The cells undergo a Warburg-like effect to generate building blocks and other metabolites needed in a state of increased proliferation.

4.1.4 The role of mitochondria in VSMC dedifferentiation

Although studies have shown that cancer cells undergoing the Warburg effect did not show impaired mitochondrial function, the downregulation of various mitochondrial genes in all the models utilised here lead to the question whether mitochondria are, unlike in cancer cells, compromised in any form in dedifferentiated VSMCs [141, 142]. Lower expression of mitochondrial enzymes could indicate less mitochondrial activity but also lower mitochondrial abundance in the cell. Especially the downregulation of the expression of subunits of the respiratory complexes would suggest a lower abundance rather than reduced activity as the activity is usually not transcriptionally regulated. To test whether the processes induced by the artery ligation have a direct or indirect impact on the cells' mitochondria, a series of experiments was performed to investigate whether the down regulation of mRNA expression led to fewer mitochondria or if mitochondrial integrity was affected.

One means to investigate the abundance of mitochondria in cells is to determine the amount of mitochondrial DNA present in the cell and normalize this to the nuclear DNA. This relies on the fact that there are as many copies of mitochondrial DNA present in the cell as there are mitochondria while there is only one copy of nuclear DNA. Here, it was found that 4 weeks after artery ligation the mtDNA to nuclear DNA ratio decreased by 25%. The p-value was 0.09 and thus did not meet the significance threshold of 0.05 but still suggests a relevant difference between ligated artery and control. A lower mtDNA to nDNA ratio indicates that there were less mitochondria present in the dedifferentiated VSMCs from the ligated artery than in differentiated cells from the control artery. Again, the influence of endothelial cells on the measurement cannot be eliminated.

In order to address the problem of potential bias by other cell types in the harvested tissue, a genetic lineage tracing mouse model (SM-mT/mG) was employed. Induction

of a smooth muscle cell specific cre recombinase results in permanent labelling of VSMCs with GFP while all other cells continue expressing mTomato. VSMCs from carotid tissue taken from these mice could then be identified with flow cytometry. The cells were stained with MitoTracker™ Deep Red to label mitochondria and the fluorescence measured only in cells from VSMC descent. MitoTracker fluorescence was significantly reduced in VSMCs from ligated carotid arteries. This indicates less abundance of mitochondria in dedifferentiated VSMCs. However, there are limitations to this interpretation. There have been reports that MitoTracker™ Deep Red is potentially sensitive to the mitochondrial membrane potential although the manufacturer claims otherwise. The intermembrane mitochondrial potential $\Delta\Psi$m is defined by the proton gradient across the inner mitochondrial membrane that is generated by the electron transport chain. Although the manufacturer claims the function of MitoTracker™ Deep Red FM is not affected by the mitochondrial potential, some groups have used it as an index for it. Data generated by Xiao et al. suggest that the intensity of MitoTracker™ Deep Red changes along with mitochondrial potential [214]. This might make it an unreliable tool to assess mitochondrial mass in cells that have undergone metabolic changes.

Other groups that have investigated the role of mitochondria in VSMC phenotypic plasticity have found links between mitochondrial morphology, mitochondrial potential and VSMC proliferation. Salabei and Hill found that PDGF treatment of VSMCs resulted in mitochondrial fragmentation and a 50% decrease in mitofusin 2 (Mfn2) abundance [150]. They therefore postulated that PDGF treatment leads to increased mitochondrial fission and an impaired fusion process resulting in a fragmentation of the mitochondrial cellular network. Inhibition of mitochondrial fission with Mdivi-1 inhibited PDGF-induced mitochondrial fragmentation and reduced VSMC proliferation. A reduction of Mfn2 was also observed in highly proliferative VSMCs from atherosclerosis-prone or balloon-injured rats by Chen et al. [215, 216]. Mfn2 depletion also caused altered glucose metabolism *in vivo* [179]. Mfn2 overexpression on the other hand inhibited proliferation of neointimal VSMCs after balloon injury [215]. Along the same lines, it was found that inhibition of mitochondrial fission reduced neointima formation in response to femoral artery wire injury [53].

These data strongly suggest a link between mitochondrial fission and fusion and VSMC proliferation *in vitro* and *in vivo*. Inhibition of mitochondrial fusion was also associated with a reduction in oxygen consumption, loss of intermembrane

mitochondrial potential and mitochondrial DNA [217, 218].
The data obtained in this study suggest that this could also be true in dedifferentiated proliferating VSMCs. Decreased oxygen consumption and reduced mtDNA content were found in this study. The decrease in MitoTracker fluorescence after carotid artery ligation could possibly be due to a reduction of mitochondrial potential in proliferating VSMCs caused by increased mitochondrial fission and reduced fusion. At this point, this assumption is highly speculative however, as more data would be needed to further support this theory.

To look further into this, the morphology of mitochondria in VSMCs was assessed in this study. Cells from ligated and control carotid arteries were examined 4 weeks after surgery. As was expected, VSMCs in the vessel media were elongated, spindly and quite large while VSMCs in the neointima appeared smaller, more circular and did not show consistent orientation. This highlights that one aspect of dedifferentiation is a change in VSMC morphology. The appearance of mitochondria in the two different cell types was similar in most, but not all aspects. Mitochondria in differentiated VSMCs in the media appeared more elongated than in dedifferentiated VSMCs in the neointima. This is also reflected in the significantly higher circularity that was determined by analysing mitochondria in both cell types (Figure 25). This different shape, however, did not affect the overall size of the mitochondria. The change in shape could be due to the different morphology of the cells themselves, as the mitochondrial network could adapt to morphologic changes in the cell. It could also be indicative of an increased fission and fragmentation of the mitochondrial network as discussed above. Since electron microscopy is two-dimensional it is only possible to obtain the area and not the volume of the mitochondria. Furthermore, the mitochondrial network as a three-dimensional structure cannot be visualised with this technique. This also questions whether the number of mitochondria determined here depicts the reality in the cell. Therefore, the conclusions that can be drawn from this experiment are limited.

4.1.5 Summary - Effects of VSMC dedifferentiation on metabolism

In this first part of the study, the metabolic adaptions of VSMCs during phenotypic modulation were investigated. An experiment looking at protein expression in differentiated and dedifferentiated VSMCs generated the hypothesis that VSMC phenotypic transition is accompanied by an adaption of the metabolism towards the requirements of the respective phenotype. In the study presented here, this hypothesis was

investigated utilising two different *in vitro* models and one *in vivo* model of VSMC dedifferentiation. Results from the two *in vitro* models of VSMC dedifferentiation suggested changes in VSMC metabolism upon induction of phenotypic switching. An elevated lactate production and possibly increased glycolysis was observed with both methods upon phenotypic switching. This indicated that VSMCs undergo similar processes as cancer cells which have been shown to shift their energy generation from mitochondrial respiration towards glycolysis and lactate production, a process known as the Warburg effect. It stands to reason that VSMCs, in order to adapt to the metabolic needs of proliferative and synthetic phenotypes, underly the same mechanism.

Data from an *in vivo* carotid artery ligation model matched the data obtained from the cell culture models, also indicating a metabolic shift in VSMCs during phenotypic switching. In addition to an enhanced glycolysis, decreased oxygen consumption, reduced mtDNA content and lower MitoTracker fluorescence were found in ligated carotid arteries compared to the control. These results indicate a lower abundance of mitochondria in dedifferentiated cells compared to differentiated cells.

Electron microscopy images showed more circular shaped mitochondria in dedifferentiated VSMCs but no difference in mitochondrial number and size. These results, however, have to be interpreted carefully as electron microscopy cannot depict the three-dimensional structure of the mitochondrial network.

Taken together this study presents strong evidence for a metabolic adaptation towards increased glycolysis and lactate production in the form of a Warburg effect in dedifferentiated VSMCs. Generally, it is assumed that it is not the generation of energy in form of ATP but other metabolic requirements, that drive this effect in proliferating cells [136]. As proliferating cells need to replicate their cellular content in order to create new cells, they have a large need for cellular building blocks like nucleotides, amino acids and lipids. As dedifferentiated VSMCs not only proliferate more but can also completely change their phenotype towards a number of different cell states, they require additional cellular building blocks and metabolites to transition to and maintain these phenotypes. By reducing mitochondrial respiration and not completely catabolising glucose in the mitochondria, part of its carbon chain can be retained and used as basis for other molecules. Acetyl-CoA, for example, is needed as a building block for acyl chains to synthesise lipids. Another important pathway that generates NADPH, pentose sugars and ribose 5-phosphate, which serve as precursor molecules for nucleotide synthesis is the pentose phosphate pathway. Glucose-6-phosphate which is generated in the first step of glycolysis is shunted into

this pathway [136]. Increasing glycolysis could therefore provide more material for feeding this pathway. It is thus likely that the metabolic shift in dediffentiating VSMCs is aimed at addressing the metabolic requirements for increased proliferation and phenotypic modulation. In addition, this study showed a correlation between VSMC dedifferentiation and mitochondrial abundance, possibly but not necessarily linked to the shift in metabolic requirements. The precise role of mitochondrial abundance as well as mitochondrial fusion and fission in VSMC dedifferentiation could not be fully elucidated in this study, however.

4.2 Impact of sirtuins on VSMC proliferation and metabolism

VSMC dedifferentiation and proliferation have been shown to be accompanied by modulations of cell metabolism both in this study and in the literature. Since cell metabolism is regulated by a large variety of factors it is still unclear how the metabolic adaptations in VSMCs are regulated. One group of metabolic regulators are the sirtuins. Sirtuins are NAD^+-dependent histone deacetylases with various histone and non-histone targets. Due to their NAD dependency, they are sensors of the metabolic state of the cell and regulate metabolism accordingly. The nuclear sirtuins SIRT6 and SIRT7 have both been shown to regulate aspects of cell metabolism and expression of both, SIRT6 and SIRT7, is reduced in various cancers. SIRT6 was also shown to be protective against the Warburg effect in cancer cells. As the preferred metabolic state of dedifferentiated and proliferating VSMCs is reminiscent of the Warburg effect in cancer cells, it stands to reason that SIRT6 could also regulate this metabolic shift in VSMCs.

In this study it was also found that the expression of mitochondrial respiratory genes is down-regulated upon VSMC dedifferentiation and that the abundance and integrity of the mitochondrial network might be impaired. SIRT7 has been shown to be a master regulator of mitochondrial biogenesis through its interaction with GABP and NRF1. The parallels between metabolic regulation by sirtuins in different cell types, especially cancer cells, and the found metabolic adaptations in VSMCs are striking. If SIRT6 and SIRT7 act similarly on VSMC metabolism as on other cell types, inhibiting increased glycolysis and the Warburg effect and regulating mitochondrial biogenesis, they could potentially inhibit VSMC dedifferentiation and proliferation. This could indicate a protective role of these sirtuins in vascular diseases where VSMC plasticity plays an essential role.

Another sirtuin, SIRT1, has already been found to play a protective role in various cardiovascular diseases such as atherosclerosis. Therefore, it was one of the aims

of this study to investigate whether SIRT6 and SIRT7 impact dedifferentiation by regulating VSMC metabolism and could potentially protect against vascular diseases.

Expression of Sirt6 and Sirt7 was first assessed in the cholesterol driven *in vitro* model of VSMC dedifferentiation. After 24 h, 48 h and 72 h cholesterol treatment the mRNA levels of Sirt6 as well as Sirt7 were reduced in isolated primary mouse VSMCs. This could indicate that Sirt6 and Sirt7 play a role in maintaining VSMC differentiation. In the carotid artery ligation model Sirt6 expression was also moderately reduced 3 days after surgery. This supports the results from the *in vitro* model. Sirt7 expression however, was increased 3 days after carotid artery ligation. This was unexpected regarding the results from the *in vitro* model and the hypothesis that Sirt7 helps maintain VSMC differentiation. As the functions of SIRT7 in the cell are diverse and often intertwining with other cellular pathways however, it could very well be that an elevated expression of Sirt7 is still protective against increased VSMC dedifferentiation.

To investigate whether Sirt6 and Sirt7 play a role in VSMC dedifferentiation, possibly via modulating cell metabolism, VSMC specific Sirt6 knock-out and Sirt7 knock-out mouse strains were created. The deletion of exons 4-6 from Sirt6 and exons 6-9 from Sirt7 was achieved with a tamoxifen inducible cre recombinase at 6-8 weeks of age. The knock-out was confirmed in mice crossed with the mT/mG reporter construct. Permanently labelled VSMCs were sorted from mouse carotids and aorta and analysed for Sirt6 and Sirt7 gene expression, respectively. Both Sirt6 and Sirt7 expression was almost completely abolished in tamoxifen treated mice. It was not tested however whether truncated Sirt6 or Sirt7 mRNA and protein was made as the expression analysis only checked for the floxed exons that were supposed to be deleted.

4.2.1 Sirt6

Sirt6 knock-out did not affect neointima formation after carotid artery ligation
After successfully confirming the VSMC specific knock-out, Sirt6 WT and Sirt6 KO mice were subjected to carotid artery ligation. The neointima formation in KO versus wildtype mice was assessed histologically 28 days after surgery. VSMC-specific Sirt6 knock-out did not result in any difference in neointima formation which did not meet expectations. As mentioned earlier, it was shown that a deletion of SIRT6 promotes glycolysis and reduces mitochondrial respiration, effectively promoting the

Warburg effect in cancer cells. If the function of Sirt6 was the same in VSMCs, a metabolic shift towards the Warburg effect would be expected in response to Sirt6 knock-out. As was found earlier in this study, a metabolic adaptation like the Warburg effect occurred in VSMCs that were undergoing dedifferentiation and proliferation in this same artery ligation model. However, an enhanced glycolysis and inhibited mitochondrial respiration upon Sirt6 knock-out would be expected to lead to increased proliferation and to promote dedifferentiation. Therefore, neointima formation in Sirt6 knock-out mice would be expected to be enhanced. This was not the case in this model, however. In addition, the ligation model is at least partly hypoxia driven. HIF1α is usually negatively regulated by SIRT6 so a knock-out of this regulator would be expected to amplify the effect of hypoxia-induced glycolysis on proliferation. It could be that the effect of the Sirt6 knock-out could not be observed under these conditions as the neointima formation was not assessed until after 4 weeks after surgery. Possibly, effects could have been observed earlier in the development of the neointima. The proliferation might have been at a maximum already and could not be increased further. It would also be interesting to investigate the effect of VSMC-specific knock-out of Sirt6 in other models of vascular injury and VSMC dedifferentiation.

Sirt6 knock-out did not influence gene expression after carotid artery ligation The results from the artery ligation model and the connection between neointima formation and VSMC metabolism, found earlier in this study, gave rise to the hypothesis that Sirt6 or Sirt7 would influence neointima formation through regulating VSMC metabolism. However, a screen of metabolic gene expression after carotid artery ligation in VSMC-specific Sirt6 knock-out mice did not reveal any differences when compared to wildtype. This could suggest that Sirt6 knock-out might not impact expression of these genes in VSMCs in a major way. The sample size in this study was very small however, so more data would be needed for an ascertained assessment of this question.

Sirt6 knock-out did not influence development of atherosclerosis in ApoE$^{-/-}$ mice While the carotid artery ligation model is useful to investigate the dedifferentiation of VSMCs *in vivo*, it cannot depict the complex pathology of real vascular diseases. Therefore, the effect of Sirt6 depletion in VSMCs was also investigated in a mouse model for atherosclerosis. For this purpose, the SM-Sirt6 mouse strain was crossed with ApoE knock-out mice to create SM-Sirt6-ApoE$^{-/-}$ mice. In these mice

the apolipoprotein E (ApoE) is globally knocked-out and they possess floxed Sirt6 alleles as well as the smooth-muscle cell specific cre recombinase.
Knock-out of Sirt6 had no impact on triglyceride, total cholesterol and HDL levels in the serum of SM-Sirt6-ApoE$^{-/-}$ mice after 12 weeks of Western diet. Previously, SIRT6 deletion in the liver had been shown to lead to increased triglyceride synthesis as well as increased glycolysis and reduced β-oxidation [177]. These findings do not match with the results obtained in this study, as there was no change in triglyceride levels in this model. This might be due to the fact that the Sirt6 knock-out in this model was restricted to VSMCs in contrast to the liver-specific knock-out in the described study by Kim et al. [177]. Apparently the VSMC specific knock-out had no effect on the systemic triglyceride metabolism. There was also no evidence for increased glycolysis upon Sirt6 knock-out in the present study. The expression of three genes involved in fatty acid β-oxidation was moderately reduced, however (Figure 29). In a study using a Sirt6 knock-down model of small hairpin RNAs (shRNAs) lentivirus injection in ApoE$^{-/-}$ mice, total cholesterol levels were elevated but HDL and triglyceride levels remained the same [219]. In the present study, there was no change in cholesterol level observed. Since the lentivirus injection model primarily targets endothelial cells, it is possible that the change in systemic cholesterol level was mediated by endothelial cells upon Sirt6 knock-out. As there was a VSMC-specific knock-out in this study and endothelial cells were expressing Sirt6 normally, this effect was not observed here.

In this study, there was no difference in plaque area or plaque volume observed in SM-Sirt6-ApoE$^{-/-}$ mice compared to Sirt6 WT mice after 12 weeks of Western diet. This did not meet the hypothesis that Sirt6 could have an atheroprotective role. It is also contradictory to other studies. Grootaert et al. reported that Sirt6 reduces atherosclerosis by protecting against senescence [220]. They found that SIRT6 protein, but not mRNA, expression was reduced in human and mouse atherosclerotic plaques. This is supported by the results from Zhang et al. who also observed a lower SIRT6 protein level in human atherosclerotic plaques [221]. Another group found decreased Sirt6 mRNA expression in aortas of ApoE$^{-/-}$ mice fed a high cholesterol diet [219]. In the study presented here, Sirt6 expression was measured after carotid artery ligation and mRNA levels were moderately decreased. However, Sirt6 expression was not measured in plaques or on protein level.
Liu et al. knocked down Sirt6 in ApoE$^{-/-}$ mice using shRNA lentivirus injection. In SIRT6-shRNA-treated ApoE$^{-/-}$ mice, they found increased plaque size and augmented

plaque vulnerability, shown by increased necrotic core areas, increased macrophage accumulation and reduced collagen content. Since the lentivirus was injected into the circulation, knock-out of Sirt6 was primarily achieved in endothelial cells but also in VSMCs. Sirt6 knock-out led to endothelial dysfunction and increased atherosclerosis formation but the authors did not specifically investigate the role of VSMCs in this context [219]. Zhang et al. utilised mice that were heterozygous for Sirt6 in their study. $Sirt6^{+/-}$ $ApoE^{-/-}$ mice fed a high fat diet for 16 weeks showed increased plaque formation and features of plaque instability [221]. These results were not confirmed in the study presented here, as cre-mediated VSMC-specific knock-out of Sirt6 did not result in increased atherosclerotic plaque burden in $ApoE^{-/-}$ mice after 12 weeks of Western type diet. This inconsistency could be due to the usage of different models of Sirt6 knock-down. Since the lentivirus was injected into the bloodstream it automatically targets the endothelium first and VSMCs second. Thus, the influence of Sirt6 knock-out in endothelial cells might have overridden the effect in VSMCs. The heterozygous model was a global model whereas the model used here was VSMCs specific. Global and cell-specific knock-out might have different effects on a systemic disease like atherosclerosis.

However, Grootaert et al. also found that Sirt6 inhibits atherosclerosis although by utilising an overexpression model. In Grootaert's study, SIRT6 regulated telomere maintenance, enhanced VSMC lifespan and prevented senescence associated metabolic changes. SIRT6 overexpressing $ApoE^{-/-}$ mice showed reduced atherosclerosis, markers of senescence and inflammation compared to controls. This was dependent on the deacetylase activity of SIRT6 [220].

Regarding these results, an increase in atherosclerosis upon knock-out of Sirt6 in the model presented here would have been expected. This was not the case, however, which can be due to different reasons. After 12 weeks of Western type diet, the atherosclerotic plaques observed in this model were already quite large and depict the late stages of atherosclerosis. The diet given to the animals contained a high amount of cholesterol so that the disease was heavily driven forward. It is possible that the effects of Sirt6 knock-out were not visible in the later stages of the disease anymore as plaque burden had already reached a very high level. In addition, Grootaert et al. used a Sirt6 overexpression model while a knock-out model was used here. There might be different effects of Sirt6 overexpression and loss-of-function on a cellular level and in the pathology of the disease.

It must also be noted that different genetic backgrounds of the mice bred and used for the experiments can influence the outcome of these studies.

Taken together, the expected atheroprotective effects of Sirt6 were not observed in this study. This contrasts with other studies that did show protective effects of Sirt6 in the context of atherosclerosis although these results were obtained in models different to the one presented here. There is also not enough evidence to confirm or reject a possible link between Sirt6 mediated regulation of metabolism and VSMC dedifferentiation in disease.

4.2.2 Sirt7

Neointima formation was increased after carotid artery ligation in Sirt7 knock-out mice Sirt7 knock-out in VSMCs on the other hand did enhance the formation of neointima in the carotid artery ligation model. The Sirt7 knock-out might influence VSMC behaviour in this setting in multiple ways. One major role of Sirt7 is the regulation of mitochondrial biogenesis, as it was shown to regulate GABP as well as NRF1, both important transcription factors of mitochondrial genes.
In this study, VSMCs displayed reduced expression of several mitochondrial genes and possibly a lower abundance of mitochondria after carotid artery ligation. As was discussed above, mitochondrial dysfunction, loss of integrity and mitochondrial fission promotes VSMC proliferation, so the impairment of mitochondria could be a possible mechanism via which loss of Sirt7 resulted in increased neointima formation. SIRT7 was also found to impact glycolysis by suppressing PGK1 activity in liver cancer cells [187]. Consequently, a knock-out of Sirt7 could lead to higher PGK1 activity and thus to increased glycolysis. As enhanced glycolysis has been associated with increased cell proliferation, this is another pathway via which Sirt7 could regulate VSMC proliferation.
Like SIRT6, SIRT7 also negatively regulates the expression of HIF-1α and HIF-2α proteins. Overexpression of SIRT7 reduced the levels of HIF proteins and their transcriptional targets, consequently repressing glycolysis [189]. A Sirt7 knock-out would therefore be expected to increase expression of HIF-1α and HIF-2α proteins. This could potentially drive proliferation via an enhanced glycolytic activity.
While the knock-out of Sirt7 lead to enhanced neointima formation in this study, Kimura et al. recently reported that Sirt7 deficiency reduced neointimal formation following vascular injury in their study [222]. 28 days after femoral artery wire injury, there was less neointima formation in Sirt7 knock-out mice compared to control mice. This was true for a systemic Sirt7 knock-out as well as a VSMC specific knock-out of Sirt7. The authors attribute this to reduced VSMC proliferation based on *in vitro*

results of serum-induced VSMC proliferation. However, this seems to be reversed in the study presented here as more neointima formation was detected which indicates increased VSMC proliferation in this setting.

Sirt7 knock-out promotes the development of atherosclerosis in ApoE$^{-/-}$ mice

The effect of Sirt7 depletion in VSMCs was also investigated in a mouse model for atherosclerosis. For this purpose, the SM-Sirt7 mouse strain was crossed with ApoE knock-out mice to create SM-Sirt7-ApoE$^{-/-}$ mice. In these mice the apolipoprotein E (ApoE) is globally knocked-out and they possess floxed Sirt7 alleles, as well as a smooth-muscle cell specific cre recombinase.

Knock-out of Sirt7 had no impact on body weight and did not significantly influence triglyceride, total cholesterol or HDL levels in the serum of SM-Sirt7-ApoE$^{-/-}$ mice after 12 weeks of Western type diet. Previously, loss of Sirt7 was found to both reduce and increase plasma levels of triglycerides. Shin et al. found low levels of plasma triglycerides in a global Sirt7 knock-out mouse model. These mice also developed chronic hepatosteatosis resembling human fatty liver disease. The lower levels of triglycerides were due to reduced very-low-density lipoprotein (VLDL) secretion [223]. Another group, however, found increased plasma levels of triglycerides and fatty acids in Sirt7 knock-out mice [121]. These studies illustrate that data on the role of Sirt7 in lipid metabolism is still contradictory and that further investigation is needed. In the model presented here, VSMC-specific knock-out did not impact plasma triglyceride levels or cholesterol levels.

Sirt7 did have an impact on plaque size, however. The area and volume of atherosclerotic plaques was significantly larger in the brachiocephalic artery (BCA) of SM-Sirt7-ApoE$^{-/-}$ mice after 12 weeks of Western type diet compared to the control. This is consistent with the results from the carotid artery ligation model where Sirt7 knock-out led to an increased neointima formation. These results indicate that Sirt7 impacts VSMC dedifferentiation and proliferation. There have been no reports from other groups on the effect of Sirt7 in atherosclerosis up to this point.

Taken together, VSMC-specific knock-out of Sirt7 did not influence cholesterol or triglyceride plasma levels but resulted in significantly larger plaque size. This suggests that Sirt7 plays a role in the development of atherosclerosis and might act atheroprotective.

Knock-out of Sirt7 did not alter gene expression after carotid artery ligation As discussed above, Sirt7 might influence VSMC proliferation by regulating metabolism in the cell. The connection between neointima formation and VSMC metabolism found earlier in this study, supports the theory that metabolic adaptation can regulate dedifferentiation and proliferation of VSMCs. To further investigate this hypothesis, carotid tissue from SM-Sirt7 WT and SM-Sirt7 KO mice were screened for expression of metabolic genes after induction of VSMC dedifferentiation by carotid artery ligation. This screen, however, did not reveal any differences in gene expression patterns after artery ligation when compared to the wildtype.

Sirt7 knock-out did not impact expression of genes involved in metabolism and mitochondrial homeostasis Ryu et al. found that SIRT7 regulates mitochondrial biogenesis via deacetylating GABP. Therefore, target genes identified in their study were also analysed here. Ryu et al. found significantly decreased expression of several mitochondrial ribosomal proteins (Mrpl49, Mrps5, Mrps9), mitochondrial polymerase, mitochondrial transcription factor A (Tfam), caseinolytic mitochondrial matrix peptidase (Clpp) and mitofusins 1 and 2 (Mfn1, Mfn2) in hearts and livers from $Sirt^{-/-}$ mice as well as in primary mouse hepatocytes and cardiomyocytes with shRNA mediated knock-down of Sirt7 [121].
However, in A7r5 cells, immortalised VSMCs, expression of these genes was not significantly lowered upon siRNA knock-down of Sirt7, except for Mfn1, Mfn2 and Polrmt which were all down-regulated moderately (Figure 35).

Expression of these genes that were termed as Sirt7 target genes by Ryu et al., was also investigated *in vivo*. None of these genes, however, were regulated in aortic tissue from SM-Sirt7 KO mice compared to wildtype mice (Figure 36). Together, the *in vitro* and *in vivo* results collected in this study indicate that Sirt7 does not regulate expression of these Sirt7 target genes in VSMCs. However, more data would be needed to fully rule out a possible regulation of these genes by Sirt7 in VSMCs.

Sirt7 knock-down did not impact metabolic output of VSMCs *in vitro* Results from metabolic flux analyses support the conclusion that Sirt7 does not regulate genes involved in metabolic pathways and mitochondrial homeostasis in VSMCs. There was no difference in oxygen consumption rate or extracellular acidification rate in A7r5 cells with siRNA mediated knock-down of Sirt7 (Figure 37). The same was true when VSMCs were induced to dedifferentiate by cholesterol loading. There was

no impact of Sirt7 knock-down in differentiated or dedifferentiated A7r5 cells (Figure 38).

Since Sirt7 knock-out was reported to lead to mitochondrial dysfunction, the mitochondrial abundance in carotid arteries from SM-Sirt7 WT and KO mice was analysed after carotid artery ligation. There was no difference in MitoTracker fluorescence in ligated or sham operated carotid arteries upon VSMC-specific Sirt7 knock-out, indicating that Sirt7 does not influence mitochondrial abundance in VSMCs. As discussed in 4.1.4, MitoTracker fluorescence might not only equal mitochondrial abundance but can also be dependent on mitochondrial membrane potential which is an indicator of mitochondrial integrity. As fluorescence levels were not different between Sirt7 WT and KO mice this suggests that neither mitochondrial abundance nor mitochondrial integrity were changed upon Sirt7 depletion.

Taken together, in this study and the models used here, Sirt7 did not regulate expression of genes involved in metabolic pathways and in mitochondrial biogenesis and homeostasis, did not impact metabolic output in metabolic flux analyses and did not alter mitochondrial abundance or integrity.
Considering the evidence for Sirt7 mediated regulation of various metabolic pathways in the literature, these results were unexpected. It has been shown to regulate mitochondrial biogenesis by interacting with the transcription factors GABP and NRF1, both master regulators of mitochondrial biogenesis. These results, however, were not obtained in VSMCs but in other cell types. *In vivo* data on mitochondrial dysfunction and the role of Sirt7 in glucose and lipid metabolism was mostly obtained in mouse models with global knock-outs whereas in this study only VSMC-specific knock-outs were analysed. *In vitro* data was obtained in primary mouse hepatocytes and primary mouse cardiomyocytes [121]. To the present, the effect of Sirt7 on metabolism has not been investigated in any other studies.
The utilisation of immortalised VSMCs in some of the *in vitro* experiments presented here could possibly explain the discrepancy as the mechanisms might be different in cells that were artificially immortalised. The natural differentiation and dedifferentiation processes are also altered in these cells, so that they might not depict the *in vivo* situation very well. However, all data obtained *in vivo* in this study also consistently show no effect of Sirt7 on metabolism.
In summary, these results indicate that Sirt7 does not impact metabolic output and mitochondrial biogenesis and homeostasis in VSMCs, neither under physiological

conditions nor in the disease setting.

Sirt7 does not regulate VSMC proliferation in VSMCs In this study, Sirt7 clearly has a function in VSMCs as depletion of Sirt7 in VSMCs led to significantly increased neointima formation in the carotid artery ligation model and significantly increased plaque size in the atherosclerosis model. These effects, however, seem to not be mediated through regulation of metabolism as was previously expected. Besides cellular metabolism, there are many factors that could cause elevated neointima formation and increased plaque sizes. A change in apoptotic processes and cell senescence as well as proliferation characteristics can all lead to changes in neointima and plaque formation and composition. Furthermore, an interference in the transition of VSMCs to the different phenotypes they display in atherosclerotic lesions can also influence plaque formation. If cells transitioned to more inflammatory cell states, for example, this could be an explanation for altered plaques. Selection of one phenotype over others could therefore be of great impact in the progression of the disease. One other major factor of neointima and plaque formation is VSMC proliferation. VSMC proliferation in plaque formation can have both beneficial as well as detrimental effects. One possible scenario for the formation of larger neointima as well as larger plaques found in this study could be that loss of Sirt7 influenced VSMC proliferation which then resulted in more neointima formation and larger plaques.

Several groups have associated Sirt7 with the regulation of cell proliferation. Fang et al. showed that Sirt7 knock-down inhibited the proliferation, promoted the apoptosis and reduced the migration of mouse airways smooth muscle cells by modulating the expression of TGF-β receptor I [224]. Consequently, Sirt7 overexpression had the opposite effects in their study i.e., it increased proliferation, reduced apoptosis and promoted migration. Along the same lines, overexpression of Sirt7 in colorectal cancer cell lines increased growth rates and invasiveness in *in vitro* and *in vivo* models [225, 226]. Knock-down of Sirt7 reversed these phenotypes. Although data on the role of Sirt7 in cancer is controversial, it is mostly perceived as a potential oncogene due to its effects on proliferation and migration. Several other studies reported a role of Sirt7 in cancer. Increased levels of Sirt7 have been found in cancer samples from patients and in cancer cell lines [181, 227]. Furthermore, knock-out of Sirt7 in hepatocellular cancerous cells and in bladder cancer cell lines resulted in decreased proliferation and migration [227, 228].
However, there were also reports that contradict these studies. Vakhrusheva et al.

for example, did not find any effect of Sirt7 on proliferation [183]. These differences could be due to the different types of tissue and different cell lines that were used in these studies. Sirt7 might have differential functions in highly proliferative tissue like cancer versus postmitotic tissue such as the heart as in Vakhrusheva's study.
In VSMCs, Zheng et al. reported that knock-down of Sirt7 significantly promoted cell proliferation and migration while overexpression had reverse results. They studied the impact of Sirt7 in a cell culture model of atherosclerosis where they treated human vascular smooth muscle cells (HAVSMCs) with ox-LDL. They propose that Sirt7 inhibited HAVSMCs proliferation and migration via enhancing Wnt / β-catenin activation [203]. In the present study however, there was no difference in proliferation of VSMCs observed after Sirt7 knock-down *in vitro* (Figure 40A). There was also no difference in expression of β-catenin (CtnnB1) or cyclin D1 (CcnD1), both directly involved in the Wnt / β-catenin signalling pathway and down-regulated in the Zheng et al. study upon Sirt7 knock-down (Figure 40B). Expression of the proliferation marker Ki67 (Mki67) was also not significantly changed after siRNA mediated knock-down of Sirt7 in the study presented here.

In addition to these *in vitro* results, the proliferation of VSMCs was investigated in the atherosclerosis disease model. Therefore, the number of VSMCs within the plaques of Sirt7 WT and Sirt7 KO animals was determined. However, as described before, it is difficult to determine whether cells in the plaque originate from VSMCs or from other cells. To address this difficulty, genetic lineage tracing was employed again and SM-Sirt7-floxed-ApoE$^{-/-}$-mT/mG mice and respective controls were created. VSMCs were thus permanently labelled with GFP while other cell types continued to express mTomato. The fraction of cells in the plaque that originated from VSMCs was determined based on the green fluorescence. The percentage of VSMCs averaged around 20% and was not different in Sirt7-KO animals compared to the control.

These data suggest that Sirt7 does not regulate proliferation in VSMCs. This is contrary to the data from Zheng et al. who found increased cell proliferation and migration upon Sirt7 knock-out and the reverse upon Sirt7 overexpression. They suggest that Sirt7 regulates VSMC proliferation by a Wnt / β-catenin-dependent mechanism [203]. Wnt signaling has previously been shown to impact mitochondrial homeostasis in several ways [134]. Considering the link between mitochondrial homeostasis and VSMC dedifferentiation and proliferation that was found earlier in the presented study, this could be a potential mechanism how Wnt signaling

impacts VSMC proliferation. However, expression of important participants of the Wnt signaling pathway was not altered in the Sirt7 knock-down setting in the present study, suggesting that this mechanism is only present in specific conditions.
Also contrary to the data presented here, Kimura et al. reported that Sirt7-deficient VSMCs showed lower levels of proliferation capacity. They propose a miRNA-dependent regulation of cell cycle-related protein expression as the underlying mechanism [222]. In the study presented here, however, Sirt7 knock-out enhanced neointima formation in the carotid artery ligation model and plaque size in the atherosclerosis model. These phenotypes did not result from a regulation of cell metabolism by Sirt7 or by an impact on cell proliferation by Sirt7. The contradictory nature of these results could be due to the different cell culture models as well as different *in vivo* models used in the various studies. *In vitro* models of VSMC proliferation have strong limitations as the non-proliferative, quiescent state of the differentiated VSMC phenotype is difficult to mimic in cell culture. The different culture conditions chosen may influence the role of Sirt7 in these settings. *In vivo* Kimura et al. employed a wire-injury model which uses the injury as a trigger for VSMC dedifferentiation, while here the carotid artery ligation model was used which is at least partly hypoxia driven. The genetic background of the mice used in these studies could also contribute to the contradictory results. The role of Sirt7 knock-out in atherosclerosis has not yet been investigated in a VSMC specific atherosclerosis mouse model other than in this study.
Taking into account the results for Sirt7 knock-out and overexpression in cancer studies, these results indicate that the precise role of Sirt7 might be dependent on the specific cell type, the cellular context and the surrounding conditions, as well as on the proliferative characteristics of the respective cells and tissues.

Taken together, Sirt7 did show an atheroprotective effect in this study. The hypothesis that this effect is mediated by Sirt7 impacting VSMC metabolism, especially mitochondrial homeostasis, could not be confirmed however. Sirt7 also did not regulate VSMC proliferation in this study and therefore probably did not impact neointima or plaque formation via this pathway. Other studies, however, have shown contradictory data and indicate a regulation of VSMC proliferation by Sirt7. Therefore, the exact role of Sirt7 in VSMCs and how it affects neointima and plaque formation still needs further investigation.

4.3 Conclusion

The aim of this study was to investigate the metabolic adaptions VSMCs exhibit during phenotypic switching and identify possible regulators thereof. An experiment looking at protein expression in differentiated and dedifferentiated VSMCs generated the hypothesis that VSMC phenotypic transition is accompanied by an adaption of the metabolism towards the requirements of the respective phenotype.
In the study presented here, this hypothesis was investigated utilising two different *in vitro* models and one *in vivo* model of VSMC dedifferentiation. Results from the two *in vitro* models of VSMC dedifferentiation suggested changes in VSMC metabolism upon induction of phenotypic modulation. An elevated lactate production and indicators for an increased glycolysis were observed with both methods upon phenotypic transitioning. This indicates that VSMCs undergo similar processes as cancer cells which have been shown to shift their energy generation from mitochondrial respiration towards glycolysis and lactate production, a process known as the Warburg effect. The underlying motivation for this shift is assumed to be the generation of cellular building blocks for lipids and amino acids and other metabolites necessary for a highly proliferative phenotype. It stands to reason that VSMCs, in order to adapt to proliferative and synthetic phenotypes, underly the same mechanism.
Data from the *in vivo* carotid artery ligation model, matched the data obtained from the cell culture models, also indicating a metabolic shift in VSMCs during phenotypic modulation. In addition to an enhanced glycolysis, decreased oxygen consumption, reduced mtDNA content and lower MitoTracker fluorescence were found in ligated carotid arteries compared to control. These results indicate a lower abundance of mitochondria in dedifferentiated cells compared to differentiated cells. Together with results from electron microscopy and the findings of other groups there is strong evidence that mitochondria play an important role in VSMC plasticity. The exact regulation of this connection could not be elucidated in this study, however.
As these results showed a strong link between VSMC plasticity and metabolism in different settings, the next step was to identify regulators of metabolism and whether their loss of function would affect VSMC dedifferentiation in the same settings. For this, Sirt6 and Sirt7 were chosen for their known regulatory function in glucose and mitochondrial metabolism, respectively. According to their known functions in other cell types, especially cancer and their close relationship with Sirt1 which was shown to exhibit atheroprotective effects before, Sirt6 and Sirt7 were expected to display similar effects and atheroprotective functions. Therefore, loss-of function of either of these sirtuins was expected to result in increased neointima formation and larger

atherosclerotic plaques in the disease models utilised here. This could be shown for the VSMC-specific knock-out of Sirt7 as it resulted in elevated neointima formation and increased plaque size but not for VSMC-specific Sirt6 knock-out which did not impact both these parameters. The hypothesis that Sirt7 mediates this effect by impacting VSMC metabolism, especially mitochondrial homeostasis, could not be confirmed, however. In this study, there was also no evidence that Sirt7 regulated the mitochondrial target genes it was shown to regulate in other cell types before. Another possible mechanism of action, namely an impact of Sirt7 on VSMC proliferation in vascular disease, was also investigated here. However, Sirt7 did not regulate VSMC proliferation in this study and therefore probably did not impact neointima or plaque formation via this pathway.

Taken together, this study showed a close association between adaptions in metabolism and VSMC dedifferentiation and proliferation. Knock-out of the metabolic regulator Sirt7 resulted in increased neointima and plaque formation which was neither due to a regulation of mitochondrial homeostasis nor an impact on cell proliferation by Sirt7. Therefore, the role of Sirt7 in VSMCs and how it affects neointima and plaque formation still needs further investigation.

4.4 Limitations and Outlook

This study has several limitations. As discussed earlier, cell culture models are not ideal to investigate VSMC dedifferentiation and the processes involved therein. Upon isolation and transfer of mVSMCs into culture the differentiated phenotype predominantly displayed in the healthy vessel media already begins to shift towards more synthetic and proliferative phenotypes. In culture, cells are stimulated to proliferate in order to gain sufficient cell numbers to conduct experiments. As increased proliferation, however, is a sign of dedifferentiation it is difficult to obtain and maintain differentiated cells in culture. Especially when investigating cell metabolism as in this study, cell culture models have significant drawbacks as culture media and its components already influence the cells' metabolism. Moreover, reagents used to induce VSMC dedifferentiation in culture, like PDGF and cholesterol, have been shown to directly alter metabolism in the cell.

Due to the limited number of primary cells that can be obtained from mouse vessels, a VSMC cell line was used for *in vitro* experiments in the second part of this study. This poses its own problems as immortalised cells usually display different characteristics compared to primary cells. Especially regarding their proliferative potential, immortalised VSMCs do not reflect the differentiated, quiescent phenotype

anymore. In addition, different VSMC culture models used by different groups may lead to discrepancies in results as could be seen with the investigation of the Sirt7 knock-out. Despite these drawbacks of the *in vitro* systems, they are still needed for investigation and unravelling of underlying mechanisms in simplified settings compared to the complex *in vivo* situation. Working towards animal welfare and conservation of resources it is also desirable to employ *in vitro* models.

The two *in vivo* models used in this study both have strengths and weaknesses. The carotid artery ligation is a very effective means to induce VSMC dedifferentiation *in vivo* without provoking inflammation. This makes it a good model to investigate VSMC specific processes without the possible interference of inflammatory reactions. However, at the same time, this is also its greatest drawback as it does not reflect a commonly found vascular injury. The atherosclerosis model on the other hand depicts the processes of vascular disease development quite well. It involves, however, cell types other than VSMCs, namely endothelial cells, macrophages and other cells from the immune system. This impedes the systematic investigation of VSMCs and their role in this setting. Utilisation of VSMC lineage tracing was used here to address this problem but since these mice had to be crossed and bred during the already ongoing study, not all experiments could be performed with these mice. It would be advisable to conduct coming experiments with these reporter mouse lines to forgo the mentioned problems.

Although the BCA is the clinically most relevant site of lesion development other groups additionally analyse plaque formation in the aortic root or the aorta. This could be interesting to pursue in the Sirt6 knock-out model where no difference in plaque formation in the BCA was found. Analysing these other parts might render new results. As was discussed before, the disease progression in this model was very fast as it was driven by a high amount of cholesterol in the diet. Looking at earlier stages of plaque formation could reveal differences between knock-out and control groups that are not distinguishable any more in the later more advanced stages.
This study was limited to male mice as the VSMC-specific cre recombinase is located on the Y-chromosome in these strains. For thoroughness' sake these studies should also be conducted in female mice especially since it is known that cardiovascular diseases manifest differently in the genders.

The precise role of mitochondrial abundance and function in VSMC plasticity could not be fully elucidated here. There is also no concluding answer to whether the observed changes in metabolism are a consequence of VSMC dedifferentiation or if they regulate it. These complex interactions need more investigation before they are fully understood. Manipulating the metabolism, for example by inhibiting glycolysis, could then become a potential strategy to inhibit VSMC plasticity in vascular disease. This approach was tried in this study by looking at Sirt6 and Sirt7 which had been shown to regulate metabolism in different cell types beforehand. However, knock-out of Sirt6 did not influence neointima or plaque formation in the *in vivo* models used here. Since Sirt6 was reported to reduce atherosclerosis by another group, it might still be worth investigating it further. Looking at earlier stages of atherosclerosis and other vascular injury models would be interesting in this context. A better understanding of whether Sirt6 regulates metabolism in VSMCs and in which ways, is also needed to determine whether it is a good target for medical intervention in vascular disease.

Although Sirt7 did affect neointima and plaque formation in this study it did not do so by regulating mitochondrial homeostasis or other metabolic pathways. It also did not regulate VSMC proliferation directly. This means it is probably not suited as a target to intervene in vascular disease by manipulating cell metabolism. It is, however, still an interesting target as it clearly does play an atheroprotective role as knock-out of Sirt7 led to aggravated neointima and plaque formation. The next steps now need to shed light on how Sirt7 achieves that.
A very likely possibility is that Sirt7 reduces atherosclerosis by protecting VSMCs from senescence as was reported for Sirt6 [220]. Sirt7 knock-out mice have a shorter lifespan compared to control and show an aging phenotype as well as increased sensitivity to oxidative and genotoxic stress [121, 183]. Sirt7 levels are reduced in senescent cells and decline with age in mice and rats [121, 185, 229]. These findings indicate that Sirt7 plays a role in cell senescence. It also maintains genomic stability by regulating p53 and DNA damage repair. It is recruited to DNA damage sites in a PARP1-dependent manner and attenuates DNA damage response [182, 230, 231]. It may also regulate aging and senescence by interacting with tripeptidyl peptidase II (TPPII) which has regulatory effects on apoptosis and senescence [182, 232]. Sirt7 also plays a critical role in protecting against cellular senescence by stabilising ribosomal RNA (rRNA) [233].

These results strongly suggest an essential role for Sirt7 in aging and senescence. As cell senescence plays a major role in atherosclerosis, it should be investigated whether Sirt7 functions as atheroprotective by protecting VSMCs from senescence.

Apart from protecting VSMCs from senescence, Sirt7 could also influence neointima formation and plaque development in other ways. Loss of Sirt7 could redirect VSMC dedifferentiation towards stronger transdifferentiation towards the macrophage like, inflammatory phenotype. This would lead to elevated inflammation and a higher amount of foam cells within the plaque which could explain the increased plaque size found in this study. To investigate this, the plaque composition should be analysed with VSMC lineage tracing as well as macrophage lineage tracing models in order to differentiate between the origins of cells displaying macrophage like characteristics. Generally, results gathered in this study need to be confirmed by further experiments and by the work of other groups. It is possible that existing correlations, changes and effects have been overlooked due to relatively small sample sizes in this study.

This study worked with knock-out models to investigate the role of Sirt6 and Sirt7 in vascular disease. However, as they are expected to have atheroprotective functions, a knock-out will likely worsen the disease as was seen in this study for the knock-out of Sirt7 and the resulting increased neointima formation and larger atherosclerotic plaque burden compared to wildtype. If the manifestations of the disease are already very pronounced in the wildtype however, differences could be difficult to detect. Therefore, it would also be of interest to create gain-of-function models and observe the effect on neointima formation and atherosclerotic plaque size. If Sirt7 indeed regulates VSMCs in these settings, overexpressing it should attenuate neointima and plaque formation. This could also help to shed more light on the underlying mechanisms.
In addition to a genetic overexpression model, activity of sirtuins can also be increased by sirtuin-activating compounds (STACs) or NAD^+ boosters. Known STACs are resveratrol, SRT1720 and SRT2104. STACs act as allosteric activators of SIRT1 by increasing the binding affinity for substrates. Clinical trials of resveratrol mostly show beneficial cardiovascular and metabolic effects, making STACs prominent candidates for future treatment of cardiovascular and metabolic diseases. It is, however, not completely understood whether STACs also activate sirtuins other than SIRT1 [165]. As the results from the presented study clearly indicate an atheroprotective effect of Sirt7 it would be of great interest to find a STAC that would enhance its activity.

Another means to activate sirtuins is the appliance of NAD^+ boosters. Since sirtuins are NAD^+ dependent, higher levels of NAD^+ increase their activity. There are several NAD^+ boosters known and some have been tested in clinical trials. This approach, however, is not very specific as NAD levels affect all sirtuins. Nevertheless, enhancing sirtuin activity may be a promising approach in the treatment of vascular diseases which should be further explored in the future.

5 References

[1] R. H. Adams and K. Alitalo, "Molecular regulation of angiogenesis and lymphangiogenesis.," *Nature reviews. Molecular cell biology*, vol. 8, no. 6, pp. 464–78, Jun. 2007, ISSN: 1471-0072. DOI: 10.1038/nrm2183. [Online]. Available: http://www.ncbi.nlm.nih.gov/pubmed/17522591.

[2] W. C. Aird, "Phenotypic heterogeneity of the endothelium: I. Structure, function, and mechanisms.," *Circulation research*, vol. 100, no. 2, pp. 158–73, Mar. 2007, ISSN: 1524-4571. DOI: 10.1161/01.RES.0000255691.76142.4a. [Online]. Available: http://www.ncbi.nlm.nih.gov/pubmed/17272818.

[3] H. M. Eilken and R. H. Adams, "Dynamics of endothelial cell behavior in sprouting angiogenesis.," *Current opinion in cell biology*, vol. 22, no. 5, pp. 617–25, Oct. 2010, ISSN: 1879-0410. DOI: 10.1016/j.ceb.2010.08.010. [Online]. Available: http://www.ncbi.nlm.nih.gov/pubmed/20817428.

[4] R. C. a. Sainson and A. L. Harris, "Regulation of angiogenesis by homotypic and heterotypic notch signalling in endothelial cells and pericytes: from basic research to potential therapies.," *Angiogenesis*, vol. 11, no. 1, pp. 41–51, Jan. 2008, ISSN: 0969-6970. DOI: 10.1007/s10456-008-9098-0. [Online]. Available: http://www.ncbi.nlm.nih.gov/pubmed/18256896.

[5] G. Bergers and S. Song, "The role of pericytes in blood-vessel formation and maintenance.," *Neuro-oncology*, vol. 7, no. 4, pp. 452–64, Oct. 2005, ISSN: 1522-8517. DOI: 10.1215/S1152851705000232.

[6] A. Armulik, A. Abramsson, and C. Betsholtz, "Endothelial/pericyte interactions.," *Circulation research*, vol. 97, no. 6, pp. 512–23, Sep. 2005, ISSN: 1524-4571. DOI: 10.1161/01.RES.0000182903.16652.d7. [Online]. Available: http://www.ncbi.nlm.nih.gov/pubmed/16166562.

[7] S. S. M. Rensen, P. a. F. M. Doevendans, and G. J. J. M. van Eys, "Regulation and characteristics of vascular smooth muscle cell phenotypic diversity.," *Netherlands heart journal : monthly journal of the Netherlands Society of Cardiology and the Netherlands Heart Foundation*, vol. 15, no. 3, pp. 100–8, Jan. 2007, ISSN: 1568-5888.

[8] O. Cleaver and D. A. Melton, "Endothelial signaling during development," *Nature Medicine*, vol. 9, no. 6, pp. 661–668, 2003, ISSN: 10788956. DOI: 10.1038/nm0603-661.

[9] B. staff, “Medical gallery of Blausen Medical 2014,” *WikiJournal of Medicine*, vol. 1, no. 2, Aug. 2014, ISSN: 20024436. DOI: 10.15347/wjm/2014.010. [Online]. Available: https://en.wikiversity.org/wiki/WikiJournal_of_Medicine/Medical_gallery_of_Blausen_Medical_2014.

[10] M. W. Majesky, “Vascular development,” *Arteriosclerosis, Thrombosis, and Vascular Biology*, vol. 38, no. 3, E17–E24, 2018, ISSN: 15244636. DOI: 10.1161/ATVBAHA.118.310223.

[11] H. Naito, T. Iba, and N. Takakura, “Mechanisms of new blood-vessel formation and proliferative heterogeneity of endothelial cells,” *International Immunology*, vol. 32, no. 5, pp. 295–305, 2021, ISSN: 14602377. DOI: 10.1093/intimm/dxaa008.

[12] World Health Organisation (WHO), *Cardiovascular diseases*.

[13] G. Dangas and F. Kuepper, “Restenosis: Repeat narrowing of a coronary artery - Prevention and treatment,” *Circulation*, vol. 105, no. 22, pp. 2586–2587, 2002, ISSN: 00097322. DOI: 10.1161/01.CIR.0000019122.00032.DF.

[14] S. O. Marx, H. Totary-Jain, and A. R. Marks, “Vascular smooth muscle cell proliferation in restenosis,” *Circulation: Cardiovascular Interventions*, vol. 4, no. 1, pp. 104–111, 2011, ISSN: 19417640. DOI: 10.1161/CIRCINTERVENTIONS.110.957332.

[15] J. B. Michel, G. Jondeau, and D. M. Milewicz, “From genetics to response to injury: Vascular smooth muscle cells in aneurysms and dissections of the ascending aorta,” *Cardiovascular Research*, vol. 114, no. 4, pp. 578–589, 2018, ISSN: 17553245. DOI: 10.1093/cvr/cvy006.

[16] A. J. Lusis, “Atherosclerosis - Insight Review Articles,” *Nature*, vol. 407, no. September, pp. 233–241, 2000, ISSN: 0028-0836.

[17] J. Gimbrone, *Vascular endothelium, hemodynamic forces, and atherogenesis*, 1999. DOI: 10.1016/s0002-9440(10)65090-0.

[18] M. R. Bennett, S. Sinha, and G. K. Owens, “Vascular Smooth Muscle Cells in Atherosclerosis,” *Circulation Research*, vol. 118, no. 4, pp. 692–702, 2016, ISSN: 15244571. DOI: 10.1161/CIRCRESAHA.115.306361.

[19] P. Libby and P. M. Ridker, “Progress and challenges in translating,” 2011. DOI: 10.1038/nature10146.

[20] P. Libby, *The forgotten majority: Unfinished business in cardiovascular risk reduction*, Oct. 2005. DOI: 10.1016/j.jacc.2005.07.006.

[21] S. C. Bergheanu, ·. M. C. Bodde, ·. J. W. Jukema, J. W. Jukema, and W. J. Nl, "Pathophysiology and treatment of atherosclerosis Current view and future perspective on lipoprotein modification treatment," *Netherlands Heart Journal*, 2017. DOI: 10.1007/s12471-017-0959-2.

[22] S. Agewall, G. Baró n-Esquivias, J. Boré, E. Bruckert, A. Cordero, A. Corsini, and P. Giannuzzi, "ESC/EAS GUIDELINES 2016 ESC/EAS Guidelines for the Management of Dyslipidaemias," DOI: 10.1093/eurheartj/ehw272. [Online]. Available: https://academic.oup.com/eurheartj/article/37/39/2999/2414995.

[23] K. J. Greenow Nigel Pearce Dipak P Ramji, "The key role of apolipoprotein E in atherosclerosis," *J Mol Med*, vol. 83, pp. 329–342, 2005. DOI: 10.1007/s00109-004-0631-3.

[24] S. Oppi, T. F. Lüscher, and S. Stein, "Mouse Models for Atherosclerosis Research—Which Is My Line?" *Frontiers in Cardiovascular Medicine*, vol. 6, p. 46, Apr. 2019, ISSN: 2297-055X. DOI: 10.3389/fcvm.2019.00046. [Online]. Available: https://www.frontiersin.org/article/10.3389/fcvm.2019.00046/full.

[25] G. K. Owens, G. K. Owens, M. S. Kumar, M. S. Kumar, B. R. Wamhoff, and B. R. Wamhoff, "Molecular regulation of vascular smooth muscle cell differentiation in development and disease.," *Physiological reviews*, vol. 84, no. 3, pp. 767–801, 2004, ISSN: 0031-9333. DOI: 10.1152/physrev.00041.2003. [Online]. Available: http://www.ncbi.nlm.nih.gov/pubmed/15269336.

[26] G. K. Owens, *Regulation of differentiation of vascular smooth muscle cells*, 1995. DOI: 10.1152/physrev.1995.75.3.487. [Online]. Available: https://pubmed.ncbi.nlm.nih.gov/7624392/.

[27] L. Bacakova, M. Travnickova, E. Filova, R. Matějka, J. Stepanovska, J. Musilkova, J. Zarubova, and M. Molitor, "The Role of Vascular Smooth Muscle Cells in the Physiology and Pathophysiology of Blood Vessels," in *Muscle Cell and Tissue - Current Status of Research Field*, InTech, Oct. 2018. DOI: 10.5772/intechopen.77115. [Online]. Available: http://dx.doi.org/10.5772/intechopen.77115.

[28] J. Hungerford and C. Little, “Developmental Biology of the Vascular Smooth Muscle Cell: Building a Multilayered Vessel Wall,” *Journal of Vascular Research*, vol. 36, no. 1, pp. 2–27, 1999, ISSN: 1018-1172. DOI: 10.1159/000025622. [Online]. Available: https://www.karger.com/Article/FullText/25622.

[29] G. Wang, L. Jacquet, E. Karamariti, and Q. Xu, “Origin and differentiation of vascular smooth muscle cells,” *Journal of Physiology*, vol. 593, no. 14, pp. 3013–3030, 2015, ISSN: 14697793. DOI: 10.1113/JP270033. [Online]. Available: https://pubmed.ncbi.nlm.nih.gov/25952975/.

[30] P. J. Psaltis, A. Harbuzariu, S. Delacroix, E. W. Holroyd, and R. D. Simari, *Resident vascular progenitor cells-diverse origins, phenotype, and function*, Apr. 2011. DOI: 10.1007/s12265-010-9248-9. [Online]. Available: https://portal.sahmriresearch.org/en/publications/resident-vascular-progenitor-cells-diverse-origins-phenotype-and-.

[31] P. Babij, S. Kawamoto, S. White, R. S. Adelstein, and M. Periasamy, “Differential expression of SM1 and SM2 myosin isoforms in cultured vascular smooth muscle,” *American Journal of Physiology - Cell Physiology*, vol. 262, no. 3 31-3, 1992, ISSN: 00029513. DOI: 10.1152/ajpcell.1992.262.3.c607. [Online]. Available: https://pubmed.ncbi.nlm.nih.gov/1550206/.

[32] L.-H. Dong, P. Lv, and M. Han, “Roles of SM22α in Cellular Plasticity and Vascular Diseases,” *Cardiovascular & Hematological Disorders-Drug Targets*, vol. 12, no. 2, pp. 119–125, Jan. 2013, ISSN: 1871529X. DOI: 10.2174/1871529x11202020119. [Online]. Available: https://pubmed.ncbi.nlm.nih.gov/23030444/.

[33] J. E. Hungerford, G. K. Owens, W. S. Argraves, and C. D. Little, “Development of the aortic vessel wall as defined by vascular smooth muscle and extracellular matrix markers,” *Developmental Biology*, vol. 178, no. 2, pp. 375–392, Sep. 1996, ISSN: 00121606. DOI: 10.1006/dbio.1996.0225. [Online]. Available: https://pubmed.ncbi.nlm.nih.gov/8812136/.

[34] L. V. Rodríguez, Z. Alfonso, R. Zhang, J. Leung, B. Wu, and L. J. Ignarro, “Clonogenic multipotent stem cells in human adipose tissue differentiate into functional smooth muscle cells,” *Proceedings of the National Academy of Sciences of the United States of America*, vol. 103, no. 32, pp. 12 167–12 172, Aug. 2006, ISSN: 00278424. DOI: 10.1073/pnas.0604850103. [Online]. Available: https://pubmed.ncbi.nlm.nih.gov/16880387/.

[35] M. Han, L.-H. Dong, B. Zheng, J.-H. Shi, J.-K. Wen, and Y. Cheng, "Smooth muscle 22 alpha maintains the differentiated phenotype of vascular smooth muscle cells by inducing filamentous actin bundling," *Life Sciences*, vol. 84, no. 13-14, pp. 394–401, Mar. 2009, ISSN: 00243205. DOI: 10.1016/j.lfs.2008.11.017. [Online]. Available: https://linkinghub.elsevier.com/retrieve/pii/S002432050800475X.

[36] Y. Kiyan, A. Limbourg, R. Kiyan, S. Tkachuk, F. P. Limbourg, A. Ovsianikov, B. N. Chichkov, H. Haller, and I. Dumler, "Urokinase receptor associates with myocardin to control vascular smooth muscle cells phenotype in vascular disease," *Arteriosclerosis, Thrombosis, and Vascular Biology*, vol. 32, no. 1, pp. 110–122, Jan. 2012, ISSN: 10795642. DOI: 10.1161/ATVBAHA.111.234369. [Online]. Available: https://pubmed.ncbi.nlm.nih.gov/22075245/.

[37] M. Ackers-Johnson, A. Talasila, A. P. Sage, X. Long, I. Bot, N. W. Morrell, M. R. Bennett, J. M. Miano, and S. Sinha, "Myocardin regulates vascular smooth muscle cell inflammatory activation and disease," *Arteriosclerosis, Thrombosis, and Vascular Biology*, vol. 35, no. 4, pp. 817–828, Apr. 2015, ISSN: 15244636. DOI: 10.1161/ATVBAHA.114.305218. [Online]. Available: https://pubmed.ncbi.nlm.nih.gov/25614278/.

[38] Z. Wang, D.-Z. Wang, D. Hockemeyer, J. McAnally, A. Nordheim, and E. N. Olson, "Myocardin and ternary complex factors compete for SRF to control smooth muscle gene expression.," *Nature*, vol. 428, no. 6979, pp. 185–189, 2004, ISSN: 0028-0836. DOI: 10.1038/nature02331.1..

[39] P. A. Huber, "Caldesmon," *International Journal of Biochemistry and Cell Biology*, vol. 29, no. 8-9, pp. 1047–1051, 1997, ISSN: 13572725. DOI: 10.1016/S1357-2725(97)00004-6. [Online]. Available: https://pubmed.ncbi.nlm.nih.gov/9415999/.

[40] S. F. D'Addario, M. Morgan, L. Talley, and B. R. Smoller, "h-Caldesmon as a specific marker of smooth muscle cell differentiation in some soft tissue tumors of the skin," *Journal of Cutaneous Pathology*, vol. 29, no. 7, pp. 426–429, 2002, ISSN: 03036987. DOI: 10.1034/j.1600-0560.2002.290707.x. [Online]. Available: https://pubmed.ncbi.nlm.nih.gov/12139638/.

[41] S. J. Winder and M. P. Walsh, *Calponin: Thin filament-linked regulation of smooth muscle contraction*, 1993. DOI: 10.1016/0898-6568(93)90029-L. [Online]. Available: https://pubmed.ncbi.nlm.nih.gov/8130072/.

[42] R. Liu and J. P. Jin, *Calponin isoforms CNN1, CNN2 and CNN3: Regulators for actin cytoskeleton functions in smooth muscle and non-muscle cells*, Jul. 2016. DOI: 10.1016/j.gene.2016.02.040.

[43] S. Taniguchi, "Suppression of cancer phenotypes through a multifunctional actin-binding protein, calponin, that attacks cancer cells and simultaneously protects the host from invasion," *Cancer Science*, vol. 96, no. 11, pp. 738–746, Nov. 2005, ISSN: 1347-9032. DOI: 10.1111/j.1349-7006.2005.00118.x. [Online]. Available: https://onlinelibrary.wiley.com/doi/10.1111/j.1349-7006.2005.00118.x.

[44] L. J. Harris, H. Abdollahi, P. Zhang, S. McIlhenny, T. N. Tulenko, and P. J. DiMuzio, "Differentiation of adult stem cells into smooth muscle for vascular tissue engineering," *Journal of Surgical Research*, vol. 168, no. 2, pp. 306–314, Jun. 2011, ISSN: 00224804. DOI: 10.1016/j.jss.2009.08.001.

[45] T. Meyer, U. Brink, C. Unterberg, S. Stöhr, H. Kreuzer, and A. B. Buchwald, "Expression of meta-vinculin in human coronary arteriosclerosis is related to the histological grade of plaque formation," *Atherosclerosis*, vol. 111, no. 1, pp. 111–119, 1994, ISSN: 00219150. DOI: 10.1016/0021-9150(94)90196-1. [Online]. Available: https://pubmed.ncbi.nlm.nih.gov/7840806/.

[46] A. M. Belkin, O. I. Ornatsky, M. A. Glukhova, and V. E. Koteliansky, "Immunolocalization of meta-vinculin in human smooth and cardiac muscles," *Journal of Cell Biology*, vol. 107, no. 2, pp. 545–553, 1988, ISSN: 00219525. DOI: 10.1083/jcb.107.2.545.

[47] S. Sartore, A. Chiavegato, R. Franch, E. Faggin, and P. Pauletto, *Myosin gene expression and cell phenotypes in vascular smooth muscle during development, in experimental models, and in vascular disease*, 1997. DOI: 10.1161/01.ATV.17.7.1210. [Online]. Available: http://ahajournals.org.

[48] M. Aikawa, Y. Sakomura, M. Ueda, K. Kimura, I. Manabe, S. Ishiwata, N. Komiyama, H. Yamaguchi, Y. Yazaki, and R. Nagai, "Redifferentiation of smooth muscle cells after coronary angioplasty determined via myosin heavy chain expression," *Circulation*, vol. 96, no. 1, pp. 82–90, Jul. 1997, ISSN: 00097322. DOI: 10.1161/01.CIR.96.1.82. [Online]. Available: https://www.ahajournals.org/doi/abs/10.1161/01.cir.96.1.82.

[49] F. T. Van Der Loop, G. Schaart, E. D. Timmer, F. C. Ramaekers, and G. J. Van Eys, "Smoothelin, a novel cytoskeletal protein specific for smooth muscle cells," *Journal of Cell Biology*, vol. 134, no. 2, pp. 401–411, Jul. 1996, ISSN: 00219525. DOI: 10.1083/jcb.134.2.401. [Online]. Available: /pmc/articles/PMC2120883/?report=abstract%20https://www.ncbi.nlm.nih.gov/pmc/articles/PMC2120883/.

[50] S. R. Turner and J. A. Macdonald, "Novel contributions of the smoothelin-like 1 protein in vascular smooth muscle contraction and its potential involvement in myogenic tone," *Microcirculation*, vol. 21, no. 3, pp. 249–258, 2014, ISSN: 15498719. DOI: 10.1111/micc.12108. [Online]. Available: https://pubmed.ncbi.nlm.nih.gov/24267201/.

[51] M. R. Alexander and G. K. Owens, "Epigenetic Control of Smooth Muscle Cell Differentiation and Phenotypic Switching in Vascular Development and Disease," *Annual Review of Physiology*, vol. 74, pp. 13–40, 2012, ISSN: 0066-4278. DOI: 10.1146/annurev-physiol-012110-142315.

[52] S. M. Schwartz, G. R. Campbell, and J. H. Campbell, *Replication of smooth muscle cells in vascular disease*, 1986. DOI: 10.1161/01.RES.58.4.427.

[53] L. Wang, T. Yu, H. Lee, D. K. O. Brien, H. Sesaki, and Y. Yoon, "Decreasing mitochondrial fission diminishes vascular smooth muscle cell migration and ameliorates intimal hyperplasia," *Cardiovascular Research*, vol. 1, pp. 272–283, 2015. DOI: 10.1093/cvr/cvv005.

[54] Z. Li, H. Cheng, W. J. Lederer, J. Froehlich, and E. G. Lakatta, "Enhanced proliferation and migration and altered cytoskeletal proteins in early passage smooth muscle cells from young and old rat aortic explants," *Experimental and Molecular Pathology*, vol. 64, no. 1, pp. 1–11, Feb. 1997, ISSN: 00144800. DOI: 10.1006/exmp.1997.2204.

[55] Y. Qi, F. Dai, J. Gu, and W. Yao, "Biomarkers in VSMC phenotypic modulation and vascular remodeling," *Die Pharmazie*, vol. 74, no. 12, pp. 711–714, 2019, ISSN: 00317144. DOI: 10.1691/ph.2019.9743.

[56] A. C. Finney and A. W. Orr, *Guidance molecules in vascular smooth muscle*, Sep. 2018. DOI: 10.3389/fphys.2018.01311. [Online]. Available: https://pubmed.ncbi.nlm.nih.gov/30283356/.

[57] J. M. Miano, E. A. Fisher, and M. W. Majesky, “Fate and State of Vascular Smooth Muscle Cells in Atherosclerosis,” *Circulation*, pp. 2110–2116, May 2021, ISSN: 15244539. DOI: 10.1161/CIRCULATIONAHA.120.049922. [Online]. Available: https://www.ahajournals.org/doi/abs/10.1161/CIRCULATIONAHA.120.049922.

[58] L. S. Shankman, D. Gomez, O. A. Cherepanova, M. Salmon, G. F. Alencar, R. M. Haskins, P. Swiatlowska, A. A. C. Newman, E. S. Greene, A. C. Straub, B. Isakson, G. J. Randolph, and G. K. Owens, “KLF4-dependent phenotypic modulation of smooth muscle cells has a key role in atherosclerotic plaque pathogenesis,” vol. 21, no. 6, 2015. DOI: 10.1038/nm.3866.

[59] D. Gomez, L. S. Shankman, A. T. Nguyen, and G. K. Owens, “Detection of histone modifications at specific gene loci in single cells in histological sections,” *Nature Methods*, vol. 10, no. 2, pp. 171–177, 2013, ISSN: 15487091. DOI: 10.1038/nmeth.2332.

[60] S. Feil, B. Fehrenbacher, R. Lukowski, F. Essmann, K. Schulze-Osthoff, M. Schaller, and R. Feil, “Transdifferentiation of vascular smooth muscle cells to macrophage-like cells during atherogenesis,” *Circulation Research*, vol. 115, no. 7, pp. 662–667, 2014, ISSN: 15244571. DOI: 10.1161/CIRCRESAHA.115.304634.

[61] G. F. Alencar, K. M. Owsiany, S. Karnewar, K. Sukhavasi, G. Mocci, A. T. Nguyen, C. M. Williams, S. Shamsuzzaman, M. Mokry, C. A. Henderson, R. Haskins, R. A. Baylis, A. V. Finn, C. A. McNamara, E. R. Zunder, V. Venkata, G. Pasterkamp, J. Björkegren, S. Bekiranov, and G. K. Owens, “Stem Cell Pluripotency Genes Klf4 and Oct4 Regulate Complex SMC Phenotypic Changes Critical in Late-Stage Atherosclerotic Lesion Pathogenesis,” *Circulation*, pp. 2045–2059, Nov. 2020, ISSN: 15244539. DOI: 10.1161/CIRCULATIONAHA.120.046672. [Online]. Available: https://www.ahajournals.org/doi/abs/10.1161/CIRCULATIONAHA.120.046672.

[62] H. Pan, C. Xue, B. J. Auerbach, J. Fan, A. C. Bashore, J. Cui, D. Y. Yang, S. B. Trignano, W. Liu, J. Shi, C. O. Ihuegbu, E. C. Bush, J. Worley, L. Vlahos, P. Laise, R. A. Solomon, E. S. Connolly, A. Califano, P. A. Sims, H. Zhang, M. Li, and M. P. Reilly, “Single-Cell Genomics Reveals a Novel Cell State during Smooth Muscle Cell Phenotypic Switching and Potential Therapeutic Targets for Atherosclerosis in Mouse and Human,” *Circulation*, pp. 2060–2075, Nov. 2020, ISSN: 15244539. DOI: 10.1161/CIRCULATIONAHA.120.048378.

[Online]. Available: https://www.ahajournals.org/doi/abs/10.1161/CIRCULATIONAHA.120.048378.

[63] R. C. Wirka, D. Wagh, D. T. Paik, M. Pjanic, T. Nguyen, C. L. Miller, R. Kundu, M. Nagao, J. Coller, T. K. Koyano, R. Fong, Y. J. Woo, B. Liu, S. B. Montgomery, J. C. Wu, K. Zhu, R. Chang, M. Alamprese, M. D. Tallquist, J. B. Kim, and T. Quertermous, "Atheroprotective roles of smooth muscle cell phenotypic modulation and the TCF21 disease gene as revealed by single-cell analysis," *Nature Medicine 2019 25:8*, vol. 25, no. 8, pp. 1280–1289, Jul. 2019, ISSN: 1546-170X. DOI: 10.1038/s41591-019-0512-5. [Online]. Available: https://www.nature.com/articles/s41591-019-0512-5.

[64] H. Iwata, I. Manabe, K. Fujiu, T. Yamamoto, N. Takeda, K. Eguchi, A. Furuya, M. Kuro-O, M. Sata, and R. Nagai, "Bone marrow-derived cells contribute to vascular inflammation but do not differentiate into smooth muscle cell lineages," *Circulation*, vol. 122, no. 20, pp. 2048–2057, Nov. 2010, ISSN: 00097322. DOI: 10.1161/CIRCULATIONAHA.110.965202. [Online]. Available: http://circ.ahajournals.org.

[65] S. Allahverdian, A. C. Chehroudi, B. M. Mcmanus, T. Abraham, and G. A. Francis, "Coronary Heart Disease Contribution of Intimal Smooth Muscle Cells to Cholesterol Accumulation and Macrophage-Like Cells in Human Atherosclerosis," *Circulation*, 2014. DOI: 10.1161/CIRCULATIONAHA.113.005015.

[66] B. P. Herring, A. M. Hoggatt, C. Burlak, and S. Offermanns, "Previously differentiated medial vascular smooth muscle cells contribute to neointima formation following vascular injury," *Vascular Cell*, vol. 6, no. 1, pp. 1–13, 2014, ISSN: 2045824X. DOI: 10.1186/2045-824X-6-21.

[67] J. Chappell, J. L. Harman, V. M. Narasimhan, H. Yu, K. Foote, B. D. Simons, M. R. Bennett, and H. F. Jørgensen, "Extensive Proliferation of a Subset of Differentiated, yet Plastic, Medial Vascular Smooth Muscle Cells Contributes to Neointimal Formation in Mouse Injury and Atherosclerosis Models," *Circulation Research*, vol. 119, no. 12, pp. 1313–1323, 2016, ISSN: 15244571. DOI: 10.1161/CIRCRESAHA.116.309799.

[68] G. Zhao, H. Lu, Z. Chang, Y. Zhao, T. Zhu, L. Chang, Y. Guo, M. T. Garcia-Barrio, Y. E. Chen, and J. Zhang, "Single-cell RNA sequencing reveals the cellular heterogeneity of aneurysmal infrarenal abdominal aorta," *Cardiovascular research*, vol. 117, no. 5, pp. 1402–1416, May 2021, ISSN: 1755-3245.

DOI: 10.1093/CVR/CVAA214. [Online]. Available: https://pubmed.ncbi.nlm.nih.gov/32678909/.

[69] W. Wu, C. Wang, H. Zang, L. Qi, M. Azhar, M. Nagarkatti, P. Nagarkatti, G. Cai, M. C. Weiser-Evans, and T. Cui, "Mature vascular smooth muscle cells, but not endothelial cells, serve as the major cellular source of intimal hyperplasia in vein grafts," *Arteriosclerosis, Thrombosis, and Vascular Biology*, vol. 40, no. 8, pp. 1870–1890, Aug. 2020, ISSN: 15244636. DOI: 10.1161/ATVBAHA.120.314465. [Online]. Available: https://www.ahajournals.org/doi/abs/10.1161/ATVBAHA.120.314465.

[70] E. Lutgens, E. D. De Muinck, P. J. Kitslaar, J. H. Tordoir, H. J. Wellens, and M. J. Daemen, "Biphasic pattern of cell turnover characterizes the progression from fatty streaks to ruptured human atherosclerotic plaques," *Cardiovascular Research*, vol. 41, no. 2, pp. 473–479, 1999, ISSN: 00086363. DOI: 10.1016/S0008-6363(98)00311-3.

[71] S. K. Moon, B. Y. Cha, and C. H. Kim, "In vitro cellular aging is associated with enhanced proliferative capacity, G1 cell cycle modulation, and matrix metalloproteinase-9 regulation in mouse aortic smooth muscle cells," *Archives of Biochemistry and Biophysics*, vol. 418, no. 1, pp. 39–48, Oct. 2003, ISSN: 00039861. DOI: 10.1016/S0003-9861(03)00402-8.

[72] R. J. Hariri, D. P. Hajjar, D. Coletti, D. R. Alonso, M. E. Weksler, and E. Rabellino, "Aging and arteriosclerosis. Cell cycle kinetics of young and old arterial smooth muscle cells," *American Journal of Pathology*, vol. 131, no. 1, pp. 132–136, 1988, ISSN: 00029440.

[73] M. B. Stemerman, R. Weinstein, J. W. Rowe, T. Maciag, R. Fuhro, and R. Gardner, "Vascular smooth muscle cell growth kinetics in vivo in aged rats," *Proceedings of the National Academy of Sciences of the United States of America*, vol. 79, no. 12 I, pp. 3863–3866, 1982, ISSN: 00278424. DOI: 10.1073/pnas.79.12.3863.

[74] Y. J. Geng and P. Libby, "Evidence for apoptosis in advanced human atheroma: Colocalization with interleukin-1β-converting enzyme," *American Journal of Pathology*, vol. 147, no. 2, pp. 251–266, 1995, ISSN: 00029440.

[75] M. R. Bennett, G. I. Evan, and S. M. Schwartz, "Apoptosis of human vascular smooth muscle cells derived from normal vessels and coronary atherosclerotic plaques," *Journal of Clinical Investigation*, vol. 95, no. 5, pp. 2266–2274, 1995,

ISSN: 00219738. DOI: 10.1172/JCI117917. [Online]. Available: https://pubmed.ncbi.nlm.nih.gov/7738191/.

[76] M. C. Clarke, N. Figg, J. J. Maguire, A. P. Davenport, M. Goddard, T. D. Littlewood, and M. R. Bennett, "Apoptosis of vascular smooth muscle cells induces features of plaque vulnerability in atherosclerosis," *Nature Medicine*, vol. 12, no. 9, pp. 1075–1080, Sep. 2006, ISSN: 10788956. DOI: 10.1038/nm1459.

[77] D. M. Schrijvers, G. R. De Meyer, M. M. Kockx, A. G. Herman, and W. Martinet, "Phagocytosis of apoptotic cells by macrophages is impaired in atherosclerosis," *Arteriosclerosis, Thrombosis, and Vascular Biology*, vol. 25, no. 6, pp. 1256–1261, Jun. 2005, ISSN: 10795642. DOI: 10.1161/01.ATV.0000166517.18801.a7. [Online]. Available: https://pubmed.ncbi.nlm.nih.gov/15831805/.

[78] C. Matthews, I. Gorenne, S. Scott, N. Figg, P. Kirkpatrick, A. Ritchie, M. Goddard, and M. Bennett, "Vascular smooth muscle cells undergo telomere-based senescence in human atherosclerosis: Effects of telomerase and oxidative stress," *Circulation Research*, vol. 99, no. 2, pp. 156–164, Jul. 2006, ISSN: 00097330. DOI: 10.1161/01.RES.0000233315.38086.bc.

[79] M. Ogami, Y. Ikura, M. Ohsawa, T. Matsuo, S. Kayo, N. Yoshimi, E. Hai, N. Shirai, S. Ehara, R. Komatsu, T. Naruko, and M. Ueda, "Telomere Shortening in Human Coronary Artery Diseases," *Arteriosclerosis, Thrombosis, and Vascular Biology*, vol. 24, no. 3, pp. 546–550, Mar. 2004, ISSN: 10795642. DOI: 10.1161/01.ATV.0000117200.46938.e7.

[80] Y. Song, H. Shen, D. Schenten, P. Shan, P. J. Lee, and D. R. Goldstein, "Aging enhances the basal production of IL-6 and CCL2 in vascular smooth muscle cells," *Arteriosclerosis, Thrombosis, and Vascular Biology*, vol. 32, no. 1, pp. 103–109, Jan. 2012, ISSN: 10795642. DOI: 10.1161/ATVBAHA.111.236349. [Online]. Available: https://pubmed.ncbi.nlm.nih.gov/22034510/.

[81] T. Yoshida, Q. Gan, Y. Shang, and G. K. Owens, "Platelet-derived growth factor-BB represses smooth muscle cell marker genes via changes in binding of MKL factors and histone deacetylases to their promoters," *American Journal of Physiology - Cell Physiology*, vol. 292, no. 2, Feb. 2007, ISSN: 03636143. DOI: 10.1152/ajpcell.00449.2006. [Online]. Available: https://pubmed.ncbi.nlm.nih.gov/16987998/.

[82] T. Yoshida, Q. Gan, and G. K. Owens, “Krüppel-like factor 4, Elk-1, and histone deacetylases cooperatively suppress smooth muscle cell differentiation markers in response to oxidized phospholipids,” *American Journal of Physiology - Cell Physiology*, vol. 295, no. 5, p. C1175, Nov. 2008, ISSN: 03636143. DOI: 10.1152/ajpcell.00288.2008.

[83] R. A. Deaton, Q. Gan, and G. K. Owens, “Spl-dependent activation of KLF4 is required for PDGF-BB-induced phenotypic modulation of smooth muscle,” *American Journal of Physiology - Heart and Circulatory Physiology*, vol. 296, no. 4, Apr. 2009, ISSN: 03636135. DOI: 10.1152/ajpheart.01230.2008. [Online]. Available: https://pubmed.ncbi.nlm.nih.gov/19168719/.

[84] N. A. Pidkovka, O. A. Cherepanova, T. Yoshida, M. R. Alexander, R. A. Deaton, J. A. Thomas, N. Leitinger, and G. K. Owens, “Oxidized phospholipids induce phenotypic switching of vascular smooth muscle cells in vivo and in vitro,” *Circulation Research*, vol. 101, no. 8, pp. 792–801, Oct. 2007, ISSN: 00097330. DOI: 10.1161/CIRCRESAHA.107.152736. [Online]. Available: https://pubmed.ncbi.nlm.nih.gov/17704209/.

[85] M. R. Alexander, M. Murgai, C. W. Moehle, and G. K. Owens, “Interleukin-1β modulates smooth muscle cell phenotype to a distinct inflammatory state relative to PDGF-DD via NF-κB-dependent mechanisms,” *Physiological Genomics*, vol. 44, no. 7, pp. 417–429, Apr. 2012, ISSN: 10948341. DOI: 10.1152/physiolgenomics.00160.2011. [Online]. Available: https://pubmed.ncbi.nlm.nih.gov/22318995/.

[86] C. Yang, X. Xiao, L. Huang, F. Zhou, L. h. Chen, Y. Y. Zhao, S. L. Qu, and C. Zhang, “Role of Kruppel-like factor 4 in atherosclerosis,” *Clinica Chimica Acta*, vol. 512, pp. 135–141, 2021, ISSN: 18733492. DOI: 10.1016/j.cca.2020.11.002. [Online]. Available: https://doi.org/10.1016/j.cca.2020.11.002.

[87] T. Yoshida, K. H. Kaestner, and G. K. Owens, “Conditional deletion of Krüppel-like factor 4 delays downregulation of smooth muscle cell differentiation markers but accelerates neointimal formation following vascular injury,” *Circulation Research*, vol. 102, no. 12, pp. 1548–1557, Jun. 2008, ISSN: 00097330. DOI: 10.1161/CIRCRESAHA.108.176974.

[88] M. E. Rosenfeld, *Converting smooth muscle cells to macrophage-like cells with KLF4 in atherosclerotic plaques*, Jun. 2015. DOI: 10.1038/nm.3875. [Online]. Available: https://www.nature.com/articles/nm.3875.

[89] O. G. McDonald, B. R. Wamhoff, M. H. Hoofnagle, and G. K. Owens, "Control of SRF binding to CArG box chromatin regulates smooth muscle gene expression in vivo," *Journal of Clinical Investigation*, vol. 116, no. 1, pp. 36–48, 2006, ISSN: 00219738. DOI: 10.1172/JCI26505.

[90] O. A. Cherepanova, D. Gomez, L. S. Shankman, P. Swiatlowska, J. Williams, O. F. Sarmento, G. F. Alencar, D. L. Hess, M. H. Bevard, E. S. Greene, M. Murgai, S. D. Turner, Y. J. Geng, S. Bekiranov, J. J. Connelly, A. Tomilin, and G. K. Owens, "Activation of the pluripotency factor OCT4 in smooth muscle cells is atheroprotective," *Nature Medicine*, vol. 22, no. 6, pp. 657–665, 2016, ISSN: 1546170X. DOI: 10.1038/nm.4109.

[91] J. M. Miano and B. C. Berk, "Retinoids," *Circulation Research*, vol. 87, no. 5, pp. 355–362, Sep. 2000, ISSN: 00097330. DOI: 10.1161/01.RES.87.5.355. [Online]. Available: https://www.ahajournals.org/doi/abs/10.1161/01.res.87.5.355.

[92] C. Xie, H. Huang, X. Sun, Y. Guo, M. Hamblin, R. P. Ritchie, M. T. Garcia-Barrio, J. Zhang, and Y. E. Chen, "MicroRNA-1 regulates smooth muscle cell differentiation by repressing kruppel-like factor 4," *Stem Cells and Development*, vol. 20, no. 2, pp. 205–210, 2011, ISSN: 15473287. DOI: 10.1089/scd.2010.0283.

[93] T. Boettger, N. Beetz, S. Kostin, J. Schneider, M. Krüger, L. Hein, and T. Braun, "Acquisition of the contractile phenotype by murine arterial smooth muscle cells depends on the Mir143/145 gene cluster," *Journal of Clinical Investigation*, vol. 119, no. 9, pp. 2634–2647, 2009, ISSN: 00219738. DOI: 10.1172/JCI38864.

[94] Y. Vengrenyuk, H. Nishi, X. Long, M. Ouimet, N. Savji, F. O. Martinez, C. P. Cassella, K. J. Moore, S. A. Ramsey, J. M. Miano, and E. A. Fisher, "Cholesterol Loading Reprograms the MicroRNA-143/145–Myocardin Axis to Convert Aortic Smooth Muscle Cells to a Dysfunctional Macrophage-Like Phenotype," 2015. DOI: 10.1161/ATVBAHA.114.304029.

[95] K. R. Cordes, N. T. Sheehy, M. P. White, E. C. Berry, S. U. Morton, A. N. Muth, T. H. Lee, J. M. Miano, K. N. Ivey, and D. Srivastava, "MiR-145 and miR-143 regulate smooth muscle cell fate and plasticity," *Nature*, vol. 460, no. 7256, pp. 705–710, 2009, ISSN: 00280836. DOI: 10.1038/nature08195.

[96] N. C. Mackenzie, K. A. Staines, D. Zhu, P. Genever, and V. E. Macrae, "miRNA-221 and miRNA-222 synergistically function to promote vascular calcification," *Cell Biochemistry and Function*, vol. 32, no. 2, pp. 209–216, 2014, ISSN: 10990844. DOI: 10.1002/cbf.3005.

[97] X. Liu, Y. Cheng, S. Zhang, Y. Lin, J. Yang, and C. Zhang, "A Necessary role of miR-221 and miR-222 in vascular smooth muscle cell proliferation and neointimal hyperplasia," *Circulation Research*, vol. 104, no. 4, pp. 476–486, 2009, ISSN: 00097330. DOI: 10.1161/CIRCRESAHA.108.185363.

[98] B. J. Holycross, R. S. Blank, M. M. Thompson, M. J. Peach, and G. K. Owens, "Platelet-derived growth factor-BB-induced suppression of smooth muscle cell differentiation," *Circulation Research*, vol. 71, no. 6, pp. 1525–1532, 1992, ISSN: 00097330. DOI: 10.1161/01.RES.71.6.1525.

[99] D. Gomez and G. K. Owens, "Smooth muscle cell phenotypic switching in atherosclerosis," *Cardiovascular Research*, vol. 95, pp. 156–164, 2012, ISSN: 00086363. DOI: 10.1093/cvr/cvs115.

[100] J. X. Rong, M. Shapiro, E. Trogan, and E. A. Fisher, "Transdifferentiation of mouse aortic smooth muscle cells to a macrophage-like state after cholesterol loading," vol. 100, no. 23, 2003.

[101] H. Koyama, E. W. Raines, K. E. Bornfeldt, J. M. Roberts, and R. Ross, "Fibrillar collagen inhibits arterial smooth muscle proliferation through regulation of Cdk2 inhibitors," *Cell*, vol. 87, no. 6, pp. 1069–1078, Dec. 1996, ISSN: 00928674. DOI: 10.1016/S0092-8674(00)81801-2. [Online]. Available: https://pubmed.ncbi.nlm.nih.gov/8978611/.

[102] D. Y. Li, B. Brooke, E. C. Davis, R. P. Mecham, L. K. Sorensen, B. B. Boak, E. Eichwald, and M. T. Keating, "Elastin is an essential determinant of arterial morphogenesis," *Nature*, vol. 393, no. 6682, pp. 276–280, May 1998, ISSN: 00280836. DOI: 10.1038/30522. [Online]. Available: https://pubmed.ncbi.nlm.nih.gov/9607766/.

[103] I. Rohwedder, E. Montanez, K. Beckmann, E. Bengtsson, P. Dunér, J. Nilsson, O. Soehnlein, and R. Fässler, "Plasma fibronectin deficiency impedes atherosclerosis progression and fibrous cap formation," *EMBO Molecular Medicine*, vol. 4, no. 7, pp. 564–576, Jul. 2012, ISSN: 17574676. DOI: 10.1002/emmm.201200237.

[104] U. Kansakar, S. S. Jankauskas, J. Gambardella, and G. Santulli, “Targeting the phenotypic switch of vascular smooth muscle cells to tackle atherosclerosis,” 2021. DOI: 10.1016/j.atherosclerosis.2021.03.034. [Online]. Available: https://doi.org/10.1016/j.atherosclerosis.2021.03.034.

[105] D. Voet, J. Voet, and C. Pratt, *Lehrbuch der Biochemie*. WILEY-VCH Verlag, 2002.

[106] K. P. C. Vollhardt and N. E. Schore, *Organische Chemie*, 4. Auflage. WILEY-VCH Verlag, 2005.

[107] Nature Education, *Scitable by Nature Education*, 2014. [Online]. Available: https://www.nature.com/scitable/.

[108] Cell Signaling Technology, *Overview of Metabolism and Metabolic Disorders*, 2021. [Online]. Available: https://www.cellsignal.com/science-resources/overview-of-metabolism.

[109] S. Malandraki-Miller, C. A. Lopez, H. Al-Siddiqi, and C. A. Carr, *Changing Metabolism in Differentiating Cardiac Progenitor Cells—Can Stem Cells Become Metabolically Flexible Cardiomyocytes?* Sep. 2018. DOI: 10.3389/fcvm.2018.00119.

[110] M. W. Gray, “Mitochondria,” *Brenner’s Encyclopedia of Genetics: Second Edition*, vol. 4, pp. 430–432, 2013, ISSN: 0044-0086. DOI: 10.1016/B978-0-12-374984-0.00957-8.

[111] I. E. Scheffler, “Mitochondria make a come back,” *Advanced Drug Delivery Reviews*, vol. 49, no. 1-2, pp. 3–26, Jul. 2001, ISSN: 0169409X. DOI: 10.1016/S0169-409X(01)00123-5.

[112] S. L. Archer, “Mitochondrial Dynamics — Mitochondrial Fission and Fusion in Human Diseases,” *New England Journal of Medicine*, vol. 369, no. 23, D. L. Longo, Ed., pp. 2236–2251, Dec. 2013, ISSN: 0028-4793. DOI: 10.1056/nejmra1215233. [Online]. Available: http://www.nejm.org/doi/10.1056/NEJMra1215233.

[113] Y. J. Liu, R. L. McIntyre, G. E. Janssens, and R. H. Houtkooper, “Mitochondrial fission and fusion: A dynamic role in aging and potential target for age-related disease,” *Mechanisms of Ageing and Development*, vol. 186, p. 111 212, Mar. 2020, ISSN: 18726216. DOI: 10.1016/j.mad.2020.111212.

[114] I. M. Grumbach and E. K. Nguyen, "Metabolic Stress: Mitochondrial Function in Neointimal Formation," *Arteriosclerosis, Thrombosis, and Vascular Biology*, vol. 39, no. 6, pp. 991–997, Jun. 2019, ISSN: 15244636. DOI: 10.1161/ATVBAHA.118.312196.

[115] K. Mitra, C. Wunder, B. Roysam, G. Lin, and J. Lippincott-Schwartz, "A hyperfused mitochondrial state achieved at G1-S regulates cyclin E buildup and entry into S phase," *Proceedings of the National Academy of Sciences of the United States of America*, vol. 106, no. 29, pp. 11 960–11 965, Jul. 2009, ISSN: 00278424. DOI: 10.1073/pnas.0904875106.

[116] C. Ploumi, I. Daskalaki, and N. Tavernarakis, *Mitochondrial biogenesis and clearance: a balancing act*, Jan. 2017. DOI: 10.1111/febs.13820. [Online]. Available: https://pubmed.ncbi.nlm.nih.gov/27462821/.

[117] R. C. Scarpulla, R. B. Vega, and D. P. Kelly, *Transcriptional integration of mitochondrial biogenesis*, Sep. 2012. DOI: 10.1016/j.tem.2012.06.006. [Online]. Available: https://pubmed.ncbi.nlm.nih.gov/22817841/.

[118] A. R. D'Souza and M. Minczuk, "Mitochondrial transcription and translation: Overview," *Essays in Biochemistry*, vol. 62, no. 3, pp. 309–320, 2018, ISSN: 00711365. DOI: 10.1042/EBC20170102.

[119] J. I. Satoh, N. Kawana, and Y. Yamamoto, "Pathway Analysis of ChIP-Seq-Based NRF1 Target Genes Suggests a Logical Hypothesis of their Involvement in the pathogenesis of Neurodegenerative Diseases," *Gene Regulation and Systems Biology*, vol. 2013, no. 7, pp. 139–152, Nov. 2013, ISSN: 11776250. DOI: 10.4137/GRSB.S13204. [Online]. Available: https://pubmed.ncbi.nlm.nih.gov/24250222/.

[120] F. Bruni, P. L. Polosa, M. N. Gadaleta, P. Cantatore, and M. Roberti, "Nuclear respiratory factor 2 induces the expression of many but not all human proteins acting in mitochondrial DNA transcription and replication," *Journal of Biological Chemistry*, vol. 285, no. 6, pp. 3939–3948, Feb. 2010, ISSN: 00219258. DOI: 10.1074/jbc.M109.044305. [Online]. Available: https://pubmed.ncbi.nlm.nih.gov/19951946/.

[121] D. Ryu, Y. S. Jo, G. Lo Sasso, S. Stein, H. Zhang, A. Perino, J. U. Lee, M. Zeviani, R. Romand, M. O. Hottiger, K. Schoonjans, and J. Auwerx, "A SIRT7-dependent acetylation switch of GABPβ1 controls mitochondrial function," *Cell Metabolism*, vol. 20, no. 5, pp. 856–869, Nov. 2014, ISSN: 19327420. DOI:

10.1016/j.cmet.2014.08.001. [Online]. Available: https://pubmed.ncbi.nlm.nih.gov/25200183/.

[122] Z.-F. Yang, K. Drumea, S. Mott, J. Wang, and A. G. Rosmarin, "GABP Transcription Factor (Nuclear Respiratory Factor 2) Is Required for Mitochondrial Biogenesis," *Molecular and Cellular Biology*, vol. 34, no. 17, pp. 3194–3201, Sep. 2014, ISSN: 0270-7306. DOI: 10.1128/mcb.00492-12. [Online]. Available: https://pubmed.ncbi.nlm.nih.gov/24958105/.

[123] J. A. Madrazo and D. P. Kelly, *The PPAR trio: Regulators of myocardial energy metabolism in health and disease*, Jun. 2008. DOI: 10.1016/j.yjmcc.2008.03.021. [Online]. Available: https://pubmed.ncbi.nlm.nih.gov/18462747/.

[124] L. J. Eichner and V. Giguère, *Estrogen related receptors (ERRs): A new dawn in transcriptional control of mitochondrial gene networks*, Jul. 2011. DOI: 10.1016/j.mito.2011.03.121. [Online]. Available: https://pubmed.ncbi.nlm.nih.gov/21497207/.

[125] B. N. Finck and D. P. Kelly, *PGC-1 coactivators: Inducible regulators of energy metabolism in health and disease*, Mar. 2006. DOI: 10.1172/JCI27794. [Online]. Available: https://pubmed.ncbi.nlm.nih.gov/16511594/.

[126] J. Hirst, "Energy transduction by respiratory complex I - An evaluation of current knowledge," in *Biochemical Society Transactions*, vol. 33, Biochem Soc Trans, Jun. 2005, pp. 525–529. DOI: 10.1042/BST0330525. [Online]. Available: https://pubmed.ncbi.nlm.nih.gov/15916556/.

[127] G. Cecchini, *Function and structure of complex II of the respiratory chain*, 2003. DOI: 10.1146/annurev.biochem.72.121801.161700. [Online]. Available: https://pubmed.ncbi.nlm.nih.gov/14527321/.

[128] R. R. Ramsay, D. J. Steenkamp, and M. Husain, "Reactions of electron-transfer flavoprotein and electron-transfer flavoprotein: ubiquinone oxidoreductase.," *The Biochemical journal*, vol. 241, no. 3, pp. 883–892, 1987, ISSN: 02646021. DOI: 10.1042/bj2410883. [Online]. Available: https://pubmed.ncbi.nlm.nih.gov/3593226/.

[129] E. A. Berry, M. Guergova-Kuras, L. S. Huang, and A. R. Crofts, "Structure and function of cytochrome bc complexes," *Annual Review of Biochemistry*, vol. 69, pp. 1005–1075, 2000, ISSN: 00664154. DOI: 10.1146/annurev.biochem.

69.1.1005. [Online]. Available: https://pubmed.ncbi.nlm.nih.gov/10966481/.

[130] M. W. Calhoun, J. W. Thomas, and R. B. Gennis, *The cytochrome oxidase superfamily of redox-driven proton pumps*, 1994. DOI: 10.1016/0968-0004(94)90071-X. [Online]. Available: https://pubmed.ncbi.nlm.nih.gov/7940677/.

[131] M. Yoshida, E. Muneyuki, and T. Hisabori, *ATP synthase - A marvellous rotary engine of the cell*, Sep. 2001. DOI: 10.1038/35089509. [Online]. Available: https://pubmed.ncbi.nlm.nih.gov/11533724/.

[132] J. F. Turrens, *Mitochondrial formation of reactive oxygen species*, Oct. 2003. DOI: 10.1113/jphysiol.2003.049478.

[133] S. Miriyala, A. K. Holley, and D. K. St Clair, "Mitochondrial Superoxide Dismutase - Signals of Distinction," *Anti-Cancer Agents in Medicinal Chemistry*, vol. 11, no. 2, pp. 181–190, Nov. 2012, ISSN: 18715206. DOI: 10.2174/187152011795255920.

[134] A. Kasahara and L. Scorrano, "Mitochondria : from cell death executioners to regulators of cell differentiation," *Trends in Cell Biology*, vol. 24, no. 12, pp. 761–770, 2014, ISSN: 0962-8924. DOI: 10.1016/j.tcb.2014.08.005. [Online]. Available: http://dx.doi.org/10.1016/j.tcb.2014.08.005.

[135] R. A. Smith, R. C. Hartley, H. M. Cochemé, and M. P. Murphy, *Mitochondrial pharmacology*, Jun. 2012. DOI: 10.1016/j.tips.2012.03.010.

[136] M. G. Heiden, L. C. Cantley, and C. B. Thompson, *Understanding the warburg effect: The metabolic requirements of cell proliferation*, May 2009. DOI: 10.1126/science.1160809. [Online]. Available: https://pubmed.ncbi.nlm.nih.gov/19460998/.

[137] P. P. Hsu and D. M. Sabatini, *Cancer cell metabolism: Warburg and beyond*, Sep. 2008. DOI: 10.1016/j.cell.2008.08.021. [Online]. Available: https://pubmed.ncbi.nlm.nih.gov/18775299/.

[138] R. J. DeBerardinis, J. J. Lum, G. Hatzivassiliou, and C. B. Thompson, *The Biology of Cancer: Metabolic Reprogramming Fuels Cell Growth and Proliferation*, Jan. 2008. DOI: 10.1016/j.cmet.2007.10.002.

[139] O. Warburg, F. Wind, and E. Negelein, “The metabolism of tumors in the body,” *Journal of General Physiology*, vol. 8, no. 6, pp. 519–530, Mar. 1927, ISSN: 15407748. DOI: 10.1085/jgp.8.6.519. [Online]. Available: https://pubmed.ncbi.nlm.nih.gov/19872213/.

[140] O. Warburg, “On the origin of cancer cells,” *Science*, vol. 123, no. 3191, pp. 309–314, 1956, ISSN: 00368075. DOI: 10.1126/science.123.3191.309. [Online]. Available: https://pubmed.ncbi.nlm.nih.gov/13298683/.

[141] V. R. Fantin, J. St-Pierre, and P. Leder, “Attenuation of LDH-A expression uncovers a link between glycolysis, mitochondrial physiology, and tumor maintenance,” *Cancer Cell*, vol. 9, no. 6, pp. 425–434, Jun. 2006, ISSN: 15356108. DOI: 10.1016/j.ccr.2006.04.023. [Online]. Available: https://pubmed.ncbi.nlm.nih.gov/16766262/.

[142] R. Moreno-Sánchez, S. Rodríguez-Enríquez, A. Marín-Hernández, and E. Saavedra, *Energy metabolism in tumor cells*, Mar. 2007. DOI: 10.1111/j.1742-4658.2007.05686.x. [Online]. Available: https://pubmed.ncbi.nlm.nih.gov/17302740/.

[143] K. De Bock, M. Georgiadou, S. Schoors, A. Kuchnio, B. W. Wong, A. R. Cantelmo, A. Quaegebeur, B. Ghesquière, S. Cauwenberghs, G. Eelen, L. K. Phng, I. Betz, B. Tembuyser, K. Brepoels, J. Welti, I. Geudens, I. Segura, B. Cruys, F. Bifari, I. Decimo, R. Blanco, S. Wyns, J. Vangindertael, S. Rocha, R. T. Collins, S. Munck, D. Daelemans, H. Imamura, R. Devlieger, M. Rider, P. P. Van Veldhoven, F. Schuit, R. Bartrons, J. Hofkens, P. Fraisl, S. Telang, R. J. Deberardinis, L. Schoonjans, S. Vinckier, J. Chesney, H. Gerhardt, M. Dewerchin, and P. Carmeliet, “Role of PFKFB3-driven glycolysis in vessel sprouting,” *Cell*, vol. 154, no. 3, pp. 651–663, Aug. 2013, ISSN: 10974172. DOI: 10.1016/j.cell.2013.06.037.

[144] A. Viola, F. Munari, R. Sánchez-rodríguez, T. Scolaro, and A. Castegna, “The Metabolic Signature of Macrophage Responses,” *frontiers in Immunology*, vol. 10, no. July, pp. 1–16, 2019. DOI: 10.3389/fimmu.2019.01462.

[145] J. Shi, Y. Yang, A. Cheng, G. Xu, and F. He, “Metabolism of vascular smooth muscle cells in vascular diseases,” *Am J Physiol Heart Circ Physiol*, vol. 319, pp. 613–631, 2020.

[146] J. T. Barron and J. E. Parrillo, “Production of lactic acid and energy metabolism in vascular smooth muscle: Effect of dichloroacetate,” *American Journal of Physiology - Heart and Circulatory Physiology*, vol. 268, no. 2 37-2, 1995, ISSN: 03636135. DOI: 10.1152/ajpheart.1995.268.2.h713. [Online]. Available: https://pubmed.ncbi.nlm.nih.gov/7864198/.

[147] L. Yang, L. Gao, T. Nickel, J. Yang, J. Zhou, A. Gilbertsen, Z. Geng, C. Johnson, B. Young, C. Henke, G. R. Gourley, and J. Zhang, “Lactate Promotes Synthetic Phenotype in Vascular Smooth Muscle Cells,” *Circulation Research*, pp. 1251–1262, 2017. DOI: 10.1161/CIRCRESAHA.117.311819.

[148] Y. Xiao, H. Peng, C. Hong, Z. Chen, X. Deng, A. Wang, F. Yang, L. Yang, C. Chen, and X. Qin, “PDGF Promotes the Warburg Effect in Pulmonary Arterial Smooth Muscle Cells via Activation of the PI3K/AKT/mTOR/HIF-1α Signaling Pathway,” *Cellular Physiology and Biochemistry*, vol. 42, no. 4, pp. 1603–1613, 2017, ISSN: 14219778. DOI: 10.1159/000479401.

[149] J. Perez, B. G. Hill, G. A. Benavides, B. P. Dranka, and V. M. Darley-Usmar, “Role of cellular bioenergetics in smooth muscle cell proliferation induced by platelet-derived growth factor.,” *The Biochemical journal*, vol. 428, no. 2, pp. 255–67, Jun. 2010, ISSN: 1470-8728. DOI: 10.1042/BJ20100090.

[150] J. K. Salabei and B. G. Hill, “Mitochondrial fission induced by platelet-derived growth factor regulates vascular smooth muscle cell bioenergetics and cell proliferation.,” *Redox biology*, vol. 1, pp. 542–51, Jan. 2013, ISSN: 2213-2317. DOI: 10.1016/j.redox.2013.10.011.

[151] E. P. Yu and M. R. Bennett, *Mitochondrial DNA damage and atherosclerosis*, 2014. DOI: 10.1016/j.tem.2014.06.008.

[152] E. Yu, P. A. Calvert, J. R. Mercer, J. Harrison, L. Baker, N. L. Figg, S. Kumar, J. C. Wang, L. A. Hurst, D. R. Obaid, A. Logan, N. E. West, M. C. Clarke, A. Vidal-Puig, M. P. Murphy, and M. R. Bennett, “Mitochondrial DNA damage can promote atherosclerosis independently of reactive oxygen species through effects on smooth muscle cells and monocytes and correlates with higher-risk plaques in humans,” *Circulation*, vol. 128, no. 7, pp. 702–712, Aug. 2013, ISSN: 00097322. DOI: 10.1161/CIRCULATIONAHA.113.002271.

[153] C. K. Docherty, A. Carswell, E. Friel, and J. R. Mercer, “Impaired mitochondrial respiration in human carotid plaque atherosclerosis : A potential role for Pink1 in vascular smooth muscle cell energetics,” *Atherosclerosis*, vol. 268, pp. 1–11, 2018, ISSN: 0021-9150. DOI: 10.1016/j.atherosclerosis.

2017 . 11 . 009. [Online]. Available: https : / / doi . org / 10 . 1016 / j . atherosclerosis.2017.11.009.

[154] M. Kaeberlein, M. McVey, and L. Guarente, "The SIR2/3/4 complex and SIR2 alone promote longevity in Saccharomyces cerevisiae by two different mechanisms," *Genes and Development*, vol. 13, no. 19, pp. 2570–2580, Oct. 1999, ISSN: 08909369. DOI: 10.1101/gad.13.19.2570. [Online]. Available: https://pubmed.ncbi.nlm.nih.gov/10521401/.

[155] J. L. Feldman, K. E. Dittenhafer-Reed, and J. M. Denu, *Sirtuin catalysis and regulation*, Dec. 2012. DOI: 10.1074/jbc.R112.378877.

[156] M. S. Bonkowski and D. A. Sinclair, *Slowing ageing by design: The rise of NAD+ and sirtuin-activating compounds*, Nov. 2016. DOI: 10 . 1038 / nrm . 2016 . 93. [Online]. Available: https : / / pubmed . ncbi . nlm . nih . gov / 27552971/.

[157] S. i. Imai and L. Guarente, *NAD+ and sirtuins in aging and disease*, 2014. DOI: 10.1016/j.tcb.2014.04.002. [Online]. Available: https://pubmed.ncbi.nlm.nih.gov/24786309/.

[158] M. C. Haigis and D. A. Sinclair, *Mammalian sirtuins: Biological insights and disease relevance*, Feb. 2010. DOI: 10.1146/annurev.pathol.4.110807.092250. [Online]. Available: https : / / pubmed . ncbi . nlm . nih . gov / 20078221/.

[159] H. C. Chang and L. Guarente, *SIRT1 and other sirtuins in metabolism*, Mar. 2014. DOI: 10 . 1016 / j . tem . 2013 . 12 . 001. [Online]. Available: https : //pubmed.ncbi.nlm.nih.gov/24388149/.

[160] H. Vaziri, S. K. Dessain, E. N. Eaton, S. I. Imai, R. A. Frye, T. K. Pandita, L. Guarente, and R. A. Weinberg, "hSIR2SIRT1 functions as an NAD-dependent p53 deacetylase," *Cell*, vol. 107, no. 2, pp. 149–159, Oct. 2001, ISSN: 00928674. DOI: 10.1016/S0092-8674(01)00527-X. [Online]. Available: https://pubmed.ncbi.nlm.nih.gov/11672523/.

[161] L. Mouchiroud, R. H. Houtkooper, N. Moullan, E. Katsyuba, D. Ryu, C. Cantó, A. Mottis, Y. S. Jo, M. Viswanathan, K. Schoonjans, L. Guarente, and J. Auwerx, "XThe NAD+/sirtuin pathway modulates longevity through activation of mitochondrial UPR and FOXO signaling," *Cell*, vol. 154, no. 2, p. 430, Jul. 2013, ISSN: 10974172. DOI: 10.1016/j.cell.2013.06.016.

[162] F. Yeung, J. E. Hoberg, C. S. Ramsey, M. D. Keller, D. R. Jones, R. A. Frye, and M. W. Mayo, "Modulation of NF-κB-dependent transcription and cell survival by the SIRT1 deacetylase," *EMBO Journal*, vol. 23, no. 12, pp. 2369–2380, Jun. 2004, ISSN: 02614189. DOI: 10.1038/sj.emboj.7600244. [Online]. Available: https://pubmed.ncbi.nlm.nih.gov/15152190/.

[163] S. B. Rajamohan, V. B. Pillai, M. Gupta, N. R. Sundaresan, K. G. Birukov, S. Samant, M. O. Hottiger, and M. P. Gupta, "SIRT1 Promotes Cell Survival under Stress by Deacetylation-Dependent Deactivation of Poly(ADP-Ribose) Polymerase 1," *Molecular and Cellular Biology*, vol. 29, no. 15, pp. 4116–4129, Aug. 2009, ISSN: 0270-7306. DOI: 10.1128/mcb.00121-09. [Online]. Available: https://pubmed.ncbi.nlm.nih.gov/19470756/.

[164] J. T. Rodgers, C. Lerin, W. Haas, S. P. Gygi, B. M. Spiegelman, and P. Puigserver, "Nutrient control of glucose homeostasis through a complex of PGC-1α and SIRT1," *Nature*, vol. 434, no. 7029, pp. 113–118, Mar. 2005, ISSN: 00280836. DOI: 10.1038/nature03354. [Online]. Available: https://pubmed.ncbi.nlm.nih.gov/15744310/.

[165] A. E. Kane and D. A. Sinclair, "Cardiovascular Aging Compendium Sirtuins and NAD + in the Development and Treatment of Metabolic and Cardiovascular Diseases," *Circulation Research*, pp. 868–885, 2018. DOI: 10.1161/CIRCRESAHA.118.312498.

[166] Q. J. Zhang, Z. Wang, H. Z. Chen, S. Zhou, W. Zheng, G. Liu, Y. S. Wei, H. Cai, D. P. Liu, and C. C. Liang, "Endothelium-specific overexpression of class III deacetylase SIRT1 decreases atherosclerosis in apolipoprotein E-deficient mice," *Cardiovascular Research*, vol. 80, no. 2, pp. 191–199, Nov. 2008, ISSN: 00086363. DOI: 10.1093/cvr/cvn224. [Online]. Available: https://pubmed.ncbi.nlm.nih.gov/18689793/.

[167] I. Gorenne, S. Kumar, K. Gray, N. Figg, H. Yu, J. Mercer, and M. Bennett, "Vascular smooth muscle cell sirtuin 1 protects against dna damage and inhibits atherosclerosis," *Circulation*, vol. 127, no. 3, pp. 386–396, Jan. 2013, ISSN: 00097322. DOI: 10.1161/CIRCULATIONAHA.112.124404. [Online]. Available: https://pubmed.ncbi.nlm.nih.gov/23224247/.

[168] A. W. Man, H. Li, and N. Xia, *The role of sirtuin1 in regulating endothelial function, arterial remodeling and vascular aging*, Sep. 2019. DOI: 10.3389/fphys.2019.01173.

[169] E. Michishita, R. A. McCord, E. Berber, M. Kioi, H. Padilla-Nash, M. Damian, P. Cheung, R. Kusumoto, T. L. Kawahara, J. C. Barrett, H. Y. Chang, V. A. Bohr, T. Ried, O. Gozani, and K. F. Chua, "SIRT6 is a histone H3 lysine 9 deacetylase that modulates telomeric chromatin," *Nature*, vol. 452, no. 7186, pp. 492–496, Mar. 2008, ISSN: 14764687. DOI: 10.1038/nature06736. [Online]. Available: https://www.nature.com/articles/nature06736.

[170] B. Yang, B. M. Zwaans, M. Eckersdorff, and D. B. Lombard, *The sirtuin SIRT6 deacetylates H3 K56Ac in vivo to promote genomic stability*, Aug. 2009. DOI: 10.4161/cc.8.16.9329. [Online]. Available: https://www.tandfonline.com/action/journalInformation?journalCode=kccy20.

[171] H. Jiang, S. Khan, Y. Wang, G. Charron, B. He, C. Sebastian, J. Du, R. Kim, E. Ge, R. Mostoslavsky, H. C. Hang, Q. Hao, and H. Lin, "SIRT6 regulates TNF-α secretion through hydrolysis of long-chain fatty acyl lysine," *Nature*, vol. 496, no. 7443, pp. 110–113, Apr. 2013, ISSN: 00280836. DOI: 10.1038/nature12038. [Online]. Available: https://www.nature.com/articles/nature12038.

[172] Z. Mao, C. Hine, X. Tian, M. Van Meter, M. Au, A. Vaidya, A. Seluanov, and V. Gorbunova, "SIRT6 promotes DNA repair under stress by activating PARP1," *Science*, vol. 332, no. 6036, pp. 1443–1446, Jun. 2011, ISSN: 00368075. DOI: 10.1126/science.1202723.

[173] S. Kugel and R. Mostoslavsky, "Chromatin and beyond: the multitasking roles for SIRT6.," *Trends in biochemical sciences*, vol. 39, no. 2, pp. 72–81, Feb. 2014, ISSN: 0968-0004. DOI: 10.1016/j.tibs.2013.12.002. [Online]. Available: http://www.sciencedirect.com/science/article/pii/S0968000413002016.

[174] L. Onn, M. Portillo, S. Ilic, G. Cleitman, D. Stein, S. Kaluski, I. Shirat, Z. Slobodnik, M. Einav, F. Erdel, B. Akabayov, and D. Toiber, "SIRT6 is a DNA double-strand break sensor," *eLife*, vol. 9, Jan. 2020, ISSN: 2050084X. DOI: 10.7554/eLife.51636.

[175] R. Mostoslavsky, K. F. Chua, D. B. Lombard, W. W. Pang, M. R. Fischer, L. Gellon, P. Liu, G. Mostoslavsky, S. Franco, M. M. Murphy, K. D. Mills, P. Patel, J. T. Hsu, A. L. Hong, E. Ford, H. L. Cheng, C. Kennedy, N. Nunez, R. Bronson, D. Frendewey, W. Auerbach, D. Valenzuela, M. Karow, M. O. Hottiger, S. Hursting, J. C. Barrett, L. Guarente, R. Mulligan, B. Demple, G. D. Yancopoulos, and F. W. Alt, "Genomic instability and aging-like phenotype in

the absence of mammalian SIRT6," *Cell*, vol. 124, no. 2, pp. 315–329, Jan. 2006, ISSN: 00928674. DOI: 10.1016/j.cell.2005.11.044.

[176] L. Zhong, A. D'Urso, D. Toiber, C. Sebastian, R. E. Henry, D. D. Vadysirisack, A. Guimaraes, B. Marinelli, J. D. Wikstrom, T. Nir, C. B. Clish, B. Vaitheesvaran, O. Iliopoulos, I. Kurland, Y. Dor, R. Weissleder, O. S. Shirihai, L. W. Ellisen, J. M. Espinosa, and R. Mostoslavsky, "The Histone Deacetylase Sirt6 Regulates Glucose Homeostasis via Hif1α," *Cell*, vol. 140, no. 2, pp. 280–293, Jan. 2010, ISSN: 00928674. DOI: 10.1016/j.cell.2009.12.041.

[177] H. S. Kim, C. Xiao, R. H. Wang, T. Lahusen, X. Xu, A. Vassilopoulos, G. Vazquez-Ortiz, W. I. Jeong, O. Park, S. H. Ki, B. Gao, and C. X. Deng, "Hepatic-specific disruption of SIRT6 in mice results in fatty liver formation due to enhanced glycolysis and triglyceride synthesis," *Cell Metabolism*, vol. 12, no. 3, pp. 224–236, Sep. 2010, ISSN: 15504131. DOI: 10.1016/j.cmet.2010.06.009.

[178] S. Naiman, F. K. Huynh, R. Gil, Y. Glick, Y. Shahar, N. Touitou, L. Nahum, M. Y. Avivi, A. Roichman, Y. Kanfi, A. A. Gertler, T. Doniger, O. R. Ilkayeva, I. Abramovich, O. Yaron, B. Lerrer, E. Gottlieb, R. A. Harris, D. Gerber, M. D. Hirschey, and H. Y. Cohen, "SIRT6 Promotes Hepatic Beta-Oxidation via Activation of PPARα," *Cell Reports*, vol. 29, no. 12, pp. 4127–4143, Dec. 2019, ISSN: 22111247. DOI: 10.1016/j.celrep.2019.11.067. [Online]. Available: https://pubmed.ncbi.nlm.nih.gov/31851938/.

[179] C. Sebastián, B. M. Zwaans, D. M. Silberman, M. Gymrek, A. Goren, L. Zhong, O. Ram, J. Truelove, A. R. Guimaraes, D. Toiber, C. Cosentino, J. K. Greenson, A. I. MacDonald, L. McGlynn, F. Maxwell, J. Edwards, S. Giacosa, E. Guccione, R. Weissleder, B. E. Bernstein, A. Regev, P. G. Shiels, D. B. Lombard, and R. Mostoslavsky, "The histone deacetylase SIRT6 Is a tumor suppressor that controls cancer metabolism," *Cell*, vol. 151, no. 6, pp. 1185–1199, Dec. 2012, ISSN: 10974172. DOI: 10.1016/j.cell.2012.10.047.

[180] E. Michishita, J. Y. Park, J. M. Burneskis, J. C. Barrett, and I. Horikawa, "Evolutionarily conserved and nonconserved cellular localizations and functions of human SIRT proteins," *Molecular Biology of the Cell*, vol. 16, no. 10, pp. 4623–4635, Oct. 2005, ISSN: 10591524. DOI: 10.1091/mbc.E05-01-0033. [Online]. Available: https://pubmed.ncbi.nlm.nih.gov/16079181/.

[181] M. F. Barber, E. Michishita-Kioi, Y. Xi, L. Tasselli, M. Kioi, Z. Moqtaderi, R. I. Tennen, S. Paredes, N. L. Young, K. Chen, K. Struhl, B. A. Garcia, O. Gozani1, W. Li, and K. F. Chua, "SIRT7 links H3K18 deacetylation to maintenance of oncogenic transformation," *Nature*, vol. 487, no. 7405, pp. 114–118, 2012, ISSN: 00280836. DOI: 10.1038/nature11043. [Online]. Available: https://pubmed.ncbi.nlm.nih.gov/22722849/.

[182] D. Wu, Y. Li, K. S. Zhu, H. Wang, and W. G. Zhu, *Advances in Cellular Characterization of the Sirtuin Isoform, SIRT7*, Nov. 2018. DOI: 10.3389/fendo.2018.00652.

[183] O. Vakhrusheva, C. Smolka, P. Gajawada, S. Kostin, T. Boettger, T. Kubin, T. Braun, and E. Bober, "Sirt7 increases stress resistance of cardiomyocytes and prevents apoptosis and inflammatory cardiomyopathy in mice," *Circulation Research*, vol. 102, no. 6, pp. 703–710, Mar. 2008, ISSN: 00097330. DOI: 10.1161/CIRCRESAHA.107.164558.

[184] B. N. Vazquez, J. K. Thackray, N. G. Simonet, N. Kane-Goldsmith, P. Martinez-Redondo, T. Nguyen, S. Bunting, A. Vaquero, J. A. Tischfield, and L. Serrano, " SIRT 7 promotes genome integrity and modulates non-homologous end joining DNA repair," *The EMBO Journal*, vol. 35, no. 14, pp. 1488–1503, Jul. 2016, ISSN: 0261-4189. DOI: 10.15252/embj.201593499. [Online]. Available: https://pubmed.ncbi.nlm.nih.gov/27225932/.

[185] N. Lee, D. K. Kim, E. S. Kim, S. J. Park, J. H. Kwon, J. Shin, S. M. Park, Y. H. Moon, H. J. Wang, Y. S. Gho, and K. Y. Choi, "Comparative interactomes of SIRT6 and SIRT7: Implication of functional links to aging," *Proteomics*, vol. 14, no. 13-14, pp. 1610–1622, 2014, ISSN: 16159861. DOI: 10.1002/pmic.201400001. [Online]. Available: https://pubmed.ncbi.nlm.nih.gov/24782448/.

[186] S. Chen, J. Seiler, M. Santiago-Reichelt, K. Felbel, I. Grummt, and R. Voit, "Repression of RNA Polymerase I upon Stress Is Caused by Inhibition of RNA-Dependent Deacetylation of PAF53 by SIRT7," *Molecular Cell*, vol. 52, no. 3, pp. 303–313, Nov. 2013, ISSN: 10972765. DOI: 10.1016/j.molcel.2013.10.010. [Online]. Available: https://pubmed.ncbi.nlm.nih.gov/24207024/.

[187] H. Hu, W. Zhu, J. Qin, M. Chen, L. Gong, L. Li, X. Liu, Y. Tao, H. Yin, H. Zhou, L. Zhou, D. Ye, Q. Ye, and D. Gao, "Acetylation of PGK1 promotes liver cancer cell proliferation and tumorigenesis," *Hepatology*, vol. 65, no. 2, pp. 515–528,

Feb. 2017, ISSN: 15273350. DOI: 10.1002/hep.28887. [Online]. Available: https://pubmed.ncbi.nlm.nih.gov/27774669/.

[188] L. Jiang, J. Xiong, J. Zhan, F. Yuan, M. Tang, C. Zhang, Z. Cao, Y. Chen, X. Lu, Y. Li, H. Wang, L. Wang, J. Wang, W. G. Zhu, and H. Wang, "Ubiquitin-specific peptidase 7 (USP7)-mediated deubiquitination of the histone deacetylase SIRT7 regulates gluconeogenesis," *Journal of Biological Chemistry*, vol. 292, no. 32, pp. 13 296–13 311, Aug. 2017, ISSN: 1083351X. DOI: 10.1074/jbc.M117.780130.

[189] M. E. Hubbi, H. Hu, Kshitiz, D. M. Gilkes, and G. L. Semenza, "Sirtuin-7 inhibits the activity of hypoxia-inducible factors," *Journal of Biological Chemistry*, vol. 288, no. 29, pp. 20 768–20 775, Jul. 2013, ISSN: 00219258. DOI: 10.1074/jbc.M113.476903. [Online]. Available: https://pubmed.ncbi.nlm.nih.gov/23750001/.

[190] M. Mohrin, J. Shin, Y. Liu, K. Brown, H. Luo, Y. Xi, C. M. Haynes, and D. Chen, "A mitochondrial UPR-mediated metabolic checkpoint regulates hematopoietic stem cell aging," *Science*, vol. 347, no. 6228, pp. 1374–1377, Mar. 2015, ISSN: 10959203. DOI: 10.1126/science.aaa2361. [Online]. Available: https://pubmed.ncbi.nlm.nih.gov/25792330/.

[191] S. Shahgaldi and F. R. Kahmini, "A comprehensive review of Sirtuins: With a major focus on redox homeostasis and metabolism," *Life Sciences*, vol. 282, p. 119 803, Oct. 2021, ISSN: 18790631. DOI: 10.1016/j.lfs.2021.119803.

[192] A. Wirth, Z. Benyó, M. Lukasova, B. Leutgeb, N. Wettschureck, S. Gorbey, P. Orsy, B. Horváth, C. Maser-Gluth, E. Greiner, B. Lemmer, G. Schütz, S. Gutkind, and S. Offermanns, "G12-G13-LARG-mediated signaling in vascular smooth muscle is required for salt-induced hypertension," *Nature Medicine*, vol. 14, no. 1, pp. 64–68, Jan. 2008, ISSN: 10788956. DOI: 10.1038/nm1666.

[193] M. D. Muzumdar, B. Tasic, K. Miyamichi, N. Li, and L. Luo, "A global double-fluorescent cre reporter mouse," *Genesis*, vol. 45, no. 9, pp. 593–605, Sep. 2007, ISSN: 1526954X. DOI: 10.1002/dvg.20335.

[194] Inaugural-dissertation, "Analyse der biologischen Funktionen von Sirt6 in metabolischen Prozessen Christian Smolka," Tech. Rep., 2012.

[195] T. Yoshizawa, M. F. Karim, Y. Sato, T. Senokuchi, K. Miyata, T. Fukuda, C. Go, M. Tasaki, K. Uchimura, T. Kadomatsu, Z. Tian, C. Smolka, T. Sawa, M. Takeya, K. Tomizawa, Y. Ando, E. Araki, T. Akaike, T. Braun, Y. Oike, E. Bober,

and K. Yamagata, “SIRT7 controls hepatic lipid metabolism by regulating the ubiquitin-proteasome pathway,” *Cell Metabolism*, vol. 19, no. 4, pp. 712–721, Apr. 2014, ISSN: 19327420. DOI: 10.1016/j.cmet.2014.03.006. [Online]. Available: http://dx..

[196] Agilent, *Seahorse XF Cell Mito Stress Test Kit Usermanual*. [Online]. Available: https://www.agilent.com/.

[197] S. M. Peterson, L. Liaw, and V. Lindner, “Ligation of the mouse common carotid artery,” in *Mouse Models of Vascular Diseases*, Tokyo: Springer Japan, Jan. 2016, pp. 43–68, ISBN: 9784431558132. DOI: 10.1007/978-4-431-55813-2{_}3. [Online]. Available: http://link.springer.com/10.1007/978-4-431-55813-2_3.

[198] K. J. Harmon, L. L. Couper, and V. Lindner, “Strain-Dependent Vascular Remodeling Phenotypes in Inbred Mice,” *The American Journal of Pathology*, vol. 156, no. 5, p. 1741, 2000, ISSN: 00029440. DOI: 10.1016/S0002-9440(10)65045-6.

[199] D. L. Myers and L. Liaw, “Improved Analysis of the Vascular Response to Arterial Ligation Using a Multivariate Approach,” *The American Journal of Pathology*, vol. 164, no. 1, p. 43, 2004, ISSN: 00029440. DOI: 10.1016/S0002-9440(10)63094-5.

[200] A. W. Holt and D. A. Tulis, “Experimental Rat and Mouse Carotid Artery Surgery: Injury and Remodeling Studies,” *ISRN Minimally Invasive Surgery*, vol. 2013, pp. 1–10, May 2013, ISSN: 2090-9438. DOI: 10.1155/2013/167407.

[201] *BioRender*. [Online]. Available: https://biorender.com/.

[202] C. L. Jackson and A. R. Bond, “The Fat-Fed Apolipoprotein E Knockout Mouse Brachiocephalic Artery in the Study of Atherosclerotic Plaque Rupture,” *Journal of Biomedicine and Biotechnology*, vol. 2011, 2011, ISSN: 11107243. DOI: 10.1155/2011/379069.

[203] J. Zheng, K. Chen, H. Wang, Z. Chen, Y. Xi, H. Yin, K. Lai, and Y. Liu, “SIRT7 Regulates the Vascular Smooth Muscle Cells Proliferation and Migration via Wnt/ β -Catenin Signaling Pathway,” *BioMed Research International*, vol. 2018, 2018, ISSN: 23146141. DOI: 10.1155/2018/4769596.

[204] R. S. Blank and G. K. Owens, “Platelet-derived growth factor regulates actin isoform expression and growth factor regulates actin isoform expression and growth state in cultured rat aortic smooth muscle cells,” *Journal of Cellular Physiology*, vol. 142, no. 3, pp. 635–642, Mar. 1990, ISSN: 0021-9541. DOI: 10.1002/jcp.1041420325. [Online]. Available: http://doi.wiley.com/10.1002/jcp.1041420325.

[205] H. M. Nef, H. Möllmann, A. Joseph, C. Troidl, S. Voss, A. Vogt, M. Weber, C. W. Hamm, and A. Elsasser, “Effects of 2-Deoxy-D-glucose on proliferation of vascular smooth muscle cells and endothelial cells,” *Journal of International Medical Research*, vol. 36, no. 5, pp. 986–991, 2008, ISSN: 03000605. DOI: 10.1177/147323000803600515.

[206] K. De Bock, M. Georgiadou, S. Schoors, A. Kuchnio, B. W. Wong, A. R. Cantelmo, A. Quaegebeur, B. Ghesquière, S. Cauwenberghs, G. Eelen, L.-K. Phng, I. Betz, B. Tembuyser, K. Brepoels, J. Welti, I. Geudens, I. Segura, B. Cruys, F. Bifari, I. Decimo, R. Blanco, S. Wyns, J. Vangindertael, S. Rocha, R. T. Collins, S. Munck, D. Daelemans, H. Imamura, R. Devlieger, M. Rider, P. P. Van Veldhoven, F. Schuit, R. Bartrons, J. Hofkens, P. Fraisl, S. Telang, R. J. Deberardinis, L. Schoonjans, S. Vinckier, J. Chesney, H. Gerhardt, M. Dewerchin, and P. Carmeliet, “Role of PFKFB3-driven glycolysis in vessel sprouting.,” *Cell*, vol. 154, no. 3, pp. 651–63, Aug. 2013, ISSN: 1097-4172. DOI: 10.1016/j.cell.2013.06.037.

[207] E. Solsona-Vilarrasa, R. Fucho, S. Torres, S. Nuñez, N. Nuño-Lámbarri, C. Enrich, C. García-Ruiz, and J. C. Fernández-Checa, “Cholesterol enrichment in liver mitochondria impairs oxidative phosphorylation and disrupts the assembly of respiratory supercomplexes,” *Redox Biology*, vol. 24, Jun. 2019, ISSN: 22132317. DOI: 10.1016/j.redox.2019.101214.

[208] X. Li, Y. Jiang, J. Meisenhelder, W. Yang, D. H. Hawke, Y. Zheng, Y. Xia, K. Aldape, J. He, T. Hunter, L. Wang, and Z. Lu, “Mitochondria-Translocated PGK1 Functions as a Protein Kinase to Coordinate Glycolysis and the TCA Cycle in Tumorigenesis,” *Molecular Cell*, vol. 61, no. 5, pp. 705–719, 2016, ISSN: 10974164. DOI: 10.1016/j.molcel.2016.02.009. [Online]. Available: http://dx.doi.org/10.1016/j.molcel.2016.02.009.

[209] S. Chen, H. Chen, C. Yu, R. Lu, T. Song, X. Wang, W. Tang, and Y. Gao, “MiR-638 repressed vascular smooth muscle cell glycolysis by targeting LDHA,”

Open Medicine (Poland), vol. 14, no. 1, pp. 663–672, 2019, ISSN: 23915463. DOI: 10.1515/med-2019-0077.

[210] J. H. Kim, K. H. Bae, J. K. Byun, S. Lee, J. G. Kim, I. K. Lee, G. S. Jung, Y. M. Lee, and K. G. Park, "Lactate dehydrogenase-A is indispensable for vascular smooth muscle cell proliferation and migration," *Biochemical and Biophysical Research Communications*, vol. 492, no. 1, pp. 41–47, 2017, ISSN: 10902104. DOI: 10.1016/j.bbrc.2017.08.041. [Online]. Available: http://dx.doi.org/10.1016/j.bbrc.2017.08.041.

[211] J. Guo, R. Zhang, Z. Yang, Z. Duan, D. Yin, and Y. Zhou, *Biological Roles and Therapeutic Applications of IDH2 Mutations in Human Cancer*, Apr. 2021. DOI: 10.3389/fonc.2021.644857.

[212] C. Scheede-Bergdahl and A. Bergdahl, "Adaptation of mitochondrial expression and ATP production in dedifferentiating vascular smooth muscle cells," *Canadian Journal of Physiology and Pharmacology*, vol. 95, no. 12, pp. 1473–1479, 2017, ISSN: 12057541. DOI: 10.1139/cjpp-2017-0227.

[213] S. Feng, N. Bowden, M. Fragiadaki, C. Souilhol, S. Hsiao, M. Mahmoud, S. Allen, D. Pirri, B. T. Ayllon, S. Akhtar, A. A. Roger Thompson, H. Jo, C. Weber, V. Ridger, A. Schober, and P. C. Evans, "Mechanical activation of hypoxia-inducible factor 1a drives endothelial dysfunction at atheroprone sites," *Arteriosclerosis, Thrombosis, and Vascular Biology*, vol. 37, no. 11, pp. 2087–2101, 2017, ISSN: 15244636. DOI: 10.1161/ATVBAHA.117.309249.

[214] B. Xiao, X. Deng, W. Zhou, and E. K. Tan, *Flow cytometry-based assessment of mitophagy using mitotracker*, Mar. 2016. DOI: 10.3389/fncel.2016.00076.

[215] K. H. Chen, X. Guo, D. Ma, Y. Guo, Q. Li, D. Yang, P. Li, X. Qiu, S. Wen, R. P. Xiao, and J. Tang, "Dysregulation of HSG triggers vascular proliferative disorders," *Nature Cell Biology*, vol. 6, no. 9, pp. 872–883, Sep. 2004, ISSN: 14657392. DOI: 10.1038/ncb1161. [Online]. Available: https://pubmed.ncbi.nlm.nih.gov/15322553/.

[216] M. Chiong, B. Cartes-Saavedra, I. Norambuena-Soto, D. Mondaca-Ruff, P. E. Morales, M. García-Miguel, and R. Mellado, *Mitochondrial metabolism and the control of vascular smooth muscle cell proliferation*, Dec. 2014. DOI: 10.3389/fcell.2014.00072.

[217] H. Chen, S. A. Detmer, A. J. Ewald, E. E. Griffin, S. E. Fraser, and D. C. Chan, "Mitofusins Mfn1 and Mfn2 coordinately regulate mitochondrial fusion and are essential for embryonic development," *Journal of Cell Biology*, vol. 160, no. 2, pp. 189–200, Jan. 2003, ISSN: 00219525. DOI: 10.1083/jcb.200211046. [Online]. Available: https://pubmed.ncbi.nlm.nih.gov/12527753/.

[218] H. Chen and D. C. Chan, *Emerging functions of mammalian mitochondrial fusion and fission*, Oct. 2005. DOI: 10.1093/hmg/ddi270. [Online]. Available: https://pubmed.ncbi.nlm.nih.gov/16244327/.

[219] Z. Liu, J. Wang, X. Huang, Z. Li, and P. Liu, "Deletion of sirtuin 6 accelerates endothelial dysfunction and atherosclerosis in apolipoprotein E-deficient mice," *Translational Research*, vol. 172, pp. 18–29, Jun. 2016, ISSN: 18781810. DOI: 10.1016/j.trsl.2016.02.005.

[220] M. O. Grootaert, A. Finigan, N. L. Figg, A. K. Uryga, and M. R. Bennett, "SIRT6 Protects Smooth Muscle Cells from Senescence and Reduces Atherosclerosis," *Circulation Research*, pp. 474–491, 2021, ISSN: 15244571. DOI: 10.1161/CIRCRESAHA.120.318353.

[221] Z. Q. Zhang, S. C. Ren, Y. Tan, Z. Z. Li, X. Tang, T. T. Wang, D. L. Hao, X. Zhao, H. Z. Chen, and D. P. Liu, "Epigenetic regulation of NKG2D ligands is involved in exacerbated atherosclerosis development in Sirt6 heterozygous mice," *Scientific Reports*, vol. 6, Apr. 2016, ISSN: 20452322. DOI: 10.1038/srep23912.

[222] Y. Kimura, Y. Izumiya, S. Araki, S. Yamamura, S. Hanatani, Y. Onoue, T. Ishida, Y. Arima, T. Nakamura, E. Yamamoto, T. Senokuchi, T. Yoshizawa, M. Sata, S. Kim-Mitsuyama, N. Nakagata, E. Bober, T. Braun, K. Kaikita, K. Yamagata, and K. Tsujita, "Sirt7 Deficiency Attenuates Neointimal Formation Following Vascular Injury by Modulating Vascular Smooth Muscle Cell Proliferation," *Circulation Journal*, pp. 1–4, 2021, ISSN: 1346-9843. DOI: 10.1253/circj.cj-20-0936.

[223] J. Shin, M. He, Y. Liu, S. Paredes, L. Villanova, K. Brown, X. Qiu, N. Nabavi, M. Mohrin, K. Wojnoonski, P. Li, H.-L. Cheng, A. J. Murphy, D. M. Valenzuela, H. Luo, P. Kapahi, R. Krauss, R. Mostoslavsky, G. D. Yancopoulos, F. W. Alt, K. F. Chua, and D. Chen, "SIRT7 Represses Myc Activity to Suppress ER Stress and Prevent Fatty Liver Disease," *CELREP*, vol. 5, pp. 654–665, 2013. DOI: 10.1016/j.celrep.2013.10.007. [Online]. Available: http://dx.doi.org/10.1016/j.celrep.2013.10.007.

[224] P. Fang, Y. Xue, Y. Zhang, N. Fan, L. Ou, L. Leng, J. Pan, and X. Wang, "SIRT7 regulates the TGF-β1-induced proliferation and migration of mouse airway smooth muscle cells by modulating the expression of TGF-β receptor I," *Biomedicine and Pharmacotherapy*, vol. 104, pp. 781–787, Aug. 2018, ISSN: 19506007. DOI: 10.1016/j.biopha.2018.05.060.

[225] Z. Deng, X. Wang, X. Long, W. Liu, C. Xiang, F. Bao, and D. Wang, "Sirtuin 7 promotes colorectal carcinoma proliferation and invasion through the inhibition of E-cadherin," *Experimental and Therapeutic Medicine*, vol. 15, no. 3, pp. 2333–2342, Mar. 2018, ISSN: 17921015. DOI: 10.3892/etm.2017.5673.

[226] H. Yu, W. Ye, J. Wu, X. Meng, R. Y. Liu, X. Ying, Y. Zhou, H. Wang, C. Pan, and W. Huang, "Overexpression of Sirt7 exhibits oncogenic property and serves as a prognostic factor in colorectal cancer," *Clinical Cancer Research*, vol. 20, no. 13, pp. 3434–3445, Jul. 2014, ISSN: 15573265. DOI: 10.1158/1078-0432.CCR-13-2952. [Online]. Available: http://clincancerres.aacrjournals.org/.

[227] J. K. Kim, J. H. Noh, K. H. Jung, J. W. Eun, H. J. Bae, M. G. Kim, Y. G. Chang, Q. Shen, W. S. Park, J. Y. Lee, J. Borlak, and S. W. Nam, "Sirtuin7 oncogenic potential in human hepatocellular carcinoma and its regulation by the tumor suppressors MiR-125a-5p and MiR-125b," *Hepatology*, vol. 57, no. 3, pp. 1055–1067, Mar. 2013, ISSN: 02709139. DOI: 10.1002/hep.26101. [Online]. Available: https://onlinelibrary.wiley.com/doi/10.1002/hep.26101.

[228] Y. Han, Y. Liu, H. Zhang, T. Wang, R. Diao, Z. Jiang, Y. Gui, and Z. Cai, "Hsa-miR-125b suppresses bladder cancer development by down-regulating oncogene SIRT7 and oncogenic long non-coding RNA MALAT1," *FEBS Letters*, vol. 587, no. 23, pp. 3875–3882, Nov. 2013, ISSN: 00145793. DOI: 10.1016/j.febslet.2013.10.023.

[229] A. Wronska, A. Lawniczak, P. M. Wierzbicki, and Z. Kmiec, "Age-related changes in sirtuin 7 expression in calorie-restricted and refed rats," *Gerontology*, vol. 62, no. 3, pp. 304–310, Apr. 2016, ISSN: 14230003. DOI: 10.1159/000441603. [Online]. Available: https://pubmed.ncbi.nlm.nih.gov/26595207/.

[230] S. Kiran, T. Anwar, M. Kiran, and G. Ramakrishna, *Sirtuin 7 in cell proliferation, stress and disease: Rise of the Seventh Sirtuin!* Mar. 2015. DOI: 10.1016/j.

cellsig.2014.11.026. [Online]. Available: https://pubmed.ncbi.nlm.nih.gov/25435428/.

[231] B. N. Vazquez, J. K. Thackray, and L. Serrano, "Sirtuins and DNA damage repair: SIRT7 comes to play," *Nucleus*, vol. 8, no. 2, pp. 107–115, Jan. 2017, ISSN: 19491042. DOI: 10.1080/19491034.2016.1264552. [Online]. Available: https://pubmed.ncbi.nlm.nih.gov/28406750/.

[232] S. Araki, Y. Izumiya, T. Rokutanda, A. Ianni, S. Hanatani, Y. Kimura, Y. Onoue, T. Senokuchi, T. Yoshizawa, O. Yasuda, N. Koitabashi, M. Kurabayashi, T. Braun, E. Bober, K. Yamagata, and H. Ogawa, "Sirt7 Contributes to Myocardial Tissue Repair by Maintaining Transforming Growth Factor-β Signaling Pathway," *Circulation*, vol. 132, no. 12, pp. 1081–1093, Sep. 2015, ISSN: 0009-7322. DOI: 10.1161/CIRCULATIONAHA.114.014821. [Online]. Available: https://www.ahajournals.org/doi/10.1161/CIRCULATIONAHA.114.014821.

[233] S. Paredes, M. Angulo-Ibanez, L. Tasselli, S. M. Carlson, W. Zheng, T. M. Li, and K. F. Chua, "The epigenetic regulator SIRT7 guards against mammalian cellular senescence induced by ribosomal DNA instability," *Journal of Biological Chemistry*, vol. 293, no. 28, pp. 11 242–11 250, Jul. 2018, ISSN: 1083351X. DOI: 10.1074/jbc.AC118.003325. [Online]. Available: https://pubmed.ncbi.nlm.nih.gov/29728458/.

6 Appendix

6.1 List of mentioned genes, proteins, receptors and transcription factors

Abca1	ATP-binding cassette, sub-family A (ABC1), member 1
Acadm	acyl-Coenzyme A dehydrogenase, medium chain
Ace	angiotensin-converting enzyme
Aco2	aconitase 2, mitochondrial
Acta2	actin, alpha 2, smooth muscle
Aldoa	aldolase A
ANT	adenine nucleotide translocase
ApoE	apolipoprotein E
Atp5h	ATP synthase, H+ transporting, mitochondrial F0 complex, subunit D
Atp5o	ATP synthase, H+ transporting, mitochondrial F1 complex, O subunit
CaU	calcium uniporter
Ccnd1	cyclin D1
CCR2	chemokine receptor 2
CD68	CD68 antigen
Clpp	caseinolytic mitochondrial matrix peptidase proteolytic subunit
COXIV	cytochrome c oxidase subunit IV
CPT	carnitine palmitoyltransferase
Cpt1a	carnitine palmitoyltransferase 1a
Ctnnb1	catenin beta 1
Dnm1l	dynamin 1-like
DRP1	dynamin-related protein 1
Echs1	enoyl-CoA hydratase, short chain 1
Eef2	eukaryotic translation elongation factor 2
EGFP	enhanced green fluorescent protein
Elk1	ETS Like-1 protein
Eno1	enolase 1

Etfa	electron transfer flavoprotein subunit alpha
ETF-Q	electron transfer flavoprotein-ubiquinone
ETS-domain	E26 transformation-specific
Fh1	fumarate hydratase 1
FOXO	forkhead box
GABP	GA-binding protein
GABPα	GA-binding protein alpha
GABPβ	GA-binding protein beta
GFP	green fluorescent protein
Glut1	glucose transporter 1
Got2	glutamatic-oxaloacetic transaminase 2
h-caldesmon	high molecular weight caldesmon
HIF-1α	hypoxia inducible factor 1α
HIF-2α	hypoxia inducible factor 2α
ICAM	intercellular adhesion molecule
Idh2	isocitrate dehydrogenase 2 (NADP)
IL-1	interleukin 1
KLF4	Kruppel-like factor 4
l-caldesmon	low molecular weight caldesmon
Ldha	lactate dehydrogenase A
Lgals3	galectin 3 / lectin, galactose binding, soluble 3
MCP-1	monocyte chemotactic protein
M-CSF	macrophage colony-stimulating factor
Mfn1	mitofusin 1
Mfn2	mitofusin 2
Mki67	marker of proliferation Ki-67
Mn-SOD	manganese superoxide dismutase
Mrpl49	mitochondrial ribosomal protein L49
Mrps5	mitochondrial ribosomal protein S5
Mrps9	mitochondrial ribosomal protein S9
mt-Nd1	NADH dehydrogenase 1, mitochondrial
Myh11	myosin heavy chain 11, smooth muscle
Ndufa13	NADH:ubiquinone oxidoreductase subunit A13
Ndufs1	NADH:ubiquinone oxidoreductase core subunit S1
NFκB	kappa-light-chain-enhancer of activated B cells

NRF1	nuclear respiratory factor 1
NRF2	nuclear respiratory factor 2
OPA1	optic atrophy 1
PARP1	poly-ADP-ribose-polymerase 1
Pcx	pyruvate carboxylase
PDH	pyruvate dehydrogenase
Pdha1	pyruvate dehydrogenase E1 subunit alpha 1
Pdhb	pyruvate dehydrogenase E1 subunit beta
Pdhx	pyruvate dehydrogenase complex, component X
PDK1	pyruvate dehydrogenase kinase 1
Pdk2	pyruvate dehydrogenase kinase 2
Pdpr	pyruvate dehydrogenase phosphatase regulatory subunit
Pfkfb3	6-phosphofructo-2-kinase/fructose-2,6-biphosphatase 3
Pfkm	phosphofructokinase, muscle
PGC-1	PPARγ coactivator 1
PGC-1α	PPARγ coactivator 1 alpha
Pgk1	phosphoglycerate kinase 1
Polrmt	RNA polymerase mitochondrial
PPARα	peroxisome proliferator-activated receptor alpha
Rpl19	ribosomal protein L19
Rps11	ribosomal protein S11
Sir2	silent regulator 2
Sirt1	sirtuin 1
Sirt6	sirtuin 6
Sirt7	sirtuin 7
Sirt7 E5-6	sirtuin 7 exon 5-6
Sirt7 E9-10	sirtuin 7 exon 9-10
Slc2a1	solute carrier family 2 member 1
SMA	smooth muscle actin
SM-MHC/SMMHC	smooth muscle myosin heavy chain
SMTN	smoothelin
Tcf21	transcription factor 21
Tfam	transcription factor A, mitochondrial
TFMB	transcription factor B, mitochondrial

TGF-β	transforming growth factor beta
Tigar	Trp53 induced glycolysis regulatory phosphatase
TNF-α	tumor necrosis factor alpha
Uqcrh	ubiquinol-cytochrome c reductase hinge protein
VCAM-1	vascular cell adhesion molecule 1